

XLIIIrd RENCONTRES DE MORIOND

Electroweak Interactions and Unified Theories

III - Flavour Physics

FLAVOUR IN WARPED EXTRA DIMENSIONS

G. CACCIAPAGLIA

*Institut de Physique Nucléaire de Lyon, Université Lyon 1, CNRS/IN2P3,
F-69622 Villeurbanne Cedex, France*

Models in warped extra dimensions are very attractive because they can easily explain the hierarchy between the Planck and Electroweak scale, and generate the hierarchies in the fermion spectrum. The bounds on flavour are naturally less severe than in 4D extensions of the Standard Model, however they are still more severe than the electroweak precision tests, therefore worsening the fine tuning or little hierarchy problem. We review some recent attempts to soften such bounds either by means of flavour symmetries in the bulk or of a 5D minimal flavour violation paradigm.

1 Introduction

The Higgs sector is the only part of the Standard Model (SM) that has not been unveiled by experimental searches yet. What puzzles theorists is not only the lack of direct evidence of a Higgs boson so far, but also a theoretical prejudice against a light fundamental scalar particle. In fact, quantum corrections would like to push the Higgs mass and the electroweak scale near the cutoff, that can be as high as the Planck scale. Recent efforts, however, have focused on a less severe problem that has more impact on the LHC experiments: the little hierarchy problem. The stability of the electroweak scale would require the presence of new particles below or around a TeV, however precision electroweak measurements generically push such scale above 5-10 TeV. This bound is severely worsened if flavour is also taken into account: measurements in the Kaon and B systems push the scale of new physics up to 10^4 TeV, thus requiring a fine tuning of several orders of magnitude unless a protection mechanism is summoned.

In the early '90, it has been realized that extra space dimensions are a rich playground for models of new physics. L. Randall and R. Sundrum¹ proposed an interesting metric in 5 dimensions that may account for large hierarchies in a natural way: such metric can be written as

$$ds^2 = \left(\frac{R}{z}\right)^2 (dx_\mu dx^\mu - dz^2) . \quad (1)$$

In this parametrization the 5D metric is explicitly invariant if we rescale the 4D coordinates x_μ and z by the same amount: this means that moving along the coordinate z is equivalent, from the 4D point of view, to a rescaling of lengths and energies. The space is compactified by placing two branes at the boundaries. The brane at small z (UV-brane) will feel a large fundamental scale and therefore acts as

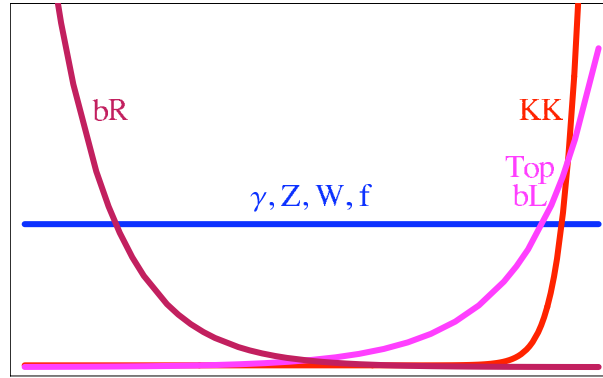


Figure 1: Portrait of a generic model of EWSB in warped space.

a fundamental cutoff of the theory, while the brane at large z will feel a smaller scale which could be identified with the electroweak scale. In this setup a large hierarchy is rephrased in terms of order one parameters thanks to the exponential nature of the metric: this is more evident if one uses the coordinate $z = R \exp \frac{y}{R}$.

This idea has sprouted many interesting models. Among them, one can identify the Higgs as the 5th polarization of a gauge boson from a broken bulk symmetry²: gauge invariance itself will protect the Higgs potential and solve the little hierarchy problem, given that the Kaluza-Klein (KK) resonances that cut off the loop divergencies are light enough. However, precision electroweak tests (PEWTs) require the heavy bosons to be above 2 TeV. Flavour physics plays an important role in these models: in fact one can use warped geometry to generate the hierarchies in the fermion mass spectrum naturally³. Once the fermions propagate in the bulk of the extra dimension, there will be more sources of flavour than in the SM: schematically the relevant terms in the action can be written as

$$S = \int d^4x \int_{z_{UV}}^{z_{IR}} dz \left(\frac{R}{z} \right)^4 \left[\frac{c_{Q,u,d}}{z} \bar{\psi}_{Q,u,d} \psi_{Q,u,d} + Y_{u,d} \bar{\psi}_Q H \psi_{u,d} \delta(z - z_{IR}) \right] + \dots, \quad (2)$$

where the dots represent eventual UV localized terms and higher order operators. The SM fermion masses are generated by the interactions with the Higgs which is localized on or near the IR brane: for instance in gauge-Higgs unification models the delta function is replaced by the Higgs profile, peaked at large z . The bulk masses c , matrices in flavour space, are not real masses: they control the fermion localization along the extra dimension, and therefore the overlap with the Higgs. The wave functions are in fact exponentially sensitive to the c 's. Generically, this flavour-dependence of the wave functions will induce flavour non-universal couplings with the gauge KK modes, in particular the KK gluons, which will generate flavour changing neutral currents (FCNCs) at tree level. Flavour therefore may constrain the KK masses well above the TeV scale! Moreover, one needs to worry about new CP violating phases and higher order operators which may be suppressed by the IR scale.

If the bounds were as tight as in 4 dimensions, it would be the death of such models: however this is not the case. In order to understand this statement, we need to understand better the structure of a generic model of EWSB in warped geometry. The key is the localization of the wave functions: in fact it will determine both the spectrum via the boundary conditions, and the strength of their couplings via their overlap with other fields. Therefore, a generic model of EWSB can be portrayed in Fig. 1: the gauge boson wave functions are flat due to gauge invariance; the light fermions are localized towards the UV brane in order to suppress their coupling to the Higgs, or any other source of EWSB; on the other hand the top is necessarily localized toward the IR brane due to its heaviness. Finally the KK modes of all the bulk fields are localized towards the IR brane: as a generic consequence, they will couple more to the heavy SM particles than to the light ones. Assuming anarchic Yukawa couplings, the spectrum and mixings are both determined by the values of the fermion wave functions on the IR brane. The couplings of light fermions to the KK modes are small due to the localizations, and universal up to corrections of order $\mathcal{O}(m_f^2/m_{KK}^2)$ ⁴: the light fermion are localized away from the IR brane, where KK wave functions are small and approximately constant. The flavour non-universal contribution comes from the values of the fermion wave functions on the IR brane, which are proportional to the fermion masses: this is the origin of the so-called Randall-Sundrum-GIM (Glashow Iliopoulos Maiani) mechanism. The situation is

different for the top, which is localized on the IR brane. Therefore, all the FCNCs are induced by the third generation, and they are proportional to the mixing angles to the top. This mechanism allows to lower considerably the flavour bounds on KK masses from thousands to 8 TeV. However, bounds from flavour are still generally more severe than EWPTs, and reopen the little hierarchy problem and a fine tuning in the Higgs potential.

In recent years a lot of work has been dedicated to weaken this flavour bounds and push them below the EWPTs bounds^{5,6,7}. In the rest of the paper we will review the two mechanisms involving flavour symmetries in the bulk⁵ and minimal flavour violation in the bulk⁶.

2 Flavour Symmetries in the Bulk

The easier way to avoid flavour bounds is to introduce flavour symmetries in the bulk. The simplest choice is to impose an $SU(3)_L \times SU(3)_R$ in the bulk for both quarks and leptons, where we impose a single flavour symmetry $SU(3)_R$ for the right handed fermions due to an eventual custodial symmetry in the bulk⁸ which will contain them in the same multiplet. The symmetry will be broken to the diagonal $SU(3)_D$ on the IR brane by the Yukawa couplings: in this way Yukawas, bulk masses and bulk operators are all flavour diagonal. The $SU(3)_R$ is broken on the UV brane where localized kinetic operators for the right-handed fermions will generate both the mass hierarchies and the mixings: therefore the number of flavour matrices in this model is the same as in the SM and no extra CP violating phases appear. Also, the symmetries forbid FCNCs: one can use two $SU(3)$ rotations in the up and down sector to diagonalize the kinetic operators. The neutral sector of the gauge bosons will remain flavour universal, while flavour violation will only appear in the interactions with charged gauge bosons like the W . Finally the only flavour violating higher order operators will be localized on the UV brane and will be suppressed by the large UV cutoff of the theory, therefore they can be safely neglected.

We can look more in detail to the main features of this scenario: the only flavour structure appears in the UV boundary conditions for the right-handed fields:

$$f_R(m, z_{UV}) \bar{A}_{u,d} = m g_R(m, z_{UV}) \mathcal{K}_{u,d} \cdot \bar{A}_{u,d}, \quad (3)$$

where f and g are generic flavour-blind wave functions, \bar{A} is the normalization - a vector in flavour space, and $\mathcal{K}_{u,d}$ are the UV kinetic matrices. One can diagonalize the kinetic matrices

$$\mathcal{K}_{u,d} = U_{u,d}^\dagger \cdot \mathcal{K}_{u,d}^{\text{diag}} \cdot U_{u,d}, \quad (4)$$

so the spectrum will be determined by the eigenvalues k_i while the mixing matrices will fix the normalization coefficients \bar{A} . Now, the couplings of neutral gauge bosons are diagonal, because they are proportional either to $U \cdot U^\dagger = 1$ or $U \cdot \mathcal{K} \cdot U^\dagger = \mathcal{K}^{\text{diag}}$; on the other hand, the charged boson couplings will be proportional to $U_u^\dagger U_d$. Therefore

$$V_{CKM} = U_u^\dagger U_d + \mathcal{O}(m_i^2) \quad (5)$$

where the corrections are due to the mass dependence of the wave functions, and all the flavour violating contributions will be proportional to the Cabibbo-Kobayashi-Maskawa matrix.

This model can be realized easily for the leptons, however it has problems when applied to quarks. The reason is that the top is very heavy and, due to the flavour symmetries, all the quarks share the same Yukawa coupling on the IR brane. The large Yukawa coupling will modify the fermion wave functions and generate universal corrections to the couplings. The flavour bound is therefore projected into EWPTs: the latter will push the KK masses above 10 TeV.

In order to solve this issue one needs to separate the top Yukawa from the light quarks. One can use different representations for the up and down right-handed quarks: using a singlet for the up quarks, including the top, can also help in lowering the bound from the coupling of the bottom with the Z boson⁹. Moreover, one can impose a looser $U(1)^3$ flavour symmetry for the right-handed up-type quarks and leave it unbroken. In this way the up type quarks Yukawas are all different:

$$Q \begin{pmatrix} m_u & & \\ & m_c & \\ & & m_t \end{pmatrix} u + m_b Q \begin{pmatrix} 1 & & \\ & 1 & \\ & & 1 \end{pmatrix} d \quad (6)$$

The down sector is as before, therefore all the flavour mixing is induced in the down sector. One can show that in this model FCNCs are still forbidden, and the strongest bound on the KK masses is again the 2 TeV from precision measurements⁵.

3 5D MFV: 5 Dimensional Minimal Flavour Violation

Another interesting approach is to impose minimal flavour violation on the 5 dimensional model: flavour violating effects are not protected by a symmetry, but by the assumption that all the flavour structure can only be determined by the Yukawa matrices. In this case, the bulk masses in Eq. 2 are

$$c_{u,d} \sim Y_{u,d}^\dagger + \dots \quad c_Q \sim rY_u^\dagger Y_u + Y_d^\dagger Y_d + \dots \quad (7)$$

The advantage of this approach is that one can still use different bulk masses to explain the hierarchies in the spectrum and the mixing angles, and at the same time gain a factor of ~ 3 suppression in the flavour bounds that makes them again as low as the precision tests. Assuming anarchic Yukawa matrices is still enough to generate the required hierarchies due to the exponential sensitivity to the c parameters. Moreover, in the limit when c_Q only depends on one Yukawa, for instance when $r \rightarrow 0$, one can diagonalize the down sector and eliminate all the flavour violating effects involving down type quarks. This means that the processes that violates flavour by 2 units, like for example the neutral Kaon mixing which gives the strongest bounds, are suppressed by small r . Therefore a moderately small r can provide the required factor of 3 in the bound without any flavour symmetry. Those small values are also preferred by the fit of the masses and mixing angles. Moreover the CP problem is also removed, because there isn't any additional phase besides the SM one: for instance one can check that electric dipole moments only arise at two loops and they do not pose any additional bound⁶.

4 Conclusion and Outlook

Flavour physics is an important component of models in warped extra dimension. In fact, flavour bounds generically apply to the KK masses of the gauge bosons which play an important role in the electroweak symmetry breaking sector and are required to be at or around a TeV in order for the model to be natural. The bounds are much lower than in a generic 4 dimensional model due to a Randall-Sundrum GIM mechanism, however they are still one order of magnitude tighter than bounds from precision electroweak tests. Moreover, the warped geometry offer the possibility to construct an elegant model of flavour where both the hierarchies in the masses and in the mixing angles are explained in terms of order one parameters. If we were not concerned by the two orders of magnitude still separating the scale of new physics and the electroweak scale, this would be one of the most appealing models of flavour.

However, trying to lower the bounds from flavour has inspired a dense activity in recent years. We reviewed two nice ideas. One involving the use of bulk flavour symmetry, and one proposal of a minimal flavour violation paradigm. In the former case, one can eliminate all the flavour changing neutral currents at the price of giving up the nice explanation of the hierarchies. The heaviness of the top quark still requires some massaging as the light quarks cannot share its large Yukawa, however it is still possible to construct models with a relaxed flavour symmetry where the flavour bound is as low as 2 TeV.

In the case of minimal flavour violation, no symmetry is needed and a relation between the Yukawa matrices and all the other sources of flavour violation is enough to solve the CP problem and to parametrically suppress the most dangerous flavour violating effects. It is important to notice that the required suppression is just a factor of 3, and that this suppression is also preferred by the fit of the fermion masses and mixing angles.

The precise bound from flavour physics is therefore very important as it can have severe consequences on the phenomenology and viability of such models. It can easily push the new physics above the reach of the LHC and the electroweak sector of the model un-natural. There cannot be a viable model unless its flavour structure is studied in detail.

Acknowledgments

I would like to thank C. Csaki, J. Galloway, G. Marandella, J. Terning and A. Weiler for their precious collaboration, and the organizers of the Rencontres of Moriond for the always inspiring environment offered during the meeting.

References

1. L. Randall and R. Sundrum, Phys. Rev. Lett. **83** (1999) 3370 [arXiv:hep-ph/9905221].
2. K. Agashe, R. Contino and A. Pomarol, Nucl. Phys. B **719** (2005) 165 [arXiv:hep-ph/0412089];
K. Agashe and R. Contino, Nucl. Phys. B **742** (2006) 59 [arXiv:hep-ph/0510164].
3. Y. Grossman and M. Neubert, Phys. Lett. B **474** (2000) 361 [arXiv:hep-ph/9912408];
T. Gherghetta and A. Pomarol, Nucl. Phys. B **586** (2000) 141 [arXiv:hep-ph/0003129].
4. K. Agashe, G. Perez and A. Soni, Phys. Rev. Lett. **93** (2004) 201804 [arXiv:hep-ph/0406101];
K. Agashe, G. Perez and A. Soni, Phys. Rev. D **71** (2005) 016002 [arXiv:hep-ph/0408134].
5. G. Cacciapaglia, C. Csaki, J. Galloway, G. Marandella, J. Terning and A. Weiler, JHEP **0804** (2008) 006 [arXiv:0709.1714 [hep-ph]].
6. A. L. Fitzpatrick, G. Perez and L. Randall, arXiv:0710.1869 [hep-ph].
7. C. Cheung, A. L. Fitzpatrick and L. Randall, JHEP **0801** (2008) 069 [arXiv:0711.4421 [hep-th]];
C. Csaki, A. Falkowski and A. Weiler, arXiv:0804.1954 [hep-ph];
M. C. Chen and H. B. Yu, arXiv:0804.2503 [hep-ph];
G. Perez and L. Randall, arXiv:0805.4652 [hep-ph];
C. Csaki, C. Delaunay, C. Grojean and Y. Grossman, arXiv:0806.0356 [hep-ph];
J. Santiago, arXiv:0806.1230 [hep-ph].
8. K. Agashe, A. Delgado, M. J. May and R. Sundrum, JHEP **0308** (2003) 050 [arXiv:hep-ph/0308036].
9. K. Agashe, R. Contino, L. Da Rold and A. Pomarol, Phys. Lett. B **641** (2006) 62 [arXiv:hep-ph/0605341].

$\Delta F = 1$ CONSTRAINTS ON MINIMAL FLAVOR VIOLATION

J. F. KAMENIK

*INFN Laboratori Nazionali di Frascati,
Via E. Fermi 40, I-00044 Frascati, Italy,**J. Stefan Institute,
Jamova 39, P. O. Box 3000, 1001 Ljubljana, Slovenia*

We present an updated phenomenological analysis of the minimal flavor violating (MFV) effective theory, both at small and large $\tan\beta$, in the sector of $\Delta F = 1$ processes. We evaluate the bounds on the scale of new physics derived from recent measurements (in particular from $B \rightarrow X_s\gamma$, $B \rightarrow X_s\ell^+\ell^-$, $B_s \rightarrow \mu^+\mu^-$ and $K \rightarrow \pi\nu\bar{\nu}$) and we use such bounds to derive a series of model-independent predictions within MFV for future experimental searches in the flavor sector.

1 Introduction

The Standard Model (SM) accurately describes high energy physical phenomena up to the electro-weak (EW) scale $\mu_W \sim 100$ GeV. It is however known to be incomplete due to the lack of description of gravity, proper unification of forces as well as neutrino masses. In view of these shortcomings, it can be regarded as a low-energy effective description of physics below a UV cut-off scale Λ . But if it is an effective theory, at what scale Λ below the unification or the Planck scale does it break down? The only dimensionful parameter in the renormalizable part of the Lagrangian is the Higgs mass, which is known to be quadratically sensitive to the cut-off scale of the theory. Then the EW hierarchy problem suggests that new physics (NP) should appear around or below $\Lambda \lesssim 1$ TeV. The non-renormalizable higher dimensional terms, formally suppressed by the increasing powers of the cut-off scale on the other hand mediate flavor changing neutral currents (FCNCs), may contain additional sources of CP violation and can violate baryon and lepton numbers. Even in absence of the later, precision measurements of low energy experiments put severe constraints on the scale of flavor and CP violating NP. Excellent agreement between SM predictions and experiment on ϵ_K (constraining $s-d$ sector), $A_{CP}(B_d \rightarrow \Psi K_s)$ and Δm_d (in the $b-d$ sector) and $B \rightarrow X_s\gamma$ (for $b \rightarrow s$ transitions) constrains

a general flavor violating NP to appear above $\Lambda \gtrsim 2 \times 10^5$ TeV, 2×10^3 TeV and 40 TeV respectively. The resulting tension between the two estimates of the NP scale illustrates what is often called the new physics flavor problem.

The Minimal Flavor Violation (MFV) hypothesis^{1,2} aims to solve the issue by demanding that all flavor symmetry breaking in and also beyond the SM is proportional to the SM Yukawas. A few direct consequences follow from this assumption: Firstly the Cabibbo-Kobayashi-Maskawa (CKM) matrix is the only source of flavor mixing and CP violation even beyond the SM. Thus, all (non-helicity suppressed) tree level and CP violating processes are constrained to their SM values. Finally, CKM unitarity is maintained and a (universal) unitarity triangle (UUT) can be determined from a constrained set of observables³. Other details of phenomenology depend on the form of the EW Higgs sector of the theory. In case of a SM-like single Higgs doublet, the FCNCs in the down quark sector are all driven by the large top Yukawa (λ_t). At the same time, when performing the operator product expansion (OPE) at the EW scale, the SM basis of operators contributing to the effective weak Hamiltonian is complete also in presence of NP, making the MFV effective theory approach predictive. The same holds true at low $\tan \beta \equiv v_u/v_d$ if the Higgs sector is described in terms of an effective two Higgs doublet model of type II with the vacuum expectation values of the Higgses coupling to up(down) quarks denoted by $v_{u(d)}$. However, bottom Yukawa (λ_b) contributions become important at large $\tan \beta$ as $\lambda_b (\sim m_b \tan \beta / v_u) \sim \lambda_t$. Accompanied by the partial lifting of helicity suppression in the down sector, contributions due to new density operators have to be taken into account in the effective weak Hamiltonian. Still, the predictivity of the MFV effective theory approach is maintained by the small number of additional operators which need to be considered.

The symmetry principles underlying the MFV hypothesis establish solid links among different flavor observables at low energy and allow to probe and constrain the scale of MFV NP. Since (non-helicity suppressed) charged current interactions are not affected, bounds can be derived from $\Delta F = 2$ and $\Delta F = 1$ FCNC phenomenology. The $\Delta F = 2$ processes are box loop mediated in the SM, and only a few operators contribute to the effective weak Hamiltonian. The main observables here are the K , B_q oscillation parameters to which MFV NP at low $\tan \beta$ contributes universally². A recent analysis⁴ was able to constrain this contribution and put a lower bound on the effective NP scale $\Lambda > 5.5$ TeV at 95% probability. The $\lambda_b \tan \beta$ contributions break the universality among kaon and B meson sectors at large $\tan \beta$, resulting in a slightly weaker bounds of $\Lambda > 5.1$ TeV. New operators due to Higgs exchange in the loop start contributing only at very large values of $\tan \beta$, resulting in a bound on a certain combination of charged Higgs parameters. $\Delta F = 1$ processes on the other hand are penguin loop mediated in the SM, with many operators contributing. In concrete MFV models, they are often related to the $\Delta F = 2$ as well as flavour conserving phenomenology⁵. On the other hand in our effective theory bottom-up approach they have to be considered completely orthogonal. An analysis of bounds coming from radiative, and (semi)leptonic decays of K and B mesons was performed a while ago², however limited experimental information at the time barred from exploring in particular the interesting role of the large $\tan \beta$ scenario. In the meantime, the situation has drastically improved and the new updated experimental and theoretical results on $\Delta F = 1$ FCNC mediated processes further motivate the revisiting and updating of this analysis. In the following we present a selection of results from such a study, the details of which will be presented elsewhere⁶.

2 Updating Analysis of $\Delta F = 1$ Constraints

In the SM the effective weak Hamiltonian describing $\Delta F = 1$ FCNC processes among down-type quark flavors $q_i - q_j$ can be written as²

$$\mathcal{H}_{eff}^{\Delta F=1} = \frac{G_F \alpha_{em}}{2\sqrt{2}\pi \sin^2 \theta_W} V_{ti}^* V_{tj} \sum_n C_n \mathcal{Q}_n + \text{h.c.}, \quad (1)$$

where G_F is the Fermi constant, α_{em} is the fine structure constant, θ_W is the Weinberg angle and V_{ij} are the CKM matrix elements. The short distance SM contributions are encoded in the Wilson coefficients C_n , computed via perturbative matching procedure at the EW scale. MFV NP manifests itself in the shifts of the individual Wilson coefficients in respect to the SM values $C_n(\mu_W) = C_n^{SM} + \delta C_n$. These shifts can be translated in terms of the tested NP energy scale Λ as $\delta C_n = 2a\Lambda_0^2/\Lambda^2$, where $\Lambda_0 = \lambda_t \sin^2(\theta_W)m_W/\alpha_{em} \sim 2.4$ TeV is the corresponding typical SM effective energy scale. The value of the free variable a depends on the details of a particular MFV NP model. In general $a \sim 1$ for tree level NP contributions, while $a \sim 1/16\pi^2$ for loop suppressed NP contributions. In our numerical results we put a to unity.

In order to address low energy phenomenology, one needs to evaluate the appropriate matrix elements of the corresponding effective dimension 6 operators \mathcal{Q}_n . At low $\tan\beta$ we consider the EM and QCD dipole operators

$$\mathcal{Q}_{7\gamma} = \frac{2}{g^2}m_j\bar{d}_{iL}\sigma_{\mu\nu}d_{jR}(eF_{\mu\nu}), \quad \mathcal{Q}_{8G} = \frac{2}{g^2}m_j\bar{d}_{iL}\sigma_{\mu\nu}T^a d_{jR}(g_s G_{\mu\nu}^a), \quad (2)$$

where g is the EW $SU(2)_L$ coupling, e is the EM coupling, g_s is the QCD coupling, T^a are the $SU(3)_c$ generator matrices, while $F_{\mu\nu}$ and $G_{\mu\nu}^a$ are the EM and QCD field tensors. They contribute to $B \rightarrow X_s\gamma$ decay as well as to the $B \rightarrow X_s\ell^+\ell^-$ phenomenology, where in addition we get contributions from the EW-penguin operators

$$\mathcal{Q}_{9V} = 2\bar{d}_{iL}\gamma_\mu d_{jL} \bar{\ell}\gamma_\mu\ell, \quad \mathcal{Q}_{10A} = 2\bar{d}_{iL}\gamma_\mu d_{jL} \bar{\ell}\gamma_\mu\gamma_5\ell. \quad (3)$$

Here $\ell = e, \mu, \tau$ denotes the charged leptons. \mathcal{Q}_{10A} also mediates $B_q \rightarrow \ell^+\ell^-$. Finally the Z-penguin operator

$$\mathcal{Q}_{\nu\bar{\nu}} = 4\bar{d}_{iL}\gamma_\mu d_{jL} \bar{\nu}_L\gamma_\mu\nu_L \quad (4)$$

enters solely in $B \rightarrow X_s\nu\bar{\nu}$ and $K \rightarrow \pi\nu\bar{\nu}$ decays and can thus be constrained independently of the others. We do not consider NP contributions to QCD penguin operators as their impact on phenomenology is subdominant compared to long distance effects. At large $\tan\beta$, one needs to take into account an additional density operator

$$\mathcal{Q}_{S-P} = 4(\bar{d}_{iL}d_{jR})(\bar{\ell}_R\ell_L) \quad (5)$$

contributing to $B \rightarrow X_s\ell^+\ell^-$ and $B_q \rightarrow \ell^+\ell^-$. On the other hand, contributions from additional four quark density operators^{7 a} which are also $\tan\beta$ enhanced and enter $B \rightarrow X_s\gamma$ and $B \rightarrow X_s\ell^+\ell^-$ through one loop mixing with $\mathcal{Q}_{7\gamma,8G}$ are $\alpha_{em}/4\pi \sim 0.001$ suppressed relative to those of \mathcal{Q}_{S-P} and thus turn out to be negligible after imposing the bounds on \mathcal{Q}_{S-P} .

In our analysis we consider the most theoretically clean observables in order to derive reliable bounds on possible NP contributions. In particular, we use the inclusive branching ratio of the radiative $B \rightarrow X_s\gamma$ decay, measured with a lower cut on the photon energy. The latest HFAG value averaged over different measurements¹⁰ is $Br(B \rightarrow X_s\gamma)_{E_\gamma > 1.6 \text{ GeV}}^{\text{exp}} = 3.52(23)(9) \times 10^{-4}$, where the first error is statistical and the second systematic. Theoretically, the SM value is known to better than 8% and the expansion in terms of δC_n evaluated at the weak scale is⁸

$$Br(B \rightarrow X_s\gamma)_{E_\gamma > 1.6 \text{ GeV}}^{\text{th}} = 3.16(23) (1 - 2.28\delta C_{7\gamma} - 0.71\delta C_{8G} + 1.51\delta C_{7\gamma}^2 + 0.78\delta C_{8G}\delta C_{7\gamma} + 0.25\delta C_{8G}^2) \times 10^{-4}, \quad (6)$$

where the central value and its error have been adjusted to take into account the CKM matrix element determination from the UUT analysis⁴. Since δC_7 and δC_8 in absence of four quark density operator contributions enter in the same fixed combination to all relevant observables (any differences being artifacts of the truncated perturbative expansion) one can always eliminate

^aWe thank Ulrich Haisch for pointing out these potential contributions.

one of them (e.g. δC_{8G}) from the analysis and then reconstruct the bound on both from the quadratic combination in eq (6).

A completely different combination of operators contributes to the helicity suppressed decay $B_s \rightarrow \mu^+ \mu^-$. Experimentally the best upper bound on the branching ratio was recently put by the CDF collaboration⁹ $Br(B_s \rightarrow \mu^+ \mu^-)^{\text{exp}} < 4.7 \times 10^{-8}$ at 90% C.L., which is only an order of magnitude above the SM prediction. The theoretical error of which is around 23% and is dominated by the lattice QCD determination of the B_s decay constant. Again using UUT CKM inputs, the expansion in terms of δC_i reads

$$Br(B_s \rightarrow \mu^+ \mu^-)^{\text{th}} = 3.8(9) (1 - 2.1\delta C_{10A} - 2.3\delta C_{S-P} + 1.1\delta C_{10A}^2 + 2.4\delta C_{S-P}\delta C_{10A} + 2.7\delta C_{S-P}^2) \times 10^{-9}. \quad (7)$$

Analysis of $B \rightarrow X_s \ell^+ \ell^-$ is more involved since, not only do almost all of the above mentioned operators ($\mathcal{Q}_{7\gamma, 8G, 9V, 10A, S-P}$) contribute here, experimentally there are already a number of inclusive as well as exclusive measurements available, constraining different combinations of NP parameters. On the inclusive side, only the branching ratio $Br(B \rightarrow X_s \ell^+ \ell^-)$, where $\ell = e, \mu$ is measured by the B factories¹¹ in several bins of di-lepton invariant mass squared (q^2). The errors vary from almost 90% in the first bin where only Belle has obtained a relevant signal, to around 30% in the other bins. The latest calculations estimate the theoretical error at around 7% for the bins below the charmonium region and around 10% for the high q^2 bin¹². The relevant formulae including NP contributions are rather lengthy and can be found in ref.^{6,12}.

Much more experimental information is available for exclusive channels where the $B \rightarrow K^{(*)} \ell^+ \ell^-$ branching ratios as well as several angular distributions have already been measured¹³. Theoretically however, despite considerable theoretical progress on the evaluation of the non-perturbative matrix elements of \mathcal{Q}_n entering exclusive channels in the recent years¹⁴, a reliable determination can only be expected from fundamentally non-perturbative methods, such as lattice QCD. In the meantime, any phenomenological implications based on existing form factor estimates should be treated with care. We will present an analysis of the impact of the exclusive modes on the MFV NP bounds elsewhere⁶.

Finally MFV NP contributions to the Z-penguin operators can be constrained using the first experimental hints¹⁵ of the $K^+ \rightarrow \pi^+ \nu \bar{\nu}$ decay $Br(K^+ \rightarrow \pi^+ \nu \bar{\nu}(\gamma))^{\text{exp}} = 147(120) \times 10^{-12}$ and comparing them to the theoretical predictions, which are brought under control by the use of experimental data on $K\ell 3$ decays¹⁶ resulting in only 11% theoretical error. In presence of MFV NP the corresponding expression reads

$$Br(K^+ \rightarrow \pi^+ \nu \bar{\nu}(\gamma))^{\text{th}} = 7.53(82)(1 + 0.93\delta C_{\nu\bar{\nu}} + 0.22\delta C_{\nu\bar{\nu}}^2) \times 10^{-11}. \quad (8)$$

Common parametric inputs in our analysis are the particle masses and lifetimes from PDG¹⁷ as well as the parameters of the CKM matrix, which, as already mentioned, we take from the UUT analysis⁴. We perform a correlated fit of subsets of observables turning on NP contributions and extract probability bounds on the shifts of the Wilson coefficients away from their SM values.

3 Results

The compilation of bounds on the MFV NP scale in respect to all the probed operators is summarized in table 1. We present two sets of bounds. In the conservative estimate we take into account all the possible fine-tunings and cancellations among the various operator contributions, including discrete ambiguities in cases where the NP contributions might flip the sign of the SM pieces. For the second, more natural bounds, we consider each δC_n individually and also discard flipped-sign fine-tuned solutions. The strongest bounds come naturally from the $B \rightarrow X_s \gamma$ decay rate and affect $\mathcal{Q}_{7\gamma, 8G}$. As can be seen, the effect of the discrete ambiguity is large and

Table 1: Summary of bounds on the MFV NP scales related to the probed effective operators. All the numerical values are the lower bounds at 95% probability on the MFV NP scale Λ as explained in the text.

Operator	Conservative bound [TeV]	Natural bound [TeV]
$Q_{7\gamma}$	1.6	5.3
Q_{8G}	1.2	3.1
Q_{9V}	1.4	1.6
Q_{10A}	1.5	1.5
Q_{S-P}	1.2	/
$Q_{\nu\bar{\nu}}$	1.5	/

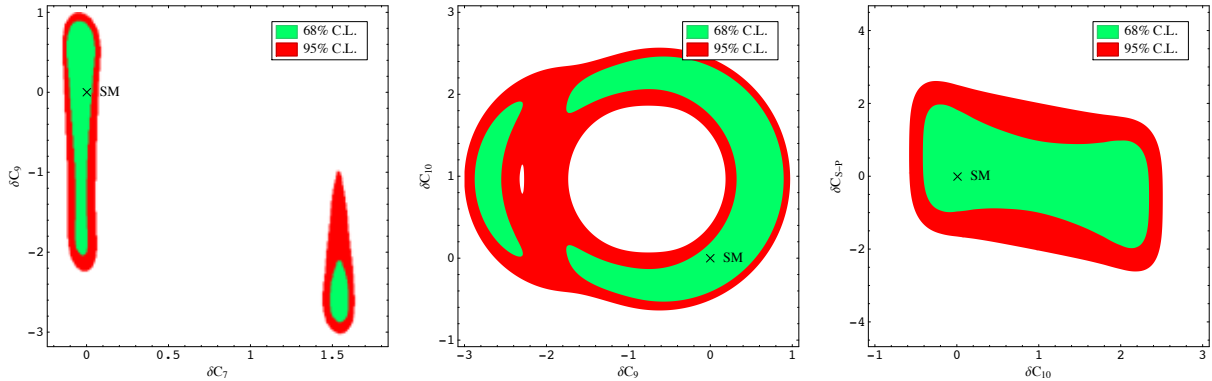


Figure 1: Correlation plots showing the most pronounced correlations among the bounds on the various NP Wilson coefficient shifts. The 68% (95%) probability regions are shown in green (red).

only the natural bounds on $\Lambda > 5.2(3.1)$ for $Q_{7\gamma(8G)}$ are competitive with the ones on $\Delta F = 2$ operators⁴. The discrete ambiguity (also seen on utmost left plot in figure 1) could however be completely removed in the future once the experimental situation concerning the lowest q^2 region in $B \rightarrow X_s \ell^+ \ell^-$ rate and especially the forward-backward asymmetry (FBA) improves. As expected, $Q_{S-P, \nu\bar{\nu}}$ operators are mainly bounded from single observables ($B_s \rightarrow \mu^+ \mu^-$ and $K^+ \rightarrow \pi^+ \nu\bar{\nu}$ respectively) leading to robust bounds around 1.2 TeV and 1.5 TeV respectively. Finally $\delta C_{9V, 10A}$ are mainly bounded by $B \rightarrow X_s \ell^+ \ell^-$ and using only presently available inclusive information the bounds are around 1.5 TeV. In all of the considered observables except $B \rightarrow X_s \gamma$ the experimental uncertainties strongly dominate and at present do not allow to discern discrete ambiguities or strong correlations as can be also deduced from figure 1 showing the most interesting pairwise correlation plots of the 68% and 95% allowed parameter regions.

4 Discussion and Outlook

In summary, immense experimental and theoretical progress in the area of flavor physics in the last decade has made it possible to constrain in a model independent way the complete set of possible beyond SM contributions to $\Delta F = 1$ and $\Delta F = 2$ processes due to possible MFV NP both at small and large $\tan \beta$. Bounds coming from $\Delta F = 2$ phenomenology are already very constraining, pushing the effective MFV NP scale beyond 5 TeV. In $\Delta F = 1$ sector, at present only the bounds coming from $B \rightarrow X_s \gamma$ are of comparable strength. However most uncertainties are dominated by experiments and one can look forward for the results of full dataset analyses by the B factories.

Using the derived bounds on the MFV NP contributions in $\Delta F = 1$ processes we are able to

make predictions for other potentially interesting observables to be probed at LHCb or a future Super Flavor Factory. As already mentioned, angular distributions like the FBA probe different combinations of the operators and would provide complimentary bounds. At the moment, considering bounds from inclusive measurements alone, no firm constraints on the FBA or its zero can be imposed within MFV models. This conclusion reinforces the importance of these observables and their potentiality of discovering relevant deviations.

Another set of observables displays interesting sensitivity to the $\tan\beta$ enhanced C_{S-P} contributions. Such are lepton flavor universality ratios $\Gamma(B \rightarrow K^{(*)}\mu^+\mu^-)/\Gamma(B \rightarrow K^{(*)}e^+e^-)$, which are very close to 1 with the SM as well as MFV models with low $\tan\beta$. However even at $\tan\beta$ present constraints already disallow deviations larger than 10% from unity for such ratios.

Finally the derived bounds allow to construct tests able to potentially rule out of MFV. Beside the interesting CP violation signals already emerging in the B_s sector¹⁸, in $\Delta F = 1$ sector first there are the firm relations among the different flavor transitions $[(b \leftrightarrow s)/(b \leftrightarrow d)/(s \leftrightarrow d) \sim |V_{tb}V_{ts}^*|/|V_{tb}V_{td}^*|/|V_{ts}V_{td}^*|]$ which might be probed with $K \rightarrow \pi\ell^+\ell^-$, $B \rightarrow X_s\nu\bar{\nu}$ or $B_d \rightarrow \mu^+\mu^-$ processes. Also interesting in this respect is the FBA in $B \rightarrow K\ell^+\ell^-$ which is already restricted to be below 1% within MFV models regardless of $\tan\beta$.

Acknowledgments

The author wishes to thank the organizers of the Rencontres de Moriond EW 2008 for their invitation and hospitality, as well as the collaborators on this project T. Hurth, G. Isidori and F. Mescia for discussions and comments on the manuscript. An Experienced Researcher position supported by the EU-RTN Programme, Contract No. MRTN-CT-2006-035482, “Flavianet” is gratefully acknowledged.

References

1. R. S. Chivukola and H. Georgi, *Phys. Lett. B* **188**, 99 (1987), J. L. Hall and L. Randall, *Phys. Rev. Lett.* **65**, 2939 (1990).
2. G. D’Ambrosio *et al*, *Nucl. Phys. B* **645**, 155 (2002).
3. A. J. Buras *et al*, *Phys. Lett. B* **500**, 161 (2001).
4. M. Bona *et al*, *JHEP* **0803**, 49 (2008), *Phys. Rev. Lett.* **97**, 151803 (2006).
5. A. J. Buras, *Phys. Lett. B* **566**, 115 (2003), U. Haisch and A. Weiler, *Phys. Rev. D* **76**, 74027 (2007).
6. T. Hurth, G. Isidori, J. F. Kamenik and F. Mescia, in preparation.
7. G. Hiller and F. Kruger, *Phys. Rev. D* **69**, 74020 (2004)
8. M. Misiak *et al*, *Phys. Rev. Lett.* **98**, 22002 (2007), M. Misiak, private communication.
9. T. Aaltonen *et al*, *Phys. Rev. Lett.* **100**, 101802 (2008).
10. HFAG, <http://www.slac.stanford.edu/xorg/hfag>, (Updated April 2008).
11. B. Aubert *et al*, *Phys. Rev. Lett.* **93**, 81802 (2004), M. Iwasaki *et al*, *Phys. Rev. D* **72**, 92005 (2005).
12. T. Huber *et al*, *Nucl. Phys. B* **740**, 105 (2006), T. Huber *et al*, arXiv:0712.3009[hep-ph].
13. A. Ishikawa *et al*, *Phys. Rev. Lett.* **96**, 251801 (2006), B. Aubert *et al*, *Phys. Rev. D* **73**, 92001 (2006), B. Aubert *et al*, arXiv:0804.4412.
14. M. Beneke *et al*, *Eur. Phys. J. C* **41**, 173 (2005), F. Krüger and J. Matias, *Phys. Rev. D* **71**, 94009 (2005), P. Ball and R. Zwicky, *Phys. Rev. D* **71**, 14015 (2005), *ibid.* 14029.
15. S. S. A. *et al*, *Phys. Rev. Lett.* **88**, 41803 (2002), V. V. Anisimovsky *et al*, *Phys. Rev. Lett.* **93**, 31801 (2004).
16. F. Mescia and C. Smith, *Phys. Rev. D* **76**, 34017 (2007).
17. W.-M. Yao *et al*, *Journal of Physics G* **33**, 1 (2006).
18. M. Bona *et al*, arXiv:0803.0659 [hep-ph].

Flavour Permutation Symmetry and Fermion Mixing ^a

P.F. Harrison ^b and D.R.J. Roythorne
*Department of Physics, University of Warwick, Coventry,
 CV4 7AL, England.*

W.G. Scott
*Rutherford Appleton Laboratory, Chilton, Didcot,
 OXON, OX11 0QX, England.*



We discuss our recently proposed $S3_{\downarrow} \times S3_{\uparrow}$ flavour-permutation-symmetric mixing observables, giving expressions for them in terms of (moduli-squared) of the mixing matrix elements. We outline their successful use in providing flavour-symmetric descriptions of (non-flavour-symmetric) lepton mixing schemes. We develop our partially unified flavour-symmetric description of both quark and lepton mixings, providing testable predictions for CP -violating phases in both B decays and neutrino oscillations.

1 Introduction

Flavour observables, namely quark and lepton masses and mixings are neither predicted nor predictable in the Standard Model. Neither are they correlated with each other in any way. However, their experimentally determined values display striking structure: viewed on a logarithmic scale, the fermion masses of any given non-zero charge are approximately equi-spaced; the spectrum of quark mixing angles is described by the Wolfenstein form, ¹ suggestive of correlations between mixing angles and quark masses, and the lepton mixing matrix is well-approximated by the tri-bimaximal form. ² These striking patterns are the modern-day equivalents of the regularities observed around a century ago in hydrogen emission spectra, which were mathematically well-described by the Rydberg formula, but nevertheless had no theoretical basis before the advent of quantum mechanics. While consistent with the Standard Model, they lie completely outside its predictive scope, and are surely evidence for some new physics beyond it.

^aTalk given at the 43rd Rencontres de Moriond, La Thuile, Italy, March 2008.

^bSpeaker.

In this talk, we report on our recent attempts³ to find a new description of fermion mixing which builds on the Standard Model and allows constraints on the mixing observables which make no reference to individual flavours, while describing mixing structures which are manifestly not flavour-symmetric, as observed experimentally. This approach does not in itself constitute a complete theory of flavour mixing beyond the Standard Model, but we hope that it might help stimulate new developments in that direction.

2 The Jarlskogian and Plaquette Invariance

Jarlskog's celebrated CP -violating invariant,⁴ J , is important in the phenomenology of both quarks and leptons. As well as parameterising the violation of a specific symmetry, it has two other properties which set it apart from most other mixing observables. First, its value (up to its sign) is independent of any flavour labels.^c Mixing observables are in general dependent on flavour labels, eg. the moduli-squared of mixing matrix elements, $|U_{\alpha i}|^2$, certainly depend on α and i . Indeed, J itself is often calculated in terms of a subset of four mixing matrix elements, namely those forming a given plaquette⁵ (whose elements are defined by deleting the γ -row and the k -column^d to leave a rectangle of four elements):

$$J = \text{Im}(\Pi_{\gamma k}) = \text{Im}(U_{\alpha i} U_{\alpha j}^* U_{\beta i}^* U_{\beta j}). \quad (1)$$

However, it is well-known⁴ that the value of J does not depend on the choice of plaquette (ie. on its flavour labels, γ and k above) - it is "plaquette-invariant". This special feature originates in the fact that J is *flavour-symmetric*, carrying information sampled evenly across the whole mixing matrix. We recently pointed-out³ that in fact, *any* observable function of the mixing matrix elements, flavour-symmetrised (eg. by summing over both rows and columns), and written in terms of the elements of a single plaquette (eg. using unitarity constraints), will be similarly plaquette-invariant. Both its expression in terms of mixing matrix elements, as well as its value, will be independent of the particular choice of plaquette.

The second exceptional property of J is that it may be particularly simply related to the fermion mass (or Yukawa) matrices:

$$J = -i \frac{\text{Det}[L, N]}{2L_{\Delta} N_{\Delta}} \quad (2)$$

where for leptons, L and N are the charged-lepton and neutrino mass matrices respectively^e (in an arbitrary weak basis) and $L_{\Delta} = (m_e - m_{\mu})(m_{\mu} - m_{\tau})(m_{\tau} - m_e)$ (with an analogous definition for N_{Δ} in terms of neutrino masses and likewise for the quarks). This is useful, as, despite J being defined purely in terms of mixing observables via Eq. (1), by contrast, Eq. (2) relates it to the mass matrices, which appear in the Standard Model Lagrangian.

We will discuss our recently proposed³ plaquette-invariant (ie. flavour-symmetric mixing) observables, which, in common with J , are independent of flavour labels and can be simply related to the mass matrices. Again like J , we find that our observables parameterise the violation of certain phenomenological symmetries which have already been considered significant^{6 7 8 9} in leptonic mixing. In the next section, we define more precisely what we mean by flavour symmetry.

^cWe focus first on the leptons, although many of our considerations may be applied equally well to the quarks. In the leptonic case, neutrino mass eigenstate labels $i = 1..3$ take the analogous role to the charge $-\frac{1}{3}$ quark flavour labels in the quark case. In this sense, we will often use the term "flavour" to include neutrino mass eigenstate labels, as well as charged lepton flavour labels.

^dWe use a cyclic labelling convention such that $\beta = \alpha + 1$, $\gamma = \beta + 1$, $j = i + 1$, $k = j + 1$, all indices evaluated mod 3.

^eThroughout this paper, L and N are taken to be Hermitian, either by appropriate choice of the flavour basis for the right-handed fields, or as the Hermitian squares, MM^{\dagger} , of the relevant mass or Yukawa coupling matrices. The symbols m_{α} , m_i generically refer to their eigenvalues in either case.

3 The $S3_{\downarrow} \times S3_{\uparrow}$ Flavour Permutation Group

The $S3_{\downarrow}$ group is the group of the six possible permutations of the charged lepton flavours and/or of the charge $-\frac{1}{3}$ quark flavours, while the $S3_{\uparrow}$ group is the group of the six possible permutations of the neutrino flavours (ie. mass eigenstates) or of the charge $\frac{2}{3}$ quark flavours (the arrow subscript corresponds to the direction of the z-component of weak isospin of the corresponding left-handed fields). We consider all possible such permutations, which together constitute the direct product $S3_{\downarrow} \times S3_{\uparrow}$ flavour permutation group (FPG)³ with 36 elements.

We next consider the P matrix (for ‘‘probability’’) ¹⁰ of moduli-squared of the mixing matrix elements, eg. for leptons:

$$P = \begin{pmatrix} |U_{e1}|^2 & |U_{e2}|^2 & |U_{e3}|^2 \\ |U_{\mu1}|^2 & |U_{\mu2}|^2 & |U_{\mu3}|^2 \\ |U_{\tau1}|^2 & |U_{\tau2}|^2 & |U_{\tau3}|^2 \end{pmatrix}. \quad (3)$$

It should be familiar: for quarks, semileptonic weak decay rates of hadrons are proportional to its elements, while for leptons, the magnitudes of neutrino oscillation probabilities may be written in terms of its elements.¹⁰ Moreover, the P matrix may easily be related to the fermion mass matrices, as we will see in Section 5 below. The P matrix manifestly transforms as the natural representation of $S3_{\downarrow} \times S3_{\uparrow}$, the transformations being effected by pre- and/or post-multiplying by 3×3 real permutation matrices.^f

Jarlskog’s invariant J is a pseudoscalar under the FPG: under even permutations, it is invariant, while under odd permutations (eg. single swaps of rows or columns of the mixing matrix, or odd numbers of them), it simply changes sign. This is our prototype Flavour Symmetric Mixing Observable (FSMO). As we commented in the previous section, it is easy to find other similar such quantities, which, surprisingly had not appeared in the literature until recently.³ There are two types of singlets under the $S3$ group: even ($\mathbf{1}$) which remain invariant under all permutations, and odd ($\bar{\mathbf{1}}$) which flip sign under odd permutations. So, under the FPG, there are four types of singlet: $\mathbf{1} \times \mathbf{1}$, $\bar{\mathbf{1}} \times \bar{\mathbf{1}}$ (like J), $\mathbf{1} \times \bar{\mathbf{1}}$ and $\bar{\mathbf{1}} \times \mathbf{1}$. By Flavour Symmetric Observables (FSOs), we mean observables with any of these transformation properties under the FPG. They may be functions of mixing matrix elements alone (FSMOs), or functions of mass eigenvalues alone, or functions of both.

Starting with elements of P and combining and (anti-)symmetrising them over flavour labels in various ways, we find that, apart from their (trivial) overall normalisation, and possibly scalar offsets, there are a finite number of independent FSMOs at any given order in P . Enumerating them, we found that there are no non-trivial ones linear in P , while at 2nd order in P , there is only one each of $\mathbf{1} \times \mathbf{1}$, $\bar{\mathbf{1}} \times \bar{\mathbf{1}}$. At third order, there is exactly one each of the four types of singlet, while at higher orders in P , there are multiple instances of each. Recognising that we need only four independent variables to specify the mixing, it is clearly enough to stop at third order, up to which, the singlets are essentially uniquely defined by their order in P and their transformation property under the FPG.

4 Flavour-Symmetric Mixing Observables

We introduce four FSMOs,³ uniquely defined as outlined above:

$$\begin{array}{ll} \mathbf{1} \times \mathbf{1} & \bar{\mathbf{1}} \times \bar{\mathbf{1}} \\ \text{2nd Order in } P: & \mathcal{G} = \frac{1}{2} [\sum_{\alpha i} (P_{\alpha i})^2 - 1] & \mathcal{F} = \text{Det} P \\ \text{3rd Order in } P: & \mathcal{C} = \frac{3}{2} \sum_{\alpha i} [(P_{\alpha i})^3 - (P_{\alpha i})^2] + 1 & \mathcal{A} = \frac{1}{18} \sum_{\gamma k} (L_{\gamma k})^3 \end{array} \quad (4)$$

^fLess obviously, any given plaquette of P transforms as a 2-dimensional (real) irreducible representation of $S3_{\downarrow} \times S3_{\uparrow}$.

where $L_{\gamma k} = (P_{\alpha i} + P_{\beta j} - P_{\beta i} - P_{\alpha j})$. Alternative, but equivalent definitions in terms of the elements of a single plaquette are given elsewhere.³ Note that \mathcal{F} is only quadratic in P , because of the constraints of unitarity. We comment briefly on the normalisations and offsets we have given them. \mathcal{F} and \mathcal{A} , being anti-symmetric, need no offset, as they are already centred on zero, which they reach for threefold maximal mixing¹¹ (uniquely defined by all 9 elements of the mixing matrix having magnitude $\frac{1}{\sqrt{3}}$). \mathcal{G} and \mathcal{C} are defined with offsets such that they likewise vanish for threefold maximal mixing. All four variables are normalised so that their maximum value is unity, which they attain for no mixing. In Ref.³, we also give the $\bar{\mathbf{1}} \times \mathbf{1}$ and the $\mathbf{1} \times \bar{\mathbf{1}}$ FSMOs at 3rd order (called \mathcal{B} and \mathcal{D} respectively), but they will not concern us here.

The four FSMOs introduced in Eq. 4 are the simplest ones⁹ in terms of P and are sufficient to completely specify the mixing, up to a number of discrete ambiguities associated with the built-in flavour symmetry. J is of course not independent, and is given by $18J^2 = 1/6 - \mathcal{G} + (4/3)\mathcal{C} - (1/2)\mathcal{F}^2$. In Table 1, we summarise their properties and values (estimated at 90% CL from compilations of current experimental results) for both quarks¹² and leptons.¹³

Table 1: Properties and values of flavour-symmetric mixing observables for quarks and leptons. The experimentally allowed ranges are estimated (90% CL) from compilations of current experimental results, neglecting any correlations between the input quantities.

Observable Name	Order in P	Symmetry: $S3_{\downarrow} \times S3_{\uparrow}$	Theoretical Range	Experimental Range for Leptons	Experimental Range for Quarks
\mathcal{F}	2	$\bar{\mathbf{1}} \times \bar{\mathbf{1}}$	$(-1, 1)$	$(-0.14, 0.12)$	$(0.893, 0.896)$
\mathcal{G}	2	$\mathbf{1} \times \mathbf{1}$	$(0, 1)$	$(0.15, 0.23)$	$(0.898, 0.901)$
\mathcal{A}	3	$\bar{\mathbf{1}} \times \bar{\mathbf{1}}$	$(-1, 1)$	$(-0.065, 0.052)$	$(0.848, 0.852)$
\mathcal{C}	3	$\mathbf{1} \times \mathbf{1}$	$(-\frac{1}{27}, 1)$	$(-0.005, 0.057)$	$(0.848, 0.852)$

5 Flavour-Symmetric Mixing Observables in Terms of Mass Matrices

Equation (2) gives J , our prototype FSMO, in terms of the fermion mass matrices, which in turn are proportional to the matrices of Yukawa couplings which appear in the Standard Model Lagrangian. In this section, we show how to write the FSMOs of Section 4 above also in terms of the mass matrices. It is useful to define a reduced P matrix:

$$\tilde{P} = P - D \quad (5)$$

where D is the 3×3 democratic matrix with all 9 elements equal to $\frac{1}{3}$. We also define the reduced (ie. traceless) powers of the fermion mass matrices: $\widetilde{L}^m := L^m - \frac{1}{3}\text{Tr}(L^m)$ (similarly for \widetilde{N}^m), in terms of which, we can define the 2×2 matrix of weak basis-invariants:

$$\tilde{T}_{mn} := \text{Tr}(\widetilde{L}^m \widetilde{N}^n), \quad m, n = 1, 2. \quad (6)$$

For known lepton masses, \tilde{T} is completely equivalent to P . In fact, it is straightforward to show that \tilde{P} is a mass-moment transform of \tilde{T} :

$$\tilde{P} = \widetilde{M}_\ell^T \cdot \tilde{T} \cdot \widetilde{M}_\nu \quad (7)$$

where

$$\widetilde{M}_\ell = \frac{1}{L_\Delta} \begin{pmatrix} m_\mu^2 - m_\tau^2 & m_\tau^2 - m_e^2 & m_e^2 - m_\mu^2 \\ m_\mu - m_\tau & m_\tau - m_e & m_e - m_\mu \end{pmatrix}, \quad (8)$$

⁹They also treat the two weak-isospin sectors symmetrically, though this is not an essential feature.

with an analogous definition for \widetilde{M}_ν (the inverse transform is easily obtained).

Starting from Eq. (4) and substituting for P from Eqs. (5) and (7), we find that:

$$\mathcal{F} \equiv \text{Det } P = 3 \frac{\text{Det } \widetilde{T}}{L_\Delta N_\Delta}; \quad \left[\text{cf. Eq. (2)} : J = -i \frac{\text{Det}[L, N]}{2L_\Delta N_\Delta} \right] \quad (9)$$

$$\mathcal{G} = \frac{\widetilde{T}_{mn} \widetilde{T}_{pq} \mathcal{L}^{mp} \mathcal{N}^{nq}}{(L_\Delta N_\Delta)^2}; \quad \mathcal{C}, \mathcal{A} = \frac{\widetilde{T}_{mn} \widetilde{T}_{pq} \widetilde{T}_{rs} \mathcal{L}_{\mathcal{C}, \mathcal{A}}^{(mpr)} \mathcal{N}_{\mathcal{C}, \mathcal{A}}^{(nqs)}}{(L_\Delta N_\Delta)^{n_{\mathcal{C}, \mathcal{A}}}}, \quad (10)$$

where the \mathcal{L} (\mathcal{N}) are simple functions of traces of \widetilde{L}^m (\widetilde{N}^m), given in Ref.³, and $n_{\mathcal{C}}$ ($n_{\mathcal{A}}$) = 2(3).

6 Application 1: Flavour-Symmetric Descriptions of Leptonic Mixing

The tribimaximal mixing² ansatz for the MNS lepton mixing matrix:

$$U \simeq \begin{pmatrix} -2/\sqrt{6} & 1/\sqrt{3} & 0 \\ 1/\sqrt{6} & 1/\sqrt{3} & 1/\sqrt{2} \\ 1/\sqrt{6} & 1/\sqrt{3} & -1/\sqrt{2} \end{pmatrix} \quad (11)$$

is compatible with all confirmed leptonic mixing measurements from neutrino oscillation experiments, and may be considered a useful leading-order approximation to the data. It is defined by three phenomenological symmetries:⁶ CP symmetry, μ - τ -reflection symmetry and Democracy, which may each be expressed (flavour-symmetrically) in terms of our FSMOs. For example, as is well known, the zero in the U_{e3} position, if exact, ensures that no CP violation can arise from the mixing matrix. CP symmetry is thus represented simply by $J = 0$ (which is a necessary, but not sufficient condition for a single zero in the mixing matrix, see Section 7 below). μ - τ -reflection symmetry⁷ means that corresponding elements in the μ and τ rows have equal moduli: $|U_{\mu i}| = |U_{\tau i}|$, $\forall i$, and this implies the two flavour-symmetric constraints:

$$\mathcal{F} = \mathcal{A} = 0 \quad (12)$$

(flavour symmetry means that although these two constraints imply just such a set of equalities, they do not define *which* pair of rows or columns are constrained). Democracy^{8,9} ensures that one row or column is trimaximally mixed, ie. has the form $\frac{1}{\sqrt{3}}(1, 1, 1)^{(T)}$, as is the case for the ν_2 column in tribimaximal mixing. Democracy is ensured flavour-symmetrically by the two constraints:

$$\mathcal{F} = \mathcal{C} = 0. \quad (13)$$

Taking all three symmetries, tribimaximal mixing (or one of its trivial permutations) is ensured by the complete set of constraints $\mathcal{F} = \mathcal{C} = \mathcal{A} = J = 0$, which may be written as the single flavour-symmetric condition:

$$\mathcal{F}^2 + \mathcal{C}^2 + \mathcal{A}^2 + J^2 = 0. \quad (14)$$

Tribimaximal mixing is manifestly not flavour symmetric. The flavour-symmetry of our constraint, Eq. (14), is spontaneously broken by its tribimaximal solutions. The symmetry is manifested by the existence of a complete set of solutions of the generalised tribimaximal form, each related to the other by a member of the flavour permutation group.

Of course, generalisations of the tribimaximal form⁶ possessing subsets of its three symmetries may be similarly defined, and their corresponding flavour-symmetric constraints may be obtained by analogy to the above. These, and those of other special mixing forms^{14,15} are tabulated in Ref.³.

7 Application 2: A Partially Unified, Flavour-Symmetric Description of Quark and Lepton Mixings

A unified understanding of quark and lepton mixings is highly desirable. This is difficult because their mixing matrices have starkly different forms: the quark mixing matrix is characterised by small mixing angles,¹² while the lepton mixing matrix is characterised mostly by large ones.¹³ Many authors have ascribed this difference to the effect of the heavy majorana mass matrix in the leptonic case, via the see-saw mechanism.¹⁷ Notwithstanding the attractiveness of this explanation, it is clearly still worthwhile to ask if there are any features of the respective mixings which the quark and lepton sectors have in common.

Neutrino oscillation data¹³ require that $|U_{e3}|^2 \lesssim 0.05$, significantly less than the other MNS matrix elements-squared. At least one *small* mixing element is hence a common feature of both quark and lepton mixing matrices. We are thus led first to ask the question: “what is the flavour-symmetric condition for at least one zero element in the mixing matrix?” We should perhaps anticipate two constraints, as the condition implies that both real and imaginary parts vanish. A zero mixing element implies CP conservation, so that $J = 0$. A clue to the second constraint is that with μ - τ -reflection symmetry, $J = 0$ ensures a zero somewhere in the ν_e row of the MNS matrix. However, μ - τ -reflection symmetry implies two more constraints, Eq. (12).

In order to find a single additional constraint we consider the K matrix^{16 10} with elements:

$$K_{\gamma k} = \text{Re}(U_{\alpha i} U_{\alpha j}^* U_{\beta i}^* U_{\beta j}), \quad (15)$$

which is the CP -conserving analogue of J (cf. the definition of J , Eq. (1)). K should be familiar: in the leptonic case, its elements are often used to write the magnitudes of the oscillatory terms in neutrino appearance probabilities;¹⁰ in the quark case, its elements are just the CKM factors of the CP -conserving parts of the interference terms in penguin-dominated decay rates. A single zero in the mixing matrix leads to four zeroes in a plaquette of K and this clearly implies:

$$\text{Det } K = 0, \quad (16)$$

which is our sufficient second condition, along with $J = 0$.^h We note that Eq. (16) can easily be cast in terms of our complete set of FSMOs, since $54 \text{Det } K \equiv 2\mathcal{A} + \mathcal{F}(\mathcal{F}^2 - 2\mathcal{C} - 1)$. Hence, μ - τ -reflection symmetry, Eq. (12), is a special case of Eq. (16).

Experimentally, there is no exactly zero element in the CKM matrix, so that $\text{Det } K = 0$ and $J = 0$ cannot *both* be exact for quarks. Moreover, for leptons, despite there being no experimental lower limit for $|U_{e3}|$, there is no reason to suppose that the MNS matrix has an exact zero either. In order to ensure a small, but non-zero element in the mixing matrices, we need to consider a modest relaxation of either condition, or of both. For quarks, we know from experiment that CP is slightly violated, with¹² $|J_q/J_{max}| \simeq 3 \times 10^{-4}$, whileⁱ for leptons, fits to oscillation data¹³ imply a fairly loose upper bound on their CP violation: $|J_\ell/J_{max}| \lesssim 0.33$. Turning to $\text{Det } K$, we find that for quarks, $|\text{Det } K_q/(\text{Det } K)_{max}| \lesssim 3 \times 10^{-7}$, while for leptons, $|\text{Det } K_\ell/(\text{Det } K)_{max}| \lesssim 0.6$ (the precision of lepton mixing data does not yet allow a strong constraint). However, there is no experimental lower limit for $|\text{Det } K|$ for quarks or for leptons, each being compatible with zero, so that it is sufficient to relax only the condition on J .

We are thus led to conjecture that for both quarks and leptons:

$$\text{Det } K = 0; \quad |J/J_{max}| = \text{small} \quad (17)$$

(it is not implied that the small quantity necessarily has the same value in both sectors). Equation (17) is a unified and flavour-symmetric, partial description of both lepton and quark mixing

^hThe two conditions may even be expressed as one, noting that the product of all nine elements of P is given by $\frac{1}{144} \prod_{\alpha i} P_{\alpha i} = (\text{Det } K)^2 + J^2(2J^2 + \mathcal{R})^2$, which is zero iff $\text{Det } K = 0$ and $J = 0$ (as $\mathcal{R} > 0$, as long as $J \neq 0$).

ⁱWe note that $J_{max} = \frac{1}{6\sqrt{3}} \simeq 0.1$ and $(\text{Det } K)_{max} = \frac{2^6}{3^9} \simeq 0.0033$.

matrices, being associated with the existence of at least one small element in each mixing matrix, U_{e3} and V_{ub} respectively (it is partial in the sense that only two degrees of freedom are constrained for each matrix). However, in the case that J is not exactly zero, the condition $\text{Det } K = 0$ also implies that in the limit, as $J \rightarrow 0$, there is at least one unitarity triangle angle which $\rightarrow 90^\circ$. This is rather obvious in the μ - τ -symmetry case, but is less obvious more generally. While the flavour symmetry prevents an a priori prediction of *which* angle is $\simeq 90^\circ$, we know from experiment¹² that for quarks, $\alpha \simeq 90^\circ$. A detailed calculation shows that our conjecture, Eq. (17), predicts, in terms of Wolfenstein parameters:¹

$$(90^\circ - \alpha) = \bar{\eta}\lambda^2 = 1^\circ \pm 0.2^\circ \quad (18)$$

at leading order in small quantities, to be compared with its current experimental determination:¹²

$$(90^\circ - \alpha) = 0^{+3^\circ}_{-7^\circ}. \quad (19)$$

It will be interesting to test Eq. (18) more precisely in future experiments with B mesons, in particular, at LHCb and at a possible future Super Flavour Factory. For leptons, experiment tells us not only that it is the U_{e3} MNS matrix element which is small but also that only the unitarity triangle angles^j $\phi_{\mu 1}$ or $\phi_{\tau 1}$ can be close to 90° . Then Eq. (17) implies that:

$$|90^\circ - \delta| = 2\sqrt{2} \sin \theta_{13} \sin \left(\theta_{23} - \frac{\pi}{4}\right) \lesssim 4^\circ \quad (20)$$

at leading order in small quantities (we use the PDG convention here). It thus requires a large CP -violating phase in the MNS matrix, which is promising for the discovery of leptonic CP violation at eg. a future Neutrino Factory.

8 Discussion and Conclusions

Given that our flavour-symmetric variables are defined (essentially) uniquely by their flavour symmetry properties and by their order in P , it is remarkable that the leptonic data may be described simply by the constraints $\mathcal{F} = \mathcal{A} = \mathcal{C} = J = 0$. This is suggestive that these variables may be fundamental in some way. It is furthermore tantalising that the smallness of one element in each mixing matrix, the approximate μ - τ -symmetry in lepton mixing and the existence of a right unitarity triangle may all be related to each other, through our simple partially-unified constraint, Eq. (17). The precision of the resulting prediction, Eq. (18), motivates more sensitive tests at future B physics facilities, while the synergy with tests at a neutrino factory is manifest.

All elements of the Standard Model, apart from the Yukawa couplings of the fermions to the Higgs, treat each fermion of any given charge on an equal footing - they are already flavour-symmetric. The Yukawa couplings, on the other hand, depend on flavour in such a way that each flavour has unique mass and mixing matrix elements. Using our flavour-symmetric observables, or combinations of them appropriately chosen, we have shown how it is also possible to specify the flavour-dependent mixings in a flavour-independent way.^k This recovers flavour symmetry at the level of the mixing description, the symmetry being broken only spontaneously by its solutions, which define and differentiate the flavours in terms of their mixings.

Acknowledgments

PFH thanks the organisers of the 43rd Rencontres de Moriond for organising a very stimulating conference. PFH also acknowledges the hospitality of the Centre for Fundamental Physics (CfFP) at the STFC Rutherford Appleton Laboratory. This work was supported by the UK Science and Technology Facilities Council (STFC).

^jWe use the nomenclature of unitarity triangle angles we defined in reference [46] of Ref.⁹.

^kWe illustrated another variant of this in Ref.¹⁸.

References

1. L. Wolfenstein, Phys. Rev. Lett. 51 (1983) 1945.
2. P. F. Harrison, D. H. Perkins, and W. G. Scott, Phys. Lett. B530 (2002) 167, hep-ph/0202074; Phys. Lett. B458 (1999) 79, hep-ph/9904297; Z. Xing Phys. Lett. B533 (2002) 85, hep-ph/0204049; X. He and A. Zee, Phys. Lett. B560 (2003) 87, hep-ph/0301092; E. Ma, Phys. Rev. Lett. 90 (2003) 221802, hep-ph/0303126; Phys. Lett. B583 (2004) 157, hep-ph/0308282; Phys. Rev. D70 (2004) 031901, hep-ph/0404199; C. I. Low and R. R. Volkas, Phys. Rev. D68 (2003) 033007, hep-ph/0305243; G. Altarelli and F. Feruglio, Nucl. Phys. B 720 (2005) 64, hep-ph/0504165.
3. P.F. Harrison, D.R.J. Roythorne and W.G. Scott, Phys. Lett. B657 (2007) 210, arXiv:0709.1439.
4. C. Jarlskog, Phys. Rev. Lett. 55 (1985) 1039; Z. Phys. C29 (1985) 491; Phys. Rev. D35 (1987) 1685; Phys. Rev. Lett. 57 (1986) 2875; Phys. Rev. D36 (1987) 2128; Phys. Rev. D39 (1989) 988; Phys. Lett. B609 (2005) 323, hep-ph/0412288; Phys. Scripta, T127 (2006) 64, hep-ph/0606050; C. Jarlskog and A. Kleppe, Nucl. Phys. B286 (1987) 245.
5. J. D. Bjorken and I. Duniety, Phys. Rev. D36 (1987) 2109.
6. P. F. Harrison and W. G. Scott, Phys. Lett. B535 (2002) 163, hep-ph/0203209.
7. C. S. Lam, Phys. Lett. B507 (2001) 214, hep-ph/0104116; M. Kitabayashi and M. Yasue, Phys. Lett. B524 (2002) 308, hep-ph/0110303; P. F. Harrison and W. G. Scott, Phys. Lett. B547 (2002) 219, hep-ph/0210197; J. F. Beacom et al. Phys. Rev. D69 (2004) 017303, hep-ph/0309267; W. Grimus and L. Lavoura, Phys. Lett. B579 (2004) 113, hep-ph/0305309.
8. P. F. Harrison and W. G. Scott, Phys. Lett. B557 (2003) 76, hep-ph/0302025; Proc. NOVE-II, Venice (2003) hep-ph/0402006; Phys. Lett. B594 (2004) 324, hep-ph/0403278; R. Friedberg and T. D. Lee, HEP & NP 30 (2006) 591, hep-ph/0606071; arXiv:0705.4156; C. S. Lam, Phys. Lett. B640 (2006) 260, hep-ph/0606220; Phys. Rev. D74 (2006), 113004, hep-ph/0611017.
9. J. D. Bjorken, P. F. Harrison and W. G. Scott, Phys. Rev. D74 (2006) 073012, hep-ph/0511201;
10. P. F. Harrison, W. G. Scott and T. J. Weiler, Phys. Lett. B641 (2006) 372, hep-ph/0607335.
11. P. F. Harrison and W. G. Scott, Phys. Lett. B349 (1995) 137, hep-ph/9503190.
12. CKMfitter Group (J. Charles et al.), Eur. Phys. J. C41 (2005) 1, hep-ph/0406184, updated results and plots: <http://ckmfitter.in2p3.fr>; M. Bona et al. (UTfit Collaboration), hep-ph/0701204.
13. A. Strumia and F. Vissani, (2007), hep-ph/0606054.
14. G. Altarelli and F. Feruglio, J. HEP 9811 (1998) 021, hep-ph/9809596.
15. V.D. Barger, S. Pakvasa, T.J. Weiler and K. Whisnant, Phys. Lett. B437 (1998) 107, hep-ph/9806387.
16. P.F. Harrison and W.G. Scott, Phys. Lett. B535 (2002) 229, hep-ph/0203021; P.F. Harrison, W.G. Scott and T.J. Weiler, Phys. Lett. B565 (2003) 159, hep-ph/0305175.
17. P. Minkowski Phys. Lett. B67 (1977) 421.
18. P. F. Harrison and W. G. Scott, Phys. Lett. B628 (2005) 93, hep-ph/0508012.

Lepton flavour violation in constrained MSSM-seesaw models

E. Arganda, M.J. Herrero

Departamento de Física Teórica C-XI and Instituto de Física Teórica C-XVI, Universidad Autónoma de Madrid, Cantoblanco, E-28049 Madrid, Spain

We calculate the predictions for lepton flavour violating (LFV) tau and muon decays, $l_j \rightarrow l_i \gamma$, $l_j \rightarrow 3l_i$, $\mu - e$ conversion in nuclei and LFV semileptonic tau decays $\tau \rightarrow \mu PP$ with $PP = \pi^+ \pi^-, \pi^0 \pi^0, K^+ K^-, K^0 \bar{K}^0$ $\tau \rightarrow \mu P$ with $P = \pi^0, \eta, \eta'$ and $\tau \rightarrow \mu V$ with $V = \rho^0, \phi$, performing the hadronisation of quark bilinears within the chiral framework. We work within a SUSY-seesaw context where the particle content of the Minimal Supersymmetric Standard Model is extended by three right-handed neutrinos plus their corresponding SUSY partners, and where a seesaw mechanism for neutrino mass generation is implemented. Two different scenarios with either universal or non-universal soft supersymmetry breaking Higgs masses at the gauge coupling unification scale are considered. After comparing the predictions with present experimental bounds and future sensitivities, the most promising processes are particularly emphasised.

1 LFV within SUSY-seesaw models

The current knowledge of neutrino mass differences and mixing angles clearly indicates that lepton flavour number is not a conserved quantum number in Nature. However, the lepton flavour violation (LFV) has so far been observed only in the neutrino sector. One challenging task for the present and future experiments will then be to test if there is or there is not LFV in the charged lepton sector as well.

Here we focus in the Minimal Supersymmetric Standard Model (MSSM) enlarged by three right-handed neutrinos and their SUSY partners where potentially observable LFV effects in the charge lepton sector are expected to occur. We further assume a seesaw mechanism for neutrino mass generation and use, in particular, the parameterisation proposed in ¹ where the solution to the seesaw equation is written as $m_D = Y_\nu v_2 = \sqrt{m_N^{\text{diag}}} R \sqrt{m_\nu^{\text{diag}}} U_{\text{MNS}}^\dagger$. Here, R is defined by θ_i ($i = 1, 2, 3$); $v_{1(2)} = v \cos(\sin)\beta$, $v = 174$ GeV; $m_\nu^{\text{diag}} = \text{diag}(m_{\nu_1}, m_{\nu_2}, m_{\nu_3})$ denotes the three light neutrino masses, and $m_N^{\text{diag}} = \text{diag}(m_{N_1}, m_{N_2}, m_{N_3})$ the three heavy ones. U_{MNS} is given by the three (light) neutrino mixing angles θ_{12}, θ_{23} and θ_{13} , and three phases, δ, ϕ_1 and ϕ_2 . With this parameterisation is easy to accommodate the neutrino data, while leaving room for extra neutrino mixings (from the right-handed sector). It further allows for large Yukawa couplings $Y_\nu \sim \mathcal{O}(1)$ by choosing large entries in m_N^{diag} and/or θ_i .

The predictions in the following are for two different constrained MSSM-seesaw scenarios, with universal and non-universal Higgs soft masses and with respective parameters (in addition to the previous neutrino sector parameters): 1) CMSSM-seesaw: $M_0, M_{1/2}, A_0 \tan \beta$, and $\text{sign}(\mu)$, and 2) NUHM-seesaw: $M_0, M_{1/2}, A_0 \tan \beta, \text{sign}(\mu), M_{H_1} = M_0(1 + \delta_1)^{1/2}$ and $M_{H_2} = M_0(1 + \delta_2)^{1/2}$. All the predictions presented here include the full set of SUSY one-loop contributing diagrams, mediated by γ, Z , and Higgs bosons, as well as boxes, and do not use the Leading Logarithmic (LLog) nor the mass insertion approximations. The hadronisation of quark bilinears is performed within the chiral framework. This is a very short summary of several publications ^{2,3,4,5} to which we refer the reader for more details.

2 Results and Discussion

We focus on the dependence on the most relevant parameters which, for the case of hierarchical (degenerate) heavy neutrinos, are: the neutrino mass m_{N_3} (m_N), $\tan \beta$, θ_1 and θ_2 . We also

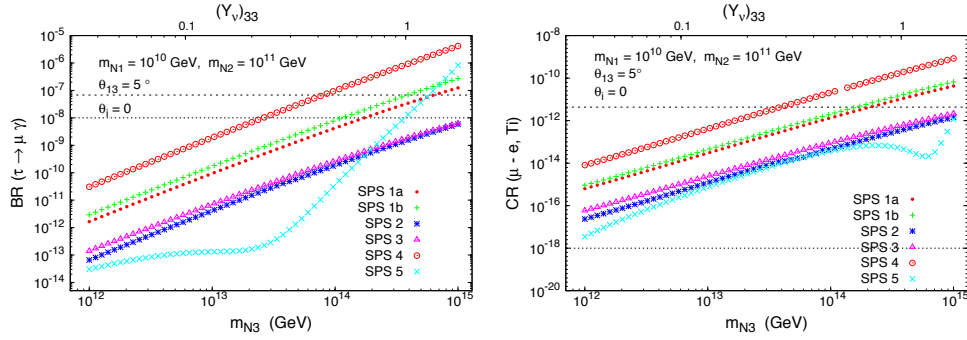


Figure 1: $\tau \rightarrow \mu\gamma$ and $\text{CR}(\mu - e, \text{Ti})$ as a function of m_{N_3} . The predictions for SPS 1a (dots), 1b (crosses), 2 (asterisks), 3 (triangles), 4 (circles) and 5 (times) are included. On the upper horizontal axis we display the associated value of $(Y_\nu)_{33}$. In each case, we set $\theta_{13} = 5^\circ$, and $\theta_i = 0$. The upper (lower) horizontal line denotes the present experimental bound (future sensitivity).

study the sensitivity of the BRs to θ_{13} . The other input seesaw parameters m_{N_1} , m_{N_2} and θ_3 , play a secondary role since the BRs do not strongly depend on them. The light neutrino parameters are fixed to: $m_{\nu_2}^2 = \Delta m_{\text{sol}}^2 + m_{\nu_1}^2$, $m_{\nu_3}^2 = \Delta m_{\text{atm}}^2 + m_{\nu_1}^2$, $\Delta m_{\text{sol}}^2 = 8 \times 10^{-5} \text{ eV}^2$, $\Delta m_{\text{atm}}^2 = 2.5 \times 10^{-3} \text{ eV}^2$, $m_{\nu_1} = 10^{-3} \text{ eV}$, $\theta_{12} = 30^\circ$, $\theta_{23} = 45^\circ$, $\theta_{13} \lesssim 10^\circ$ and $\delta = \phi_1 = \phi_2 = 0$.

The results for the CMSSM-seesaw scenario are collected in Figs. 1 through 5. In Fig. 1, we display the predictions of $\text{BR}(\tau \rightarrow \mu\gamma)$ and $\text{CR}(\mu - e, \text{Ti})$ as a function of the heaviest neutrino mass m_{N_3} for the various SPS points, and for the particular choice $\theta_i = 0$ ($i = 1, 2, 3$) and $\theta_{13} = 5^\circ$. We have also considered the case of degenerate heavy neutrino spectra (not shown here). In both scenarios for degenerate and hierarchical heavy neutrinos, we find a strong dependence on the the heavy neutrino masses, with the expected behaviour $|m_N \log m_N|^2$ of the LLog approximation, except for SPS 5 point, which fails by a factor of $\sim 10^4$. The rates for the various SPS points exhibit the following hierarchy, $\text{BR}_4 > \text{BR}_{1b} \gtrsim \text{BR}_{1a} > \text{BR}_3 \gtrsim \text{BR}_2 > \text{BR}_5$. This behaviour can be understood in terms of the growth of the BRs with $\tan \beta$, and from the different mass spectra associated with each point. Most of the studied processes reach their experimental limit at $m_{N_3} \in [10^{13}, 10^{15}]$ which corresponds to $Y_\nu^{33,32} \sim 0.1 - 1$. At present, the most restrictive one is $\mu \rightarrow e\gamma$ (which sets bounds for SPS 1a of $m_{N_3} < 10^{13} - 10^{14} \text{ GeV}$), although $\mu - e$ conversion will be the best one in future, with a sensitivity to $m_{N_3} > 10^{12} \text{ GeV}$.

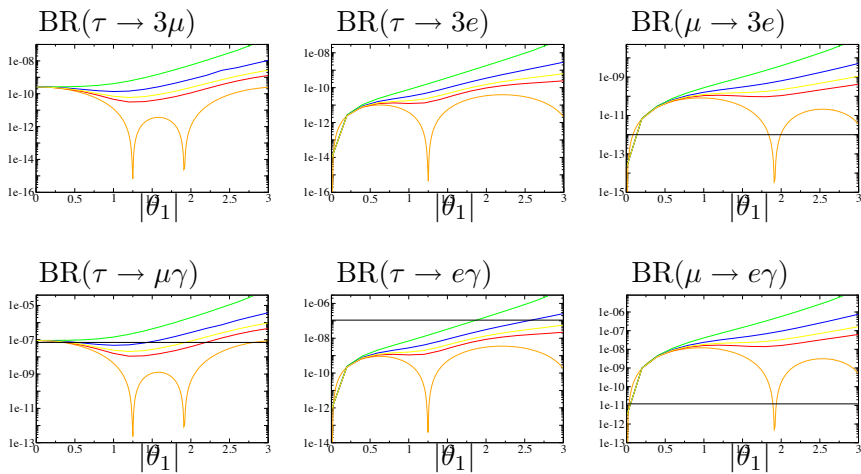


Figure 2: Dependence of LFV τ and μ decays with $|\theta_1|$ for SPS 4 case with $\arg(\theta_1) = 0, \pi/10, \pi/8, \pi/6, \pi/4$ in radians (lower to upper lines), $(m_{N_1}, m_{N_2}, m_{N_3}) = (10^8, 2 \times 10^8, 10^{14}) \text{ GeV}$, $\theta_2 = \theta_3 = 0$, $\theta_{13} = 0$ and $m_{\nu_1} = 0$. The horizontal lines are the present experimental bounds.

Fig. 2 shows the behaviour of the six considered LFV τ and μ decays, for SPS 4 point, as a function of $|\theta_1|$, for various values of $\arg\theta_1$. We see clearly that the BRs for $0 < |\theta_1| < \pi$ and $0 < \arg\theta_1 < \pi/2$ can increase up to a factor $10^2 - 10^4$ with respect to $\theta_i = 0$. Similar results have been found for θ_2 , while BRs are nearly constant with θ_3 in the case of hierarchical neutrinos. The behaviour of $\text{CR}(\mu - e, \text{Ti})$ with θ_i is very similar to that of $\text{BR}(\mu \rightarrow e\gamma)$ and $\text{BR}(\mu \rightarrow 3e)$. For instance, Fig. 3 shows the dependence of $\text{CR}(\mu - e, \text{Ti})$ with θ_2 , and illustrates that for large θ_2 , rates up to a factor $\sim 10^4$ larger than in the $\theta_i = 0$ case can be obtained.

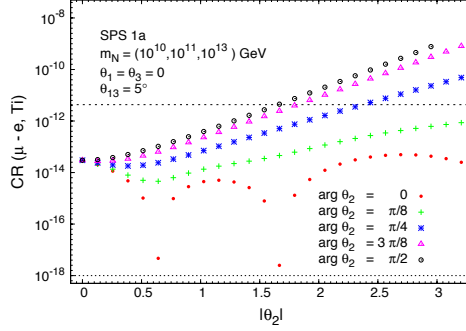


Figure 3: $\text{CR}(\mu - e, \text{Ti})$ as a function of $|\theta_2|$, for SPS 1a case with $\arg\theta_2 = \{0, \pi/8, \pi/4, 3\pi/8, \pi/2\}$ (dots, crosses, asterisks, triangles and circles, respectively), $m_{N_i} = (10^{10}, 10^{11}, 10^{13})$ GeV, $\theta_{13} = 5^\circ$. The upper (lower) horizontal line denotes the present experimental bound (future sensitivity).

In Fig. 4 we show the dependence of $\mu \rightarrow e\gamma$, $\mu \rightarrow 3e$ and $\mu - e$ conversion on the light neutrino mixing angle θ_{13} . These figures clearly manifest the very strong sensitivity of their rates to the θ_{13} mixing angle for hierarchical heavy neutrinos. Indeed, varying θ_{13} from 0 to 10° leads to an increase in the rates by as much as five orders of magnitude.

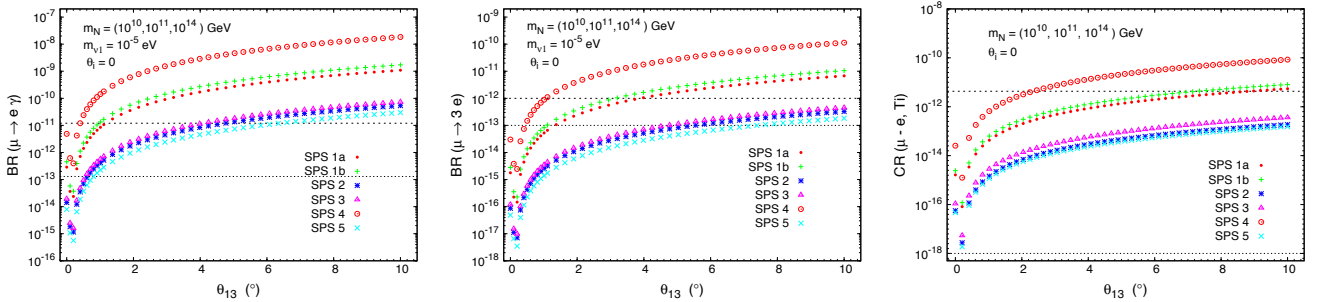


Figure 4: $\text{BR}(\mu \rightarrow e\gamma)$, $\text{BR}(\mu \rightarrow 3e)$ and $\text{CR}(\mu - e, \text{Ti})$ as a function of θ_{13} (in degrees), for SPS 1a (dots), 1b (crosses), 2 (asterisks), 3 (triangles), 4 (circles) and 5 (times), with $\theta_i = 0$ and $m_{N_i} = (10^{10}, 10^{11}, 10^{14})$ GeV. The upper (lower) horizontal line denotes the present experimental bound (future sensitivity).

On the other hand, since $\mu \rightarrow e\gamma$ is very sensitive to θ_{13} , but $\text{BR}(\tau \rightarrow \mu\gamma)$ is clearly not, and since both BRs display the same approximate behaviour with m_{N_3} and $\tan\beta$, one can study the impact that a potential future measurement of θ_{13} and these two rates can have on the knowledge of the otherwise unreachable heavy neutrino parameters. The correlation of these two observables as a function of m_{N_3} , is shown in Fig. 5 for SPS 1a. Comparing these predictions for the shaded areas along the expected diagonal “corridor”, with the allowed experimental region, allows to conclude about the impact of a θ_{13} measurement on the allowed/excluded m_{N_3} values. The most important conclusion from Fig. 5 is that for SPS 1a, and for the parameter space defined in the caption, an hypothetical θ_{13} measurement larger than 1° , together with the present experimental bound on the $\text{BR}(\mu \rightarrow e\gamma)$, will have the impact of excluding values

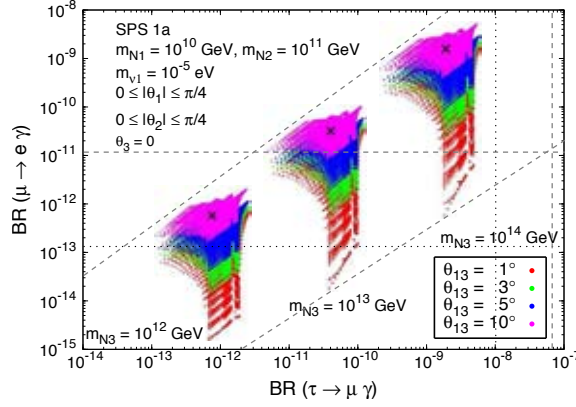


Figure 5: Correlation between $\text{BR}(\mu \rightarrow e \gamma)$ and $\text{BR}(\tau \rightarrow \mu \gamma)$ as a function of m_{N_3} , for SPS 1a, and impact of θ_{13} . The areas displayed represent the scan over θ_i . From bottom to top, the coloured regions correspond to $\theta_{13} = 1^\circ, 3^\circ, 5^\circ$ and 10° (red, green, blue and pink, respectively). Horizontal and vertical dashed (dotted) lines denote the experimental bounds (future sensitivities).

of $m_{N_3} \gtrsim 10^{14}$ GeV. Moreover, with the planned MEG sensitivity, the same θ_{13} measurement could further exclude $m_{N_3} \gtrsim 3 \times 10^{12}$ GeV.

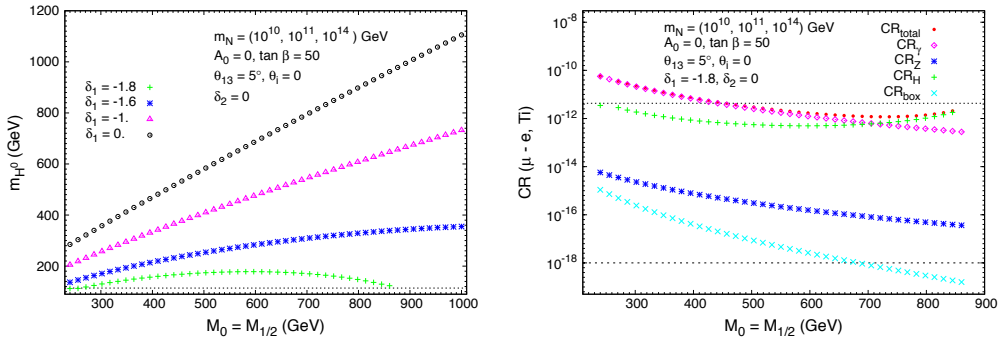


Figure 6: Left panel: Mass of m_{H^0} as a function of $M_0 = M_{1/2}$, for fixed values of $\delta_1 = \{-1.8, -1.6, -1, 0\}$ (respectively crosses, asterisks, triangles and circles), with $m_{N_i} = (10^{10}, 10^{11}, 10^{14})$ GeV, $\theta_i = 0$, $A_0 = 0$, $\tan \beta = 50$ and $\theta_{13} = 5^\circ$. Right panel: Contributions to $\text{CR}(\mu - e, \text{Ti})$: total (dots), γ -penguins (diamonds), Z -penguins (asterisks), H -penguins (crosses) and box diagrams (times) as a function of $M_0 (= M_{1/2})$ for the NUHM case with $\delta_1 = -1.8$, $\delta_2 = 0$, $\tan \beta = 50$, $m_{N_i} = (10^{10}, 10^{11}, 10^{14})$ GeV, $\theta_{13} = 5^\circ$ and $R = 1$ ($\theta_i = 0$). The upper (lower) horizontal line denotes the present experimental bound (future sensitivity).

The numerical results for the NUHM-seesaw scenario as a function of $M_0 = M_{1/2} = M_{\text{SUSY}}$ are collected in Figs. 6 and 7. The behaviour of the predicted m_{H^0} as a function of M_{SUSY} is shown in Fig. 6 (left panel). The most interesting solutions with important phenomenological implications are found for negative δ_1 and positive δ_2 . Notice that, for all the explored $\delta_{1,2}$ values, we find a value of m_{H^0} that is significantly smaller than in the universal case ($\delta_{1,2} = 0$).

In Fig. 6 (right panel) the various contributions from the γ -, Z -, Higgs mediated penguins and box diagrams as a function of M_{SUSY} are shown. Here, we choose $\delta_1 = -1.8$ and $\delta_2 = 0$. We observe a very distinct behaviour with M_{SUSY} of the Higgs-mediated contributions compared to those of the CMSSM case. In fact, the Higgs-mediated contribution can equal, or even exceed that of the photon, dominating the total conversion rate in the large $M_0 = M_{1/2}$ region. These larger Higgs contributions are the consequence of their exclusive SUSY non-decoupling behaviour for large M_{SUSY} , and of the lighter Higgs boson mass values encountered in this region, as previously illustrated in Fig. 6.

In Fig. 7 we display the predicted $\mu - e$ conversion rates for other nuclei, concretely Al, Ti,

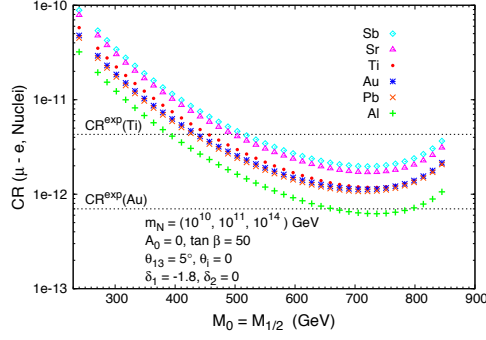


Figure 7: $\mu - e$ conversion rates as a function of $M_0 = M_{1/2}$ in the NUHM-seesaw for various nuclei: Sb, Sr, Ti, Au, Pb and Al nuclei (diamonds, triangles, dots, asterisks, times and crosses, respectively), with $m_{N_i} = (10^{10}, 10^{11}, 10^{14})$ GeV, $A_0 = 0$, $\tan \beta = 50$, $\theta_{13} = 5^\circ$, $\theta_i = 0$, $\delta_1 = -1.8$ and $\delta_2 = 0$. From top to bottom, the horizontal dashed lines denote the present experimental bounds for $\text{CR}(\mu - e, \text{Ti})$ and $\text{CR}(\mu - e, \text{Au})$.

Sr, Sb, Au and Pb, as a function of M_{SUSY} . We clearly see that $\text{CR}(\mu - e, \text{Sb}) > \text{CR}(\mu - e, \text{Sr}) > \text{CR}(\mu - e, \text{Ti}) > \text{CR}(\mu - e, \text{Au}) > \text{CR}(\mu - e, \text{Pb}) > \text{CR}(\mu - e, \text{Al})$. The most important conclusion from Fig. 7 is that we have found predictions for Gold nuclei which, for the input parameters in this plot, are above its present experimental bound throughout the explored M_{SUSY} interval. Finally, although not shown here for shortness, we have also found an interesting loss of correlation between the predicted $\text{CR}(\mu - e, \text{Ti})$ and $\text{BR}(\mu \rightarrow e\gamma)$ in the NUHM-seesaw scenario compared to the universal case where these are known to be strongly correlated. This loss of correlation occurs when the Higgs-contributions dominate the photon-contributions and could be tested if the announced future sensitivities in these quantities are reached.

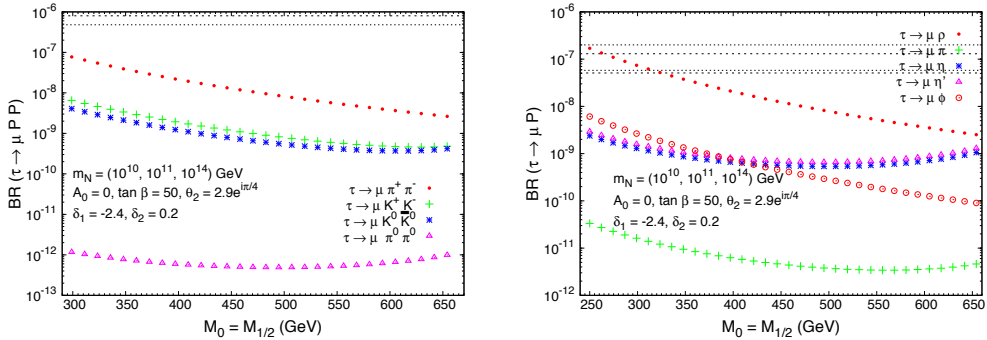


Figure 8: Predictions of $\text{BR}(\tau \rightarrow \mu PP)$ and $\text{BR}(\tau \rightarrow \mu P)$ as a function of M_{SUSY} in the NUHM scenario for a large $\tau - \mu$ mixing driven by $\theta_2 = 2.9e^{i\pi/4}$.

The corresponding predictions for $\theta_2 = 2.9e^{i\pi/4}$ of the nine LFV semileptonic τ decays studied in this work as a function of M_{SUSY} are shown in Fig. 8. In this case, we work with $\delta_1 = -2.4$ and $\delta_2 = 0.2$, that drive us to Higgs boson masses around 150 GeV even for heavy SUSY spectra. In this Fig. 8 we can see that, the choice of θ_2 increase all the rates about two orders of magnitude respect to the case $\theta_i = 0$, not shown here for brevity. $\text{BR}(\tau \rightarrow \mu\pi^+\pi^-)$ and $\text{BR}(\tau \rightarrow \mu\rho)$ the largest rates and, indeed, the predictions of these two latter channels reach their present experimental sensitivities at the low M_{SUSY} region, below 200 GeV and 250 GeV respectively, for this particular choice of input parameters.

In Fig. 9 we plot finally the predictions for $\text{BR}(\tau \rightarrow \mu K^+ K^-)$ and $\text{BR}(\tau \rightarrow \mu\eta)$ as a function of one the most relevant parameters for these Higgs-mediated processes which is the corresponding Higgs boson mass.

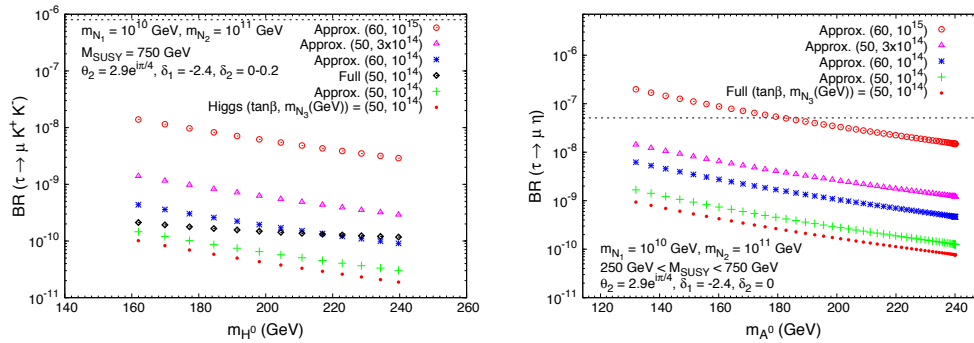


Figure 9: Predictions for $BR(\tau \rightarrow \mu K^+ K^-)$ and $BR(\tau \rightarrow \mu \eta)$ as a function of m_{H^0} in the NUHM scenario.

Firstly, we see that the approximate and exact results of the Higgs contribution agree within a factor of two for both channels, but the agreement of the full result with respect to the Higgs contribution is clearly worse in the case of $\tau \rightarrow \mu K^+ K^-$ than in $\tau \rightarrow \mu \eta$. In the latter, the agreement is quite good because the Z -mediated contribution is negligible, and this holds for all M_{SUSY} values in the studied interval, $250 \text{ GeV} < M_{\text{SUSY}} < 750 \text{ GeV}$. In the first, it is only for large M_{SUSY} that the H -mediated contribution competes with the γ -mediated one and the Higgs rates approach the total rates. For instance, the predictions for $BR(\tau \rightarrow \mu K^+ K^-)$ shows that for $M_{\text{SUSY}} = 750 \text{ GeV}$ and $m_{H^0} = 160 \text{ GeV}$ the total rate is about a factor 2 above the Higgs rate, but for $m_{H^0} = 240 \text{ GeV}$ it is already more than a factor 5 above.

In this figure we have also explored larger values of m_{N_3} and $\tan \beta$, by using in those cases the approximate formula, and in order to conclude about the values that predict rates comparable with the present experimental sensitivity. We can conclude then that, at present, it is certainly $\tau \rightarrow \mu \eta$ the most competitive LFV semileptonic tau decay channel. The parameter values that provide rates being comparable to the present sensitivities in this channel are $\tan \beta = 60$ and $m_{N_3} = 10^{15} \text{ GeV}$ which correspond to $|\delta_{32}| \simeq 2$.

Interestingly, the most competitive channels to explore simultaneously LFV $\tau - \mu$ transitions and the Higgs sector are $\tau \rightarrow \mu \eta$, $\tau \rightarrow \mu \eta'$ and also $\tau \rightarrow \mu K^+ K^-$. Otherwise, the golden channels to tackle the Higgs sector are undoubtedly $\tau \rightarrow \mu \eta$ and $\tau \rightarrow \mu \eta'$. On the other hand, the rest of the studied semileptonic channels, $\tau \rightarrow \mu \pi^+ \pi^-$, etc., will not provide additional information on LFV with respect to that provided by $\tau \rightarrow \mu \gamma$.

In conclusion, we believe that a joint measurement of the LFV branching ratios, the $\mu - e$ conversion rates, θ_{13} and the SUSY spectrum will be a powerful tool for shedding some light on the otherwise unreachable heavy neutrino parameters. Furthermore, in the case of a NUHM scenario, it may also provide interesting information on the Higgs sector. It is clear from this study that the connection between LFV and neutrino physics will play a relevant role for the searches of new physics beyond the SM.

We acknowledge Ana M. Teixeira, Stefan Antusch and Jorge Portolés for their participation in our works. E. Arganda thanks the organizers for his invitation to this fruitful conference.

1. J. A. Casas and A. Ibarra, Nucl. Phys. B 618 (2001) 171 [arXiv:hep-ph/0103065].
2. E. Arganda and M. J. Herrero, Phys. Rev. D **73** (2006) 055003 [arXiv:hep-ph/0510405].
3. S. Antusch, E. Arganda, M. J. Herrero and A. M. Teixeira, JHEP **0611** (2006) 090 [arXiv:hep-ph/0607263].
4. E. Arganda, M. J. Herrero and A. M. Teixeira, arXiv:0707.2955 [hep-ph]. To appear in JHEP (2007).
5. E. Arganda, M. J. Herrero and J. Portoles, JHEP **0806** (2008) 079 [arXiv:0803.2039 [hep-ph]].

Top physics

TOP PAIR PRODUCTION

M.Besançon
*CEA-Saclay, DSM/Irfu/SPP,
 bat. 141, 91191 Gif sur Yvette, France*

We review the most recent results on top quark pair production at the Tevatron including production mechanism, cross sections, forward-backward asymmetry measurements and searches for resonances decaying to top quarks which were available at the time of the 2008 electroweak session of the Rencontres de Moriond conference.

1 Introduction

Since its discovery by the CDF and D0 experiments¹ the Tevatron is the only place where the top quark (t) can be studied. The year 2008 will certainly be the last possible year for such a statement due to the advent of the LHC.

Doing top quark physics means covering a wide spectrum of different subjects including studies of the t (single and pair) production, decay and properties. The present mini-review focuses on top quark pair ($t\bar{t}$) production and the emphasis is put on recent results concerning the $t\bar{t}$ production mechanism, cross section measurements and top quark mass (m_t) measurements from cross sections measurements, forward backward measurement and finally searches of resonances decaying into t quarks. Recent results concerning m_t direct measurements as well as other properties (W helicity, t charge) and the single t production can be found in these proceedings². The Tevatron is performing well and the results reported here correspond to Tevatron integrated luminosities ranging from 1 to 2 fb⁻¹.

At the Tevatron, within the Standard Model (SM), $t\bar{t}$ production is expected to occur via strong interactions namely through $q\bar{q}$ annihilation (85%) and gluon gluon (gg) fusion (15%). Typical next-to-leading (NLO) predictions range from $\sigma(p\bar{p}) \rightarrow t\bar{t} \approx 6.7 \pm 0.4$ pb for $m_t = 175$ GeV to $\sigma(p\bar{p}) \rightarrow t\bar{t} \approx 7.8 \pm 0.5$ pb for $m_t = 170$ GeV^{3,4}. The t is expected to decay before it hadronizes. The t decays into a b quark and an on-shell W gauge boson ($t \rightarrow Wb$) with a branching ratio close to 1. The final states corresponding to $t\bar{t}$ production are classified

according to the decay of the W gauge boson from the t . The results reported here concentrate on the lepton+jets channels where one W gauge boson decays leptonically i.e. $W \rightarrow l\nu$ where $l = \mu$ or e (amounting to 30% of all the $t\bar{t}$ channels) and dilepton channels where both W decay leptonically (5%). Other channels include all hadronic channels where both W gauge bosons decay hadronically ($W \rightarrow qq'$, 45%) as well as tauonic channels where both W decay leptonically into tau leptons (20%).

The main physics backgrounds from SM processes are also decay channel dependent. The main SM physics backgrounds for $t\bar{t}$ signals in the lepton+jets channel come from W +jets production as well as multijets production where one jet fakes an electron or a muon. In the dilepton channel the main physics backgrounds come from Z gauge boson production decaying into a lepton pair, Drell Yan processes and gauge boson pair production. Typical event selections require high p_T lepton (> 15 to 20 GeV), large missing transverse energy (> 15 to 20 GeV) and jets with large transverse energies (> 15 to 20 GeV). They also include cuts on several kinematical variables. In several analyses the selection uses of b -quark jets identification based either on displaced vertices (with efficiencies ranging from 50 to 60 %) or soft lepton taggers.

2 Production mechanism

The evaluation of the gg fusion process in $t\bar{t}$ production suffers from theoretical uncertainties and can vary up to a factor of 2. This motivates the CDF experiment to perform a measurement of the relative fraction C_f of gluon gluon fusion ($t\bar{t}^{gg}$) versus quark antiquark annihilation ($t\bar{t}^{q\bar{q}}$) by combining two complementary methods which were already reported elsewhere before this conference. The new CDF result presented at this conference concerns the combination.

The first method is a data driven method based on low p_t tracks⁵. Because gluons can radiate other partons and gluons, ($t\bar{t}^{gg}$) should have more low p_t tracks. The shapes of the track p_t distributions of the two components ($t\bar{t}^{gg}$ and $t\bar{t}^{q\bar{q}}$) are derived from inclusive dijets and $W + n$ jets (where $n = 0, 1, 2$) data samples. The background shape is then constructed as a combination of the $t\bar{t}^{gg}$ and $t\bar{t}^{q\bar{q}}$ shapes. The three shapes are then fit to the data sample selected for the t signal in the lepton+jets channel. The second method uses the kinematics of the production and the decay of the $t\bar{t}$ to differentiate the two production mechanisms⁶. The kinematic variables are used to train a neural network (NN) to increase the sensitivity of the method. This analysis relies on Monte Carlo (MC). A large ensemble of pseudo-experiments (PSE) are generated to calculate the statistical and systematical uncertainties and the Feldman-Cousins (FC)⁷ method is used to make the measurement. The track method and the NN method are then combined into a combined PSE method⁸. Using a total integrated luminosity of 995 pb^{-1} the CDF experiment finds: $C_f = 0.07_{-0.07}^{+0.15}$ at 68 % confidence level.

3 Top quark pair production cross section and top quark mass from cross sections measurements

3.1 Top quark pair production cross section measurements

The D0 experiment performed a new measurement of the $t\bar{t}$ production cross section in the lepton+jets channel employing two complementary methods for discrimination between signal and background namely using a likelihood discriminant and b -tagging⁹. This new measurement is based on about 0.9 fb^{-1} of data.

Events with $t\bar{t}$ decays differ in their event kinematics from background events. However no single kinematic quantity can separate signal and background very well. This motivates the development of the likelihood discriminant method which uses up to 6 kinematical quantities⁹ in each channel to discriminate the $t\bar{t}$ signal from the backgrounds. Four channels are defined

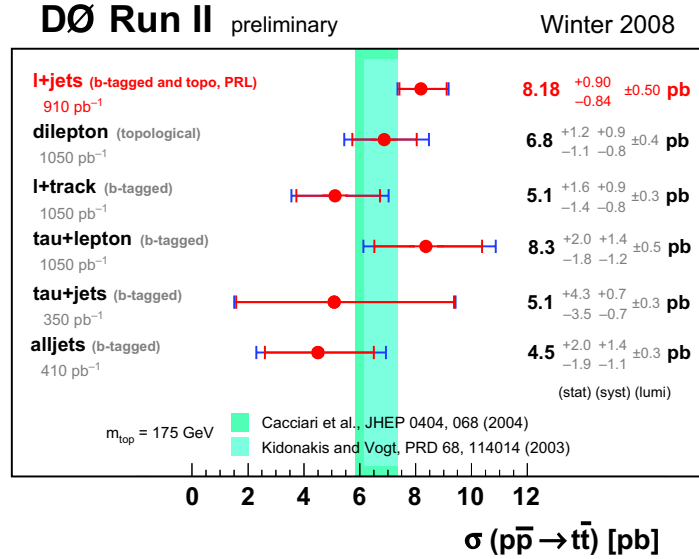


Figure 1: Summary of $t\bar{t}$ production cross-section measurements from the D0 experiment available at the time of the 2008 EW session of the Rencontres de Moriond conference.

by lepton flavor (e, μ) and jet multiplicity ($3, \geq 4$).

The probability density functions of the likelihood discriminant is determined from MC for $t\bar{t}$ signal and prompt lepton backgrounds and from a control data sample for multijets backgrounds (backgrounds without prompt leptons) both using the TMVA method¹⁰. A maximum likelihood fit to the distribution of the likelihood discriminant from the data is then performed in all four channels simultaneously with the $t\bar{t}$ production cross section as a free parameter.

The b -tagging method exploits the fact that every $t\bar{t}$ decay produces two b quark to distinguish them from the backgrounds. The signal over background ratio is enhanced by requiring at least one b -tagged jet. The $t\bar{t}$ signal and prompt lepton backgrounds are modeled with the MC and the backgrounds from multijets events are determined from the data. The cross section is calculated using a maximum likelihood fit to the number of events in eight different channels defined by the lepton flavor (e, μ), jet multiplicity ($3, \geq 4$) and b -tag multiplicity ($1, \geq 2$).

Combining the likelihood discriminant and the b -tagging methods with the help of the method described in¹¹, the D0 experiment measures the $t\bar{t}$ production cross section in the lepton+jets channel using a total integrated luminosity of 910 pb⁻¹ $\sigma(p\bar{p}) \rightarrow t\bar{t} = 7.77 \pm 0.54(stat.) \pm 0.47(syst.) \pm 0.47(lumi.)$ pb for $m_t = 170$ GeV and $\sigma(p\bar{p}) \rightarrow t\bar{t} = 7.42 \pm 0.53(stat.) \pm 0.46(syst.) \pm 0.45(lumi.)$ pb for $m_t = 175$ GeV.

Figure 1 shows that the measurements are consistent with each other and consistent with the SM predictions. New physics would show up as inconsistencies.

3.2 Top quark mass from cross sections measurements

The value of m_t can vary significantly depending on its different possible (and related) definitions from the running m_t definition in the (for example) \overline{MS} scheme (from the 1-loop up to the 3-loop level) to the $m_{t\text{pole}}$ ¹² which is itself defined up to some ambiguities such as the known renormalon ambiguity¹³.

At the Tevatron, the m_t measurements are performed by using template, ideogram, neutrino weighting or matrix element 'direct' methods¹⁴. They rely on the detailed description of the $t\bar{t}$ production in the MC simulations which currently contain only matrix elements at the leading order (LO) of quantum chromodynamics (QCD) and higher orders are simulated by applying

parton showers thus leaving in principle the m_t convention unknown. Therefore the world average of m_t is extracted in a not very well-defined scheme. The t quark mass can also be measured from the $t\bar{t}$ production cross section measurements. These 'indirect' measurements will thus provide valuable complementary informations on the value of m_t . Although efforts are put in improving their accuracy they are not meant to compete in precision with the 'direct' m_t measurements. The measurement of m_t from the most recent $t\bar{t}$ production cross section measurement from the D0 experiment reported in subsection 3.1 was not available at the time of the 2008 EW session of this conference but can be found in its QCD session¹⁵. Therefore we will only mention the results obtained with the previous set of cross-section measurements of summer 2007¹⁶ corresponding to an integrated luminosity of 910 pb^{-1} for the lepton+jets channel and 1.05 fb^{-1} for the dilepton channel. Comparing the cross section measurements in the lepton+jets channel¹⁷ with the predictions of³, and⁴ respectively, leads to $m_t = 166.9_{-5.2}^{+5.9}(\text{stat.} + \text{syst.})_{-3.8}^{+3.7}(\text{theory})$ GeV, and $m_t = 166.1_{-5.3}^{+6.1}(\text{stat.} + \text{syst.})_{-6.7}^{+4.9}(\text{theory})$ GeV respectively. This can be compared with the direct measurement from the D0 experiment with the matrix element method¹⁹ $m_t = 170.5 \pm 2.4(\text{stat.} + \text{JES}) \pm 1.2(\text{syst.})$ GeV and with the 2007 world average $m_{top} = 170.9 \pm 1.1(\text{stat.}) \pm 1.5(\text{syst.})$ GeV.

Comparing the measurements in the dilepton channel¹⁸ and predictions leads to $m_t = 174.5_{-8.2}^{+10.5}(\text{stat.} + \text{syst.})_{-3.6}^{+3.7}(\text{theory})$ GeV and $m_t = 174.1_{-8.4}^{+9.8}(\text{stat.} + \text{syst.})_{-6.0}^{+4.2}(\text{theory})$ GeV respectively. This can be compared with the direct measurement from the D0 experiment with the neutrino weighting method²⁰ $m_t = 172.5 \pm 5.8(\text{stat.}) \pm 5.5(\text{syst.})$ GeV.

The CDF experiment performed a new m_t measurement using the $t\bar{t}$ production cross section measurement in the dilepton channel, with an integrated luminosity of 1.2 fb^{-1} , as a constraint. Since the number of $t\bar{t}$ signal events depends on m_t , the observed number of events can therefore be used to measure m_t .

The kinematics of the $t\bar{t}$ system in the dilepton channel data sample is solved using the information on the momentum z-component of the $t\bar{t}$ system taken from the $t\bar{t}$ data sample in the lepton+jets channel. Solving the kinematics of the $t\bar{t}$ system in the dilepton channel allows to reconstruct m_t . The CDF experiment then uses a likelihood fit to get the final m_t measurement. The reconstructed m_t distribution from data is compared to MC signal and backgrounds templates and the number of events is compared to the expected number of events. The result of the likelihood fit gives: $m_t = 170.7_{-3.9}^{+4.2}(\text{stat.}) \pm 2.6(\text{syst.}) \pm 2.4(\text{theory})$ GeV.

4 Forward backward asymmetry

At the Tevatron the $t\bar{t}$ production is predicted to be charge symmetric at LO in QCD. However NLO calculations predicts asymmetries in the 5%-10% range²³ and next-to-next-to-leading order (NNLO) calculations predict significant corrections for $t\bar{t}$ production in association with a jet²⁴. The charge asymmetry arises from the interferences between symmetric and antisymmetric contributions under the exchange $t \leftrightarrow \bar{t}$. The charge asymmetry depends on the region of phase space being and, in particular, on the production of an additional jet. The small asymmetries expected in the SM makes this a sensitive probe for new physics²⁵.

Using a data sample corresponding to an integrated luminosity of about 0.9 fb^{-1} , the D0 experiment performed the first measurement of the forward-backward charge asymmetry in $t\bar{t}$ production in the lepton+jets channel²⁶. The forward-backward charge asymmetry can be obtained from the signed difference between the rapidities of the t and \bar{t} , $\Delta y = y_t - y_{\bar{t}}$ where the rapidity y is defined as function of the polar angle θ and the ratio of the particle's momentum to its energy β as $y(\theta, \beta) = \frac{1}{2} \ln[(1 + \beta \cos\theta)/(1 - \beta \cos\theta)]$. The asymmetry is defined as:

$$A_{fb} = \frac{N^{\Delta y > 0} - N^{\Delta y < 0}}{N^{\Delta y > 0} + N^{\Delta y < 0}}, \quad (1)$$

where $N^{\Delta y > 0}$ ($N^{\Delta y < 0}$) is the number of event with positive (negative) Δy .

Using a data sample with one lepton+ n jets, where $n \geq 4$ one jet at least being b -tagged in order to enhance the signal, the kinematics of the $t\bar{t}$ is reconstructed with the help a kinematic fitter which varies the 4-momenta of the detected objects within their resolutions and minimizes a χ^2 statistics, constraining both the known W gauge boson mass (M_W) and m_t .

The sample composition, including $t\bar{t}$ signal and W +jets from MC simulations and multijet background from data samples that fail lepton identification, as well as A_{fb} are then extracted from a simultaneous maximum-likelihood fit to data.

The observed asymmetry, uncorrected for acceptance and reconstruction effects, are $A_{fb}^{obs} = 0.12 \pm 0.08(stat.) \pm 0.01(syst.)$ for $n_{jets} \geq 4$, $A_{fb}^{obs} = 0.19 \pm 0.09(stat.) \pm 0.02(syst.)$ for $n_{jets} = 4$ and $A_{fb} = -0.16_{-0.17}^{+0.15}(stat.) \pm 0.03(syst.)$ for $n_{jets} \geq 5$.

Using a lepton+(at least 4) jets sample, where at least one jet is b -tagged, corresponding to an integrated luminosity of 1.9 fb^{-1} and containing 484 candidates events, the CDF experiment performed a forward-backward asymmetry defined by²⁷:

$$A_{fb} = \frac{N_{-Q_l \text{Cos}\Theta > 0} - N_{-Q_l \text{Cos}\Theta < 0}}{N_{-Q_l \text{Cos}\Theta > 0} + N_{-Q_l \text{Cos}\Theta < 0}}, \quad (2)$$

where Θ is the production angle of the t i.e. the angle between the t and the proton beam, and Q_l is the charge of the lepton.

The t production angle in the lepton+jets final state is reconstructed by using a kinematic fitter. In order to compare to the theoretical prediction any bias and smear of the $t\bar{t}$ asymmetry due to backgrounds, acceptance, and reconstruction have to be taken into account. The CDF experiment uses MC simulations to simulate these effects.

Including the reconstruction and acceptance corrections the forward backward asymmetry is measured to be $A_{fb} = 0.17 \pm 0.07(stat.) \pm 0.04(syst.)$

The measured is consistent (at the 2σ) level with the prediction 0.04 from the NLO MC generator MC@NLO²⁸.

The CDF experiment performed a cross-check to the measurement by reweighting the $t\bar{t}$ MC signal distribution to have a 'true' $A_{fb} = 0.17$. A Kolmogorov-Smirnov test has been performed to compare the shape of the reweighted distribution with backgrounds and data resulting into a probability of 45.6% showing a good agreement.

Due to different A_{fb} definitions and due to the usage (CDF) or not (D0) of acceptance and reconstruction corrections, the D0 and CDF results on A_{fb} are not to be compared.

5 Searches for resonances

The t is known so far as being the heaviest elementary particle. The production of $t\bar{t}$ can be sensitive to physics beyond standard model in particular top-color and unknown heavy resonances²⁹, heavy Higgs boson decaying to t ³⁰, $t\bar{t}$ condensation³¹, massive Z gauge boson in extended gauge theories³², Kaluza-Klein states of the Z gauge boson or gluon³³ and axiglons³⁴. Such new effects may produce resonances in the $t\bar{t}$ invariant mass distribution or may interfere with SM processes and cause distortion to the shape of this invariant mass distribution.

Using the same data sample in the lepton+jets channel as described in section 4 allowing also for a second b -tagged jet, the CDF experiment performed a measurement of the $t\bar{t}$ differential cross section with respect to the invariant $t\bar{t}$ mass $d\sigma/dM_{t\bar{t}}$ ³⁵. The $t\bar{t}$ invariant mass is reconstructed by combining the 4-momenta of the 4 leading jets, lepton and missing transverse energy. The neutrino momentum is taken from the missing transverse energy, the longitudinal component p_z of the neutrino being obtained by constraining the lepton and the neutrino invariant mass to be equal to M_W .

The reconstructed $M_{t\bar{t}}$ distribution is distorted from the true distribution by detector effects, resolutions and acceptances. These effects are corrected by using a regularized unfolding technique i.e. Singular Value Decomposition (SVD)³⁶. The CDF experiment then uses an Anderson-Darling³⁷ statistic to test for discrepancies from the standard model expectation. No evidence of inconsistencies with the Standard Model is seen, with an observed p-value of 0.45.

Using the same data sample as above the CDF experiment also searched for massive gluons decaying into $t\bar{t}$ ³⁸. In this search $M_{t\bar{t}}$ is reconstructed event-by-event using the Dynamical Likelihood Method (DLM)³⁹ also used for one of the CDF experiment m_t measurement⁴⁰. After reconstructing $M_{t\bar{t}}$, an unbinned likelihood fit is performed to extract the coupling strength. The fitted coupling strengths are consistent with the SM prediction within 1.7σ in the width over coupling ratio range from 0.05 to 0.5 for a massive gluon mass range from 400 to 800 GeV.

The D0 experiment searched for a narrow-width heavy resonance X decaying into $t\bar{t}$ using a lepton+jets sample with at least one b -tagged jet corresponding to an integrated luminosity of 0.9 pb^{-1} ⁴¹. The $t\bar{t}$ invariant mass is reconstructed in the same way as described above for the CDF $d\sigma/dM_{t\bar{t}}$ measurement. Model independent upper limits on $\sigma_X Br(X \rightarrow t\bar{t})$ have been obtained using a bayesian method⁴². Within a top-color-assisted technicolor model, the existence of a leptophobic Z' boson with $M_{Z'} < 690 \text{ GeV}$ and width $\Gamma_{Z'} = 0.012M_{Z'}$ is excluded at 95% confidence level.

An updated result was just available for the 2008 QCD session of the Rencontres de Moriond conference⁴³. With a data sample corresponding to an integrated luminosity of 2.1 pb^{-1} , the the existence of a leptophobic Z' boson with $M_{Z'} < 690 \text{ GeV}$ and width $\Gamma_{Z'} = 0.012M_{Z'}$ is excluded at 95% confidence level.

6 Conclusions

We review the most recent results on $t\bar{t}$ production at the Tevatron which were available at the time of the 2008 electroweak session of the Rencontres de Moriond conference and corresponding to about 1 to 2 fb^{-1} of integrated luminosity for each of the CDF and D0 experiments. These results include production mechanism, cross sections and forward-backward asymmetry measurements which are found to be consistent with the SM expectations. The $t\bar{t}$ production cross section measurements allow for complementary m_t measurements which can be compared to direct measurements. There are no evidence so far for resonances decaying into t and model independent limits on masses as well as parameters of the different possible theoretical frameworks have been set. More data and results are expected to come after the winter 2008 as the Tevatron is continuing to perform very well.

References

1. CDF collaboration, F. Abe *et al.*, *Phys. Rev. Lett.* **74**, 2626 (1995); D0 collaboration, S. Abachi *et al.*, *Phys. Rev. Lett.* **74**, 2632 (1995).
2. See Y. C. Chen and R. Schwienhorst contributions to these proceedings.
3. N. Kidonakis *et al.*, *Phys. Rev. D* **68**, 114014 (2003).
4. M. Cacciari *et al.*, *JHEP* 0404**068**2004.
5. CDF public note 8724, CDF Collaboration, T. Aaltonen *et al.*, arXiv:0712.3273.
6. CDF public note 8811.
7. G. Feldman and R. Cousins, *Phys. Rev. D* **57**, 3873 (1998).
8. CDF public note 9162.
9. D0 collaboration, *et al.*, D0 note 5591-CONF.
10. A. Höcker *et al.*, physics/0703039.

11. L. Lyons *et al.*, *Nucl. Instrum. Methods A* **270**, 110 (1988); A. Valassi, *Nucl. Instrum. Methods A* **500**, 391 (2003).
12. N. Gray *et al.*, *Z. Phys. C* **48**, 673 (1990); K. Melnikov and T. v. Ritbergen, *Phys. Lett. B* **482**, 99 (2000); K. G. Chetyrkin and M. Steinhauser, *Phys. Rev. Lett.* **83**, 4001 (1999); M. Beneke *et al.*, CERN-TH-2000-100, hep-ph/0003033.
13. M. Beneke and V. M. Braun, *Nucl. Phys. B* **426**, 301 (1994); I. I. Bigi *et al.*, *Phys. Rev. D* **50**, 2234 (1994); M. Beneke, *Phys. Lett. B* **344**, 341 (1995); M. Beneke and V. M. Braun, hep-ph/0010208.
14. See Y. C. Chen contribution to these proceedings.
15. See. S. Chevalier-Théry contribution to the proceedings of the 2008 QCD session of the Rencontres de Moriond.
16. D0 note 5449-CONF.
17. D0 note 5422.
18. D0 note 5371-CONF.
19. D0 note 5362-CONF.
20. D0 note 5347-CONF, D0 NOTE 5463-CONF.
21. FERMILAB-TM-2380-E, hep-ex/0703034.
22. CDF note 8869.
23. J. H. Kühn and G. Rodrigo, *Phys. Rev. Lett.* **81**, 49 (1998); J. H. Kühn and G. Rodrigo, *Phys. Rev. D* **59**, 054017 (1999); M. T. Bowen *et al.*, *Phys. Rev. D* **73**, 14008 (2006).
24. S. Dittmaier *et al.*, *Phys. Rev. Lett.* **98**, 262002 (2007).
25. M. Carena *et al.*, *Phys. Rev. D* **70**, 093009 (2004); C. T. Hill, *Phys. Lett. B* **345**, 483 (1998); O. Antuñao *et al.*, *Phys. Rev. D* **77**, 014003 (2008).
26. D0 collaboration, V. M. Abazov *et al.*, arXiv:0712.0851 (accepted by PRL).
27. CDF note 9169.
28. S. Frixione and B. R. Webber, *JHEP* **0206**, 029 (2002); S. Frixione *et al.*, *JHEP* **0308**, 007 (2003);
29. C. T. Hill and S. Parke, *Phys. Rev. D* **49**, 4454 (1994); R. Frederix and F. Maltoni, arXiv:0712.2355.
30. D. Dicus *et al.*, *Phys. Lett. B* **333**, 126 (1994).
31. G. Cvetic, *Rev. Mod. Phys.* **71**, 513 1999.
32. A. Leike, *Phys. Rept.* **317**, 1431999.
33. T. Rizzo, *Phys. Rev. D* **61**, 05505 (2000); B. Lillie *et al.*, *JHEP* **09**, 074 (2007).
34. L. M. Sehgal and M. Wanniger, *Phys. Lett. B* **200**, 211 (1988).
35. CDF note 9157.
36. A. Höcker and V. Kartvelishvili, *Nucl. Instrum. Methods A* **372**, 469 (1996).
37. T. W. Anderson and D. A. Darling, *The Annals of Mathematical Statistics*, **23**, 193 1952.
38. CDF note 9164.
39. K. Kondo, *J. Phys. Soc. Jpn.*, **57**, 4126 1988, K. Kondo, *J. Phys. Soc. Jpn.*, **60**, 836 1991, K. Kondo and T. Chikamatsu, *J. Phys. Soc. Jpn.*, **62**, 1177 1993, K. Kondo, hep-ex/0508035.
40. CDF collaboration, A. Abulencia *et al.*, *Phys. Rev. D* **73**, 092002 (2006).
41. D0 note 5443-CONF.
42. I. Bertram *et al.*, FERMILAB-TM-2104.
43. D0 note 5584-CONF, see also R. Eusebi contribution to the proceedings of the 2008 QCD session of the Rencontres de Moriond.

TOP MASS AND PROPERTIES

Yen-Chu Chen

On behalf of CDF and D0 collaboration

Institute of Physics, Academia Sinica,

Taipei, Taiwan, Republic of China

The top quark was discovered in 1995. The top quark mass is now well measured at the Tevatron, with uncertainty getting below 1% of the top mass. The world average from last year was $170.9 \pm 1.8 \text{ GeV}/c^2$. The new CDF measurement is $172 \pm 1.2 \text{ (stat)} \pm 1.5 \text{ (sys)} \text{ GeV}/c^2$, and D0 will soon present a new measurement. The top quark mass is an important parameter in the Standard Model, and should be measured as precisely as possible. To learn more about the top quark observed and study possible new physics, other properties also should be measured. At the Tevatron, the charge of the top quark can be measured directly. Examples of other properties studied and reported in this presentation are W helicity, top decay branching ratio to b (R_b), searches for $t \rightarrow Hb$ and for flavor changing neutral current (FCNC). The results are all consistent with the Standard Model within current statistics. With significantly more data being collected at the Tevatron, precision measurements of the top properties are just starting.

1 Introduction

Top quarks are produced at the Tevatron mainly in top anti-top pairs, $P\bar{P} \rightarrow t\bar{t}$, through quark anti-quark annihilation and gluon gluon fusion. The t (\bar{t}) quark subsequently decays into a W^+ (W^-) boson and a b (\bar{b}) quark, $t \rightarrow Wb$, with a branching ratio close to 1. From the b 's and the final products of the W decays, the mass and other properties of the top quark can be measured.

The $P\bar{P} \rightarrow t\bar{t} \rightarrow W^+bW^-\bar{b}$ production cross section and event selection have been reported in a previous talk at this Conference. Based on how the W 's decay, three analysis channels are identified: the di-lepton channel (DIL) for both W 's decaying leptonically, the lepton plus jet channel (LJ) for only one W decaying leptonically, and the all hadron channel for both W 's decaying hadronically. (In this article we consider the final leptons being electron or muon only. The case of $W \rightarrow \tau\nu$ has to be handled differently due to the nature of tau decay.) Each channel

has its own challenges and strengths. Some common methods are developed and used when applicable.

2 top mass measurement

Mass is a fundamental property of a particle. While the top has been discovered for more than ten years, we have many interesting questions about the top quark. Are we seeing the same particle in all three analysis channels (DIL, LJ and all hadron)? Precise measurement of the top mass in these three channels could provide some insight to this question. If this particle seen as top quark is truly the one of the SM, then since its mass strongly correlates with the mass of Higgs particle, precise measurement of the top mass can help the search of the Higgs particle, and will also enable stringent constraints for electroweak tests and new physics.

The three channels, DIL, LJ and all hadron, have their own challenges and methods. In the DIL channel, each event has two neutrinos that are not measured directly, with only the missing transverse energy providing partial information for these two neutrinos. The system is under-constrained. Additional assumption is used to further constrain the system to be able to reconstruct the top mass. Also, various top mass could be used as input to obtain a probability density function to determine the most probable value for top mass.

A general issue with all three channels is: which lepton and jet(s) in each $t\bar{t}$ event are decay products of the top quark and which are from the anti-top? One could try all possible combinations and select one based on reconstruction probability or simple kinematic information, such as the invariant mass of the top and anti-top system. Alternatively, one could use all possible solutions and assign weights based on the some relevant quantities, such as a weight defined by comparing missing E_t from the reconstruction to that from what is measured in each event. These techniques are also generally applied in studying properties of the top quark.

2.1 The methods

One common issue with all channels is the jet energy calibration. In prior analysis jet energy calibration was based on predefined cone sizes. In an event where at least one W decays hadronically, the known W boson mass can be used as input to further fine tune the two jets associated with this W . This is called the in-situ jet energy calibration. In top mass measurement, this W mass constraint is applied to the final events selected to find the average shift to the nominal jet energy calibration. The shift is applied to all jets including the b jets. This procedure significantly improves the determination of the uncertainty in the top mass measurement.

The Template Method is one of the main methods used to obtain the top mass. In this method, top mass is reconstructed from the kinematic information available in the event. Templates are formed based on Monte Carlo with different top mass input. Comparing these templates with the observed events reconstructed in the same way reveals the top mass. In each DIL channel event, the system is under-constrained. Additional reasonable assumption has to be made, such as taking P_z of top anti-top system from observed events¹, or weighting on the ϕ angle of the neutrino², etc. In the LJ channel, the assumption is made that the missing energy is due to the neutrino being not detected. A top mass fitter is used to find the most probable top mass, taking into account the resolution of p_t and jet energy measured. In-situ jet energy calibration is commonly applied to improve the uncertainty. In each all hadronic event, there are two W 's decaying hadronically. In-situ jet energy calibration is generally applied to the jets which form the W 's. In the Template Method with 2-dimensional fit (TMT2D)³ analysis in CDF, all possible jet pairing combinations are tried but only the one with best χ^2 is kept.

The Matrix Element Method is based on theory. This takes into account all the kinematics information contained in an event, which are top mass dependent. A conditional probability

Table 1: top mass measurement at the Tevatron

Analysis	Samples	Result
ME+NN (CDF) ⁶	DIL, 2 fb ⁻¹	171.2 ± 2.7(stat) ± 2.9(sys) GeV/c ²
TMP+NN (CDF) ³	Had., 1.9 fb ⁻¹	177.0 ± 3.7(stat + JES) ± 1.6(sys) GeV/c ²
ME+NN (CDF) ⁴	LJ, 1.9 fb ⁻¹	172.7 ± 1.2(stat) ± 1.3(JES) ± 1.2(sys) GeV/c ²
MW (D0) ⁷	DIL, 1 fb ⁻¹	175.2 ± 6.1(stat) ± 3.4(sys) GeV/c ²
NW (D0) ⁸	DIL, 1 fb ⁻¹	172.5 ± 5.8(stat) ± 3.5(sys) GeV/c ²

can be formed for a given top mass. In DIL, this probability can be expressed as

$$P(\mathbf{x}|M_t) = \frac{1}{N} \int d\Phi_8 |\mathcal{M}_{t\bar{t}}(p; M_t)|^2 \prod_{jets} W(p, j) f_{PDF}(q_1) f_{PDF}(q_2), \quad (1)$$

where M_t is the top mass, \mathbf{x} contains the lepton and jet energy measurement, $\mathcal{M}_{t\bar{t}}(p; M_t)$ is the $t\bar{t}$ production matrix⁵, q is the vector of incoming parton-level quantities, p is the vector of resulting parton-level quantities: lepton and quark momenta, $W(p, j)$ is the transfer function which gives the probability to observe a jet with energy j given a parton energy p , and finally, f_{PDF} the parton distribution functions of the two quarks from the proton and anti-proton. The integral is over the entire six-particle phase space. Scanning through the top mass, the most probable point reveals the mass of the top quark. An example of applying such method for top mass measurement is performed at CDF using DIL samples⁶.

This method “Matrix Weighting” is different from the “Matrix Element” method described previously. This method is applied to DIL samples, where the system is under-constrained due to missing neutrinos. For a given top mass, one could try to resolve for $t\bar{t}$ momentum. A weight is calculated for each solution found by comparing the missing energy calculated with the one observed in observed events. The top mass is determined from a scan through a range of top mass to find a maximum weight and the extremum of likelihood. This is described in D0’s public conference note⁷.

“Neutrino weighting” is a method applied in D0. Using DIL samples, for a given top mass η was thrown based on Monte Carlo simulation for each ν . Then the set of energy-momentum conservation equations can be resolved for ν momentums. For each event a weight template was derived based on missing energy expected and observed at each given top mass. A maximum likelihood is formed, combining all events, and the extremum of this distribution reveals the top mass. This is described in D0’s public conference note⁸.

At the Tevatron, many techniques have been developed to measure the top mass. Progress has been made to improve the uncertainty. Some of the methods have not been mentioned in this presentation. A single variable that has a distribution being sensitive to the top mass can be used to do the measurement. One such variable is the L_{xy} , which is the closet distance of the secondary vertex to the primary vertex in the transverse plan of the detector. may have a distribution which is sensitive to the top mass. The top mass measurement from the top production cross section is discussed by Marc Besancon at this Conference. All of the methods provide additional info, and could help in improving uncertainty of the combined top mass.

2.2 The results

The results on the top mass measurement at Tevatron given at this conference are listed in Table 1. All individual top mass measurement from all three channels show consistent results. There is no indication of seeing different particles in different channels.

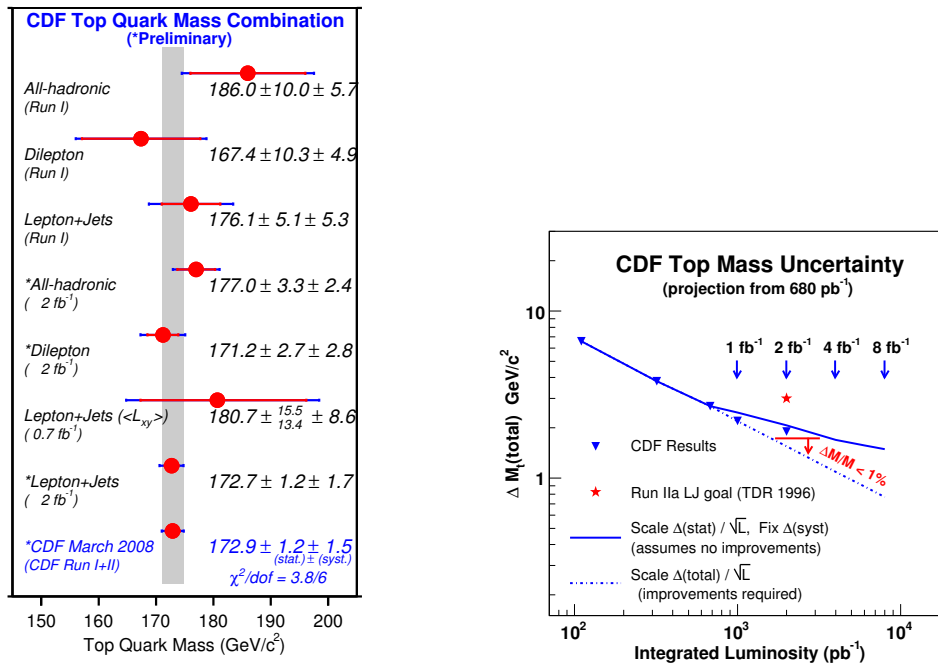


Figure 1: The combined measurement of top mass from CDF. The plot on the right shows the improvement of uncertainty with respect to the integrated luminosity. The dark blue points are the reality, compared to the projection based on including more data only (blue line) or further improving the analysis methods (dashed line). The improvement based better methods is hard to predict. The dashed line is the most optimistic case. The new results are between the two lines. CDF alone is at the same level as CDF and D0 combined last year. Combining effort from CDF and D0, the uncertainty of top mass should be less than 1% of the measured top mass.

At the moment of this presentation, CDF has already a combined result using various results from all hadronic, DIL and LJ channels. This yields $172.9 \pm 1.2(\text{stat}) \pm 1.5(\text{sys}) \text{ GeV}/c^2$ and is shown in Figure 1. This result is approaching an uncertainty of 1% of the top mass, which is similar to CDF and D0 combined result for the year 2007. Together with the updated D0 measurement, the new combined result would have an uncertainty below 1%. (This happened right after the Moriond EW 2008 conference.⁹) CDF and D0 are working together on common systematic issues to improve uncertainty at the Tevatron for the high precision era of top mass measurement.

3 Top property studies

The SM top quark has spin (1/2), charge (+2/3), and other definite properties which should be measured. In contrast, the top mass is a free parameter in SM. Any significant deviation of the top quark properties from SM would indicate new physics. The top charge is among the fundamental properties of the top quark most accessible at Tevatron. Other properties, such as top spin, lifetime, decay width, either need significantly more data or are far beyond our capability to measure with our given detector resolution. Studies from the top decay include the helicity of W boson from top decay, measurement of branching ratio, search for charged Higgs, search for flavor changing neutral current, etc.

3.1 The charge of top quark

In the SM, the charge of top quark is +2/3. An alternative possibility suggested by an exotic model (XM)¹¹ is -4/3. In this model, it is claimed that the particle seen at Tevatron may be an exotic top of charge -4/3, which decays into W^- and b , unlike in the SM where the top quark

decays into W^+ and b . The two key elements in the study are then to identify the source of a jet being b or \bar{b} , and how the b and \bar{b} jets are paired with the two W 's.

The identification of a jet being from b or \bar{b} is done via calculating the jet charge, which is sum of jet-track charges weighted by the track momentum amplitude and how close the track is to the jet axis. For true b jets this method has 60% probability of identifying b or \bar{b} correctly.

The pairing can be done by taking the measured top mass as input and check which pairing is more probable. In DIL channel, events can be selected based on the square of invariant mass of the paired lepton and jet m_{lb}^2 to improve the purity. In each event there are two possible ways of pairing and four possible m_{lb}^2 values. The pairing having the maximum m_{lb}^2 does not always provide the correct pairing. In the events with the maximum m_{lb}^2 is greater than certain value, this method can be almost 100% correct. However cutting too tight would lose too much in statistics. The best point for making such cut is 21000, assuming that SM is true and top mass is $175 \text{ GeV}/c^2$. With this selection, 94% of pairing purity can be reached with efficiency of 39%.

The charge of the top quark was first studied by D0. With 0.37 fb^{-1} of data, the result prefers the SM instead of XM¹⁰. In CDF, the study has been done with data up to 1.5 fb^{-1} . The result¹² up to date support SM over XM, and the XM is rejected at 87% confidence level (CL). Combining DIL and LJ, among 225 top or anti-top quark decays 124 decays support SM and 101 support XM. Correcting for purity of the analysis, the measured true fraction of SM over total is 0.87, which based on our sensitivity gives a p value of 0.31. An additional way of showing this is the Bayes Factor (BF), which is defined as $P(N_+|SM)/P(N_+|XM)$, i.e. the probability of observed events happening assuming SM is true over the one of XM. A common way to utilize BF is the quantity $L = 2 * \ln(BF)$. For L in the ranges (0-2), (2-6), (6-10), (>10), the result is uncertain, positive, strongly supporting SM, or very strongly supporting SM, respectively. Our result from CDF data is 12.01, thus very strongly support SM over XM. With more data, we will determine more precisely the top charge.

3.2 W helicity

In the SM, V-A rules the weak decay. The W boson from top quark decay is thus polarized. The SM predicts that the W helicity in this case should have 70% longitudinal (f_0) and 30% left-handed (f_-). The component of right-handed (f_+) is very small, 3.6×10^{-4} . Significant deviation of f_+ would indicate new physics.

The study of W helicity can be performed via looking at the $\cos\theta^*$ distribution, where θ^* is the angle of the electron or muon in the W rest frame with respect to the anti-direction of top quark in this frame. The analysis can be performed in LJ and DIL channels. In case of LJ the missing energy is assumed to be due to the missing neutrino. Events can be reconstructed using top mass as input and lepton angle in W rest frame can be calculated. The top mass used is generally $175 \text{ GeV}/c^2$. In case of DIL there are two missing neutrinos. Using top mass as input one can figure out which jet is paired with which lepton and resolve for the neutrino momenta. Lepton angle in the W rest frame can be obtained in this way. CDF does this analysis, using 1.9 fb^{-1} data, in the LJ channel. In a 2 dimensional fit where both f_0 and f_+ are fitted at the same time the result shows $f_0 = 0.65 \pm 0.19(stat) \pm 0.03(sys)$ and $f_+ = -0.03 \pm 0.07(stat) \pm 0.03(sys)$. If f_0 is fixed to the SM value CDF obtains $f_+ = -0.04 \pm 0.04(stat) \pm 0.03(sys)$ and sets upper limit for f_+ at 0.07 at 95% CL¹³. D0 collaboration does the analysis in both LJ and DIL channels. A 2-D fit of f_0 and f_+ reveals $0.425 \pm 0.166(stat) \pm 0.102(sys)$ and $0.119 \pm 0.0090(stat) \pm 0.053(sys)$ respectively. Fixing f_0 to the SM value gives $f_+ = -0.002 \pm 0.047(stat) \pm 0.047(sys)$. An upper limit of 0.13 at 95% CL is set¹⁴.

3.3 Study of R_b

A study on the $R_b = Br(t \rightarrow Wb)/Br(t \rightarrow Wq)$, where q represents all possible quarks allowed in the decay, is performed at D0. R_b is correlated with the top pair production. Noting that D0 does simultaneous fit to both values, using LJ channel from 0.9 fb^{-1} data¹⁵. The result is $R_b = 0.97_{-0.08}^{+0.09}(\text{stat} + \text{sys})$. A lower limit of R_b is set at 0.79 at 95% CL. From this a lower limit on $|V_{tb}|$ is set at 0.89 at 95% CL. From the same fit the resulted production cross section is $\sigma_{t\bar{t}} = 8.18_{-0.84}^{+0.90}(\text{stat} + \text{sys}) \pm 0.50(\text{lumi})$ pb, which is consistent with the direct measurement.

3.4 Search for $t \rightarrow Hb$

It is interesting to search for charged Higgs in the top quark decay. D0 collaboration did this analysis by comparing the production cross section of top pair from the LJ channel against the one from the DIL channel. If there were charged Higgs in the top decay, it would mostly contribute to the LJ channel but much less in the DIL channel. The ratio of the two production cross sections is $R = 1.21_{-0.26}^{+0.27}(\text{stat} + \text{sys})$, based on the assumption that $R_b = 1$. Extracting the branching ratio of $t \rightarrow Hb$ from this cross section ratio, D0 obtains $Br = 0.13_{-0.11}^{+0.12}(\text{stat} + \text{sys})$. An upper limit is set at 0.35 at 95% CL¹⁶.

3.5 Search for FCNC

At CDF an analysis to study FCNC is to search for $t \rightarrow Zq$ in the top quark decay. The SM predicts a branching ratio at the order of $O(10^{-14})$. However beyond SM up to $O(10^{-4})$ is possible. At CDF events having two high p_t leptons with at least 4 jets were selected with constraint on masses of top, Z and W. Comparing the data (1.9 fb^{-1}) with expectation, no excess is seen. An upper limit is set at 3.7% at 95% CL¹⁷.

4 Summary and Future Prospects

The top quark mass has been well measured at the Tevatron, with uncertainty getting below 1% of the top mass. The top quark mass is an important parameter in the Standard Model, and should be measured as precisely as possible. Other properties of the top quark also should be measured, to learn more about the top quark and study possible new physics. Examples of other top studies at the Tevatron are the charge of the top quark, W helicity, top decay branching ratio to b (R_b), searches for $t \rightarrow Hb$ and for flavor changing neutral current (FCNC). The results are all consistent with the Standard Model within current statistics. With significantly more data being collected at the Tevatron, precision measurements of the top properties are just starting.

Acknowledgments

Many thanks to the people working on Tevatron. With their dedicated effort to improve the accelerator discoveries are made possible. Many thanks to the funding agencies to CDF and D0 collaboration. Many thanks to the authors and conveners of both collaboration who provided critical input to this presentation. At the end I want to thank the organizers of the Moriond EW 2008 conference for their warm hospitality and well organized program.

References

1. T. Aaltonen *et al.*, *The CDF Collaboration*, *PRL* **100**, 062005 (2008).
2. B. Abbott *et al.*, *Phys. Rev. D* **60**, 052001 (1999); A. Abulencia *et al.*, *Phys. Rev. D* **73**, 112006 (2006)

3. T. Aaltonen et al., *The CDF Collaboration*, public CDF note 9165, (2007).
4. T. Aaltonen et al., *The CDF Collaboration*, public CDF note 9196, (2008).
5. G. Mahlon, S. Parke, *Phys. Lett. B* **411**, 173 (1997); G. Mahlon, S. Parke, *Phys. Rev. D* **55**, 7249 (1996).
6. T. Aaltonen et al., *The CDF Collaboration*, *Phys. Rev. D* **75**, 031105 (2007); T. Aaltonen et al., *The CDF Collaboration*, public CDF note 8951 (2007).
7. V. M. Abazo et al., *The D0 Collaboration*, *D0CONF* note 5463, (2007).
8. V. M. Abazo et al., *The D0 Collaboration*, *D0CONF* note 5347, (2007).
9. *Tevatron Eelectroweak Working Group*, <http://arxiv.org/abs/0803.1683>.
10. V. M. Abazo et al., *The D0 Collaboration*, *Phys. Rev. Lett.* **98**, 041801 (2007).
11. D. Chang, W. Chang, E. Ma, *Phys. Rev. D* **59**, 091503 (1999).
12. T. Aaltonen et al., *The CDF Collaboration*, public CDF note 8967, (2007).
13. T. Aaltonen et al., *The CDF Collaboration*, public CDF note 9215, (2008).
14. V. M. Abazo et al., *The D0 Collaboration*, *Phys. Rev. Lett.* **100**, 062004 (2008).
15. V. M. Abazo et al., *The D0 Collaboration*, *Fermilab-Pub-04/08/010-E*, (2008).
16. V. M. Abazo et al., *The D0 Collaboration*, *D0CONF* note 5466, (2007).
17. T. Aaltonen et al., *The CDF Collaboration*, public CDF note 9202, (2008).

Single top quark production at the Tevatron

R. Schwienhorst^a

Michigan State University, 3234BPS, East Lansing, MI 48824, USA



The Tevatron experiments D0 and CDF have found evidence for single top quark production, based on datasets between 0.9 fb^{-1} and 2.2 fb^{-1} . Several different multivariate techniques are used to extract the single top quark signal out of the large backgrounds. The cross section measurements are also used to provide the first direct measurement of the CKM matrix element $|V_{tb}|$.

1 Introduction

Evidence for single top quark production at the Tevatron and a first direct measurement of the CKM matrix element $|V_{tb}|$ was first reported by the D0 collaboration¹. In contrast to top quark pair production through the strong interaction, which was observed in 1995^{2,3}, single top quarks are produced via the weak interaction. The Feynman diagrams for standard model (SM) s-channel (tb) and t-channel (tqb) single top quark production are shown in Fig. 1. There is third production mode, associated production of a top quark and a W boson, but its cross section is so small that it will not be considered further. The SM cross section for the s-channel process $p\bar{p} \rightarrow t\bar{b} + X, \bar{t}b + X$ is $0.88 \pm 0.14 \text{ pb}$ at NLO for $m_{\text{top}} = 175 \text{ GeV}$ ^{4,5}. At the same order and mass, the cross section for the t-channel process $p\bar{p} \rightarrow tq\bar{b} + X, \bar{t}q\bar{b} + X$ is $1.98 \pm 0.30 \text{ pb}$ ^{4,6}.

Measuring the single top quark production cross section provides a direct measurement of the CKM matrix element $|V_{tb}|$. The single top quark final state also allows for studies of the top quark polarization, and it is sensitive to many models of new physics, for example flavor changing neutral currents via the gluon⁷ or heavy new bosons W' that only couple to quarks⁸. The s-channel process is also an important background to Higgs searches in the associated production mode, and the advanced analysis techniques used in the single top searches will be applicable to Higgs searches as well.

^aOn behalf of the D0 and CDF collaborations.



Figure 1: Feynman diagrams for s-channel (left) and t-channel (right) single top quark production at the Tevatron.

The D0 collaboration has updated two of their analysis methods using a dataset of 0.9 fb^{-1} . The updated results, including a combination of different methods are presented below. The CDF collaboration has analyzed a dataset of 2.2 fb^{-1} and significantly improved the sensitivity to single top quark production. These new results are presented below.

2 D0 results

2.1 Event selection

The D0 analysis selects electron+jets and muon+jets events in 0.9 fb^{-1} of data with the following requirements: One high- p_T lepton (electron ($p_T > 15 \text{ GeV}$) or muon ($p_T > 18 \text{ GeV}$)), missing transverse energy $\cancel{E}_T > 15 \text{ GeV}$, and between two and four jets with jet $p_T > 15 \text{ GeV}$ and jet 1 $p_T > 25 \text{ GeV}$, at least one is tagged with a neural-network based b-tagging algorithm. Additional cuts remove fake-lepton background events. Events are collected by lepton+jets trigger requirements.

The number of events observed in data and expected from the background model and SM signal is shown in Table 1. The largest sources of systematic uncertainty are the background normalization, jet energy scale, as well as b-tag and trigger modelling.

Table 1: Numbers of events expected by D0 in 0.9 fb^{-1} for electron and muon, 1 b-tag and 2 b-tag channels combined.

	2 jets	3 jets	4 jets
s-channel	16 ± 3	7 ± 2	2 ± 1
t-channel	20 ± 4	12 ± 3	4 ± 1
$t\bar{t}$	59 ± 14	134 ± 32	155 ± 36
W +jets	531 ± 129	248 ± 64	70 ± 20
Multijets	96 ± 19	77 ± 15	29 ± 6
Total background	686 ± 131	460 ± 75	253 ± 42
Data	697	455	246

Table 1 shows that after selection cuts, the expected SM single top signal is small compared to the background sum, and in fact the signal is significantly smaller than the background uncertainty. Thus, more advanced techniques are required to extract the signal.

2.2 Multivariate techniques

The D0 analysis employs three different multivariate techniques to extract the single top quark signal out of the large backgrounds. The boosted decision tree (BDT) analysis has not changed since the publication of evidence for single top quark production⁷. Here we focus on the Bayesian neural network analysis and the matrix element analysis, both of which have been re-optimized.

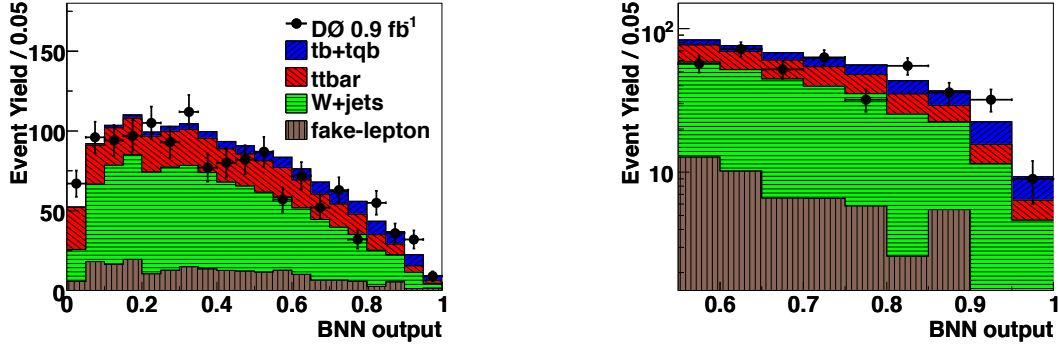


Figure 2: Comparison between data and background sum for the Bayesian neural network output. Shown is the full distribution (left), and the high-discriminant region (right). The signal has been normalized to the SM expectation.

In a conventional neural network, the network parameters and weights are determined in an optimization (training) procedure. Rather than optimizing for these network parameters once and then fixing them, the optimal network configuration can be obtained as an average over many different values for the network parameters. In this Bayesian procedure, an integration over all of the possible network parameter space is performed. The network architecture is fixed, and the weight of each set of parameters is obtained through a Bayesian integration. The final network discriminant is then the weighted average over all the individual networks. Fig. 2 shows the output of the BNN for the D0 data.

The Matrix element analysis starts from the Feynman diagrams for the single top quark processes and uses transfer functions to relate the parton level quark-level information to the reconstructed jet and other information. Matrix elements for the single top quark signal as well as the W +jets backgrounds are included. For 3-jet events, a top pair matrix element is also included. For each event, an integration over the phase space is performed, employing the transfer functions to compute the probability for this particular event to arise from a specific matrix element. A likelihood function is then formed as the ratio of the signal and signal plus background probabilities.

2.3 D0 summary

The cross section is measured as the peak of the Bayesian posterior probability density, shown in Fig. 3 for the ME analysis. The three different methods measure the following cross sections for the sum of s- and t-channel:

$$\begin{aligned} \sigma^{\text{obs}}(p\bar{p} \rightarrow tb + X, tqb + X) &= 4.9^{+1.4}_{-1.4} \text{ pb (DT)} \\ &= 4.4^{+1.6}_{-1.4} \text{ pb (BNN)} \\ &= 4.8^{+1.6}_{-1.4} \text{ pb (ME)}. \end{aligned}$$

The measured cross sections are consistent with each other and above the SM expectation.

The decision tree analysis has also measured the s- and t-channel cross sections separately,

$$\begin{aligned} \sigma^{\text{obs}}(p\bar{p} \rightarrow tb + X) &= 1.0 \pm 0.9 \text{ pb} \\ \sigma^{\text{obs}}(p\bar{p} \rightarrow tqb + X) &= 4.2^{+1.8}_{-1.4} \text{ pb}, \end{aligned}$$

where the standard model cross section is used for the single top process not being measured.

Removing the constraint of the standard model ratio allows to form the posterior probability density as a function of both the tb and tqb cross sections. This model-independent posterior is shown in Fig. 3 (right) for the DT analysis, using the $tb+tbq$ discriminant. The most probable value corresponds to cross sections of $\sigma(tb) = 0.9$ pb and $\sigma(tqb) = 3.8$ pb. Also shown are

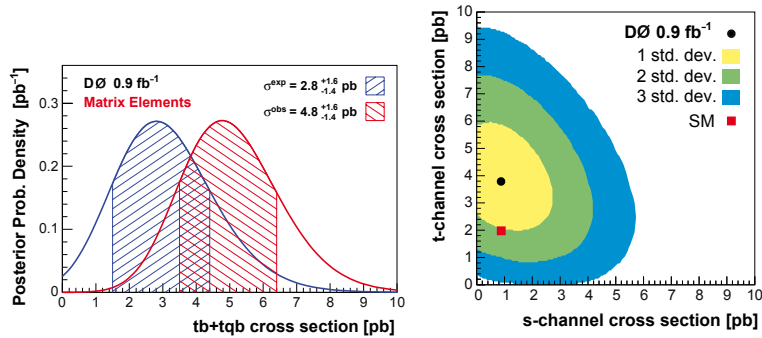


Figure 3: Posterior probability density for the matrix element analysis as a function of the sum of s-channel and t-channel cross sections (left), and for the BDT analysis as a function of both the s-channel and t-channel cross sections (right).

the one, two, and three standard deviation contours. While this result favors a higher value for the t -channel contribution than the SM expectation, the difference is not statistically significant. Several models of new physics that are also consistent with this result are shown in Ref.⁹. These updated results have recently been published¹⁰.

3 CDF results

3.1 Event selection

The CDF analysis selects electron+jets and muon+jets events in 2.2 fb^{-1} of data with the following requirements: One high- p_T lepton ($p_T > 20 \text{ GeV}$), $\cancel{E}_T > 25 \text{ GeV}$, and two or three jets with jet $p_T > 20 \text{ GeV}$, at least one of which is tagged by a displaced vertex tagging algorithm. Additional cuts remove fake-lepton background events. Events are collected by single-lepton trigger requirements. The matrix element analysis uses additional triggers in the muon channel to increase the acceptance.

The number of events observed in data and expected from the background model and SM signal is shown in Table 2. The largest sources of systematic uncertainty are the background normalization, jet energy scale, and b-tag modelling. Again, it is clear that a advanced analysis

Table 2: Numbers of events expected by CDF in 2.2 fb^{-1} for electron and muon, 1 b -tag and 2 b -tag channels combined.

	2 jets	3 jets
s-channel	41 ± 6	14 ± 2
t-channel	62 ± 9	18 ± 3
$t\bar{t}$	146 ± 21	339 ± 48
W +bottom	462 ± 139	141 ± 43
W +charm	395 ± 122	109 ± 34
W +light	340 ± 56	102 ± 17
Z +jets	27 ± 4	11 ± 2
diboson	63 ± 6	22 ± 2
Multijets	60 ± 24	21 ± 9
Total background	1492 ± 269	755 ± 91
Data	1535	752

techniques are required to extract the signal.

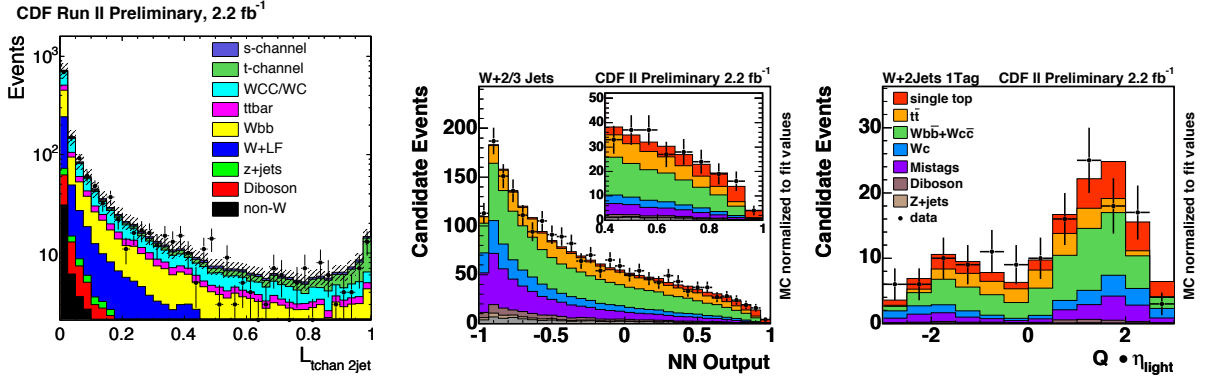


Figure 4: Comparison between data and background sum for the t-channel likelihood discriminant (left), the neural network discriminant (center), and the light quark jet pseudorapidity in the high-discriminant region for the neural network analysis (right). The signal has been normalized to the SM expectation.

3.2 CDF Likelihood Function

A multivariate likelihood is built from several kinematic variables that each separate the single top quark signal from the backgrounds. One special variable is a specially developed b-tagging neural network that aids in separating b-quark jets from light quark and c-quark jets. An additional special variable is a kinematic solver using constraints from the W boson mass and the top quark mass to determine if an event is well reconstructed. Another special variable is the t-channel matrix element, which uses the kinematic information provided by the kinematic solver. The likelihood discriminant for the t-channel likelihood is shown in Fig. 4 (left).

The measured cross section is obtained as the peak of a Bayesian posterior probability. The likelihood analysis measures a cross section of $\sigma(tb + tqb) = 1.8^{+0.9}_{-0.8}$ pb, below the SM expectation.

3.3 CDF Neural Network

Several kinematic variables as well as the b-tagging neural network output are combined in a neural network. Four different networks are built with 10-14 variables each, trained separately for 2-jet and 3-jet as well as 1-tag and 2-tag events. The full neural network output distribution is shown in Fig. 4 (center), and the signal region is shown in Fig. 4 (right). The neural network analysis measures a cross section of $\sigma(tb + tqb) = 2.0^{+0.9}_{-0.8}$ pb, below the SM expectation but consistent with the SM within uncertainties.

3.4 CDF Matrix Element

The matrix element analysis uses the same approach as described above, but also includes a top pair matrix element in the 2-jet bin. The matrix element for top quark pair events has more final state particles than the single top process, and these additional particles have to be integrated out. This is done by integrating over the kinematics of the hadronically decaying W -boson in a lepton+jets top pair event.

The Bayesian posterior probability density for the Matrix element analysis is shown in Fig. 5, showing the measured cross section and the measurement uncertainty. The measured cross section is $\sigma(tb + tqb) = 2.2^{+0.8}_{-0.7}$ pb, again below the SM expectation but consistent with the SM within uncertainties. The CKM matrix element $|V_{tb}|$ is also extracted from the posterior probability and a lower limit is found to be $|V_{tb}| > 0.59$ at the 95% confidence level.

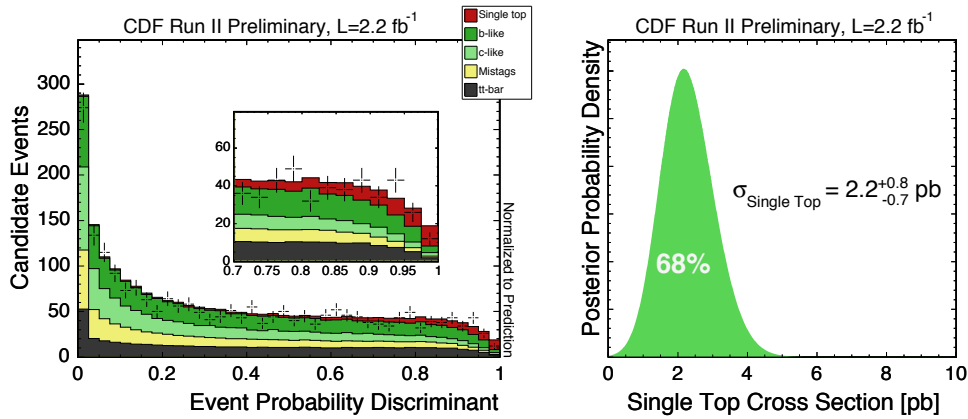


Figure 5: Data-background comparison for the matrix element discriminant (left) and Bayesian posterior density distribution observed by the Matrix element analysis.

4 Summary

Both Tevatron experiments have found better than 3 sigma evidence for single top quark production and have made the first direct measurement of the CKM matrix element $|V_{tb}|$ using advanced multivariate techniques. The CKM matrix element $|V_{tb}|$ can be measured to better than 15%. Further improvements to the analyses are in progress and both experiments are working towards observation of single top quark production at the 5 sigma level.

Acknowledgments

We thank the Fermilab staff and the technical staffs of the participating institutions for their vital contributions.

References

1. V.M. Abazov *et al.* (D0 Collaboration), Phys. Rev. Lett. **98**, 181802 (2007).
2. F. Abe *et al.* (CDF Collaboration), Phys. Rev. Lett. **74**, 2626 (1995).
3. S. Abachi *et al.* (D0 Collaboration), Phys. Rev. Lett. **74**, 2632 (1995).
4. Z. Sullivan, Phys. Rev. D **70**, 114012 (2004).
5. Q. H. Cao, R. Schwienhorst and C. P. Yuan, Phys. Rev. D **71**, 054023 (2005) [arXiv:hep-ph/0409040].
6. Q. H. Cao, R. Schwienhorst, J. A. Benitez, R. Brock and C. P. Yuan, Phys. Rev. D **72**, 094027 (2005) [arXiv:hep-ph/0504230].
7. V. M. Abazov *et al.* (D0 Collaboration), Phys. Rev. Lett. **99**, 191802 (2007) [arXiv:hep-ex/0702005].
8. V. M. Abazov *et al.* (D0 Collaboration), accepted by Phys. Rev. Lett, arXiv:0803.3256 [hep-ex].
9. T. Tait and C.P. Yuan, Phys. Rev. D **63**, 014018 (2001).
10. V. M. Abazov *et al.* (D0 Collaboration), accepted by Phys. Rev. D, arXiv:0803.0739 [hep-ex].

B, C and S physics

MEASUREMENTS OF ϕ_1 AND ϕ_2 BY BELLE AND BABAR

T.A.-Kh. Aushev^{a 1,2}

for the Belle Collaboration

¹*Swiss Federal Institute of Technology of Lausanne, EPFL*

²*Institute for Theoretical and Experimental Physics, Moscow, ITEP
Lausanne, Switzerland*

We report recent measurements of the Unitarity triangle angles ϕ_1 and ϕ_2 using large data samples collected with Belle and BaBar detectors at e^+e^- asymmetric-energy colliders.

1 Introduction

In the Standard Model (SM), CP violation in B^0 meson decays originates from an irreducible complex phase in the 3×3 Cabibbo-Kobayashi-Maskawa (CKM) mixing matrix¹. The angles ϕ_1 and ϕ_2 of the CKM unitarity triangle have been measured in several B decay modes^{2,3,4,5}. Extra studies in different decay modes are important to check the self-consistence between measurements to probe the existence of New Physics.

The results reported in this paper were obtained by two experiments, Belle and BaBar, working at e^+e^- asymmetric-energy colliders, KEKB⁶ and PEP-II, correspondingly, with the center-of-mass (CM) energy at $\Upsilon(4S)$ resonance ($\sqrt{s} = 10.58$ GeV). The Belle detector⁷ is a large-solid-angle magnetic spectrometer that consists of a silicon vertex detector (SVD), a 50-layer central drift chamber (CDC), a mosaic of aerogel threshold Cherenkov counters (ACC), time-of-flight scintillation counters (TOF), and an array of CsI(Tl) crystals (ECL) located inside a superconducting solenoid coil that provides a 1.5 T magnetic field. An iron flux-return located outside of the coil is instrumented to detect K_L mesons and to identify muons (KLM). For the results from Belle experiment the data sample of 657 million $B\bar{B}$ pairs is used.

The BaBar detector is described in detail elsewhere⁸. Charged particle momenta are measured with a tracking system consisting of a five-layer silicon vertex tracker (SVT) and a 40-layer

^a**e-mail:** aushev@itep.ru

drift chamber (DCH) surrounded by a 1.5 T solenoidal magnet. An electromagnetic calorimeter (EMC) comprising 6580 CsI(Tl) crystals is used to measure photon energies and positions. Charged hadrons are identified with a detector of internally reflected Cherenkov light (DIRC) and ionization measurements in the tracking detectors. The results from BaBar experiment are based on 383 million $B\bar{B}$ pairs data sample.

2 Study of $B^+ \rightarrow D^+\bar{D}^0$ and search for $B^0 \rightarrow D^0\bar{D}^0$

Recently, evidence of direct CP violation in the decay $B^0 \rightarrow D^+D^-$ was observed by Belle⁹, while BaBar measured an asymmetry consistent with zero¹⁰. A similar effect might occur in the charged mode $B^+ \rightarrow D^+\bar{D}^0$ ¹¹. This decay has already been observed by Belle¹² and confirmed by BaBar¹³.

Now, Belle updated their result with larger data sample¹⁴. 366 ± 32 events were found from the fit to the $\Delta E - M_{bc}$ distribution (Fig. 1(a,b)), where $\Delta E = E_B - E_{\text{beam}}$, $M_{bc} = \sqrt{E_{\text{beam}}^2 - p_B^{*2}}$, $E_B(p_B^*)$ is the energy (momentum) of B candidate in the CM system, E_{beam} is the CM beam energy. The branching fraction of $B^+ \rightarrow D^+\bar{D}^0$ is measured to be $\mathcal{B}(B^+ \rightarrow D^+\bar{D}^0) = (3.85 \pm 0.31 \pm 0.38) \times 10^{-4}$, where the first error is statistical and the second one is systematic. The charge asymmetry for this decay is measured to be consistent with zero: $A_{CP}(B^+ \rightarrow D^+\bar{D}^0) = 0.00 \pm 0.08 \pm 0.02$. Belle also searched for the decay $B^0 \rightarrow D^0\bar{D}^0$. An upper limit is established for the branching fraction: $\mathcal{B}(B^0 \rightarrow D^0\bar{D}^0) < 0.43 \times 10^{-4}$ (Fig. 1(c,d)).

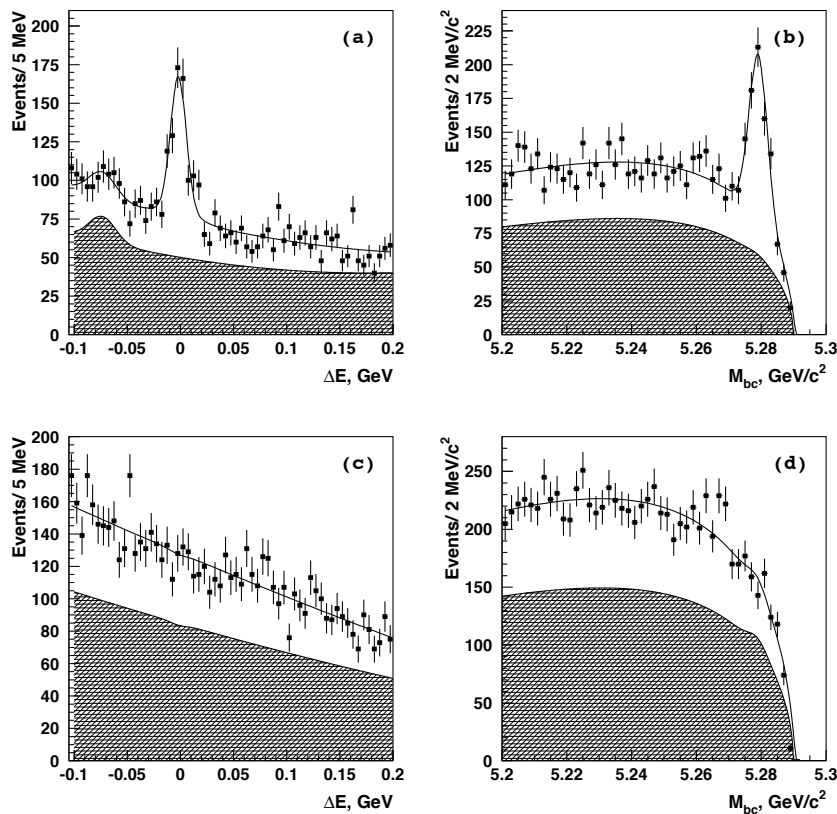


Figure 1: ΔE (a,c) and M_{bc} (b,d) distributions for the $B^+ \rightarrow D^+\bar{D}^0$ (a,b) and $B^0 \rightarrow D^0\bar{D}^0$ (c,d) candidates. Each distribution is the projection of the signal region of the other parameter. Points with errors represent the experimental data, open curves show projections from the 2D fits and cross-hatched curves show the $B\bar{B}$ background component only.

3 Study of $B^0 \rightarrow D^{*+}D^{*-}$

Another interesting decay mode to study the CP asymmetry is $B^0 \rightarrow D^{*+}D^{*-}$. Both experiments have updated their results for this decay mode and obtained high statistics signals shown in Fig. 2(a,c)¹⁵. The time-dependent decay rates of B^0 and \bar{B}^0 to a CP eigenstate, like $D^{*+}D^{*-}$, is given by formula:

$$\mathcal{P}(\Delta t) = \frac{e^{-\Delta t/\tau_{B^0}}}{4\tau_{B^0}} \left\{ 1 + q \left[\mathcal{S}_{f_{CP}} \sin(\Delta m_d \Delta t_{B^0}) + \mathcal{A}_{f_{CP}} \cos(\Delta m_d \Delta t_{B^0}) \right] \right\},$$

where q is the b -flavor charge: $q = +1(-1)$ when the tagging B meson is a B^0 (\bar{B}^0), τ_{B^0} is the neutral B lifetime, Δm_d is the mass difference between two B^0 mass eigenstates, $\Delta t_{B^0} = t_{CP} - t_{\text{tag}}$. The tree diagram dominates in this decay mode, which according to the SM gives $\mathcal{S}_{f_{CP}} = \xi_{D^{*+}D^{*-}} \sin 2\phi_1$ and $\mathcal{A}_{f_{CP}} = 0$. The parameter $\xi_{D^{*+}D^{*-}}$ is the CP eigenvalue of the $D^{*+}D^{*-}$, which is $+1$ when the decay proceeds via S and D waves, or -1 for a P wave. Therefore, the CP measurement requires helicity study to obtain the CP -odd fraction R_{odd} of the decay. It is done in both analyses from Belle and BaBar in the so-called transversity basis. The fit results are presented in Fig. 2(b,d). The parameter R_{odd} is found to be equal to $0.143 \pm 0.034(\text{stat}) \pm 0.008(\text{syst})$ by BaBar and $0.116 \pm 0.042(\text{stat}) \pm 0.004(\text{syst})$ by Belle.

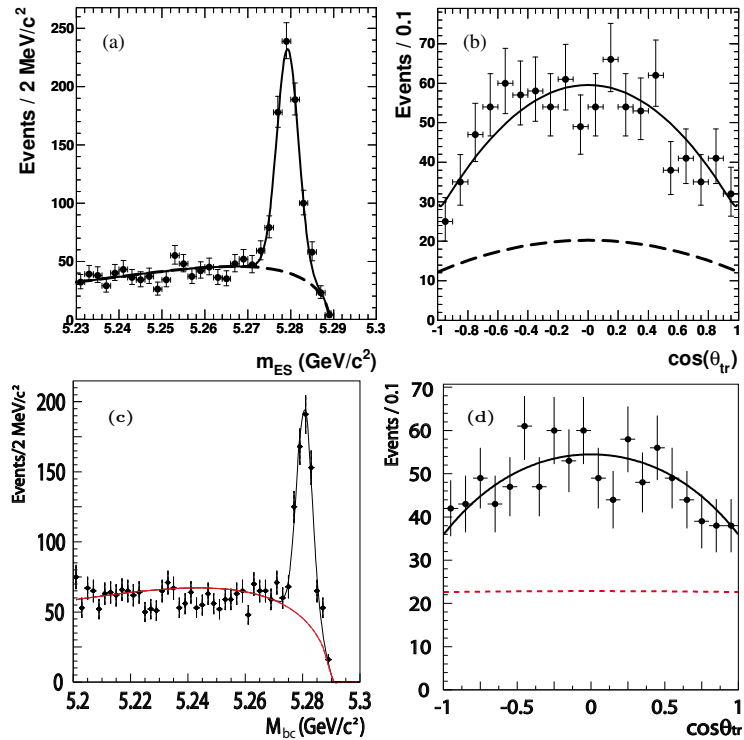


Figure 2: Measured distributions of M_{bc} (a, c) and $\cos\theta_{tr}$ in the region $M_{bc} > 5.27$ GeV/c² (b, d) for BaBar (a, b) and Belle (c, d) of $B^0 \rightarrow D^{*+}D^{*-}$ events. The solid lines are the projections of the fit results. The dotted lines represent the background components.

Finally, the unbinned maximum likelihood fit was performed to obtain the CP -violating parameters. The results of the fits are summarized in Table 1 and presented in Fig. 3. Both experiments obtained the results well consistent with each other in both the CP -odd fraction and the CP -violating parameters. Note that in the BaBar parametrization $\mathcal{A} = -\mathcal{C}$. The Belle results are preliminary.

Table 1: Results for $B^0 \rightarrow D^{*+}D^{*-}$ decay mode.

	Yield	R_{odd}	$\mathcal{A} = -\mathcal{C}$	\mathcal{S}
Belle	545 ± 29	$0.116 \pm 0.042 \pm 0.004$	$+0.16 \pm 0.13 \pm 0.02$	$-0.93 \pm 0.24 \pm 0.15$
BaBar	638 ± 38	$0.143 \pm 0.034 \pm 0.008$	$+0.02 \pm 0.11 \pm 0.02$	$-0.66 \pm 0.19 \pm 0.04$

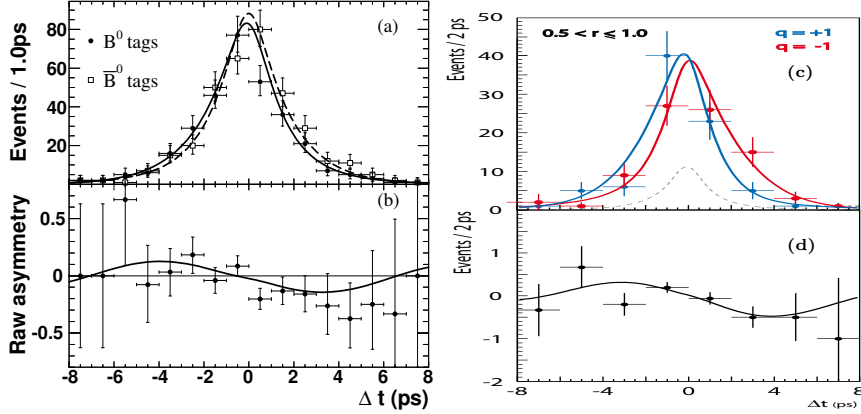


Figure 3: The Δt distributions of $B^0 \rightarrow D^{*+}D^{*-}$ events in the region $M_{bc} > 5.27 \text{ GeV}/c^2$ for $B^0(\bar{B}^0)$ tagged candidates (a,c) and the raw asymmetry $(N_{B^0} - N_{\bar{B}^0})/(N_{B^0} + N_{\bar{B}^0})$, as a function of Δt (b,d) for BaBar (a,b) and Belle (c,d). The lines represent the fit results.

4 CP -violation in $B^0 \rightarrow K_S\pi^0\pi^0$ and $B^0 \rightarrow K_S\pi^0$

In the SM, the CP violation parameters in $b \rightarrow s$ “penguin” and $b \rightarrow c$ “tree” transitions are predicted to be the same, $\mathcal{S}_f \approx -\xi_f \sin 2\phi_1$ and $\mathcal{A}_f \approx 0$, with small theoretical uncertainties. Recent measurements however, indicate that the effective $\sin 2\phi_1$ value, $\sin 2\phi_1^{\text{eff}}$, measured with penguin processes is different from $\sin 2\phi_1 = 0.687 \pm 0.025$ measured in tree decays by 2.6σ ¹⁶. New particles in loop diagrams may shift the weak phase.

Recently, Belle and BaBar measured the CP asymmetry in $B^0 \rightarrow K_S^0\pi^0\pi^0$ and $B^0 \rightarrow K_S\pi^0$ decays that proceed through $b \rightarrow s\bar{q}q$ ($q = u, d$) transitions^{17,18,19,20}. The results of CP -violating parameters measurements are presented in Table 2. Both experiments are perfectly consistent with each other. In the case of $B^0 \rightarrow K_S^0\pi^0\pi^0$ the central value of \mathcal{S} has a sign opposite to what we expect from the SM, but the errors are still too large to claim the contradiction. The estimated deviation of the average value from the SM is more than 2σ . The fit to the data for Belle for $B^0 \rightarrow K_S^0\pi^0\pi^0$ is presented in Fig. 4(a-c) and the BaBar result for $B^0 \rightarrow K_S^0\pi^0$ is shown in Fig. 4(d-f).

 Table 2: Results for $B^0 \rightarrow K_S^0\pi^0\pi^0$ and $B^0 \rightarrow K_S\pi^0$ decay modes.

	$\mathcal{A} = -\mathcal{C}$	$\mathcal{S} = -\sin 2\phi_1$
$B^0 \rightarrow K_S^0\pi^0\pi^0$		
Belle	$-0.17 \pm 0.24 \pm 0.06$	$+0.43 \pm 0.49 \pm 0.09$
BaBar	$-0.23 \pm 0.52 \pm 0.13$	$+0.72 \pm 0.71 \pm 0.08$
Average	-0.18 ± 0.22	$+0.52 \pm 0.41$
$B^0 \rightarrow K_S\pi^0$		
Belle	$-0.05 \pm 0.14 \pm 0.05$	$+0.33 \pm 0.35 \pm 0.08$
BaBar	$-0.24 \pm 0.15 \pm 0.03$	$+0.40 \pm 0.23 \pm 0.03$

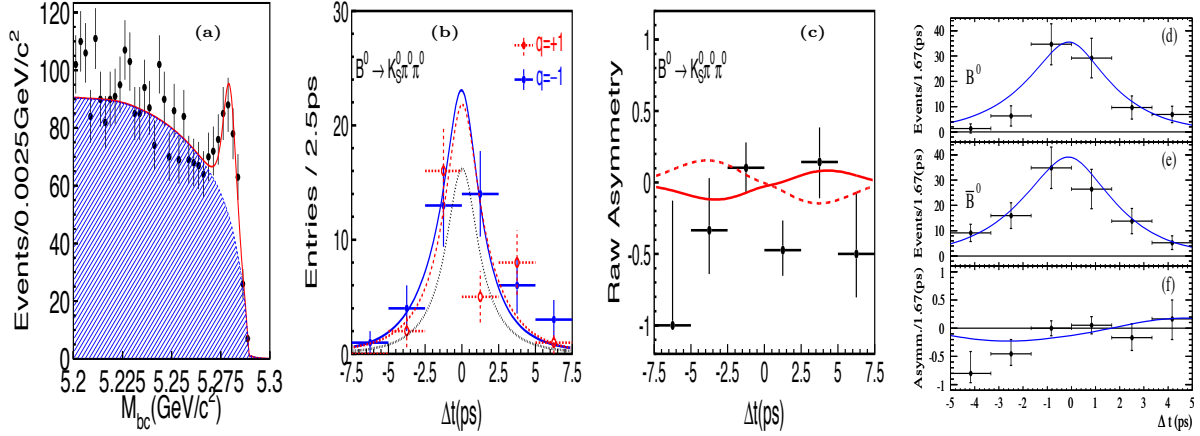


Figure 4: Distributions for the M_{bc} (a), the Δt (b) and the raw asymmetry (c) for $B^0 \rightarrow K_S^0 \pi^0 \pi^0$ decay mode from Belle. Δt distributions for the B^0 (d) and \bar{B}^0 (e) tagged events and the raw asymmetry (f) for the decay $B^0 \rightarrow K_S^0 \pi^0$ from BaBar. The lines represent the fit result.

5 ϕ_2 measurements

The CKM angle ϕ_2 have been measured in decay modes like $B^0 \rightarrow \pi\pi, \rho\rho, \rho\pi$ ²¹. Addition of new decay modes allows to improve an accuracy of ϕ_2 measurement and to check a consistency of measurements in different final states. The decay $B^0 \rightarrow a_1^\pm(1260)\pi^\mp$ proceeds through $b \rightarrow u$ transitions, hence its time-dependent CP violation is also sensitive to ϕ_2 . Belle measured the branching fraction for this decay mode to be $\mathcal{B}(B^0 \rightarrow a_1^\pm(1260)\pi^\mp)\mathcal{B}(a_1^\pm(1260) \rightarrow \pi^\pm\pi^\pm\pi^\mp) = (14.9 \pm 1.6 \pm 2.3) \times 10^{-6}$ ²², while BaBar has updated their previous measurements now with CP violation study: $\mathcal{A}_{CP} = -0.07 \pm 0.07 \pm 0.02$ and $\mathcal{S} = +0.37 \pm 0.21 \pm 0.07$ ²³. The angle ϕ_2 was measured to be $\phi_2^{\text{eff}} = 78.6^\circ \pm 7.3^\circ$. The result is presented in Fig. 5(a-c).

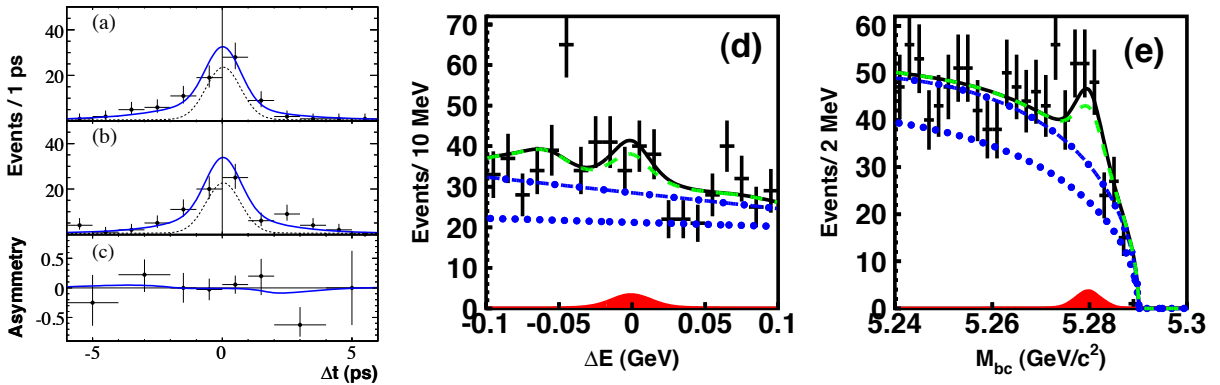


Figure 5: Δt distributions of the decay $B^0 \rightarrow a_1^\pm \pi^\mp$ for B^0 (a) and \bar{B}^0 (b) tagged events, and the raw asymmetry (c). The solid lines show the fit results, while the dotted lines show the background component. Projection of the signal region onto (d) ΔE and (e) M_{bc} for $B^0 \rightarrow \rho^0 \rho^0$ candidates. The fit result is shown as the thick solid curve; the hatched region represents the signal component. The dotted, dot-dashed and dashed curves represent, respectively, the cumulative background contributions from continuum processes, $b \rightarrow c$ decays, and charmless B decays.

Belle also performed the search for the decay $B^0 \rightarrow \rho^0 \rho^0$ and other decay modes with four pions in the final state. In the absence of the signals, the upper limits on the branching fraction were established. The signal distributions for the $B^0 \rightarrow \rho^0 \rho^0$ are shown in Fig. 5(a,b). All

Table 3: Fit results for decays relevant to ϕ_2 measurements.

Mode	Yield	ϵ (%)	$\mathcal{S}(\sigma)$	$\mathcal{B}(\times 10^{-6})$	UL($\times 10^{-6}$)@90% C.L.
Belle results					
$\rho^0 \rho^0$	$24.5^{+23.6+9.7}_{-22.1-9.9}$	9.16	1.0	$0.4 \pm 0.4^{+0.2}_{-0.2}$	< 1.0
$\rho^0 \pi^+ \pi^-$	$112.5^{+67.4+51.5}_{-65.6-53.7}$	2.90	1.3	$5.9^{+3.5+2.7}_{-3.4-2.8}$	< 11.9
$4\pi^\pm$	$161.2^{+61.2+26.0}_{-59.4-28.5}$	1.98	2.5	$12.4^{+4.7+2.0}_{-4.6-2.2}$	< 19.0
$\rho^0 f^0$	$-11.8^{+14.5+4.9}_{-12.9-3.6}$	5.10	—	—	< 0.6
$f^0 f^0$	$-7.7^{+4.7+3.0}_{-3.5-2.9}$	2.75	—	—	< 0.4
$f^0 \pi^+ \pi^-$	$6.3^{+37.0+18.0}_{-34.7-18.1}$	1.55	—	$0.6^{+3.6}_{-3.4} \pm 1.8$	< 7.3
BaBar results					
$b_1^0 \pi^+$	178^{+39}_{-37}	6.78	4.0	$6.7 \pm 1.7 \pm 1.0$	
$b_1^0 K^+$	219^{+38}_{-36}	6.73	5.3	$9.1 \pm 1.7 \pm 1.0$	
$b_1^\mp \pi^\pm$	387^{+41}_{-39}	9.54	8.9	$10.9 \pm 1.2 \pm 0.9$	
$b_1^- K^+$	267^{+33}_{-32}	9.43	6.1	$7.4 \pm 1.0 \pm 1.0$	
$a_1^0 \pi^+$	382 ± 79	7.2	3.8	$20.4 \pm 4.7 \pm 3.4$	
$a_1^- K^0$	241 ± 32	9.6	6.2	$34.9 \pm 5.0 \pm 4.4$	
$a_1^+ \pi^0$	459 ± 78	12.5	4.2	$26.4 \pm 5.4 \pm 4.2$	
$a_1^- K^+$	272 ± 44	7.9	5.1	$16.3 \pm 2.9 \pm 2.3$	

results are preliminary.

Also a number of the decay modes potentially usable for the ϕ_2 measurements have been studied by BaBar^{24,25,26}. All the results of these studies are summarized in Table 3.

6 CP -violation in $\Upsilon(4S)$ decays

In the decay $\Upsilon(4S) \rightarrow B^0 \bar{B}^0 \rightarrow f_1 f_2$, where f_1 and f_2 are CP eigenstates, the CP eigenvalue of the final state $f_1 f_2$ is $\xi = -\xi_1 \xi_2$. Here the minus sign corresponds to odd parity from the angular momentum between f_1 and f_2 . If f_1 and f_2 have the same CP eigenvalue, i.e. $(\xi_1, \xi_2) = (+1, +1)$ or $(-1, -1)$, ξ is equal to -1 . Such decays, for example $(f_1, f_2) = (J/\psi K_S^0, J/\psi K_S^0)$, violate CP conservation since the $\Upsilon(4S)$ meson has $J^{PC} = 1^{--}$ and thus has $\xi_{\Upsilon(4S)} = +1$. The branching fraction within the SM is suppressed by the factor

$$F \approx \frac{x^2}{1+x^2} (2 \sin 2\phi_1)^2 = 0.68 \pm 0.05,$$

where $x = \Delta m_d / \Gamma = 0.776 \pm 0.008$ ²⁷.

This decay was studied by Belle. Due to a small branching fractions to the final state and low reconstruction efficiencies the expected yield is very small, 0.04 events. In order to increase the signal yield, a partial reconstruction technique was used²⁸. One B^0 was fully reconstructed, while only K_S^0 was reconstructed from another one. The signal was searched in the recoil mass distribution to the reconstructed particles where, in principle, signals from $\eta_c, J/\psi, \chi_{c1}$, or $\psi(2S)$ can be seen. The method was checked using charged B decay control samples, $\Upsilon(4S) \rightarrow B^+ B^- \rightarrow (f_{B^+}, J/\psi^{\text{tag}} K^- \text{ and } \eta_c^{\text{tag}} K^-)$, where f_{B^+} stands for $J/\psi K^+$ and $\bar{D}^0 \pi^+$. Also neutral B decays were examined in the decay $\Upsilon(4S) \rightarrow B^0 \bar{B}^0 \rightarrow (f_{B^0}, J/\psi^{\text{tag}} K_S^0 \text{ and } \eta_c^{\text{tag}} K_S^0)$ with $f_{B^0} = B^0 \rightarrow D^{(*)-} h^+$. The fit yields 206 ± 57 for charged B and 35 ± 16 for neutral B signal events, which is in good agreement with the MC expectation (Fig. 6(a,b)). The results of the final fit are shown in Fig. 6(c). The extracted signal yield, $-1.5^{+3.6}_{-2.8}$ events, is consistent with zero as well as with the SM prediction (1.7 events). An upper limit for the branching fraction was obtained $\mathcal{B}(\Upsilon(4S) \rightarrow B^0 \bar{B}^0 \rightarrow J/\psi K_S^0, (J/\psi, \eta_c) K_S^0) < 4 \times 10^{-7}$ at the

90% confidence level, where the SM prediction is 1.4×10^{-7} . This corresponds to $F < 2$ at the 90% confidence level.

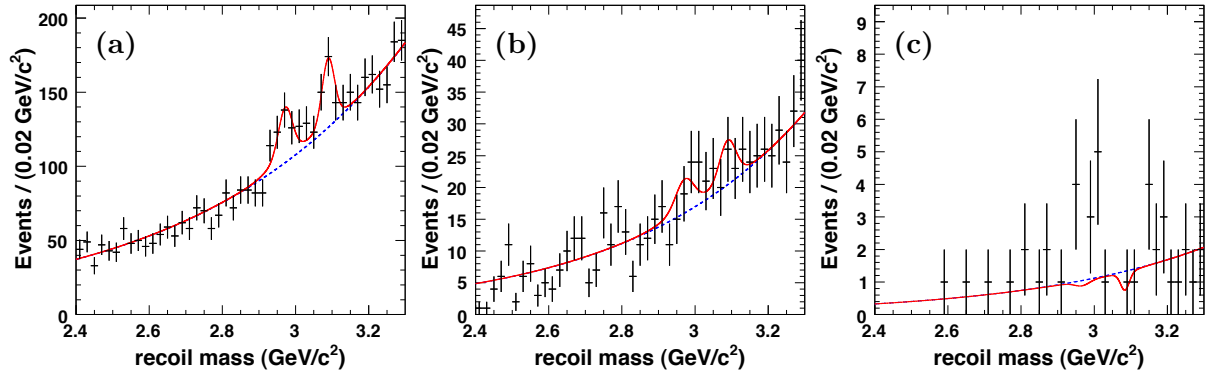


Figure 6: Recoil mass distributions for samples reconstructed as $\Upsilon(4S) \rightarrow (B^+, (J/\psi, \eta_c)^{\text{tag}} K^-)$ (a), $(B^0 \rightarrow D^{(*)-} h^+, (J/\psi, \eta_c)^{\text{tag}} K_S^0)$ (b) and $(J/\psi K_S^0, (J/\psi, \eta_c)^{\text{tag}} K_S^0)$ (c). The solid lines show the fits to signal plus background distributions while the dashed lines show the background distributions.

7 Summary

The CP violating parameters have been measured in various decay modes. Most of the measurements are in a good agreement with the SM expectations. Although a room for New Physics becomes smaller and smaller, there is still some sign that it can be found in $b \rightarrow s$ transitions. More statistics is necessary to test these possibilities.

References

1. N. Cabibbo, Phys. Rev. Lett. 10, 531 (1963); M. Kobayashi and T. Maskawa, Prog. Theor. Phys. **49**, 652 (1973).
2. K.-F. Chen *et al.* (The Belle Collaboration), Phys. Rev. Lett. **98**, 031802 (2007)
3. B. Aubert *et al.* (The BaBar Collaboration), Phys. Rev. Lett. **99** 171803 (2007).
4. A. Kusaka, C.-C. Wang *et al.* (The Belle collaboration), Phys. Rev. D **77**, 072001 (2008).
5. B. Aubert *et al.* (The BaBar Collaboration), Phys. Rev. D **76**, 052007 (2007)
6. S. Kurokawa and E. Kikutani, Nucl. Instr. and Meth. A **499**, 1 (2003).
7. A. Abashian *et al.* (The Belle Collaboration), Nucl. Instr. and Meth. A **479**, 117-232 (2002).
8. B. Aubert *et al.* (The BaBar Collaboration), Nucl. Instrum. Methods Phys. Res., Sect. A **479**, 1 (2002).
9. S. Fratina *et al.* (The Belle Collaboration), Phys. Rev. Lett. **98**, 221802 (2007).
10. B. Aubert *et al.* (The BaBar Collaboration), Phys. Rev. Lett. **99**, 071801 (2007).
11. The inclusion of charge conjugate modes is implied throughout this Letter.
12. G. Majumder *et al.* (The Belle Collaboration), Phys. Rev. Lett. **95**, 041803 (2005).
13. B. Aubert *et al.* (The BaBar Collaboration), Phys. Rev. D **73**, 112004 (2006).
14. I. Adachi *et al.* (The Belle Collaboration), Phys. Rev. D **77**, 091101(R) (2008).
15. B. Aubert *et al.* (The BaBar Collaboration), Phys. Rev. D **76**, 111102(R) (2007).
16. Heavy Flavor Averaging Group, “Winter 2007”, <http://www.slac.stanford.edu/xorg/hfag>.
17. K. Abe *et al.* (The Belle Collaboration), arXiv:hep-ex/0708.1845.
18. B. Aubert *et al.* (The BaBar Collaboration), Phys. Rev. D **76**, 071101(R) (2007).
19. K. Abe *et al.* (The Belle Collaboration), arXiv:hep-ex/0609006.

20. B. Aubert *et al.* (The BaBar Collaboration), Phys. Rev. D **77**, 012003 (2008).
21. B. Aubert *et al.* (The BaBar Collaboration), Phys. Rev. D **76**, 052007 (2007). B. Aubert *et al.* (The BaBar Collaboration), Phys. Rev. Lett. **99**, 021603 (2007). A. Kusaka, C.C. Wang *et al.* (The Belle Collaboration), Phys. Rev. D **77**, 072001 (2008). A. Somov, A. Schwartz *et al.* (The Belle Collaboration), Phys. Rev. D **76**, 011104 (2007). H. Ishino *et al.* (The Belle Collaboration), Phys. Rev. Lett. **98**, 211801 (2007).
22. K. Abe *et al.* (The Belle Collaboration), arXiv:hep-ex/0706.3279.
23. B. Aubert *et al.* (The BaBar Collaboration), Phys. Rev. Lett. **98**, 181803 (2007).
24. B. Aubert *et al.* (The BaBar Collaboration), Phys. Rev. Lett. **99**, 261801 (2007).
25. B. Aubert *et al.* (The BaBar Collaboration), Phys. Rev. Lett. **100**, 051803 (2008).
26. B. Aubert *et al.* (The BaBar Collaboration), Phys. Rev. Lett. **99**, 241803 (2007).
27. W.-M. Yao *et al.* (Particle Data Group), Journal of Phys. **G 33**, 1 (2006).
28. O. Tajima, M. Hazumi *et al.* (The Belle collaboration), Phys. Rev. Lett. **99**, 211601 (2007).

Improved Measurement of Inclusive Radiative B -meson decays

A. LIMOSANI for the Belle Collaboration
*School of Physics, Experimental Particle Physics,
 University of Melbourne 3010, Australia*

We report a fully inclusive measurement of the flavor changing neutral current decay $B \rightarrow X_s \gamma$ in the energy range $1.7 \text{ GeV} \leq E_\gamma^{\text{c.m.s}} \leq 2.8 \text{ GeV}$, covering 97% of the total spectrum, where c.m.s is the center of mass system. Using 605 fb^{-1} of data, we obtain in the rest frame of the B -meson $\mathcal{B}(B \rightarrow X_s \gamma : E_\gamma^B > 1.7 \text{ GeV}) = (3.31 \pm 0.19 \pm 0.37 \pm 0.01) \times 10^{-4}$, where the errors are statistical, systematic and from the boost correction needed to transform from the rest frame of the $\Upsilon(4S)$ (c.m.s) to that of the B -meson, respectively. We also measure the first and second moments of the photon energy spectrum as functions of various energy thresholds, which extend down to 1.7 GeV. The results are preliminary.

1 Introduction

Radiative B -meson decays may offer a view of phenomena beyond the Standard Model of particle physics (SM). In the SM, these decays proceed via a flavor changing neutral current (FCNC) decay, which consists of a loop process. Yet to be discovered particles, such as charged Higgs or supersymmetric particles, may be produced virtually in the loop and produce a measureable deviation from the branching fraction predicted by the SM.

The predictions of the branching fraction at order α_s^2 (NNLO - next to next to leading order) $(3.15 \pm 0.23) \times 10^{-41}$, $(2.98 \pm 0.26) \times 10^{-42}$ and the average of experiment measured values $(3.55 \pm 0.26) \times 10^{-43}$ are in tacit agreement. An updated experimental measurement would further test this agreement, and, moreover, give stronger constraints on extensions to the SM *e.g.* Minimal Supersymmetric Standard Model⁴ and left-right symmetric models^{5,6}. The photon energy spectrum is also of great importance. At the parton level, the photon is monochromatic with energy $E \approx m_b/2$ in the b -quark rest frame. The energy is smeared by the motion of the b -quark inside the B meson and gluon emission. A measurement of the moments of this spectrum allows for a determination of the b -quark mass and of its *Fermi motion*. This information can then be used in the extraction of the CKM matrix elements $|V_{cb}|$ and $|V_{ub}|$ from inclusive semileptonic B decays⁷. A measurement of the low-energy tail of the photon spectrum is important in this context⁸.

Belle has previously measured the $B \rightarrow X_s \gamma$ branching fraction with 5.8 fb^{-1} and 140 fb^{-1} of data using semi-inclusive⁹ and fully inclusive approaches¹⁰, respectively. Other measurements include those from CLEO¹¹ and BaBar^{12,13,14}.

Here we present an update of our fully inclusive measurement¹⁰, based on a much larger dataset and with significant refinements, which includes an unfolding of detector effects on the measured spectrum that improve the measurements of the branching fraction and spectral moments, respectively. We also extend the photon energy range to $E_\gamma^{\text{c.m.s}} > 1.7 \text{ GeV}$, covering more of the spectrum than ever before, where c.m.s refers to the centre of mass system, which is equivalent to the rest frame of the $\Upsilon(4S)$.

2 Detector and Data sample

The $B \rightarrow X_s \gamma$ decay is studied using the Belle detector at the KEKB asymmetric e^+e^- storage ring¹⁵. The data consists a of sample of 604.6 fb^{-1} taken at the $\Upsilon(4S)$ resonance corresponding to $(656.7 \pm 8.9) \times 10^6 B\bar{B}$ pairs. Another 68.3 fb^{-1} sample has been taken at an energy 60 MeV below the resonance and is used to measure the non- $B\bar{B}$ background. Throughout this manuscript, we refer to these data samples as the ON and OFF samples, respectively.

The Belle detector is a large-solid-angle magnetic spectrometer described in detail elsewhere¹⁶. The main component relevant for this analysis is the electromagnetic calorimeter (ECL) made of 16.2 radiation lengths long CsI(Tl) crystals. The photon energy resolution is about 2% for the energy range relevant in this analysis.

3 Analysis Strategy

The strategy to extract the signal $B \rightarrow X_s \gamma$ spectrum is to collect all high-energy photons, vetoing those originating from π^0 and η decays to two photons. The contribution from continuum $e^+e^- \rightarrow q\bar{q}$ ($q = u, d, s, c$) and QED type events is subtracted using the OFF sample. The remaining backgrounds from $B\bar{B}$ events are subtracted using Monte Carlo (MC) distributions scaled by data control samples.

Photon candidates are selected from ECL clusters of 5×5 crystals in the barrel region ($-0.35 \leq \cos\theta \leq 0.70$, where θ is the polar angle with respect to the beam axis, subtended from the direction opposite the positron beam. They are required to have an energy $E_\gamma^{\text{c.m.s}}$ larger than 1.4 GeV. We require 95% of the energy to be deposited in the central 3×3 crystal array and use isolation cuts to veto photons from bremsstrahlung and interaction with matter. The center of the cluster has to be displaced from any other ECL cluster with $E > 20 \text{ MeV}$ by at least 30 cm at the surface of the calorimeter, and from any reconstructed track by 30 cm, or by 50 cm for tracks with a measured momentum above 1 GeV/c. Moreover, the angle between the photon and the highest energy lepton in the event has to be larger than 0.3 radians at the interaction point.

In the Belle detector, a non-negligible background (1%) is due to the overlap of a hadronic event with energy deposits left in the calorimeter by previous QED interactions (mainly Bhabha scattering). Such composite events are completely removed using timing information for calorimeter clusters associated with the candidate photons. The cluster timing information is stored in the raw data, and is available in the reduced format used for analysis only for data processed after the summer of 2004. This divides our data set into 253.7 fb^{-1} and 350.9 fb^{-1} samples of reprocessed data without and with timing information, respectively. To minimise composite background due to Bhabha scattering and two-photon processes that contaminate both $\Upsilon(4S)$ and continuum data samples, we veto any candidate that contains an ECL cluster with energy exceeding 1 GeV within a cone of 0.2 radians in the direction opposite our photon candidate as measured in the c.m.s frame. In the second data set only photons that are in time with the rest of the event are retained. The efficiency of this selection on signal events is larger than 99.5%. We veto candidate photons from π^0 and η decays to two photons by combining each $B \rightarrow X_s \gamma$ candidate photon with all other photons in the event. We reject the photon candidate if the likelihood of being a π^0 or η is larger than 0.1 and 0.2, respectively, these yield, on average, background suppression factors of 4 and 2, respectively. These likelihoods are determined from MC and are functions of the laboratory energy of the other photon, its polar angle θ and the mass of the two-photon system.

In order to reduce the contribution from continuum events, we use two Fisher discriminants calculated in the c.m.s frame. The first discriminant exploits the topology of $B \rightarrow X_s \gamma$ events and combines three energy flows around the photon axis. These energy flow variables are obtained using all particles, except for the photon candidate, we measure the energy in the three regions defined by $\Theta < 30^\circ$, $30^\circ \leq \Theta \leq 140^\circ$, $\Theta > 140^\circ$, where Θ is the angle of the particle to the candidate photon. The second exploits the spherical shape of $B\bar{B}$ events and is built using ten event-shape variables including Fox-Wolfram moments¹⁷ for the full event and for the partial event with the photon removed, the full- and partial-event thrusts and the angles of the thrust axis with respect to the beam and the photon direction. To optimise these selection criteria, we use a MC simulation¹⁸ containing large samples of $B\bar{B}$, $q\bar{q}$ and signal weighted according to the luminosities of the ON and OFF samples. In the optimisation step the signal MC used is generated as inclusive $B \rightarrow X_s \gamma$ and exclusive $B \rightarrow K^* \gamma$. The inclusive component X_s is defined as a resonance of spin-1 with a Breit-Wigner form and a mass of $2.4 \text{ GeV}/c^2$ and width $1.5 \text{ GeV}/c^2$. The X_s system is hadronised by JETSET and subsequently reweighted to match the prediction of the DGE

model^{21 a} with $m_b(\overline{M\overline{S}}) = 4.20 \text{ GeV}/c^2$, with the mass extending no lower than $1.18 \text{ GeV}/c^2$ to agree with the corresponding world average branching fractions³. To improve the understanding of the photon energy spectrum at low energies, the selection criteria are optimised to maximize the sensitivity to the signal in the energy bin $1.8 \text{ GeV} < E_\gamma^{\text{c.m.s}} < 1.9 \text{ GeV}$.

After these selection criteria we observe 4.15×10^6 and 0.25×10^6 photon candidates in the ON and OFF data samples, respectively.

4 Background subtraction

The spectrum measured in OFF data is scaled by luminosity to the expected number of non- $B\overline{B}$ events in ON data and subtracted. The formula used to subtract continuum background is as follows:

$$N^{B\overline{B}}(E_\gamma^{\text{c.m.s(ON)}}) = N^{\text{ON}}(E_\gamma^{\text{c.m.s(ON)}}) - \alpha \cdot \frac{\epsilon_{\text{Hadronic}}^{\text{ON}}}{\epsilon_{\text{Hadronic}}^{\text{OFF}}} \cdot \frac{\epsilon_{B \rightarrow X_s \gamma}^{\text{ON}}}{\epsilon_{B \rightarrow X_s \gamma}^{\text{OFF}}} \cdot F_N \cdot N^{\text{OFF}}(F_E E_\gamma^{\text{c.m.s(OFF)}}) \quad (1)$$

where ϵ is the efficiency of Belle's hadronic selection¹⁹ or of this analysis' ($B \rightarrow X_s \gamma$) selection criteria in continuum events at either ON resonance ($\sqrt{s} = 10.58 \text{ GeV}$) or OFF resonance ($\sqrt{s} = 10.52 \text{ GeV}$) energies, and α is the ratio of ON to OFF resonance integrated luminosity corrected for the energy difference ($\alpha = 8.7557(\pm 0.3\%)$). The factors F_E and F_N compensate for the slightly lower mean energy and multiplicity of particles in OFF compared to ON events. We find $F_N = 1.0009 \pm 0.0001$, $F_E = 1.0036 \pm 0.0001$, $\frac{\epsilon_{\text{Hadronic}}^{\text{ON}}}{\epsilon_{\text{Hadronic}}^{\text{OFF}}} = 0.9986 \pm 0.0001$, and $\frac{\epsilon_{B \rightarrow X_s \gamma}^{\text{ON}}}{\epsilon_{B \rightarrow X_s \gamma}^{\text{OFF}}} = 0.9871 \pm 0.0014$. The ON and scaled OFF spectra and their difference are shown in Fig. 1.

We then subtract the backgrounds from B decays from the obtained spectrum. Six background categories are considered: (i) photons from $\pi^0 \rightarrow \gamma\gamma$; (ii) photons from $\eta \rightarrow \gamma\gamma$; (iii) other real photons (mainly decays of ω , η' , and J/ψ , and bremsstrahlung, including the short distance radiative correction (modelled with PHOTOS²²); (iv) ECL clusters not due to single photons (mainly K_L^0 's and \bar{n} 's); (v) Electrons misidentified as photons and; (vi) beam background. The spectra of the background of photons from B -meson decays with respect to the expected signal is shown in Fig. 2, their relative contributions are also listed. The net background of this type is a factor five greater than the signal.

For each of these categories we take the predicted background from MC and scale it according to measured yields wherever possible. The inclusive $B \rightarrow \pi^0 X$ and $B \rightarrow \eta X$ spectra are measured in data using pairs of photons with well-balanced energies and applying the same ON-OFF subtraction procedure. The yields obtained in data are on average 10% larger and 5% lower for π^0 and η than MC expectations. The observed discrepancy between the measured and simulated π^0 η spectra is attributed to the branching fraction assumptions used for the generator²³. Beam background is measured using a sample of randomly triggered events and added to the $B\overline{B}$ MC.

For each selection criterion and each background category we determine the $E_\gamma^{\text{c.m.s}}$ -dependent selection efficiency in OFF-subtracted ON data and MC using appropriate control samples. We then scale the MC background sample according to the ratio of these efficiencies. The efficiencies of the π^0 and η vetoes for photons not from π^0 and η are measured in data using one photon from a reconstructed π^0 , where the other photon of the π^0 is excluded from the search over the remaining photons for the next best π^0 or η candidate (highest π^0 or η likelihood). Consequently the best formed π^0 or η candidate used in the calculation of the likelihoods is most likely a random combination, and therefore suited to measuring the effect of the vetoes. The π^0 veto efficiency is measured using a sample of photons coming from measured π^0 decays. We use partially reconstructed $D^{*+} \rightarrow D^0 \pi^+$, $D^0 \rightarrow K^- \pi^+ \pi^0$ decays where the π^0 is replaced by the candidate photon in the reconstruction. The η veto efficiency for photons from π^0 's and event-shape criteria efficiencies are measured using a π^0 anti-veto sample, which is made of photons with a π^0 likelihood larger than 0.75 (*i.e.*, no π^0 veto) and passing all other selection criteria. Other efficiencies are measured using the signal sample. Beam background is negligible after the application of the OFF time veto. In the sample of data where the veto is unavailable we scale the background according to a comparison of yields between MC and data for high energy ($E_\gamma^{\text{c.m.s}} > 2.8 \text{ GeV}$) photon candidates found in the endcaps of the ECL. This sample after continuum subtraction is a clean sample of ECL clusters from beam backgrounds.

^aIn the optimisation step the choice of signal model has a negligible effect on the measure of optimisation, suffice to say the choice of signal model should not be construed as preferential.

The ratios of data and MC efficiencies versus $E_\gamma^{\text{c.m.s}}$ are fitted using first or second order polynomials, which are used to scale the background MC. Most are found to be statistically compatible with unity. An example is the effect of the π^0 veto on photons from π^0 s that escape the veto in the partially reconstructed D^* sample, which is shown in Fig. 3.

An exception is the efficiency of the requirement that 95% of the energy be deposited in the central nine cells of the 5×5 cluster, which is found to be poorly modelled by our MC for non-photon backgrounds. We estimate the efficiency for data using a sample of candidate photons in OFF-subtracted ON data after subtracting the known contribution from real photons. This increases the yield of background (iv) by 50%. The yield from the six background categories, after having been properly scaled by the above described procedures, are subtracted from the OFF-subtracted spectrum. The result is shown in Fig. 1. After these subtractions the yield in the spectrum above the endpoint of B decays is compatible with zero, 1245 ± 4349 candidates.

5 Correction for Acceptance

To measure the branching fraction and the moments we correct the raw spectrum using a three step procedure: (i) divide by the efficiency of the selection criteria *i.e.* the probability of a photon candidate passing cuts given a cluster has been found in the ECL, as a function of the measured energy in the c.m.s frame; (ii) perform an unfolding procedure based on the Singular Value Decomposition (SVD) algorithm²⁴, which maps the spectrum from measured energy to true energy thereby undoing the distortion caused by the ECL; (iii) divide by the efficiency of detection *i.e.* the probability that a photon originating at the interaction point is reconstructed in the ECL, as a function of the true energy. Data are divided into 50 MeV wide bins. Step (ii), which was not performed in our previous analysis, is essential for a consistent extraction of partial branching fractions and moments as a function of lower energy thresholds. The unfolding matrix, derived from signal MC, is calibrated to data using the results of a study of radiative di-muon events, which gave the ECL response in data and MC in an energy and acceptance range consistent with our analysis. We use five signal models: KN²⁵, BLNP^{26,27}, DGE²⁰, BBU²⁸ and GG²⁹. Values of the parameters of the signal model used in the signal MC are derived from fits to the signal spectrum shown in Fig 1. The two error bars for each point show the statistical and the total error, including the systematic error which is correlated among the points. In order to obtain the total $B \rightarrow X_s \gamma$ branching fraction we apply corrections for the contribution from Cabibbo suppressed $B \rightarrow X_d \gamma$ decays. The ratio of the $B \rightarrow X_s \gamma$ and $B \rightarrow X_d \gamma$ branching fractions is assumed to be $R_{d/s} = (4.0 \pm 0.4)\%$ ³⁰. We apply corrections to derive the measurements in the B -meson rest frame, using a toy MC approach. We generate photon 4-momentum in the rest frame of the B -meson using signal models referred to earlier, and generate B -meson 4-momentum using their known fixed energy and $1 - \cos\theta^2$ distribution in the c.m.s. Repeating this exercise many times yields photon energy spectra in the rest frame of the B -meson and the c.m.s, from which we extract corrections used to yield measurements in the B -meson frame. The correction is derived as a mean over all signal models while the root-mean-square is assigned as the uncertainty. After correcting for the acceptance we derive distributions of the partial branching fraction, first moment (mean) and second central moment (variance) of $B \rightarrow X_s \gamma$ as measured in the c.m.s and B rest frame for lower energy thresholds as shown in Fig. 1. In the range from 1.7 to 2.8 GeV in the rest frame of the B -meson, we obtain a partial branching fraction, and the first two moments of the energy spectrum:

$$\mathcal{B}(B \rightarrow X_s \gamma) = (3.31 \pm 0.19 \pm 0.37 \pm 0.01) \times 10^{-4} \quad (2)$$

$$\langle E_\gamma \rangle = 2.281 \pm 0.032 \pm 0.053 \pm 0.002 \text{ GeV} \quad (3)$$

$$\langle E_\gamma^2 \rangle - \langle E_\gamma \rangle^2 = 0.0396 \pm 0.0156 \pm 0.0214 \pm 0.0012 \text{ GeV}^2, \quad (4)$$

where the errors are statistical, systematic and from the boost correction, respectively.

6 Results

The full results, the systematic error budget and correlation coefficients for five lower energy thresholds ($E_\gamma^B = 1.7, 1.8, 1.9, 2.0, 2.1$ GeV) are listed in Table 1. The total systematic error is derived from a sum in quadrature over all sources. We vary the number of $B\bar{B}$, the ON to OFF ratio of integrated luminosities and the correction factors applied to the OFF data photon candidates and assign the observed variation as the systematic associated with continuum subtraction. The parameters of the correction functions

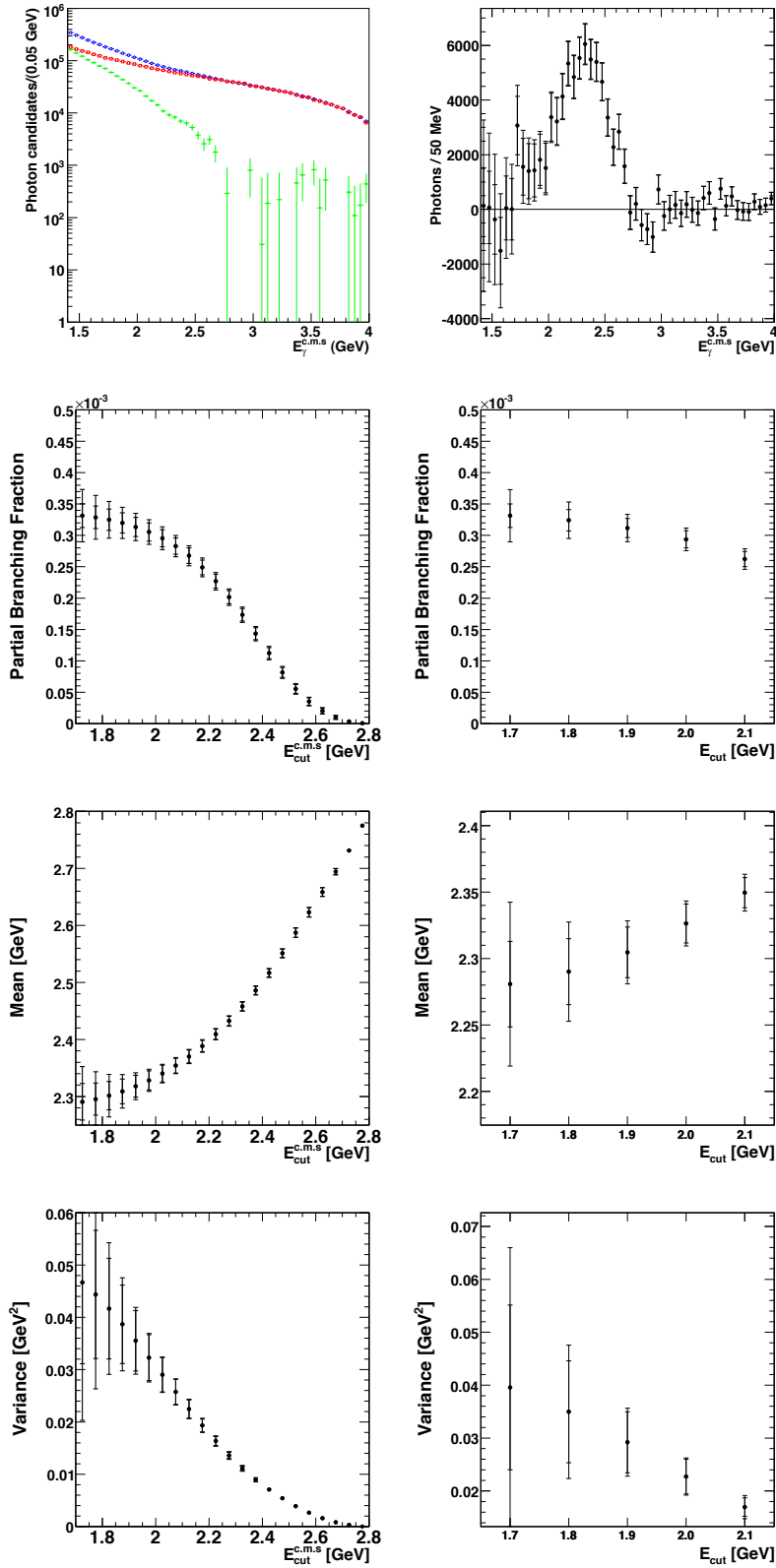


Figure 1: (1ST ROW-left) ON data (open circle), scaled OFF data (open square) and continuum background subtracted (filled circle) photon energy spectra of candidates in the c.m.s frame. (1ST ROW-right) The extracted photon energy spectrum of $B \rightarrow X_{s,d}\gamma$. The two error bars show the statistical and total errors. (2ND ROW) Partial branching fractions, (3RD ROW) mean, and (4TH ROW) variance of $B \rightarrow X_s\gamma$ in the (LEFT) c.m.s and (RIGHT) and in the rest frame of the B -meson for lower energy thresholds. The two error bars show the statistical and total errors.

Table 1: The measurements and correlation coefficients of the branching fraction, mean and variance of the photon energy spectrum for various lower energy thresholds, E_γ^B , as measured in the rest frame of the B -meson and the contributions to the systematic uncertainty.

E_γ^B [GeV]	$B(B \rightarrow X_s \gamma) (10^{-4})$					$\langle E_\gamma \rangle$ (GeV)					$\Delta E_\gamma^2 \equiv \langle E_\gamma^2 \rangle - \langle E_\gamma \rangle^2$ (GeV ²)				
	1.7	1.8	1.9	2.0	2.1	1.7	1.8	1.9	2.0	2.1	1.7	1.8	1.9	2.0	2.1
Value	3.31	3.24	3.12	2.94	2.62	2.281	2.290	2.305	2.326	2.350	0.0396	0.0350	0.0292	0.0227	0.0170
\pm statistical	0.19	0.17	0.15	0.14	0.12	0.032	0.025	0.019	0.015	0.011	0.0156	0.0096	0.0058	0.0033	0.0017
\pm systematic	0.37	0.24	0.16	0.12	0.10	0.053	0.028	0.014	0.007	0.005	0.0214	0.0081	0.0027	0.0009	0.0006
\pm boost	0.01	0.01	0.02	0.02	0.05	0.002	0.002	0.004	0.005	0.006	0.0012	0.0005	0.0008	0.0009	0.0012
Systematic Uncertainties															
Continuum	0.18	0.11	0.08	0.07	0.07	0.030	0.016	0.008	0.004	0.002	0.0101	0.0040	0.0012	0.0004	0.0004
Selection	0.20	0.15	0.11	0.08	0.06	0.023	0.012	0.006	0.003	0.001	0.0114	0.0039	0.0014	0.0005	0.0001
π^0/η	0.07	0.05	0.04	0.02	0.01	0.012	0.006	0.003	0.002	0.001	0.0075	0.0023	0.0007	0.0003	0.0001
Other B	0.24	0.13	0.06	0.02	0.01	0.033	0.016	0.007	0.002	0.000	0.0124	0.0051	0.0017	0.0004	0.0000
Beam	0.02	0.02	0.01	0.01	0.01	0.001	0.001	0.000	0.000	0.000	0.0006	0.0003	0.0001	0.0000	0.0000
resolution	0.01	0.01	0.02	0.02	0.03	0.006	0.005	0.005	0.004	0.004	0.0009	0.0006	0.0005	0.0004	0.0004
Unfolding	0.01	0.00	0.00	0.01	0.01	0.002	0.001	0.001	0.001	0.002	0.0014	0.0008	0.0006	0.0003	0.0001
Model	0.03	0.02	0.01	0.00	0.00	0.005	0.003	0.002	0.001	0.000	0.0014	0.0006	0.0002	0.0000	0.0000
γ Detection	0.03	0.02	0.01	0.00	0.00	0.005	0.003	0.002	0.001	0.000	0.0014	0.0006	0.0002	0.0000	0.0000
$B \rightarrow X_d \gamma$	0.01	0.01	0.01	0.01	0.01	0.000	0.000	0.000	0.000	0.000	0.0001	0.0000	0.0000	0.0000	0.0000
Correlation coefficients (combined statistical and systematic)															
	ΔB					$\langle E_\gamma \rangle$					ΔE_γ^2				
	1.7	1.8	1.9	2.0	2.1	1.7	1.8	1.9	2.0	2.1	1.7	1.8	1.9	2.0	2.1
1.7	1.000	0.959	0.811	0.699	0.604	0.455	0.322	0.114	-0.083	-0.142	0.848	0.857	0.722	0.528	0.445
1.8		1.000	0.942	0.839	0.720	0.269	0.129	-0.073	-0.251	-0.291	0.807	0.878	0.822	0.678	0.568
ΔB 1.9			1.000	0.939	0.823	0.031	-0.107	-0.291	-0.442	-0.464	0.680	0.817	0.869	0.814	0.700
2.0				1.000	0.959	-0.004	-0.143	-0.332	-0.494	-0.531	0.612	0.767	0.863	0.870	0.846
2.1					1.000	0.023	-0.107	-0.296	-0.476	-0.548	0.546	0.689	0.795	0.848	0.910
1.7						1.000	0.967	0.838	0.636	0.489	0.342	0.149	-0.094	-0.252	-0.174
1.8							1.000	0.946	0.793	0.645	0.155	-0.047	-0.290	-0.431	-0.329
$\langle E_\gamma \rangle$ 1.9								1.000	0.942	0.824	-0.066	-0.280	-0.516	-0.640	-0.530
2.0									1.000	0.954	-0.230	-0.438	-0.660	-0.779	-0.696
2.1										1.000	-0.252	-0.438	-0.642	-0.777	-0.751
1.7											1.000	0.945	0.782	0.581	0.497
1.8												1.000	0.935	0.782	0.677
ΔE_γ^2 1.9													1.000	0.946	0.840
2.0														1.000	0.942
2.1															1.000

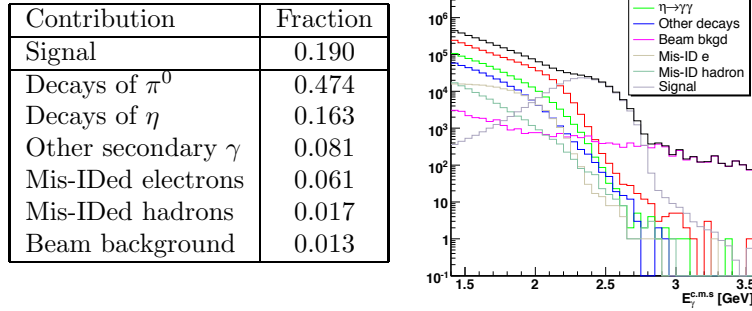


Figure 2: Relative contributions of the $B\bar{B}$ backgrounds after selection in the $1.7 < E_{\gamma}^{c.m.s}/(\text{GeV}) < 2.8$ range. The spectra of photons from B -meson decays passing selection criteria as predicted using a MC sample.

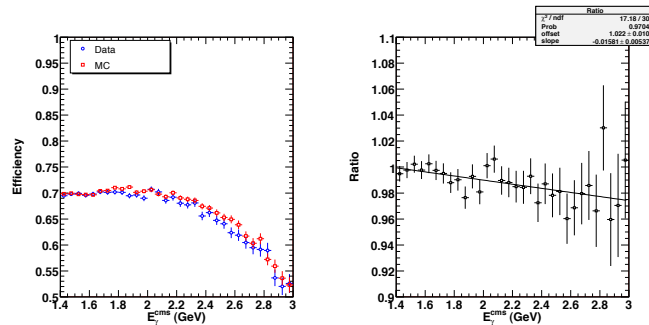


Figure 3: (LEFT) The π^0 veto efficiency in the partially reconstructed D^* sample for both Data (circles) and MC (squares) and (RIGHT) their ratio fitted with a first order polynomial.

applied to the π^0 and η yields are varied taking into account their correlations. As we do not measure the yields of photons from sources other than π^0 's and η 's in $B\bar{B}$ events, we independently vary the expected yields of these additional sources by $\pm 20\%$. For the model dependence in correcting for the acceptance we use four signal models in addition to the default model, and assign the maximum deviation from the default as the uncertainty. The error on the photon detection efficiency in the ECL is measured to be 2% using radiative μ -pair events, and also affects the estimation of photons from $B\bar{B}$. For the uncertainties related to the unfolding procedure, we vary the effective rank parameter up and down by one in the SVD algorithm.

7 Summary

In conclusion, we have measured the branching fraction and photon energy spectrum of $B \rightarrow X_s \gamma$ in the energy range $1.7 \text{ GeV} \leq E_{\gamma}^{c.m.s} \leq 2.8 \text{ GeV}$ in a fully inclusive way. For the first time 97% of the spectrum is measured³¹ allowing the theoretical uncertainties to be reduced to a very low level. Using 605 fb^{-1} of data taken at the $\Upsilon(4S)$ and 68 fb^{-1} taken below the resonance, we obtain $\mathcal{B}(B \rightarrow X_s \gamma : E_{\gamma}^B > 1.7 \text{ GeV}) = (3.31 \pm 0.19 \pm 0.37 \pm 0.01) \times 10^{-4}$, where the errors are statistical, systematic and due to the boost correction, respectively. This result is in agreement with the latest theoretical calculations^{1,2,20}. The results can be used to place constraints on new physics³² and determine SM parameters such as the b -quark mass³³.

Acknowledgments

We thank the KEKB group for excellent operation of the accelerator, the KEK cryogenics group for efficient solenoid operations, and the KEK computer group and the NII for valuable computing and SINET3 network support. We acknowledge support from MEXT and JSPS (Japan); ARC, DEST and A.J. Slocum (Australia); NSFC (China); DST (India); MOEHRD, KOSEF and KRF (Korea); KBN

(Poland); MES and RFAAE (Russia); ARRS (Slovenia); SNSF (Switzerland); NSC and MOE (Taiwan); and DOE (USA).

References

1. M. Misiak *et al.*, Phys. Rev. Lett. **98** (2007) 022002
2. T. Becher and M. Neubert, Phys. Rev. Lett. **98**, 022003 (2007)
3. W. M. Yao *et al.* [Particle Data Group], J. Phys. G **33**, 1 (2006).
4. S. Bertolini, F. Borzumati, A. Masiero and G. Ridolfi, Nucl. Phys. B **353**, 591 (1991).
5. P. L. Cho and M. Misiak, Phys. Rev. D **49**, 5894 (1994)
6. K. Fujikawa and A. Yamada, Phys. Rev. D **49**, 5890 (1994).
7. E. Barberio *et al.* [Heavy Flavor Averaging Group (HFAG) Collaboration], arXiv:0704.3575 [hep-ex].
8. I. Bigi and N. Uraltsev, Int. J. Mod. Phys. A **17**, 4709 (2002)
9. K. Abe *et al.* [Belle Collaboration], Phys. Lett. B **511**, 151 (2001)
10. P. Koppenburg *et al.* [Belle Collaboration], Phys. Rev. Lett. **93**, 061803 (2004)
11. S. Chen *et al.* [CLEO Collaboration], Phys. Rev. Lett. **87**, 251807 (2001)
12. B. Aubert *et al.* [BABAR Collaboration], Phys. Rev. D **72**, 052004 (2005)
13. B. Aubert *et al.* [BaBar Collaboration], Phys. Rev. Lett. **97**, 171803 (2006)
14. B. Aubert *et al.* [BABAR Collaboration], Phys. Rev. D **77**, 051103 (2008)
15. S. Kurokawa and E. Kikutani, Nucl. Instrum. Methods Phys. Res. Sect., **A499**, 1 (2003), and other papers included in this Volume.
16. Belle Collaboration, A. Abashian *et al.*, Nucl. Instrum. Meth. A **479**, 117 (2002).
17. G. C. Fox and S. Wolfram, Phys. Rev. Lett. **41**, 1581 (1978).
18. R. Brun, R. Hagelberg, M. Hansroul and J. C. Lassalle, "Geant: Simulation Program For Particle Physics Experiments. UserGuide And Reference Manual,"
19. B. Casey, <http://www.phys.hawaii.edu/~casey/thesis/> (2001)
20. J. R. Andersen and E. Gardi, JHEP **0701**, 029 (2007)
21. J. R. Andersen and E. Gardi, JHEP **0506**, 030(2005)
22. E. Barberio and Z. Was, Comput. Phys. Commun. **79**, 291 (1994).
23. D. J. Lange, Nucl. Instrum. Meth. A **462**, 152 (2001).
24. A. Hocker and V. Kartvelishvili, Nucl. Instrum. Meth. A **372**, 469 (1996)
25. A. L. Kagan and M. Neubert, Eur. Phys. J. C **7**, 5 (1999)
26. B. O. Lange, M. Neubert and G. Paz, B decay spectra," JHEP **0510**, 084 (2005)
27. B. O. Lange, M. Neubert and G. Paz, Phys. Rev. D **72**, 073006 (2005)
28. D. Benson, I. I. Bigi and N. Uraltsev, Nucl. Phys. B **710**, 371 (2005)
29. P. Gambino and P. Giordano, Work in progress (2008)
30. T. Hurth, E. Lunghi and W. Porod, Nucl. Phys. B **704**, 56 (2005)
31. O. Buchmuller and H. Flacher, Phys. Rev. D **73**, 073008 (2006)
32. O. Buchmuller *et al.*, Phys. Lett. B **657**, 87 (2007)
33. C. Schwanda *et al.* [Belle Collaboration], arXiv:0803.2158 [hep-ex].

New Results on Leptonic B meson decays at *BABAR*

Kim Hojeong

Stanford Linear Accelerator Center, 2575 Sand Hill Road, Menlo Park, CA, 94025, USA

We present selected new results on leptonic B meson decays from the *BABAR* experiment: searches for the decays $B^0 \rightarrow \ell^+\ell^-$, $B^+ \rightarrow \ell^+\nu$ and $B^0 \rightarrow \ell^+\tau^-$, and $B \rightarrow K\nu\bar{\nu}$, where $\ell = e$ or μ ¹. We observe no evidence for these decays and set upper limits on their branching fractions.

1 Introduction

Leptonic B meson decays provide an important tool to investigate the Standard Model (SM) and physics beyond the SM. They are highly suppressed in the SM, because they involve a $b \rightarrow d$ transition, require an internal quark annihilation, and there are also helicity suppression for $B^0 \rightarrow \ell^+\ell^-$ and $B^+ \rightarrow \ell^+\nu$ modes, and because the flavor-changing neutral-currents are forbidden at the tree level for $B \rightarrow K\nu\bar{\nu}$ mode. The decay rates can be enhanced or reduced when heavy virtual particles like Higgs or super-symmetric² (SUSY) particles replace the W boson or show up at higher orders in loop diagrams. Constraints on these decays can provide information on important SM parameters, such as B meson decay constant. They have identifiable final states with low multiplicity, but they are mostly below our sensitivity. These decay modes will play an important role at the future colliders, such as a Super-B factory, ILC, and LHC (for muon modes).

The analyses described in this paper use data recorded with the *BABAR* detector at the PEP-II asymmetric energy e^+e^- storage rings. A detailed description of the *BABAR* detector can be found elsewhere³. A full *BABAR* Monte Carlo (MC) simulation using GEANT4⁴ is used to evaluate signal efficiencies and to identify and study background sources.

Table 1: Result of $B^0 \rightarrow \ell^+ \ell^-$ analysis. Efficiency (ϵ), number of signal events (N_{sig}) from ML fit, and 90% confidence level upper limit on the branching fraction (UL(BF)) for the three leptonic decays $B^0 \rightarrow e^+ e^-$, $B^0 \rightarrow \mu^+ \mu^-$, and $B^0 \rightarrow e^\pm \mu^\mp$ are shown.

	ϵ (%)	N_{sig}	UL(BF) $\times 10^{-8}$
$B^0 \rightarrow e^+ e^-$	16.6 ± 0.3	0.6 ± 2.1	11.3
$B^0 \rightarrow \mu^+ \mu^-$	15.7 ± 0.2	-4.9 ± 1.4	5.2
$B^0 \rightarrow e^\pm \mu^\mp$	17.1 ± 0.2	1.1 ± 1.8	9.2

2 $B^0 \rightarrow \ell^+ \ell^-$

The leptonic decays $B^0 \rightarrow \ell^+ \ell^-$ are studied using 383.6×10^6 $B\bar{B}$ events. The SM prediction on the branching fractions (BFs) are 1.9×10^{-15} (8.0×10^{-11}) for the $e^+ e^-$ ($\mu^+ \mu^-$) mode, and the $B^0 \rightarrow e^\pm \mu^\mp$ decay is forbidden. The best upper limits (UL) on the BFs have been set at the order of 10^{-8} by the BABAR⁵ experiment for $e^+ e^-$ and $e^\pm \mu^\mp$ modes using 111fb^{-1} , and by CDF⁶ experiment for $\mu^+ \mu^-$ mode with 2fb^{-1} .

The B^0 candidate is reconstructed by combining two oppositely charged tracks originating from a common vertex. We use two kinematic quantities: $m_{ES} = \sqrt{(E_{\text{beam}}^*)^2 - (\sum_i \mathbf{p}_i^*)^2}$ and $\Delta E = \sum_i \sqrt{m_i^2 + (\mathbf{p}_i^*)^2} - E_{\text{beam}}^*$, where E_{beam}^* is the beam energy in the CM frame, \mathbf{p}_i^* and m_i are the momenta in the CM frame and the masses of the daughter particles i of B meson. E_{beam}^* is used instead of the measured B meson energy in the CM frame because E_{beam}^* is more precisely known. For correctly reconstructed B^0 mesons, the m_{ES} distribution has a maximum at the B^0 mass with a standard deviation of about $2.5 \text{MeV}/c^2$ and the ΔE distribution has a maximum near zero with a standard deviation of about 25MeV .

Stringent requirements on particle identification⁷ are made to reduce the contamination from misidentified hadrons and leptons. We retain about 93% (73%) of the electrons (muons), with a misidentification rate for pions of less than about 0.1% (3%). The main background are continuum processes where $e^+ e^- \rightarrow f\bar{f}$, ($f = u, d, s, c, \tau$). A Fisher discriminant⁸ (\mathcal{F}) is constructed, using their different event topology with respect to that of the signal events.

A maximum likelihood (ML) fit is performed based on the variables m_{ES} , ΔE and \mathcal{F} . The results are summarized in Table 1. The event and background *sPlot*⁹ distributions are shown in Figure 1. Using a Bayesian approach, a 90% confidence level (CL) UL on the BF is calculated. The systematic uncertainties are included as a Gaussian into the likelihood calculation.

3 $B^+ \rightarrow \ell^+ \nu$ and $B^0 \rightarrow \ell^+ \tau^-$

We present searches for the decays $B^+ \rightarrow \ell^+ \nu$ and the lepton flavor violating decays $B^0 \rightarrow \ell^+ \tau^-$, where $\ell = e$ or μ using 378×10^6 $B\bar{B}$ events. The SM predictions of the BFs are of the order of 10^{-11} (10^{-7}) for $B^+ \rightarrow e^+ \nu$ ($B^+ \rightarrow \mu^+ \nu$), and $B^0 \rightarrow \ell^+ \tau^-$ modes are forbidden. The UL on the BFs have been measured by BABAR¹⁰, Belle¹¹, and CLEO¹². The best published limits are from Belle for $B^+ \rightarrow \ell^+ \nu$, at the order of 10^{-6} with 253fb^{-1} , and CLEO for $B^0 \rightarrow \ell^+ \tau^-$, at the order of $10^{-4 \sim -5}$ with 9.6×10^6 $B\bar{B}$ events.

We fully reconstruct one of the two B mesons (B_{tag}) in the event: $B_{tag} \rightarrow D^{(*)} X_{had}$, X_{had} decays in combinations of K 's and π 's. This method has not been used for searches for these modes. To suppress the continuum backgrounds, we use their different event topologies with

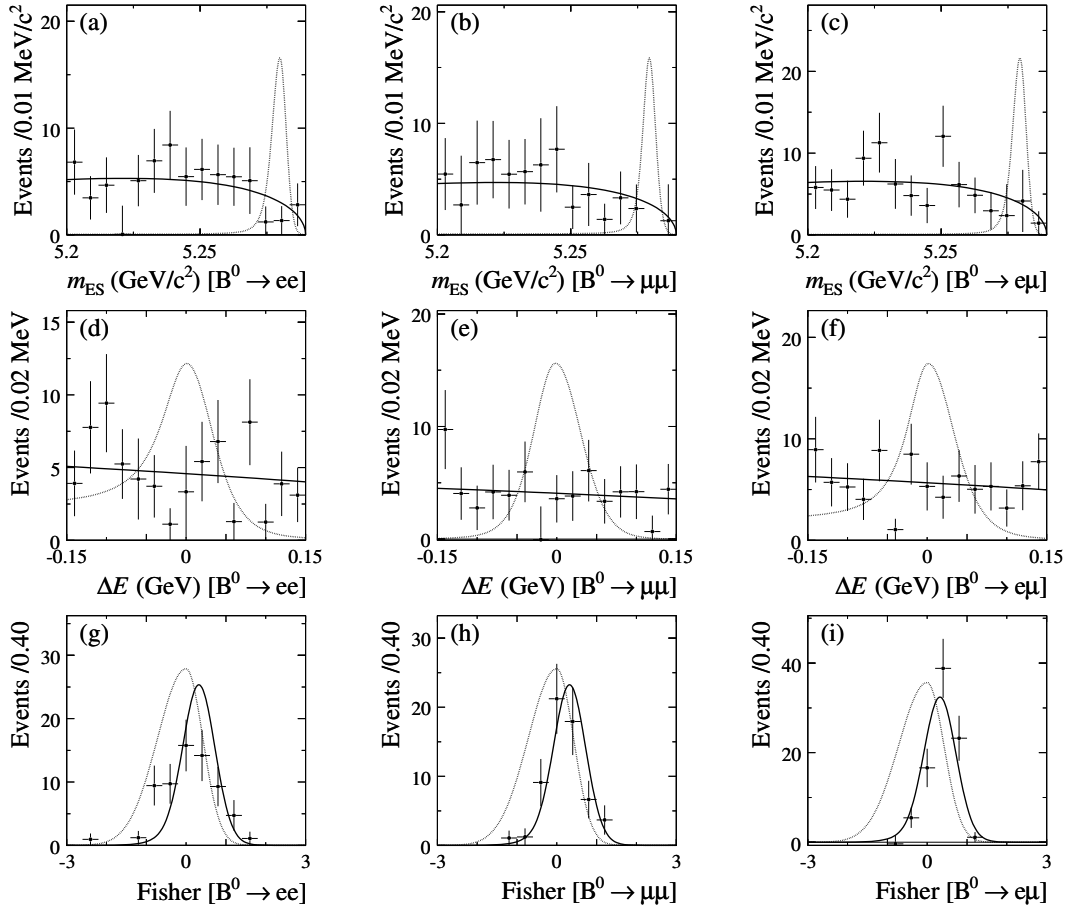


Figure 1: The distributions of events in m_{ES} (a,b,c), ΔE (d,e,f) and \mathcal{F} (g,h,i) for $B^0 \rightarrow e^+e^-$ (left), $B^0 \rightarrow \mu^+\mu^-$ (middle), $B^0 \rightarrow e^\pm\mu^\mp$ (right) are shown. The points with error bars are data. The overlaid solid curve in each plot is the background *sPlot* distribution obtained by maximizing the likelihood not using the information from the corresponding component. The dotted line, representing the signal probability density function with an arbitrary scaling, indicates where the signal is expected.

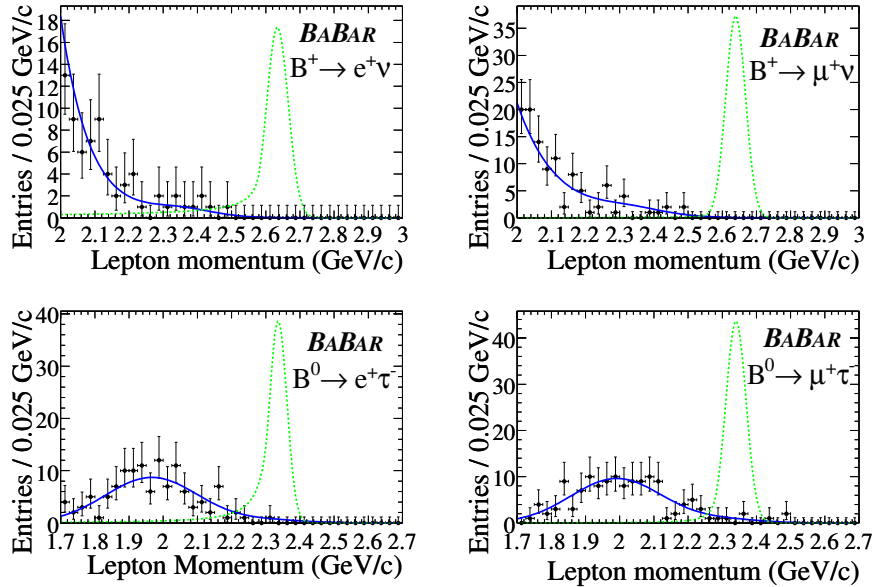


Figure 2: The unbinned maximum likelihood fits and the distributions of the lepton momentum for $B^+ \rightarrow \ell^+ \nu$ and $B^0 \rightarrow \ell^+ \tau^-$ analyses. The points with error bars are data, the solid line represents the ML fit. The dashed line, representing the signal probability density function with an arbitrary scaling, indicates where the signal is expected.

respect to that of the signal events. After all selection criteria are applied, it results in a yield of approximately 2500 (2000) correctly reconstructed B^+ (B^0) candidates per fb^{-1} of data. This hadronic tagging method yields lower statistics than other methods but it provides an almost background-free environment.

All particles not used in the B_{tag} reconstruction are included in the reconstruction of the signal B meson. From the two-body kinematics, we expect a mono-energetic lepton in the signal B rest frame: lepton momentum (p^*) of 2.64 (2.34) GeV/c for the $B^+ \rightarrow \ell^+ \nu$ ($B^0 \rightarrow \ell^+ \tau^-$) modes.

We reconstruct τ in the following modes: $e^- \bar{\nu}_e \nu_\tau$, $\mu^- \bar{\nu}_\mu \nu_\tau$, $\pi^- \nu_\tau$, $\pi^- \pi^0 \nu_\tau$, $\pi^- \pi^0 \pi^0 \nu_\tau$, and $\pi^- \pi^- \pi^+ \nu_\tau$. The second highest momentum track in the event excluding the B_{tag} daughters is assumed to be a τ daughter, and is required to have a charge opposite to the primary signal lepton.

The signal yields are extracted from unbinned ML fits to the signal lepton momentum distributions, as measured in the signal B rest frame. The fits are restricted to the ranges in p^* shown in Fig. 2. Using a Bayesian approach, a 90% CL UL on the BF is determined. The dominant systematic uncertainties are due to the fitting procedure and the determination of B_{tag} efficiencies. The total uncertainty is between 10 and 16% depending on the modes. The uncertainties are incorporated into the final results by varying the BF assumption by its uncertainty when integrating likelihood for the 90% CL UL. The results are summarized in Table 2.

4 $B \rightarrow K \nu \bar{\nu}$

The $B \rightarrow K \nu \bar{\nu}$ decays are studied using 319 fb^{-1} of data. The SM prediction of this mode¹³ is $(3.8 \pm 1.2) \times 10^{-6}$ and the best published UL is at 1.4×10^{-5} from Belle¹⁴ with $535 \times 10^6 B\bar{B}$ events.

Table 2: Result of $B^+ \rightarrow \ell^+\nu$ and $B^0 \rightarrow \ell^+\tau^-$ analyses. The efficiency (ϵ), number of signal events (N_{sig}) and 90% CL UL on the BF (UL(BF)) for the decay modes are shown.

	$\epsilon (\times 10^{-5})$	N_{sig}	UL(BF) $\times 10^{-6}$
$B^+ \rightarrow e^+\nu$	135 ± 4	-0.07 ± 0.03	5.2
$B^+ \rightarrow \mu^+\nu$	120 ± 4	-0.11 ± 0.05	5.6
$B^0 \rightarrow e^+\tau^-$	32 ± 2	0.02 ± 0.01	28
$B^0 \rightarrow \mu^+\tau^-$	27 ± 2	0.01 ± 0.01	22

We reconstruct one of the two B mesons in the event, where it decays semileptonically: $B^+ \rightarrow D^{(*)0}\ell^+\nu$. Compared to hadronic tagging method used in $B^+ \rightarrow \ell^+\nu$ and $B^0 \rightarrow \ell^+\tau^-$ analyses, this semileptonic tagging method yields higher statistics with more background.

A multivariate classifier, the Random Forest (RF) tool from StatPatternRecognition¹⁵ is used to optimize signal separation from background. Several regions of the parameter space (terminal leaf size, maximum number of input variables randomly selected for decision splits) are explored with the RF classifier. We use the Punzi Figure of Merit¹⁶, $S/(N_\sigma/2 + \sqrt{b})$, where s is signal, b is background and N_σ is the sigma level of discovery (we take $N_\sigma = 3$), and found the optimal Punzi Figure of Merit with a terminal leaf size of 35 events, after growing 100 decision trees, and sampling on at most 20 variables. The variables include number of tracks in the event (excluding tracks from the B_{tag} reconstruction), transverse momentum of tracks, event topology variables, missing energy in the event, total energy in the event, total energy deposit in the detector that are not associated with any charged or neutral particles.

The signal box is defined in the 2-dimensional space of D^0 mass and the RF output, which is blinded until we finish with all selections and estimations. The RF output ranges between 0 and 1. The signal box is RF output bigger than 0.82 and near D^0 mass peak which varies depends on the D modes. We estimate the background level in the signal box using MC events as well as data outside of the signal box.

While 30.71 ± 10.71 events are expected 38 events are observed as shown in Figure 3. The systematic uncertainties, which are estimated using double tag events, in where both B mesons decay semileptonically, are incorporated in the UL BF calculation. We set 90% UL BF at 4.2×10^{-5} , using a modified frequentist method¹⁷.

5 Summary

New leptonic B meson decays from BABAR are presented: $B^0 \rightarrow \ell^+\ell^-$, $B^+ \rightarrow \ell^+\nu$, $B^0 \rightarrow \ell^+\tau^-$ and $B \rightarrow K\nu\bar{\nu}$ decays. We have not observed signal and set upper limits on all of these decays. With much more statistics from Super-B factory or ILC, exploiting the hadronic tagging method may be powerful. The leptonic B meson decays will provide us important information on nature with more data.

References

1. Throughout this paper, decay modes imply also their charge conjugations.
2. K.S. Badu and C.F. Kolda, *Phys. Rev. Lett.* **84**, 228 (2000); S. R. Choudhury and N. Gaur, *Phys. Lett. B* **451**, 86 (1999); P.H. Chankowski and L. Slawianowska, *Phys. Rev.*

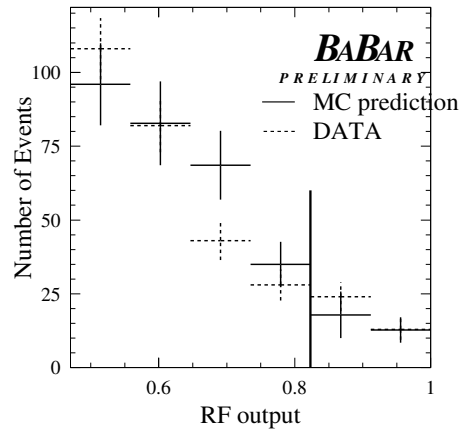


Figure 3: The output of the Random Forest for $B \rightarrow K\nu\bar{\nu}$ analysis. The right side of the black line is the signal box. The dashed line is data and the solid line is expected background from MC.

- D **63**, 054012 (2001); C. Bobeth *et al.*, *Phys. Rev. D* **64**, 074014 (2001).
3. B. Aubert *et al.*, [BABAR Collaboration], *Nucl. Instrum. Methods A* **479**, 1 (2002).
 4. S. Agostinelli *et al.*, *Nucl. Instrum. Methods A* **506**, 250 (2003).
 5. B. Aubert *et al.*, [BABAR Collaboration], *Phys. Rev. Lett.* **94**, 221803 (2005).
 6. T. Aaltonen *et al.*, [CDF Collaboration], arXiv:hep-ex/0712.1708.
 7. See for instance B. Aubert *et al.*, [BABAR Collaboration], *Phys. Rev. D* **66**, 032003 (2002).
 8. R.A. Fisher, *Annals Eugen.* **7**, 179 (1936).
 9. M. Pivk and F.R. Le Diberder, *Nucl. Instrum. Methods A* **555**, 356 (2005).
 10. B. Aubert *et al.*, [BABAR Collaboration], *Phys. Rev. Lett.* **92**, 221803 (2004).
 11. N. Satoyama *et al.*, [BELLE Collaboration], *Phys. Lett. B* **647**, 67 (2007).
 12. M. Artuso *et al.*, [CLEO Collaboration], *Phys. Rev. Lett.* **75**, 785 (1995).
 13. G. Buchalla, G. Iliesiu and G. Isidori, *Phys. Rev. D* **63**, 014015 (2001).
 14. K.F. Chen *et al.*, proceedings for Flavor Physics & CP Violation Conference, Bled, 2007 (arXiv:0708.4089).
 15. StatPatternRecognition: A C++ Package for Statistical Analysis of High energy Physics Data, I.Narsky arXiv:physics/0507143v1 [physics.data-an].
 16. G. Punzi, *Sensitivity of Searches for New Signals and Its Optimization*, Proceedings of Phystat 2004, 79-83.
 17. R. Barlow, *A Calculator for Confidence Intervals*, *Comput. Phys. Commun.* **149**, 97 (2002).

B-hadron lifetimes and rare decays at Tevatron

N. Parua

*Department of Physics, Indiana University, Swain Hall West
Bloomington, Indiana, USA*

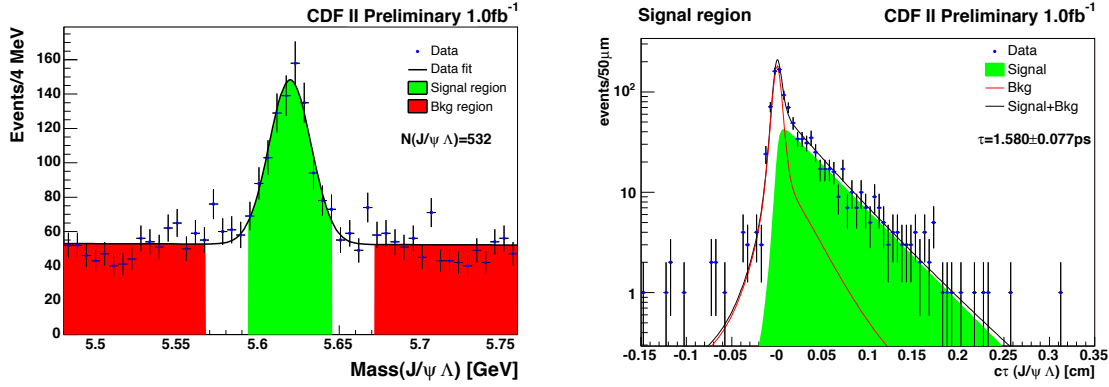
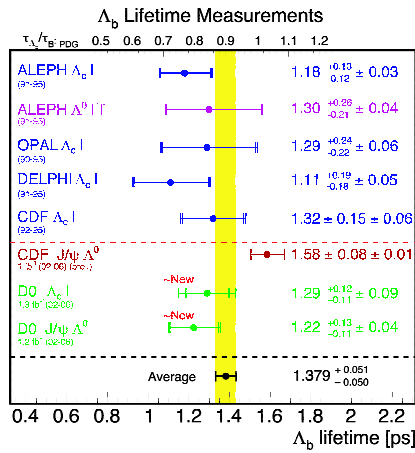
Here we present most recent results on the measurements of b-hadron lifetimes, and rare decays using data collected by both CDF and DØ experiments at Fermilab Tevatron. With large dataset collected by both experiments, most stringent limits on some of the rare decays are set.

1 Introduction

Accelerator division at Fermilab Tevatron has so far done an excellent job in delivering large amount of data. Both CDF, and DØ experiments have accumulated more than $3 fb^{-1}$ of data (at the time of the conference). A large number of measurements of b-hadron lifetimes, and rare decays are performed by these experiments. b-physics program at Tevatron is complementary to the one at B factories, where clear understanding of B^0 , and B^+ has been achieved. Although $p\bar{p}$ collision environment is not as clean, Tevatron enjoys having high $b\bar{b}$ production cross section, high integrated luminosity, and the possibility of producing heavier b-hadrons, thus a rich b-physics program.

2 Measurement of lifetimes

Lifetime measurement of b hadrons serve as a tool to understand the interaction between heavy and light quarks. Theoretical model known as Heavy Quark Effective Theory (HQET) ¹, considers in the leading order, all light quarks as spectator and predicts all b hadrons having same lifetime. Up to about 10% difference between lifetimes of b-hadrons is predicted by HQET originating from the higher order corrections that are proportional to $1/m_b^2$. In order to measure lifetime of b hadron experimentally first we determine the distance traveled by the b hadron in the plane transverse to the beam direction, and correct it for Lorentz boost. We then define


 Figure 1: Λ_b mass (left), and Proper Decay Length distribution for $\Lambda_b \rightarrow J/\psi\Lambda$ in the signal region (right).

 Figure 2: Status of $\tau(\Lambda_b)$ measurement.

proper decay length as

$$\lambda = \frac{L_{xy}}{(\beta\gamma)_T^B} = L_{xy} \frac{cM_B}{p_T} \quad (1)$$

here $(\beta\gamma)_T^B$ and M_B are the transverse boost and the mass of the b hadron. Finally the lifetime is obtained by performing a simultaneous unbinned maximum likelihood fit to the mass and proper decay length. Both CDF and DØ reported measurement of Λ_b lifetime in exclusive decay channel $\Lambda_b \rightarrow J/\psi(\rightarrow \mu^+\mu^-)\Lambda(\rightarrow p\pi)$. Figure 1 shows proper decay length distribution for Λ_b decay at CDF using 1.0 fb^{-1} of data. Measurement of lifetime of Λ_b is also presented as a ratio with the lifetime of B_d^0 decay that has very similar event topology. CDF measurement² of lifetime of Λ_b , $\tau(\Lambda_b)$ is 1.580 ± 0.077 (stat) ± 0.012 (syst) ps and $\tau(\Lambda_b)/\tau(B^0) = 1.018 \pm 0.062$ (stat) ± 0.007 (syst). This measurement is about 3σ higher than the theoretical prediction and world average. DØ measurement³ of $\tau(\Lambda_b)$ in the same channel using 1.2 fb^{-1} of data is $1.218^{+0.130}_{-0.115}$ (stat) ± 0.042 (syst) ps, and $\tau(\Lambda_b)/\tau(B^0) = 0.811^{+0.096}_{-0.034}$. DØ had also done a measurement of Λ_b lifetime in the semileptonic decay channel $\Lambda_b \rightarrow \mu\nu\Lambda_c(\rightarrow K_s^0 p)X$. This measurement⁴ benefits from having large statistics, but as full reconstruction is not possible one cannot observe Λ_b peak. The measured lifetime in this channel is $\tau(\Lambda_b) = 1.290^{+0.119}_{-0.110}$ (stat) $^{+0.087}_{-0.091}$ (syst) ps. The most recent status of all $\tau(\Lambda_b)$ measurement is summarized in Figure 2⁵. CDF has looked into the exclusive decay channels for $B^+ \rightarrow J/\psi K^+$, $B^0 \rightarrow J/\psi K^{*0}$, and $B^0 \rightarrow J/\psi K_s^0$. The measured lifetimes are² $\tau(B^+) = 1.630 \pm 0.016$ (stat) ± 0.011 (syst) ps, and $\tau(B^0) =$

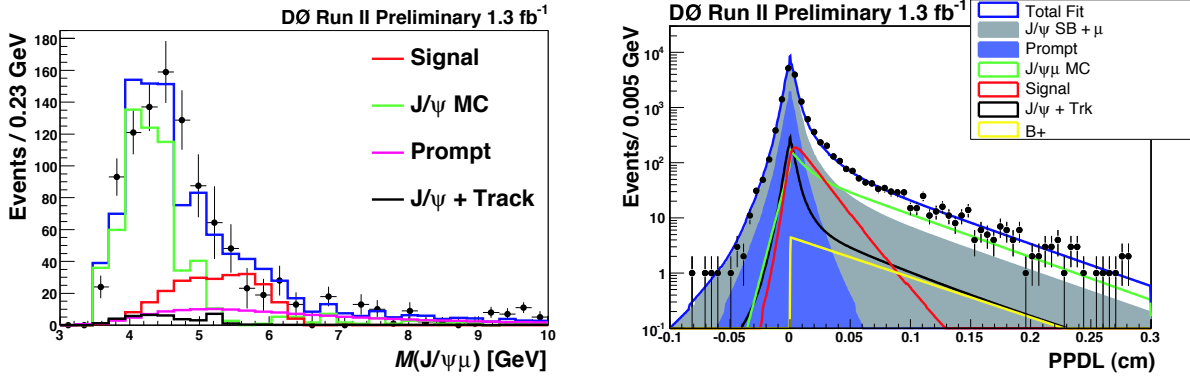


Figure 3: B_c^\pm mass signal following lifetime cut, demonstrating signal, and Pseudo-Proper Decay Length distribution for $B_c^\pm \rightarrow J/\psi\mu\nu$ in the signal region (right).

$1.551 \pm 0.019(stat) \pm 0.011(syst)$ ps. From these measurements $\tau(B^+)/\tau(B^0)$ is found to be $1.015 \pm 0.023(stat) \pm 0.004(syst)$. These measurements are in good agreement with theoretical prediction¹.

DØ has recently reported on the measurement of the lifetime of B_c^\pm meson. B_c^\pm is one of the most interesting meson studied at Tevatron in that it comprises of two different heavy quarks competing each other for decay. B_c^\pm has the shortest lifetime of weakly decaying b-hadron with explicit predictions of its lifetime to be 0.55 ± 0.15 ps using Operator Product Expansion (OPE), and 0.48 ± 0.05 using QCD sum rules⁶. This is about 1/3 of the lifetime of other B mesons. DØ has looked into the decay of $B_c^\pm \rightarrow J/\psi\mu\nu$ using $1.3 fb^{-1}$ of data. Due to the escaping ν DØ measured the pseudo-proper decay length (PPDL), and corrected it by using a factor that takes boost into account. Finally the lifetime is determined by using simultaneous fit to three-muon invariant mass and PPDL. Presence of B_c signal in the sample is demonstrated in Figure 3(left) that shows the fit to the three muon invariant mass distribution after subtracting J/ψ sideband component and B^+ component. A requirement is put on the transverse decay length significance, $L_{xy}/\sigma(L_{xy}) > 4$, where $\sigma(L_{xy})$ is the uncertainty on the measurement of L_{xy} . The probability of background fluctuating up to the signal is found to be more than 5σ . It is important to note that the transverse decay length cut that would bias the lifetime measurement is not applied in the full simultaneous mass and PPDL fit. Figure 3(right) shows the PPDL distribution. DØ measured⁷ $\tau(B_c^\pm) = 0.444_{-0.036}^{+0.039}(stat)_{-0.034}^{+0.039}(syst)$ ps. This result is in good agreement with earlier CDF measurement⁸, and theoretical prediction⁶.

Measurements of B_S lifetimes are recently done by CDF, and DØ experiment. Flavor specific lifetime measurement of B_S is done by CDF experiment using the decays of $B_s \rightarrow D_s^-(\phi\pi^-)\pi^+$, and $B_s \rightarrow D_s^-\rho^+(\pi^+\pi^0)$. The second decay channel cannot be fully reconstructed due to the presence of π^0 . Both fully and partially reconstructed channels yields about 1100 events each in $1.3 fb^{-1}$ of data. The lifetime measurement depends on two fits done sequentially. First relative fraction of events from different signal, and background decay modes is determined by performing a fit on the reconstructed mass of B_s candidates. Then using the fractions obtained from the first fit, a maximum likelihood fit for B_s meson lifetime is performed. The values of the lifetimes obtained in the fully reconstructed and partially reconstructed channels are 1.456 ± 0.067 ps, and 1.545 ± 0.051 ps respectively. Result of the combination of these two modes is $\tau(B_s) = 1.518 \pm 0.041 \pm 0.025$ ps⁹. DØ experiment has measured the average lifetime of B_s, \bar{B}_s states in the decay of $B_s \rightarrow J/\psi\phi$, using $2.8 fb^{-1}$ of data. Value of $\tau(B_s)$ is found to be $1.52 \pm 0.05 \pm 0.01$ ps¹⁰. CDF measurement in the same decay channel using $1.7 fb^{-1}$ of data is $\tau(B_s) = 1.52 \pm 0.04 \pm 0.02$ ps¹¹.

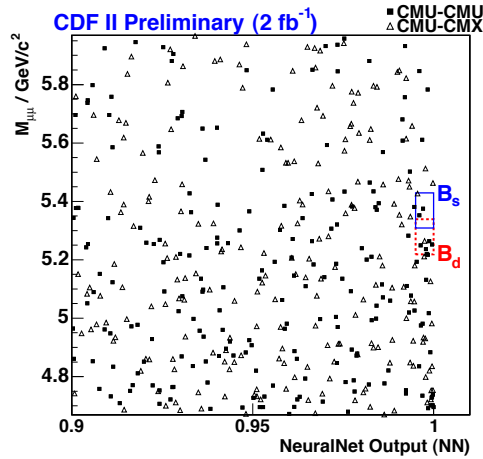


Figure 4: Neural Net output for $B_s(B_d^0) \rightarrow \mu^+\mu^-$ search. Signal windows are shown in the boxes.

3 Rare Decays

Flavor Changing Neutral Current (FCNC) processes are excellent place to study new physics beyond Standard model. The FCNC decays of $B_s(B_d^0) \rightarrow \mu^+\mu^-$ can only go through higher order Feynman diagrams, and are suppressed by the helicity factor $(m_\mu/m_B)^2$. The decay of B_d^0 is further suppressed with respect to the decay of B_s by the ratio of CKM elements, $|V_{td}/V_{ts}|^2$. The predicted branching ratios for $B_s \rightarrow \mu^+\mu^-$, and $B_d^0 \rightarrow \mu^+\mu^-$ are $(3.42 \pm 0.54) \times 10^{-9}$, and $(1.00 \pm 0.14) \times 10^{-10}$ respectively¹². Various extensions of the SM predicts branching ratios that are up to 3 orders magnitude higher¹³. For instance Minimal supersymmetric Standard Model (MSSM) predicts enhancement proportional to $\tan^6\beta$. CDF experiment has analyzed $2 fb^{-1}$ of data to look for $B_s \rightarrow \mu^+\mu^-$, and $B_d^0 \rightarrow \mu^+\mu^-$. To achieve best separation between signal and background, at the final stage of the analysis CDF has used a neural network variable, comprising of proper decay length, proper decay length significance, 3D opening angle between dimuon system and the displacement vector between primary vertex and dimuon vertex, and the track isolation of the B candidate. Figure 4 shows the distribution of the neural network output vs invariant mass of the dimuon. Indicated in the boxes are signal windows for B_s , and B_d^0 . No excess of signal over background estimation is observed. CDF has put the worlds best limits on the branching ratio (Br) of $B_s(B_d^0) \rightarrow \mu^+\mu^-$ ¹⁴. These limits at 95%(90%) C.L are $\text{Br}(B_s \rightarrow \mu^+\mu^-) < 5.8 \times 10^{-8} (4.7 \times 10^{-8})$, and $\text{Br}(B_d^0 \rightarrow \mu^+\mu^-) < 1.8 \times 10^{-8} (1.5 \times 10^{-8})$. DØ has used $2 fb^{-1}$ of data also and did not find any excess in their search for $B_s \rightarrow \mu^+\mu^-$ signal. Limits obtained by DØ experiment are $\text{Br}(B_s \rightarrow \mu^+\mu^-) < 9.3 \times 10^{-8} (7.5 \times 10^{-8})$ at 95%(90%) C.L.¹⁵.

FCNC decays are further suppressed through GIM mechanism¹⁶ in charmed mesons like D, where the standard model expectation of the branching ratio for $D^+ \rightarrow \pi^+\mu^+\mu^-$ is less than 10^{-9} ¹⁷. DØ experiment has performed a search for the continuum decay of $D^+ \rightarrow \pi^+\mu^+\mu^-$. In order to exclude events coming from the decays $D^+, D_s^+ \rightarrow \phi(\rightarrow \mu^+\mu^-)\pi^+$ the region where dimuon invariant mass is consistent with ϕ mass is excluded. In $1.3 fb^{-1}$ of data sample 19 candidate events are observed, whereas 25 ± 4.6 events from background sources are expected. This leads to the limit of $\text{Br}(D^+ \rightarrow \pi^+\mu^+\mu^-) < 3.9 \times 10^{-6} (6.1 \times 10^{-6})$ at 90% (95%) C.L.¹⁸. This is currently the world's most stringent limit on the decay mediated by $c \rightarrow u\mu^+\mu^-$ transition.

4 Summary

We have presented a lot of measurements on b-hadron lifetimes, and rare decays with improved uncertainties. For some of the FCNC rare decays most stringent limits in the world have been obtained. In some lifetime measurements uncertainties at the level of 1% have been achieved. Many uncertainties are still dominated by statistics. As we expect to double our dataset by the end of the Tevatron running, we look forward to exciting prospects on both precision lifetime measurements, and rare decays. In fact for some of the FCNC rare decays we expect to get close to the standard model prediction.

5 Acknowledgments

The author would like to thank all his Tevatron colleagues for their hard work, and the conference organizers for an enjoyable conference.

6 References

1. F. Gabbiani *et al*, *Phys. Rev. D* **70**, 094031 (2004).
2. A. Abulencia *et al*, CDF Note 8524.
3. V. Abazov *et al*, *Phys. Rev. Lett.* **99**, 142001 (2007).
4. V. Abazov *et al*, *Phys. Rev. Lett.* **99**, 182001 (2007).
5. HFAG group, www.slac.stanford.edu/xorg/hfag/
6. V. Kiselev, hep-ph/0308214 (2003).
7. V. Abazov *et al*, D0 Note 5524-CONF
8. A. Abulencia *et al*, *Phys. Rev. Lett.* **97**, 012002 (2006).
9. A. Abulencia *et al*, CDF Note 9203.
10. V. Abazov *et al*, Fermilab-Pub-08/033-E, hep-ex/0802.2255, Submitted to PRL.
11. T. Aaltonen *et al*, *Phys. Rev. Lett.* **100**, 121803 (2008).
12. G. Buchalla *et al*, *Nucl. Phys. B* **400**, 225 (1993); A.J. Buras *et al*, *Phys. Lett. B* **566**, 115 (2003)
13. R. Arnowitt *et al*, *Phys. Lett. B* **538**, 121 (2002); A. Dedes *et al*, *Phys. Lett. B* **600**, 261 (2004); J. Ellis *et al*, *Phys. Lett. B* **624**, 47 (2005).
14. T. Aaltonen *et al*, *Phys. Rev. Lett.* **100**, 101802 (2008).
15. V. Abazov *et al*, D0 Note 5344-CONF .
16. S. Glashow *et al*, *Phys. Rev. D* **2**, 1285 (1970).
17. G. Bardman *et al*, *Phys. Rev. D* **66**, 014009 (2002); S. Fajfer *et al*, *Phys. Rev. D* **64**, 114009 (2001).
18. V. Abazov *et al*, *Phys. Rev. Lett.* **100**, 101801 (2008).

B_s MIXING, $\Delta\Gamma_s$ AND CP VIOLATION AT THE TEVATRON

Gian Piero DI GIOVANNI,
for the CDF and DØ Collaborations
*LPNHE, Laboratoire de Physique Nucléaire et des Hautes Energies,
4 Place Jussieu, Tour 33 RdC, 75005,
Paris, France*

We discuss the results from the Tevatron experiments on mixing and CP violation in the $B_s^0 - \bar{B}_s^0$ system, with particular emphasis to the updated measurements of the decay-width difference $\Delta\Gamma_s$ and the first measurement of the CP-violating phase β_s using flavor tagging information. We also briefly review the charge asymmetry measurements in semileptonic B_s^0 decays and in $B^\pm \rightarrow J/\psi K^\pm$ decays.

1 Introduction

The Tevatron is a $p\bar{p}$ collider operating at the Fermi National Accelerator Laboratory. The protons and anti-protons collide at a center-of-mass energy of $\sqrt{s} = 1.96$ TeV in two interaction points, where the CDF II and DØ detectors are located. The two experiments have collected an integrated luminosity of 3 fb^{-1} and the measurements presented here span from 1.0 fb^{-1} to 2.8 fb^{-1} . The physics of the b quark is a very active research area to challenge the Standard Model predictions. Precise measurements in B^0 and B^+ meson decays, performed at the B factories, improved the understanding of flavor dynamics and proved the Standard Model description very successful. On the other hand, a comparable experimental knowledge of B_s^0 decays has been lacking. The B_s^0 oscillation observation at CDF¹ strongly constrained the magnitude of New Physics contributions in the B_s^0 mixing, while its phase, responsible for CP violating effects, is not precisely determined yet. The B_s^0 sector offers a large variety of interesting processes in which large CP violation effects are still allowed by the current experimental constraints, but are negligible small in the Standard Model. Thus, the Tevatron collider, providing a simultaneous access to large samples of strange and non-strange b -mesons necessary for precision measurements, offers a great opportunity to study the B_s^0 flavor sector, before the start-up of CERN Large Hadronic Collider (LHC).

2 Phenomenology of the B_s^0 System

Flavor oscillation, or mixing, is a very well established phenomenon in particle physics. In the Standard Model the mass and the flavor eigenstates of neutral B mesons differ. This give rise to particle-antiparticle oscillations, which proceed through forth-order flavor changing weak interactions, whose phenomenology depends on the Cabibbo-Kobayashi-Maskawa (CKM) quark mixing matrix. The rate at which the neutral $B - \bar{B}$ transitions occur is governed by the mass difference, Δm of the two mass eigenstates, B^L and B^H , where the superscripts L and H stay for

“light” and “heavy”. The phenomenology of mixing in B_s^0 and \bar{B}_s^0 mesons is, then, characterized by the mass difference of the two mass eigenstates, Δm_s , as well as by the decay width-difference $\Delta\Gamma_s \equiv \Gamma_s^L - \Gamma_s^H = 1/\tau_{B_s^L} - 1/\tau_{B_s^H}$. The latter depends on the CP violating phase defined as $\phi_s = \arg(-M_{12}/\Gamma_{12})$, through the relationship $\Delta\Gamma_s = 2|\Gamma_{12}| \times \cos(\phi_s)$. M_{12} and Γ_{12} are the off-diagonal elements of the $B_s^0 - \bar{B}_s^0$ decay matrix from the Schrödinger equation describing the time evolution of B_s^0 mesons^{2,3}. While the Standard Model expectations are small⁴, $\phi_s = 4 \times 10^{-3}$, New Physics could significantly modify the observed phase value contributing with additional processes, $\phi_s = \phi_s^{SM} + \phi_s^{NP}$. The same phase would alter the observed phase between the mixing and the $b \rightarrow c\bar{c}s$ transitions, $2\beta_s = 2\beta_s^{SM} - \phi_s^{NP}$, in which the Standard Model contribution is defined as $-2\beta_s^{SM} = -2 \arg(-\frac{V_{ts}V_{tb}^*}{V_{cs}V_{cb}^*}) \approx \mathcal{O}(0.04)$, where V_{ij} are the elements of the CKM matrix. Since both ϕ_s^{SM} and β_s^{SM} are tiny with respect to the current experimental resolution, we can approximate $\phi_s = -2\beta_s$. A measurement of sizable value of $2\beta_s$ (ϕ_s) would be a clear indication of New Physics^{2,3}.

3 B_s^0 Mixing

While Δm_d was precisely determined at the B factories^{5,6}, the B_s^0 mixing frequency has been first measured at CDF experiment¹. The $B_s^0 - \bar{B}_s^0$ oscillation observation was achieved through a combination of several data-sets of 1 fb^{-1} , in integrated luminosity, which results in:

$$\Delta m_s = 17.77 \pm 0.10 \text{ (stat.)} \pm 0.07 \text{ (syst.) ps}^{-1}, \quad (1)$$

with a significance greater than 5 standard deviations. Two independent types of flavor tags are used to identify the B_s^0 flavor at production: the Opposite Side Tagger (OST) and the Same Side Kaon Tagger (SSKT). The performance of flavor taggers are quantified by the efficiency ϵ and the dilution \mathcal{D} , defined as the probability to correctly tag a candidate. The tagging effectiveness, $\epsilon\mathcal{D}^2$ of the OST is 1.8%. The SSKT has $\epsilon\mathcal{D}^2 = 3.5\%$ (hadronic) and 4.8% (semileptonic) and thus contributes most to the sensitivity of the CDF analysis. The accurate measurement of the $B_s^0 - \bar{B}_s^0$ mixing frequency offers a powerful constraint to the ratio $|V_{ts}|^2/|V_{td}|^2$ of CKM matrix elements:

$$\frac{|V_{ts}|^2}{|V_{td}|^2} = 0.2060 \pm 0.0007 \text{ (stat.)}_{-0.0060}^{+0.0081} \text{ (theory)}. \quad (2)$$

DØ recently reported a measurement of the B_s^0 oscillation frequency⁷ using a large sample of semileptonic B_s^0 decays and their first hadronic mode, $B_s^0 \rightarrow D_s^- [\rightarrow \phi (\rightarrow K^+ K^-) \pi^-] \pi^+$. DØ combines the tagging algorithms using a likelihood-ratio method, obtaining a total effective tagging power $\epsilon\mathcal{D}^2 = (4.49 \pm 0.88)\%$. With a data-set of approximately 2.4 fb^{-1} , they obtains:

$$\Delta m_s = 18.56 \pm 0.87 \text{ (stat.)ps}^{-1}. \quad (3)$$

The result statistically exceeds the 3σ significance and it is compatible with the CDF measurement. The Δm_s is well consistent with the Standard Model unitarity hypothesis for the CKM matrix.

4 Phase of the Mixing Amplitude and Decay-Width Difference in the B_s^0 System

We present the time-dependent angular analyses of $B_s^0 \rightarrow J/\psi (\rightarrow \mu^+ \mu^-) \phi (\rightarrow K^+ K^-)$ decay mode performed at the Tevatron experiments. The decay $B_s^0 \rightarrow J/\psi \phi$ proceeds through the $b \rightarrow c\bar{c}s$ transition and gives rise to both CP-even and CP-odd final states. Through the angular distributions of the J/ψ and ϕ mesons, it is possible to statistically separate the two final states

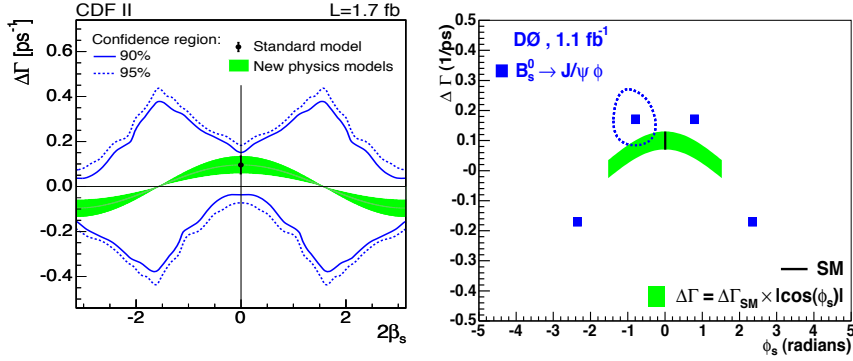


Figure 1: Left: CDF 90% (solid) and 95% (dashed) confidence level contour in the plane $2\beta_s - \Delta\Gamma_s$, compared with the SM prediction and the region allowed in New Physics model given by $\Delta\Gamma_s = 2|\Gamma_{12}|\cos(2\beta_s)$, with $\Gamma_{12} = 0.048 \pm 0.018 \text{ ps}^{-1}$. Right: $D\bar{O}$ point estimate in the plane $\Delta\Gamma_s - \phi_s$. The 39% CL contour (error ellipse) is additionally drawn in the plane $\phi_s - \Delta\Gamma_s$. It is also shown the band representing the relation $\Delta\Gamma_s = \Delta\Gamma_{SM} \times \cos(\phi_s)$, with $\Delta\Gamma_{SM} = 0.10 \pm 0.03 \text{ ps}^{-1}$. In $D\bar{O}$ nomenclature $\phi_s = -2\beta_s$. The 4-fold ambiguity is discussed in the text.

with different CP eigenvalues, thus allowing to determine the phase β_s and to separate lifetimes for the mass eigenstates, so to measure the decay-width difference $\Delta\Gamma_s$. After the $D\bar{O}$ analysis⁸ of untagged $B_s^0 \rightarrow J/\psi\phi$ decay sample of 1.1 fb^{-1} , and reported at Moriond 2007, the CDF Collaboration presents a similar analysis with a sample of 1.7 fb^{-1} in integrated luminosity⁹. CDF measures $\Delta\Gamma_s = 0.076_{-0.063}^{+0.059}$ (stat.) ± 0.006 (syst.) ps^{-1} , $c\tau_s = 456 \pm 13$ (stat.) ± 7 (syst.) μm , assuming CP conservation ($\beta_s = 0$) results. To date, this is one of the most precise B_s^0 lifetime measurements and it is in excellent agreement with both the $D\bar{O}$ results and the theoretical expectations predicting $\tau_s = \tau_d \pm \mathcal{O}(1\%)$. Allowing CP violation, a bias and non-Gaussian fit estimates are observed in pseudo-experiments for statistics similar to the present data-sets. The observed bias originates from the loss of degree of freedom of the likelihood for certain values of the parameters of interest and does not permit a point estimation of $\Delta\Gamma_s$ and β_s . Thus, CDF provides confidence level regions in the $2\beta_s - \Delta\Gamma_s$ plane using the likelihood ratio ordering of Feldman and Cousins¹⁰. For the Standard Model expectation ($\Delta\Gamma_s \approx 0.096 \text{ ps}^{-1}$ and $2\beta_s = 0.04 \text{ rad}^4$), the probability to get equal or greater likelihood ratio than the one observed in data is 22%, which corresponds to 1.2 Gaussian standard deviations. Figure 1 shows the CDF and the $D\bar{O}$ results in the $2\beta_s - \Delta\Gamma_s$ plane. Furthermore, the CDF Collaboration performed an angular analysis on the $B^0 \rightarrow J/\psi(\rightarrow \mu^+\mu^-)K^{*0}(\rightarrow K^+\pi^-)$ decay mode for the measurement of the transversity amplitudes and strong phases. Such an analysis plays a key role in the validation of the entire framework used for the $B_s^0 \rightarrow J/\psi\phi$ angular analysis. The results obtained for the transverse linear polarization amplitudes at $t = 0$, A_{\parallel} and A_{\perp} , corresponding to CP even and CP odd final states respectively, as well as the strong phases $\delta_{\parallel} = \arg(A_{\parallel}^*A_0)$ and $\delta_{\perp} = \arg(A_{\perp}^*A_0)$, are $|A_{\parallel}|^2 = 0.569 \pm 0.009$ (stat.) ± 0.009 (syst.), $|A_{\perp}|^2 = 0.211 \pm 0.012$ (stat.) ± 0.006 (syst.), $\delta_{\parallel} = -2.96 \pm 0.08$ (stat.) ± 0.03 (syst.) and $\delta_{\perp} = 2.97 \pm 0.06$ (stat.) ± 0.01 (syst.), which are in agreement and competitive with the current B factories results¹¹.

We present the first Tevatron studies of the $B_s^0 \rightarrow J/\psi\phi$ decay mode when the initial state of the B_s^0 meson is identified exploiting the flavor tagging information. In fact, such information allows to separate the time evolution of mesons originally produced as B_s^0 or \bar{B}_s^0 . The angular analyses which do not use the flavor tagging are sensitive to $|\cos(2\beta_s)|$ and $|\sin(2\beta_s)|$, leading to a 4-fold ambiguity in the likelihood for the determination of $2\beta_s$ (see Figure 1). On the other hand, utilizing flavor tagging algorithms, the analyses gain sensitivity to the sign of $\sin(2\beta_s)$ reducing by half the allowed region for β_s . CDF performed a flavor tagged analysis on a 1.35 fb^{-1} data-set of $B_s^0 \rightarrow J/\psi\phi$ reconstructed events, which yields $\simeq 2,000$ signal candidates¹².

The measured efficiencies for OST and SSKT are $\epsilon_{OST} = (96 \pm 1)\%$ and $\epsilon_{SSKT} = (50 \pm 1)\%$. The dilutions are respectively $\mathcal{D}_{OST} = (11 \pm 2)\%$ for the OST and $\mathcal{D}_{SSKT} = (27 \pm 4)\%$ for the SSKT. The addition of tagging information improves the regularity of the likelihood with respect to the untagged case, but still non-Gaussian uncertainties and biases are observed in simulated experiments with the available statistics. Thus, CDF reports a confidence region constructed according to the Feldman Cousins criterion with rigorous inclusion of systematics uncertainties. In fact, any $\Delta\Gamma_s - \beta_s$ pair is excluded at a given CL only if it can be excluded for any choice of *all* other fit parameters, sampled uniformly within $\pm 5\sigma$ of the values determined in their estimate on data. Assuming the Standard Model predicted values of $2\beta_s = 0.04$ rad and $\Delta\Gamma_s = 0.096$ ps⁻¹, the probability of a deviation as large as the observed data is 15%, which corresponds to 1.5 Gaussian standard deviations. Moreover, if $\Delta\Gamma_s$ is treated as a nuisance parameter, thus fitting only for $2\beta_s$, CDF finds $2\beta_s \in [0.31, 2.82]$ rad at the 68% confidence level. By exploiting the current experimental and theoretical information, CDF extracts tighter bounds on the CP violation phase β_s . Imposing the constraint on $|\Gamma_{12}| = 0.048 \pm 0.018$ ps⁻¹ in $\Delta\Gamma_s = 2|\Gamma_{12}|\cos(2\beta_s)$ ⁴, $2\beta_s \in [0.24, 1.36] \cup [1.78, 2.90]$ rad at the 68% CL. Additionally constraining the strong phases δ_{\parallel} and δ_{\perp} to the B factories results on $B^0 \rightarrow J/\psi K^{*0}$ ¹¹ and the B_s^0 mean width to the world average B^0 width¹³, it is found $2\beta_s \in [0.40, 1.20]$ rad at the 68% CL. The DØ Collaboration reports an analysis¹⁴ on 2,000 signal $B_s^0 \rightarrow J/\psi\phi$ candidates, reconstructed in 2.8 fb⁻¹. DØ combines the tagging algorithms, as done in their B_s^0 mixing analysis. The total tagging power is $\epsilon\mathcal{D}^2 = (4.68 \pm 0.54)\%$ and a tag is defined for 99.7% of the events. To overcome the likelihood pathologies described above, DØ decides to vary the strong phases around the world-averaged values for the $B^0 \rightarrow J/\psi K^{*0}$ decay¹⁵, applying a Gaussian constraint. This removes the 2-fold ambiguity, inherent the measurement for arbitrary strong phases. The strong phases in $B^0 \rightarrow J/\psi K^{*0}$ and $B_s^0 \rightarrow J/\psi\phi$ cannot be exactly related in the $SU(3)$ limit, so the width of the Gaussian is chosen to be $\pi/5$, allowing for some degree of $SU(3)$ symmetry violation. The fit with all floating parameters yields to the measurements

$$\begin{aligned}\phi_s &= -0.57_{-0.30}^{+0.24} \text{ (stat.)}_{-0.02}^{+0.07} \text{ (syst.) rad,} \\ \Delta\Gamma_s &= 0.19 \pm 0.07 \text{ (stat.)}_{-0.01}^{+0.02} \text{ (syst.) ps}^{-1}, \\ \tau_s &= 1.52 \pm 0.05 \text{ (stat.)} \pm 0.01 \text{ (syst.) ps.}\end{aligned}\tag{4}$$

The allowed ranges at the 90% CL for the parameters of interest are found to be $\phi_s \in [-1.20, 0.06]$ rad and $\Delta\Gamma_s \in [0.06, 0.30]$ ps⁻¹. The expected confidence level contours in the $\phi_s - \beta_s$ plane at 68% and 90% CL are depicted in Figure 2. The level of agreement with the Standard Model corresponds to 6.6%, which is obtained by generating pseudo-experiments with the initial value for ϕ_s set to -0.04 rad and counting the events whose obtained fitted value of the phase is lower than the measured -0.57 rad. The results supersede the previous DØ untagged analysis on a smaller $B_s^0 \rightarrow J/\psi\phi$ sample.

5 Charge Asymmetry in B_s^0 Semileptonic Decays

Another way of studying the CP violation induced by the B_s mixing, is to measure the charge asymmetry in semileptonically decaying mesons. The charge asymmetry is connected to the CP violating phase ϕ_s , through the relationship $A_{SL}^s = \Delta\Gamma_s/\Delta m_s \times \tan(\phi_s)$. With the underlying assumption of $\phi_s = -2\beta_s$ (see Section 2), an independent measurements on charge asymmetry could be used to constrain the CP violating phase β_s ¹⁶. DØ Collaboration performed two independent analyses to extract A_{SL}^s . The first result is based on the di-muon charge asymmetry measurement¹⁷, defined as

$$A_{SL}^{\mu\mu} = \frac{N(bb \rightarrow \mu^+\mu^+) - N(bb \rightarrow \mu^-\mu^-)}{N(bb \rightarrow \mu^+\mu^+) + N(bb \rightarrow \mu^-\mu^-)}.\tag{5}$$

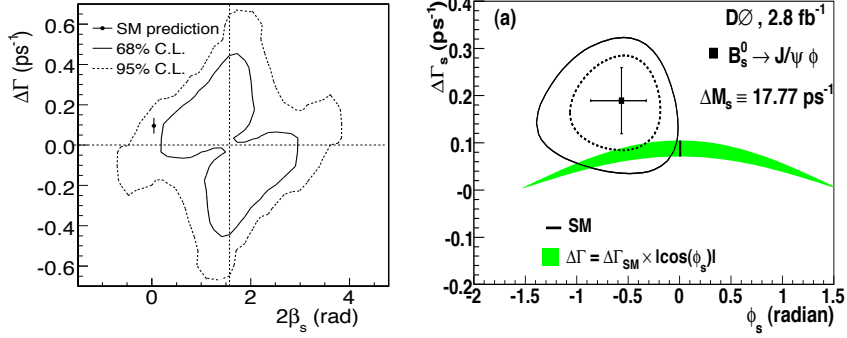


Figure 2: Left: CDF confidence level contour in the plane $2\beta_s - \Delta\Gamma_s$ when using flavor tagging. It quotes the 68% (solid) and 95% (dashed) C.L. The solution with $\Delta\Gamma_s > 0$ corresponds to $\cos(\delta_\perp) < 0$ and $\cos(\delta_\perp - \delta_\parallel) > 0$. The opposite is true for the solution with $\Delta\Gamma_s < 0$. Right: DØ confidence level contours in the $\Delta\Gamma_s - \phi_s$ plane. The curves correspond to the expected 68% (dashed) and 90% (solid) CL. The cross represents the best estimate fit with the one-dimensional uncertainties. According to DØ nomenclature, $\phi_s = -2\beta_s$.

The following asymmetry gets its contributions from both B^0 and B_s^0 : by using the world average value for B^0 and B_s^0 production fractions and the B^0 charge asymmetry measurements from the B factories, DØ extracts the B_s^0 charge asymmetry on a data-set of 1.0 fb^{-1} :

$$A_{SL}^{\mu\mu, B_s^0} = -0.0064 \pm 0.0101 \text{ (stat. + syst.)}. \quad (6)$$

CDF Collaboration also released a similar measurement of the di-muon charge asymmetry¹⁸ on a sample of 1.6 fb^{-1} data. In this analysis, the unbinned likelihood is performed using the impact parameter information of the two muons, in order to separate the $b - \bar{b}$ component of the sample from the others which arise from prompt and charm sources:

$$A_{SL}^{\mu\mu, B_s^0} = 0.020 \pm 0.021 \text{ (stat.)} \pm 0.016 \text{ (syst.)} \pm 0.009 \text{ (inputs)}. \quad (7)$$

Additionally to the statistical and systematic uncertainties, the last uncertainty term comes from the world average value for B^0 and B_s^0 production fractions and the B^0 charge asymmetry measurements already discussed in the description of DØ results. Compared to CDF, DØ analysis has strongly reduced systematics uncertainties thanks to a regular flipping of the magnet polarity. Such technique, removing most of the artificial asymmetry in the detector response, is constantly used by DØ to measure all the charge asymmetries described along this paper.

The DØ Collaboration probes the ϕ_s phase also by measuring the charge asymmetry in an untagged sample of $B_s^0 \rightarrow \mu D_s$ decays, with $D_s \rightarrow \phi(\rightarrow K^+ K^-)\pi$. With a data-set of 1.3 fb^{-1} the charge asymmetry is found to be¹⁹

$$A_{SL}^{\mu D_s} = 0.0245 \pm 0.0193 \text{ (stat.)} \pm 0.0035 \text{ (syst.)}. \quad (8)$$

6 Charge Asymmetry in $B^+ \rightarrow J/\psi K^+$ Decay

We present a search for direct CP violation in $B^+ \rightarrow J/\psi K^+$ decays²⁰. The event sample is selected from 2.8 fb^{-1} of $p\bar{p}$ collisions recorded by DØ experiment. The charge asymmetry is defined as

$$A_{CP}(B^+ \rightarrow J/\psi K^+) = \frac{N(B^- \rightarrow J/\psi K^-) - N(B^+ \rightarrow J/\psi K^+)}{N(B^- \rightarrow J/\psi K^-) + N(B^+ \rightarrow J/\psi K^+)}. \quad (9)$$

By using a sample of approximately 40,000 $B^+ \rightarrow J/\psi K^+$ decays, the asymmetry is measured to be $A_{CP} = 0.0075 \pm 0.0061 \text{ (stat.)} \pm 0.0027 \text{ (syst.)}$. The result is consistent with the

world average¹³ and the Standard Model expectation $A_{CP}(B^+ \rightarrow J/\psi K^+) \simeq 0.003$ ²¹, but has a factor of two improvement in precision, thus representing the most stringent bound for new models which predict large values of $A_{CP}(B^+ \rightarrow J/\psi K^+)$. Furthermore, DØ provides the direct CP violating asymmetry measurement in $B^+ \rightarrow J/\psi\pi^+$, $A_{CP}(B^+ \rightarrow J/\psi\pi^+) = -0.09 \pm 0.08$ (stat.) ± 0.03 (syst.). The result agrees with the previous measurements of this asymmetry¹³ and has a competitive precision.

7 Conclusions

After the successful B_s^0 oscillation observation, the CDF and DØ Collaboration directed their effort in the exploration of the mixing-induced CP violation effect in the B_s^0 system. We described the first tagged measurement in $B_s^0 \rightarrow J/\psi\phi$ performed at the CDF II detector, which improved the sensitivity to the CP violating phase β_s , excluding negative and large values for the phase itself. The DØ Collaboration promptly delivered a similar analysis confirming the results. The agreement of the analyses of $B_s^0 \rightarrow J/\psi\phi$ decays, shows an interesting fluctuations in the same direction from CDF and DØ experiments and they will certainly need further investigations to support an evidence, which would be possible exploiting the full Run II data sample, if these first indications are confirmed in the future. We also reviewed the charge asymmetry measurements of B_s^0 semileptonic decays, which provide another independent test for the CP violation in B_s^0 mixing and can be combined with the analyses on $B_s^0 \rightarrow J/\psi\phi$ to get a better understanding of the CP violating phenomena. Finally, we presented the world most precise direct CP violating asymmetry in the $B^+ \rightarrow J/\psi K^+$ decay mode. The Tevatron experiments are becoming increasingly competitive with B factories results on B^0/B^+ decays and complementary to them in corresponding B_s^0 modes. Since many of the analyses reported do not even use half of the statistics available, significant improvements are expected in the future, as the Tevatron keeps producing data.

References

1. A. Abulencia *et al.* [CDF Collaboration], Phys. Rev. Lett. **97** (2006) 242003.
2. A. S. Dighe, I. Dunietz and R. Fleischer, Eur. Phys. J. C **6** (1999) 647
3. I. Dunietz, R. Fleischer and U. Nierste, Phys. Rev. D **63**, 114015 (2001)
4. A. Lenz and U. Nierste, JHEP **0706** (2007) 072.
5. B. Aubert *et al.* [BABAR Collaboration], Phys. Rev. Lett. **88** (2002) 221802.
6. T. Tomura *et al.* [Belle Collaboration], Phys. Lett. B **542**, 207 (2002).
7. <http://www-d0.fnal.gov/Run2Physics/WWW/results/prelim/B/B51/>.
8. V. M. Abazov *et al.* [DØ Collaboration], Phys. Rev. Lett. **98** (2007) 121801.
9. T. Aaltonen *et al.* [CDF Collaboration], Phys. Rev. Lett. **100** (2008) 121803.
10. Gary J. Feldman and Robert D. Cousins, Phys. Rev. D, **57**, (1998) 3873.
11. B. Aubert *et al.* [BABAR Collaboration], Phys. Rev. D **71** (2005) 032005.
12. T. Aaltonen *et al.* [CDF Collaboration], arXiv:0712.2397 [hep-ex].
13. W. M. Yao *et al.* [Particle Data Group], J. Phys. G **33** (2006) 1.
14. V. M. Abazov *et al.* [DØ Collaboration], arXiv:0802.2255 [hep-ex].
15. E. Barberio *et al.* [HFAG Collaboration], arXiv:0704.3575 [hep-ex].
16. V. M. Abazov *et al.* [DØ Collaboration], Phys. Rev. D **76** (2007) 057101.
17. V. M. Abazov *et al.* [DØ Collaboration], Phys. Rev. D **74** (2006) 092001.
18. <http://www-cdf.fnal.gov/physics/new/bottom/070816.blessed-acp-bsemil/>.
19. V. M. Abazov *et al.* [DØ Collaboration], Phys. Rev. Lett. **98** (2007) 151801.
20. V. M. Abazov *et al.* [DØ Collaboration], arXiv:0802.3299 [hep-ex].
21. W. S. Hou, M. Nagashima and A. Soddu, arXiv:hep-ph/0605080.

BELLE NEW RESULTS ON $B \rightarrow D^{**}\ell\nu$ DECAYS

D. LIVENTSEV

*Institute for Theoretical and Experimental Physics,
B. Chermushkinskaya, 25, 117218 Moscow, Russia
(For the Belle collaboration)*

We present a study of semileptonic B decays to P -wave D^{**} mesons at Belle. Semileptonic decay to a D_2^* meson is observed for the first time and its product branching ratio is measured to be $\mathcal{B}(B^+ \rightarrow \bar{D}_2^{*0}\ell^+\nu) \times \mathcal{B}(\bar{D}_2^{*0} \rightarrow D^-\pi^+) = 0.22 \pm 0.03(\text{stat.}) \pm 0.04(\text{syst.})\%$.

1 Introduction

Heavy Quark Effective Theory (HQET) has proven to be very successful at describing semileptonic decays of B -mesons, especially inclusive transitions. However, some difficulties arise when it is applied to exclusive decays. For example, certain sum rules (in particular, the Uraltsev sum rule¹) imply the strong dominance of decays to the narrow excited D mesons over those to the wide ones, while some experimental data show the opposite trend^{2,3}. However, no complete experimental study of such semileptonic decays to excited D mesons exists, and thus no direct comparison with theoretical predictions can be performed. Here we present Belle study of $B \rightarrow D^{(*)}\pi\ell\nu$ decays and measurement of the excited D contributions to the $D^{(*)}\pi$ final state⁴.

According to HQET there are two doublets of orbitally excited (P -wave) charmed mesons (D^{**}), differentiated by their light quark angular momentum $j_q = 1/2$ or $j_q = 3/2$. Members of the $j_q = 3/2$ doublet are predicted to decay only via a D -wave and be relatively narrow, while members of the $j_q = 1/2$ doublet are predicted to decay only via an S -wave and be relatively broad⁵. The D^{**} states with spin-parity and light quark angular momentum combinations $0^+(j_q = 1/2)$, $1^+(j_q = 1/2)$, $1^+(j_q = 3/2)$ and $2^+(j_q = 3/2)$ are usually labelled D_0^* , D_1' , D_1 and D_2^* , respectively. The D^{**} states have previously been observed and studied in hadronic B decays⁶. Semileptonic B decays to narrow D_1 and D_2^* mesons have been studied by a number of experiments⁷. The semileptonic branching fractions of $B \rightarrow D^{(*)}\pi\ell\nu$ decays were measured by Belle⁸ and BaBar⁹.

This measurement is based on a data sample that contains 657 million $B\bar{B}$ pairs, which corresponds to 605fb^{-1} , collected at the $\Upsilon(4S)$ resonance with the Belle detector¹¹ operating at the KEKB asymmetric-energy e^+e^- collider¹⁰. An additional 68fb^{-1} data sample taken at a center-of-mass energy 60 MeV below the $\Upsilon(4S)$ resonance is used to study continuum $e^+e^- \rightarrow q\bar{q}$ ($q = u, d, s, c$) background.

2 Data analysis

To suppress the large combinatorial background expected in the reconstruction of final states including a neutrino, we use a full reconstruction tagging method. The first B meson (denoted as B_{sl}) is reconstructed in the semileptonic mode of interest, *i.e.* as a combination of all final particles $D^{(*)}\pi\ell$ except for the neutrino. The remainder of the event is combined into either a $D^{(*)}\pi\pi^\pm$ ($n \leq 6$) or $D^{(*)}\rho^-$ combination to form the tagging B meson (referred to below as B_{tag}). Semileptonic decays are identified by a peak around zero in the missing mass squared spectrum, $M_\nu^2 = (P_{\text{beams}} - P_{\text{tag}} - P_{\text{sl}})^2$, where P_{beams} is the total four-momentum of the beams and P_{tag} and P_{sl} are the reconstructed four-momenta of the B_{sl} and B_{tag} , respectively. This method provides significantly improved resolution in the missing momentum in comparison with non-tagging methods, thus allowing background suppression, separation of different decay modes and precise calculation of the decay kinematics. The M_ν^2 spectra for the four semileptonic decays $B \rightarrow D^{(*)}\pi\ell\nu$ are shown in Figs. 1, *1a)–1d)* as points with error bars.

We divide the backgrounds into the following categories: (1) Continuum, (2) Backgrounds with the B_{tag} misreconstructed from particles belonging to the other B meson or fake tracks, (3) B_{sl} backgrounds with the B_{tag} reconstructed correctly, which can be further separated by their source: (3a) Combinatorial background under the $D^{(*)}$ signal from B_{sl} , (3b) Hadrons misidentified as leptons, (3c) Feed-down from $B \rightarrow D^*\pi\ell\nu$ reconstructed as $B \rightarrow D\pi\ell\nu$ with lost neutral(s). All backgrounds except for (3c) are reliably determined and finally subtracted directly from the data. Background (3c) is observed only in the $B \rightarrow D\pi\ell\nu$ channels and is estimated from a Monte Carlo (MC) simulation with normalization fixed to the data using $B \rightarrow D^*(\pi)\ell\nu$ signal yields. This contribution is plotted in Figs. 1, *1a), 1c)* as open histograms.

The background-subtracted M_ν^2 distributions are shown in Figs. 1, *2a)–2d)*. These distributions are fitted with signal functions, the shapes of which are fixed from MC studies. Fitted signal yields, reconstruction efficiencies and branching ratios are summarized in Table 1. The branching ratios are calculated relative to the normalization modes $B \rightarrow D\ell\nu$ to cancel out the B_{tag} reconstruction efficiency according to the formula: $\mathcal{B}(\text{mode}) = \mathcal{B}(\text{norm}) \times N_{\text{mode}}/N_{\text{norm}} \times \epsilon_{\text{norm}}/\epsilon_{\text{mode}}$, where $N_{\text{norm}(\text{mode})}$ and $\epsilon_{\text{norm}(\text{mode})}$ are the signal yield and reconstruction efficiency of the normalization mode (mode of interest) and the normalization mode \mathcal{B} is taken from the PDG¹². Relative efficiencies are obtained from MC simulation. Intermediate branching fractions are included, while the tagging efficiency is not. The reconstruction and background subtraction procedures for the $B \rightarrow D\ell\nu$ mode are identical to those applied for the studied channels. The obtained branching fractions are in good agreement with our previous measurement⁸ and with BaBar results⁹.

Signals for semileptonic B decays to orbitally excited D^{**} are extracted from the $D^{(*)}\pi$ invariant mass distributions. We define a signal window for $B \rightarrow D^{(*)}\pi\ell\nu$ decays by the requirement $|M_\nu^2| < 0.1\text{GeV}^2/c^4$. The backgrounds are estimated in the same way as in the M_ν^2 distribution study. The $D^{(*)}\pi$ invariant mass spectra from the signal window after subtraction of backgrounds (1-3) are shown in Fig. 2. The mass distributions before background subtraction, restricted to the region near the $j_q = 3/2$ states, are shown in the insets.

To extract the D^{**} signals we perform simultaneous unbinned likelihood fits to the signal and background $D^{(*)}\pi$ mass spectra. The signal function includes all orbitally excited D^{**} contributing to the given final state (D_0 and D_2^* to $D\pi$ and D_1 , D_1' , D_2^* to $D^*\pi$), each of

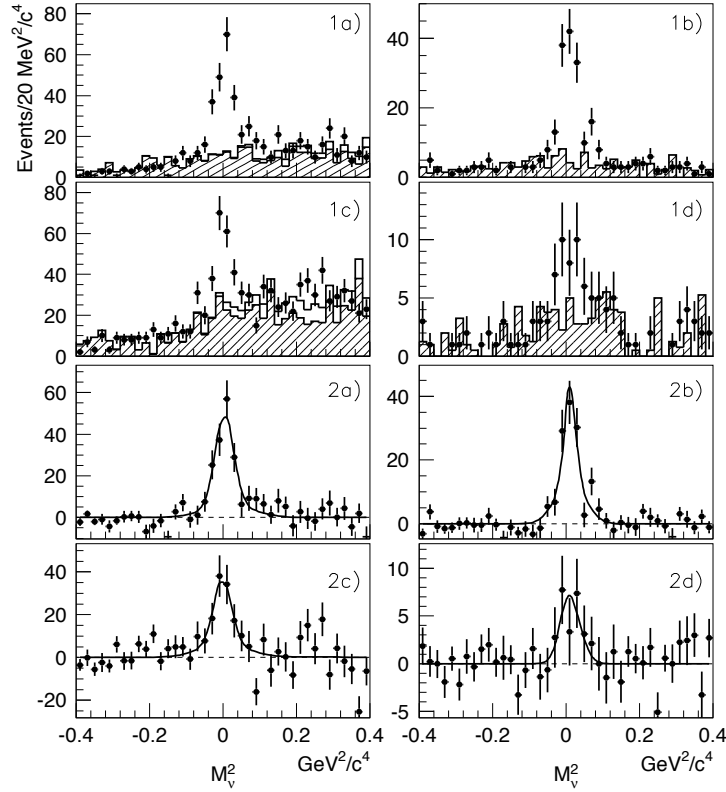


Figure 1: M_v^2 spectra before (1) and after (2) background subtraction for: a) $B^+ \rightarrow D^- \pi^+ \ell^+ \nu$, b) $B^+ \rightarrow D^{*0} \pi^+ \ell^+ \nu$, c) $B^0 \rightarrow D^- \pi^- \ell^+ \nu$, d) $B^0 \rightarrow \bar{D}^{*0} \pi^- \ell^+ \nu$. The curves are the fits, which are described in the text.

which is described by a relativistic Breit-Wigner function for a known orbital momenta, and a non-resonant part described by the Goity-Roberts model¹⁴. D^{**} masses and widths are fixed to measured values⁶. To further investigate the $D\pi$ mass spectrum we also test a $D_v^* + D_2^*$ hypothesis. Despite the $D^0\pi^+$ mass region corresponding to D^{*+} being excluded from the study, and while D^{*0} is below the $D^-\pi^+$ threshold, a virtual D_v^* can be produced off-shell. We describe the D_v^* contribution by a tail of the Breit-Wigner function with floating normalization. Fit results are shown as a dashed line for this combination.

Fitted resonance yields and corresponding product branching ratios are listed in Table 2. The contribution of the non-resonant component in all cases is consistent with zero. The $B \rightarrow D^{**}\ell\nu$ decay significance is defined as $\sqrt{-2 \ln L_{\max}/L_0}$, where L_0 is the likelihood value returned by the fit to the $D^{(*)}\pi$ distribution with the D^{**} contribution fixed to zero. Our result for $B \rightarrow \bar{D}_1 \ell^+ \nu$ is in good agreement with previous measurements⁷. For a $D_0^* + D_2^*$ hypothesis the branching

Table 1: Results for $B \rightarrow D^{(*)}\pi\ell\nu$ where the first error is statistical and the second is systematic.

Mode	Yield	Eff.,%	$\mathcal{B}(\text{mode}),\%$
$B^+ \rightarrow D^0 \ell^+ \nu$	2320 ± 60	6.4	2.15 ± 0.22 ¹³
$B^+ \rightarrow D^- \pi^+ \ell^+ \nu$	192 ± 19	2.8	$0.40 \pm 0.04 \pm 0.06$
$B^+ \rightarrow D^{*0} \pi^+ \ell^+ \nu$	123 ± 14	1.14	$0.64 \pm 0.08 \pm 0.09$
$B^0 \rightarrow D^- \ell^+ \nu$	760 ± 30	3.7	2.12 ± 0.20 ¹³
$B^0 \rightarrow \bar{D}^0 \pi^- \ell^+ \nu$	150 ± 20	3.7	$0.42 \pm 0.07 \pm 0.06$
$B^0 \rightarrow \bar{D}^{*0} \pi^- \ell^+ \nu$	22 ± 8	0.40	$0.56 \pm 0.21 \pm 0.08$

ratio of the decay to the wide D_0^* is large, in contrast to theoretical predictions³. However, the present statistics do not definitely exclude an interpretation of broadly distributed $D\pi^+$ events as the D_v^* tail.

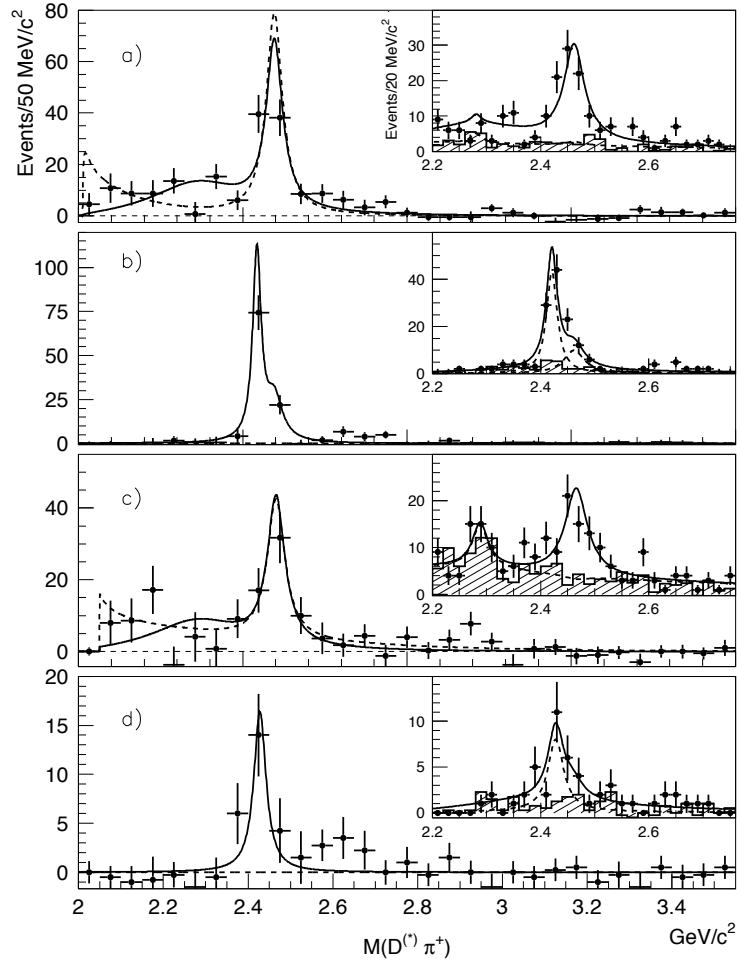


Figure 2: Hadronic invariant mass distributions for: a) $B^+ \rightarrow D^- \pi^+ \ell^+ \nu$, b) $B^+ \rightarrow D^{*-} \pi^+ \ell^+ \nu$, c) $B^0 \rightarrow \bar{D}^0 \pi^- \ell^+ \nu$, d) $B^0 \rightarrow \bar{D}^{*0} \pi^- \ell^+ \nu$. Insets show the distributions before background subtraction in the region around the narrow D^{**} 's. The background is shown as the hatched histogram. The curves are the fits, which are described in the text.

For $D^{*,**}$'s decaying into $D\pi$ we perform a study of the helicity angle distributions, which is the angle between π momentum and the direction opposite to B_{sl} -momentum in the $D^{*,**}$ rest frame. To extract the D_v^* , D_0^* and the D_2^* helicity distributions we perform a combined fit of the $M(D\pi)$ spectra for $D\pi$ combinations from both B^+ and B^0 in bins of helicity angle. The fit procedure is identical to that used for the $\mathcal{B}(B \rightarrow D^{*,**} \ell \nu)$ calculation. The results corrected for the efficiency are plotted in Fig. 3. D_2^* distributions for D_v^* and D_0^* hypothesis coincide within errors, so that only that for the $D_0^* + D_2^*$ case is shown in Fig. 3 c. The D_0^* helicity distribution is consistent with the $J = 0$ hypothesis ($\chi^2/ndf = 6.0/4$, where ndf is the number of degrees of freedom). The D_2^* helicity distribution is fitted with the function $a_0^2 |Y_2^0|^2 + 4a_1^2 |Y_2^1|^2 + 4a_2^2 |Y_2^2|^2$, where the Y_j^i are spherical harmonics and $a_0^2 + 4a_1^2 + 4a_2^2 = 1$. The fit yields $a_0^2 = 0.74 \pm 0.10$, $a_1^2 = 0.04 \pm 0.02$ and $a_2^2 = 0.02 \pm 0.02$; the fit quality is $\chi^2/ndf = 2.0/3$. The fit is consistent with the assumed quantum numbers and demonstrates that the D_2^* from semileptonic decay is dominantly in the $s_z = 0$ spin projection. Helicity distributions, predicted by theory, are shown as dashed lines. For evaluating the $D_v^* + D_2^*$ hypothesis, the obtained D_v^* helicity distribution (Fig. 3 b) is fitted with the function $b_0^2 |Y_1^0|^2 + b_1^2 |Y_1^1|^2$. This fit yields

Table 2: Results of the $D^{(*)}\pi^+$ pair invariant mass study. $\mathcal{B}(\text{mode}) \equiv \mathcal{B}(B \rightarrow D^{**}\ell\nu) \times \mathcal{B}(D^{**} \rightarrow D^{(*)}\pi^+)$. The first error is statistical and the second is systematic.

Mode	Yield	$\mathcal{B}(\text{mode}),\%$	Signif.
$B^+ \rightarrow \bar{D}_0^{*0}\ell^+\nu$	102 ± 19	$0.24 \pm 0.04 \pm 0.06$	5.4
$B^+ \rightarrow \bar{D}_2^{*0}\ell^+\nu$	94 ± 13	$0.22 \pm 0.03 \pm 0.04$	8.0
$B^0 \rightarrow D_0^{*-}\ell^+\nu$	61 ± 22	$0.20 \pm 0.07 \pm 0.05$	2.6
$B^0 \rightarrow D_2^{*-}\ell^+\nu$	68 ± 13	$0.22 \pm 0.04 \pm 0.04$	5.5
$B^+ \rightarrow \bar{D}_1^{*0}\ell^+\nu$	-5 ± 11	< 0.07 @ 90% C.L.	
$B^+ \rightarrow \bar{D}_1^0\ell^+\nu$	81 ± 13	$0.42 \pm 0.07 \pm 0.07$	6.7
$B^+ \rightarrow \bar{D}_2^{*0}\ell^+\nu$	35 ± 11	$0.18 \pm 0.06 \pm 0.03$	3.2
$B^0 \rightarrow D_1^{*-}\ell^+\nu$	4 ± 8	< 0.5 @ 90% C.L.	
$B^0 \rightarrow D_1^-\ell^+\nu$	20 ± 7	$0.54 \pm 0.19 \pm 0.09$	2.9
$B^0 \rightarrow D_2^{*-}\ell^+\nu$	1 ± 6	< 0.9 @ 90% C.L.	
		< 0.3 @ 90% C.L.	

$b_0^2 = 0.15 \pm 0.09$, $b_1^2 = 0.85 \pm 0.09$ ($\chi^2/ndf = 18.8/4$) in poor agreement with expectations from theory, shown as a dashed line.

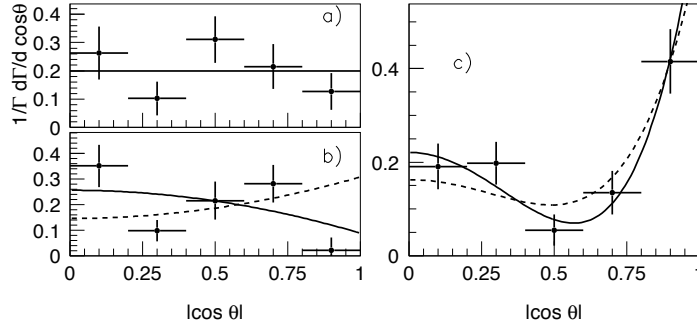


Figure 3: Helicity distributions for a) D_0^* , b) D_v^* , c) D_2^* . The curves represent the fits, described in the text.

We also study the dependence of the $B \rightarrow D^{**}$ transition on q^2 or, equivalently, on the conventional HQET variable w , which is the dot-product of B and D^{**} four-velocities: $w = v_B \cdot v_{D^{**}}$. The w -dependence is obtained from fits of $D\pi$ invariant mass in bins of w . The results are presented in Fig. 4. As with the helicity study the D_2^* distribution is shown only for the $D_0^* + D_2^*$ hypothesis in Fig. 4 c. The w distribution is fitted according to the model given in Ref. ¹⁵. In HQET, the matrix elements between the B and D states to leading order in Λ_{QCD}/m_Q are expressed in terms of three universal Isgur-Wise functions $\xi(w)$, $\tau_{1/2}(w)$ and $\tau_{3/2}(w)$ for (D, D^*) , (D_0^*, D_1^*) and (D_1, D_2^*) doublets, respectively ¹⁵. We assume a ‘‘pole’’ form for $\xi(w)$: $\xi = (2/(1+w))^{2\rho^2}$ and a linear form for $\tau_i(w)$ functions: $\tau_i(w) = \tau_i(1)[1 + \hat{\tau}'_i(w-1)]$, and the following relation: $\hat{\tau}'_{1/2} = \hat{\tau}'_{3/2} + 0.5$ ¹⁶. A simultaneous fit to the w -distributions for D_0^* and D_2^* gives $\hat{\tau}'_{3/2} = -1.8 \pm 0.3$. Using the measured branching ratios of $B \rightarrow D_{0,2}^*\ell\nu$, we also calculate $\tau_{3/2}(1) = 0.75$ and $\tau_{1/2}(1) = 1.28$. All parameters are in agreement with expectations except for $\tau_{1/2}(1)$, which is larger than predicted due to the large value of $\mathcal{B}(B \rightarrow D_0^*\ell\nu)$.

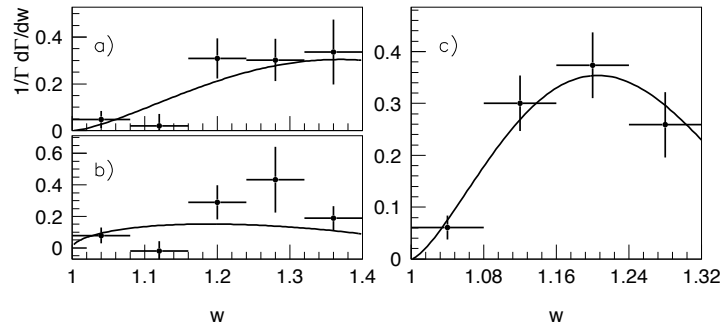


Figure 4: w distributions for a) D_0^* , b) D_v^* , c) D_2^* . The curves are the fits, which are described in the text.

3 Conclusion

In conclusion, we measured the branching fractions for $B \rightarrow D^{(*)}\pi\ell\nu$ decays. We also performed an analysis of the final state $D^{(*)}\pi$ hadronic system and obtained branching ratios for the $B \rightarrow D^{**}\ell\nu$ components. Semileptonic decay to D_2^* meson is observed and measured for the first time. Helicity and w distributions are studied for this decay. We observe a broad enhancement in the $D\pi$ mass distribution consistent with wide D_0^* production. The branching ratio of the decay to $B \rightarrow D_0^*\ell\nu$ is found to be large, in contrast with theoretical predictions³. However there is no indication of a broad D_1' in the $B \rightarrow D^*\pi\ell\nu$ channel, which should be of the same order. The combined likelihood of fits to the $D\pi$ mass, helicity and w distributions for $D_0^* + D_2^*$ hypothesis is higher than that for the $D_v^* + D_2^*$ combination by 2.8σ . However, the present data sample cannot exclude the interpretation of this enhancement as a D_v^* tail.

References

1. N. Uraltsev, Phys. Lett. **B501**, 86 (2001).
2. N. Uraltsev, hep-ph/0409125.
3. I.I. Bigi *et al.*, Eur. Phys. J. C **52**, 975 (2007).
4. D. Liventsev *et al.* (Belle Collaboration), Phys. Rev. D **77**, 091503 (2008).
5. J. Rosner, Comm. Nucl. Part. Phys. **16**, 109 (1986).
6. K. Abe *et al.* (Belle Collaboration), Phys. Rev. D **69**, 112002 (2004); A. Kuzmin *et al.* (Belle Collaboration), Phys. Rev. D **76**, 012006 (2007).
7. D. Buskulic *et al.* (ALEPH Collaboration), Z. Phys. C **73**, 601 (1997); A. Anastassov *et al.* (CLEO Collaboration), Phys. Rev. Lett. **80**, 4127 (1998); V.M. Abazov *et al.* (D0 Collaboration), Phys. Rev. Lett. **95**, 171803 (2005); J. Abdallah *et al.* (DELPHI Collaboration), Eur. Phys. J. C **45**, 35 (2006).
8. D. Liventsev *et al.* (Belle Collaboration), Phys. Rev. D **72**, 051109 (2005).
9. B. Aubert *et al.* (BaBar Collaboration), arXiv:0708.1738.
10. S. Kurokawa and E. Kikutani, Nucl. Instr. and Meth. A **499**, 1 (2003), and other papers included in this volume.
11. A. Abashian *et al.* (Belle Collaboration), Nucl. Instr. and Meth. A **479**, 117 (2002).
12. W.-M. Yao *et al.* (Particle Data Group), J. Phys. G **33**, 1 (2006).
13. Used as a reference.
14. J.L. Goity, W. Roberts, Phys. Rev. D **51**, 3459 (1995).
15. A. Le Yaouanc *et al.*, Phys. Lett. B **520**, 25 (2001).
16. S. Veseli, M.G. Olsson, Phys. Lett. B **367**, 302 (1996).

SEMILEPTONIC B AND D DECAYS — A REVIEW OF RECENT PROGRESS

M. MAZUR

*Department of Physics, University of California, Santa Barbara
Santa Barbara, CA 93106*

We present a review of semileptonic decays of B and D mesons, highlighting recent results from the B factories. We discuss measurements of both inclusive and exclusive decays, measurements of the CKM quark-mixing matrix elements $|V_{cb}|$ and $|V_{ub}|$, studies of nonperturbative QCD effects, and a search for new physics effects using decays to τ leptons.

1 Introduction

Semileptonic decays provide an excellent laboratory in which to study electroweak physics, QCD, and to search for physics beyond the Standard Model. We present recent results on semileptonic B and D meson decays from the three B factories, $BABAR$, Belle, and CLEO.

2 $|V_{cb}|$ and Heavy-quark Parameters from Inclusive B Decays

The inclusive decay mode $B \rightarrow X_c \ell^- \bar{\nu}_\ell$ ¹, where X_c indicates any charmed hadronic system, can be used both to measure the CKM matrix element² $|V_{ub}|$ and to study nonperturbative QCD effects of quarks bound inside hadrons. The differential decay rate for this process is described in Heavy Quark Effective Theory (HQET) as an expansion in terms of α_s , whose effects are perturbatively calculable, and in the b quark mass, m_b , whose effects are nonperturbative and must be measured in data. At second order in $1/m_b$, two nonperturbative parameters arise, corresponding to the kinetic energy and chromomagnetic moment of the b quark in the B meson and denoted μ_π^2 and μ_G^2 , respectively³; at third order in $1/m_b$, two further parameters arise, ρ_{LS}^3 and ρ_D^3 . By measuring moments of the lepton energy spectrum and the X_c mass spectrum in $B \rightarrow X_c \ell^- \bar{\nu}_\ell$ decays and the photon energy spectrum in $B \rightarrow X_s \gamma$ decays — and by studying the variation of these moments as a function of a low-energy cut on the lepton (or photon, in the case of $B \rightarrow X_s \gamma$) energy — we can measure these nonperturbative heavy-quark expansion

parameters. By measuring the total rate of $B \rightarrow X_x \ell^- \bar{\nu}_\ell$ decays, we can simultaneously extract the value of $|V_{cb}|$.

The Belle and *BABAR* Collaborations recently presented measurements of the moments of the E_ℓ and m_X spectra⁴. These measurements use a tagging technique where one of the two B mesons in an $\Upsilon(4S) \rightarrow B\bar{B}$ event is fully reconstructed in a hadronic decay channel; by tagging one B meson, the second B can be reconstructed with reduced background and additional kinematic constraints, both of which are helpful when reconstructing decays with unobserved neutrinos. Corrections are applied to the observed kinematic variables E_ℓ and m_X to account for finite detector resolution and the effects of unobserved particles. The Belle measurements use an unfolding technique, based on the Singular Valued Decomposition technique⁵, while the *BABAR* analysis uses a set of calibration curves to make event-by-event corrections.

A global fit^{6,7} for $|V_{cb}|$ and the heavy-quark expansion parameters is shown in Figure 1. The average includes the recent measurements from Belle and *BABAR*, as well as older measurements from CLEO, CDF, and DELPHI, and includes up to the third E_ℓ moment, the third m_X moment, and the second E_γ moment, all for a variety of lepton or photon energy cuts. The measured moments are highly correlated with one another takes into account the individual covariance matrices as well as a number of external constraints from theory and from other measurements. The measured value of $|V_{cb}|$ is $(42.04 \pm 0.34 \pm 0.59) \times 10^{-3}$, with a total error less than 2%, and the b quark mass is measured as $(4.597 \pm 0.034) \text{ GeV}/c^2$, with an error less than 1%.

Inclusion of the $B \rightarrow X_s \gamma$ photon energy moments in this global fit is somewhat problematic, both from a theoretical and an experimental point of view⁸. Theoretically, including these moments is difficult, in part because all calculations are model dependent to some degree, and in part because the operator product expansion must take into account non-local operators which are difficult to estimate. Additionally, the experimental results display some tension, with the $B \rightarrow X_s \gamma$ results pulling down the value of m_b by about 1%. If the $B \rightarrow X_s \gamma$ moments are excluded from the fit, we instead obtain $|V_{cb}| = (41.85 \pm 0.38 \pm 0.59) \times 10^{-3}$ and $m_b = (4.660 \pm 0.053) \text{ GeV}/c^2$. While the effect on $|V_{cb}|$ is rather small, the effect of this change on the value of $|V_{ub}|$ is much larger, $\approx 10\%$; for this reason, the extraction of $|V_{ub}|$ presented below uses only the $B \rightarrow X_c \ell^- \bar{\nu}_\ell$ moments.

3 $|V_{ub}|$ from Inclusive B Decays

Precision measurement of $|V_{ub}|$ is one of the main goals of the B factory physics program since, together with the angle β , $|V_{ub}|$ helps determine the apex of the Unitarity Triangle². The most precise measurements of $|V_{ub}|$ come from the inclusive $B \rightarrow X_u \ell^- \bar{\nu}_\ell$ decay rate, which is proportional to $|V_{ub}|^2$.

The $B \rightarrow X_u \ell^- \bar{\nu}_\ell$ decay rate is difficult to measure because background from $B \rightarrow X_c \ell^- \bar{\nu}_\ell$ decays is 50 times larger than the signal. Measurements of $|V_{ub}|$ use cuts on kinematic variables — including the lepton energy, m_X , q^2 , and $P_+ \equiv E_X - |p_X|$ — to suppress this $|V_{cb}|$ background, taking advantage of the fact that the c quark is much heavier than the u . The partial decay rate in this restricted phase space is then extrapolated back to the full decay rate using theoretical models⁹ based on heavy-quark parameters which are determined from $B \rightarrow X_c \ell^- \bar{\nu}_\ell$ decays as described above.

BABAR presented a measurement¹⁰ of $|V_{ub}|$ using three kinematic variables: m_X , q^2 , and P_+ . One B meson is fully reconstructed and a high-momentum lepton is identified in the recoil. Combinatorial backgrounds are subtracted by fitting distributions of the tag B mass in bins of the three kinematic variables, and a fit to the resulting kinematic distributions is used to distinguish $B \rightarrow X_u \ell^- \bar{\nu}_\ell$ signal from the residual $B \rightarrow X_c \ell^- \bar{\nu}_\ell$ events and other backgrounds. Several values of $|V_{ub}|$ are reported for different kinematic cuts and in different theoretical frameworks. A global average of inclusive $|V_{ub}|$ measurements⁶, including this latest

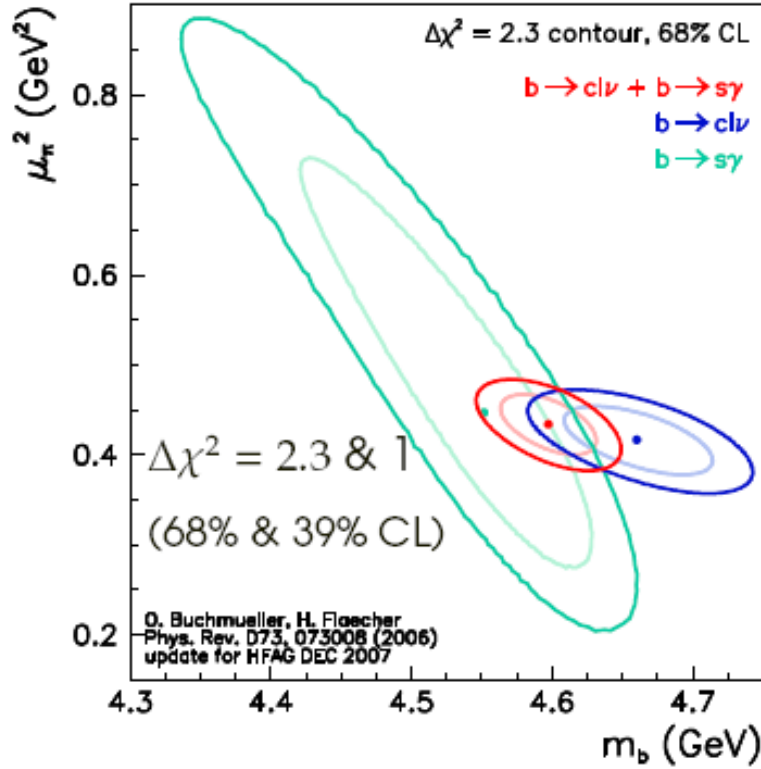


Figure 1: Projection of a global fit for $|V_{cb}|$ and heavy-quark expansion parameters using moments measurements, showing the error ellipse in the $m_b - \mu_\pi^2$ plane. The ellipse is shown for three configurations of the fit: including all moments in the fit, including just the $B \rightarrow X_c \ell^- \bar{\nu}_\ell$ moments, and including just the $B \rightarrow X_s \gamma$ moments.

one and a similar analysis from Belle¹¹, is shown in Figure 2 for the BLPN framework; $|V_{ub}|$ is measured to be $(3.98 \pm 0.15 \pm 0.30) \times 10^{-3}$, with a total error of 8%, while similar results are obtained in the other theoretical frameworks⁹.

4 Charm Semileptonic Decays and Form Factors

Studies of exclusive semileptonic decays, in which particular final state hadronic systems are selected, provide us with another approach to measuring CKM matrix elements and another way to help shed light on perturbative QCD processes. The dynamics of exclusive semileptonic decays are described by a set of form factors which are functions of the squared momentum transfer, q^2 . A variety of theoretical techniques have been used to calculate these form factors¹². Decays of charm mesons provide a clean environment in which to measure the dynamics of semileptonic decay and to study these form factors; testing form factor models in the charm sector also leads to improved understanding of the form factors in the bottom sector, improving the extraction of $|V_{cb}|$ and $|V_{ub}|$.

CLEO-c presented recent results on the semileptonic D decays $D \rightarrow \pi \ell^- \bar{\nu}_\ell$ and $D \rightarrow K \ell^- \bar{\nu}_\ell$ for both charged and neutral D mesons¹³. This analysis uses the missing four-momentum in the event to estimate the neutrino momentum, taking advantage of the good hermeticity of the detector. Signal events are required to have a squared missing mass, m_{miss}^2 , consistent with zero, indicating that a single neutrino was undetected. Signals are further discriminated from background events using two kinematic variables, the mass and energy of the reconstructed D candidate.

A fit is performed in bins of q^2 in order to measure the branching fractions and to extract

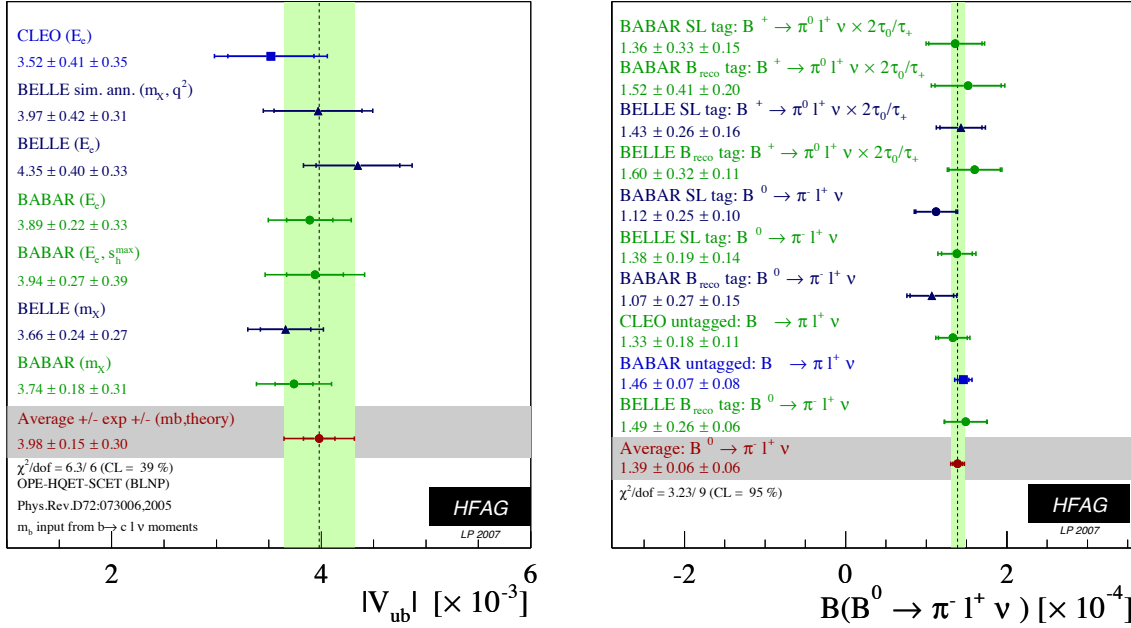


Figure 2: Global averages of inclusive $|V_{ub}|$ measurements (left) and the exclusive $B^0 \rightarrow \pi^- \ell^+ \nu_\ell$ branching fraction (right), highlighting the consistency between many different measurement techniques as well as the precision obtained in recent years from the B factories.

information about the form factors. The branching fractions measured are $\mathcal{B}(\bar{D}^0 \rightarrow \pi^+ \ell^- \bar{\nu}_\ell) = (0.299 \pm 0.011 \pm 0.009)\%$, $\mathcal{B}(D^- \rightarrow \pi^0 \ell^- \bar{\nu}_\ell) = (0.373 \pm 0.022 \pm 0.013)\%$, $\mathcal{B}(\bar{D}^0 \rightarrow K^+ \ell^- \bar{\nu}_\ell) = (3.56 \pm 0.03 \pm 0.09)\%$, and $\mathcal{B}(D^- \rightarrow K^0 \ell^- \bar{\nu}_\ell) = (8.53 \pm 0.13 \pm 0.23)\%$, consistent with similar recent results from Belle and BABAR¹⁴. The form factors for these decays are measured using both a model-independent series expansion and pole models. The expansion results are generally consistent with previous measurements. While the pole models also consistent with previous measurements, they only give a reasonable description of the data for unphysical parameter values. By using lattice QCD calculations of the form factor normalizations, they measure $|V_{cd}| = 0.217 \pm 0.009 \pm 0.004 \pm 0.023$ and $|V_{cs}| = 1.015 \pm 0.010 \pm 0.011 \pm 0.106$, in good agreement with previous measurements.

5 $|V_{ub}|$ from Exclusive B Decays

Exclusive $b \rightarrow u$ decay modes, such as $B \rightarrow \pi \ell^- \bar{\nu}_\ell$, $B \rightarrow \rho \ell^- \bar{\nu}_\ell$, $B \rightarrow \omega \ell^- \bar{\nu}_\ell$, and $B \rightarrow \eta^{(\prime)} \ell^- \bar{\nu}_\ell$, allow us to measure $|V_{ub}|$ as well as to test form factor models in heavy-to-light meson decays. The experimental and theoretical errors on $|V_{ub}|$ from exclusive decays are orthogonal to those in inclusive decays, making these modes complementary to the inclusive studies discussed above.

The CLEO Collaboration recently published¹⁵ a study of the exclusive modes $B \rightarrow h \ell^- \bar{\nu}_\ell$, where $h = \{\pi^+/\pi^0/\rho^+/\rho^0/\omega/\eta/\eta'\}$. As in the previous analysis, the missing momentum in the event must be consistent with a single neutrino, which is then used to reconstruct the $B \rightarrow h \ell^- \bar{\nu}_\ell$ candidate. Signal and background events are identified using two kinematic variables: $m_{h \ell^- \bar{\nu}_\ell}$, the mass of the $h \ell^- \bar{\nu}_\ell$ system after correcting for the neutrino energy resolution, and ΔE , the difference between the observed energy of the $h \ell^- \bar{\nu}_\ell$ system and the beam energy. For the ρ and ω modes, the invariant mass m_h of the ρ or ω is also used to discriminate signal from background. A binned fit is performed to the joint distribution of $m_{h \ell^- \bar{\nu}_\ell}$, ΔE , q^2 , m_h , and, for the ρ mode, $\cos \theta_{W \ell}$, the cosine of the angle between the lepton and the W in the B rest frame; this last variable is sensitive to the helicity of the ρ .

Using isospin to combine the π^+ with π^0 results and the ρ^+ , ρ^0 , and ω results, they obtain $\mathcal{B}(\bar{B}^0 \rightarrow \pi^+\ell^-\bar{\nu}_\ell) = (1.31 \pm 0.15 \pm 0.11) \times 10^{-4}$ and $\mathcal{B}(\bar{B}^0 \rightarrow \rho^+\ell^-\bar{\nu}_\ell) = (2.93 \pm 0.37 \pm 0.37) \times 10^{-4}$, results which are among the most precise measurements to date. The branching fraction for $\bar{B}^0 \rightarrow \pi^+\ell^-\bar{\nu}_\ell$ can be compared to the world average⁶, which is shown in Figure 2. From the π channel, they also measure $|V_{ub}| = (3.6 \pm 0.4 \pm 0.2_{-0.4}^{+0.6}) \times 10^{-3}$, comparable in precision to recent results from the *BABAR* and Belle Collaborations¹⁶ and consistent with the current world average. They find 3σ evidence for the η' mode with $\mathcal{B}(B^- \rightarrow \eta'\ell^-\bar{\nu}_\ell) = (2.66 \pm 0.80 \pm 0.56) \times 10^{-4}$ and set a 90% upper limit $\mathcal{B}(B^- \rightarrow \eta\ell^-\bar{\nu}_\ell) < 1.01 \times 10^{-4}$; these results are consistent with a previous *BABAR* upper limit at the 5% level, and may suggest a significant singlet contribution to the η' .

6 $B \rightarrow D\ell^-\bar{\nu}_\ell$, $D^*\ell^-\bar{\nu}_\ell$, and $D^{**}\ell^-\bar{\nu}_\ell$

Understanding the exclusive $b \rightarrow c$ semileptonic decays is another important part of the B factory physics program, particularly since these modes have among the largest B meson branching fractions. The dominant decay modes $B \rightarrow D\ell^-\bar{\nu}_\ell$ and $B \rightarrow D^*\ell^-\bar{\nu}_\ell$ make up about 70% of the total inclusive rate⁶, with the remaining 30% not yet well measured. These decay modes provide us with complementary measurements of $|V_{cb}|$ and allow us to study decay form factors and HQET. Additionally, these processes are backgrounds in many other analyses, so improved understanding of these decays will lead to improvements in extraction of $|V_{ub}|$ and $|V_{cb}|$.

The *BABAR* Collaboration has presented a simultaneous measurement of the branching fractions $B \rightarrow D\ell^-\bar{\nu}_\ell$, $B \rightarrow D^*\ell^-\bar{\nu}_\ell$, $B \rightarrow D\pi^\pm\ell^-\bar{\nu}_\ell$, and $B \rightarrow D^*\pi^\pm\ell^-\bar{\nu}_\ell$, for both charged and neutral B mesons¹⁷. Each of these modes is reconstructed in the recoil of a fully reconstructed B meson, and signals are extracted using a fit to the m_{miss}^2 distribution, where correctly reconstructed events with just one missing neutrino peak at zero m_{miss}^2 . Each of these eight branching fractions is the most precise measurement to date. The sum of these measurements, together with the inclusive branching fraction, suggests that $(11 \pm 4)\%$ of $B \rightarrow X_c\ell^-\bar{\nu}_\ell$ decays are still unaccounted for, and may likely be due to $B \rightarrow D^{(*)}n\pi\ell^-\bar{\nu}_\ell$ decays with $n > 1$ pions in the final state.

Studies of the decays $B \rightarrow D^{**}\ell^-\bar{\nu}_\ell$ (where D^{**} means either a charm resonance heavier than the D^* or a nonresonant $D^{(*)}n\pi$ system) are interesting because, as mentioned above, the known exclusive decay modes do not saturate the inclusive decay rate, and D^{**} is expected to make up most of the remainder. These decays are also interesting because of what is known as the 1/2–3/2 puzzle: HQET strongly favors production of resonances where the light quark has angular momentum $j_q = 3/2$ (the D_1 and D_2^* states) over those with angular momentum $j_q = 1/2$ (the D_0^* and D_1'), but experimental results¹⁸ suggest that the rates of the two angular momentum states are comparable.

Belle and *BABAR* recently presented studies of $B \rightarrow D^{**}\ell^-\bar{\nu}_\ell$ decays where the individual D^{**} states are distinguished¹⁹. Both analyses identify a clean sample of $B \rightarrow D^{(*)}\pi^\pm\ell^-\bar{\nu}_\ell$ decays by reconstructing them in the recoil of a fully reconstructed B meson and using m_{miss}^2 to identify signal events. A fit to the $D\pi$ and $D^*\pi$ mass spectra is used to disentangle the individual D^{**} contributions, and the branching fractions are summarized in Table 1. The results of the two analyses are largely consistent with one another and with previous results. The branching fractions for the $j_q = 1/2$ states are of the same magnitude as the $j_q = 3/2$ states, confirming earlier results yet perpetuating the 1/2–3/2 puzzle in HQET. Neither measurement sees evidence for a nonresonant $B \rightarrow D^{(*)}\pi\ell^-\bar{\nu}_\ell$ state. The most significant difference between the two sets of results is in the $B \rightarrow D_1'\ell^-\bar{\nu}_\ell$ state. Belle sees no evidence for these decays and sets an upper limit, while *BABAR*, with comparable sensitivity, sees a significant signal ($> 6\sigma$). It is difficult to accommodate a large rate for the $B \rightarrow D_0^*\ell^-\bar{\nu}_\ell$ state without a similarly large rate in $B \rightarrow D_1'\ell^-\bar{\nu}_\ell$, so further study of these modes will help to resolve this discrepancy.

Table 1: Measured product branching fractions $\mathcal{B}(B \rightarrow D^{**}\ell^{-}\bar{\nu}_\ell) \times \mathcal{B}(D^{**} \rightarrow D^{(*)}\pi)$. Both analyses observe nonresonant $B \rightarrow D^{(*)}\pi\ell^{-}\bar{\nu}_\ell$ yields consistent with zero.

Mode	$\mathcal{B}(B \rightarrow D^{**}\ell^{-}\bar{\nu}_\ell) \times \mathcal{B}(D^{**} \rightarrow D^{(*)}\pi)$ (%)	
	Belle	BABAR
$D\pi$ invariant mass fit		
$B^- \rightarrow D_0^{*0}\ell^{-}\bar{\nu}_\ell$	$0.24 \pm 0.04 \pm 0.06$	$0.28 \pm 0.05 \pm 0.04$
$B^- \rightarrow D_2^{*0}\ell^{-}\bar{\nu}_\ell$	$0.22 \pm 0.03 \pm 0.04$	$0.16 \pm 0.03 \pm 0.01$
$\bar{B}^0 \rightarrow D_0^{*+}\ell^{-}\bar{\nu}_\ell$	$0.20 \pm 0.07 \pm 0.05$	$0.47 \pm 0.09 \pm 0.07$
$\bar{B}^0 \rightarrow D_2^{*+}\ell^{-}\bar{\nu}_\ell$	$0.22 \pm 0.04 \pm 0.04$	$0.08 \pm 0.04 \pm 0.02$
$D^*\pi$ invariant mass fit		
$B^- \rightarrow D_1^{*0}\ell^{-}\bar{\nu}_\ell$	< 0.07 (90% CL)	$0.27 \pm 0.05 \pm 0.05$
$B^- \rightarrow D_1^0\ell^{-}\bar{\nu}_\ell$	$0.42 \pm 0.07 \pm 0.07$	$0.29 \pm 0.03 \pm 0.03$
$B^- \rightarrow D_2^{*0}\ell^{-}\bar{\nu}_\ell$	$0.18 \pm 0.06 \pm 0.03$	$0.07 \pm 0.01 \pm 0.01$
$\bar{B}^0 \rightarrow D_1^{*+}\ell^{-}\bar{\nu}_\ell$	< 0.5 (90% CL)	$0.37 \pm 0.07 \pm 0.05$
$\bar{B}^0 \rightarrow D_1^+\ell^{-}\bar{\nu}_\ell$	$0.54 \pm 0.19 \pm 0.09$	$0.25 \pm 0.05 \pm 0.03$
$\bar{B}^0 \rightarrow D_2^{*+}\ell^{-}\bar{\nu}_\ell$	< 0.3 (90% CL)	$0.04 \pm 0.02 \pm 0.01$

7 $B \rightarrow D^{(*)}\tau^{-}\bar{\nu}_\tau$

Semileptonic decays with τ leptons provide a new source of information on SM processes as well as a window into physics beyond the SM since the large τ mass gives sensitivity to decays mediated by a charged Higgs boson²⁰. Because the corresponding decays to light leptons have been studied and the form factors have been measured, theoretical predictions for the τ modes are quite clean, making these modes attractive probes of new physics. These decays are extremely challenging experimentally, however, due to the presence of multiple neutrinos in the final state.

Belle and BABAR recently presented the first results on exclusive semitauponic B decays²¹. Both experiments fully reconstruct one of the two B mesons in the event and use the kinematic constraints to measure the missing four-momentum from the second B . Care must be taken to be sure that the decay products of both B mesons are correctly reconstructed and account for all of the visible particles in the event, since mistakes tend to fake the missing momentum signature of signal events.

The Belle analysis reconstructs $\bar{B}^0 \rightarrow D^{*+}\tau^{-}\bar{\nu}_\tau$ with $\tau^{-} \rightarrow \ell^{-}\bar{\nu}_\ell\nu_\tau$ and $\tau^{-} \rightarrow \pi^{-}\nu_\tau$ and requires events to have a large value of X_{miss} , a kinematic variable closely related to the missing mass. This cut preferentially selects events in which multiple neutrinos have escaped detection. The signal yield is then extracted by fitting the tag B mass distribution, yielding the result $\mathcal{B}(\bar{B}^0 \rightarrow D^{*+}\tau^{-}\bar{\nu}_\tau) = (2.02_{-0.37}^{+0.40} \pm 0.37)\%$.

The BABAR analysis reconstructs four modes, $B^- \rightarrow D^0\tau^{-}\bar{\nu}_\tau$, $B^- \rightarrow D^{*0}\tau^{-}\bar{\nu}_\tau$, $\bar{B}^0 \rightarrow D^+\tau^{-}\bar{\nu}_\tau$, and $\bar{B}^0 \rightarrow D^{*+}\tau^{-}\bar{\nu}_\tau$, with $\tau^{-} \rightarrow \ell^{-}\bar{\nu}_\ell\nu_\tau$. The signal is extracted with a fit to the m_{miss}^2 and lepton momentum distributions (for signal events, this lepton is secondary), performed simultaneously in the D^0 , D^{*0} , D^+ , and D^{*+} final states, as well as a set of control samples which simultaneously constrain background from $B \rightarrow D^{**}\ell^{-}\bar{\nu}_\ell$ decays. Combining results from charged and neutral B modes, they obtain $\mathcal{B}(\bar{B}^0 \rightarrow D^+\tau^{-}\bar{\nu}_\tau) = (0.86 \pm 0.24 \pm 0.11 \pm 0.06)\%$ and $\mathcal{B}(\bar{B}^0 \rightarrow D^{*+}\tau^{-}\bar{\nu}_\tau) = (1.62 \pm 0.31 \pm 0.10 \pm 0.05)\%$, where the D^* result is consistent with that of Belle.

Both the Belle and BABAR results are about one standard deviation higher than the SM prediction. These measurements are statistically limited, however, and with increased statistics, studies of these modes are expected to add significant constraints to new physics models. In addition to the branching fractions, several other observables are sensitive to possible non-SM contributions, including q^2 distributions and D^* and τ polarization²⁰, which would add to the

sensitivity of future studies of $B \rightarrow D^{(*)}\tau^{-}\bar{\nu}_{\tau}$.

8 Conclusion

We have presented an overview of recent results in semileptonic decays from the B factories. $|V_{ub}|$ has been measured with several different techniques and is now known to better than 10%, while $|V_{cb}|$ is now known to better than 2%. Both of these measurements are fundamental to the B factory goal of overconstraining the Unitarity Triangle. Work is ongoing to understand the composition of the exclusive states which make up $B \rightarrow X_c\ell^{-}\bar{\nu}_{\ell}$, particularly in disentangling the various D^{**} contributions. New decay modes with τ leptons have been observed for the first time, opening up a new window into physics beyond the Standard Model.

References

1. Charge conjugate processes are implied throughout.
2. N. Cabibbo, Phys. Rev. Lett. **10** 531 (1963); M. Kobayashi and T. Maskawa, Prog. Theor. Phys. **49** 652 (1973).
3. We use here the kinetic scheme: P. Gambino and N. Uraltsev, Eur. Phys. Jour. C **34** 181 (2004); D. Benson, I.I. Bigi, and N. Uraltsev, Nucl. Phys. B **710** 371 (2005). These decays can alternatively be described in the 1S scheme: C.W. Bauer *et al.*, Phys. Rev. D **67** 054012 (2003) and Phys. Rev. D **70** 094017 (2004).
4. P. Urquijo *et al.* (Belle Collab.), Phys. Rev. D **75** 032001 (2007); C. Schwanda *et al.* (Belle Collab.), Phys. Rev. D **75** 032005 (2007); B. Aubert *et al.* (BABAR Collab.), arXiv:0707.2670.
5. A. Höcker and V. Kartvelishvili, Nucl. Instrum. Methods Phys. Res., Sect. A **372** 469 (1996).
6. E. Barberio *et al.* (HFAG), arXiv:0704.3575 and online updates.
7. O. Buchmüller and H. Flächer, Phys. Rev. D **73** 073008 (2006).
8. M. Neubert at the Joint Workshop on $|V_{ub}|$ and $|V_{cb}|$ at the B Factories, Heidelberg, (2007).
9. C.W. Bauer, Z. Ligeti, and M. Luke, Phys. Rev. D **64** 113004 (2001); B.O. Lange, M. Neubert, and G. Paz, Phys. Rev. D **72** 073006 (2005); J.R. Andersen and E. Gardi, JHEP **0601** 097 (2006).
10. B. Aubert *et al.* (BABAR Collab.), Phys. Rev. Lett. **100** 171802 (2008).
11. I. Bizjak *et al.* (Belle Collab.), Phys. Rev. Lett. **95** 241801 (2005).
12. A common model-independent parameterization is C.G. Boyd and M.J. Savage, Phys. Rev. D **56** 303 (1997). Some commonly used models include D. Scora and N. Isgur, Phys. Rev. D **52** 2783 (1995); I. Caprini, L. Lellouch, and M. Neubert, Nucl. Phys. B **530** 153 (1998); D. Becirevic and A.B. Kaidalov, Phys. Lett. B **478** 417 (2000); and A. Khodjamirian *et al.*, Phys. Rev. D **62** 114002 (2000). Lattice QCD calculations include C. Aubin *et al.*, Phys. Rev. Lett. **94** 011601 (2005).
13. S. Dobbs *et al.* (CLEO Collab.), arXiv:0712.1020.
14. L. Widhalm *et al.* (Belle Collab.), Phys. Rev. Lett. **97** 061804 (2006); B. Aubert *et al.* (BABAR Collab.), Phys. Rev. D **76** 052005 (2007).
15. D. Asner *et al.* (CLEO Collab.), Phys. Rev. D **76** 012007 (2007).
16. T. Hokuue *et al.* (Belle Collab.), Phys. Lett. B **648** 139 (2007); B. Aubert *et al.* (BABAR Collab.), Phys. Rev. Lett. **98** 091801 (2007).
17. B. Aubert *et al.* (BABAR Collab.), Phys. Rev. Lett. **100** 151802 (2008).
18. J. Abdallah *et al.* (Delphi Collab.), Eur. Phys. Jour. C **45** 35 (2006).
19. D. Liventsev *et al.* (Belle Collab.), Phys. Rev. D **77** 091503 (2008); see also the contribution from D. Liventsev in these proceedings.

20. J.G. Körner and G.A. Schuler, *Z. Phys. C* **46** 93 (1990); A.F. Falk *et al.*, *Phys. Lett. B* **326** 145 (1994); M. Tanaka, *Z. Phys. C* **67** 321 (1995); K. Kiers and A. Soni, *Phys. Rev. D* **56** 5786 (1997); D.S. Hwang and D.-W. Kim, *Eur. Phys. Jour. C* **14** 271 (2000); H. Itoh, S. Komine, and Y. Okada, *Prog. Theor. Phys.* **114** 179 (2005); C.-H. Chen and C.-Q. Geng, *JHEP* **0610** 053 (2006); U. Nierste, S. Trine, and S. Westhoff, arXiv:0801.4938.
21. A. Matyja *et al.* (Belle Collab.), *Phys. Rev. Lett.* **99** 191807 (2007); B. Aubert *et al.* (BABAR Collab.), *Phys. Rev. Lett.* **100** 021801 (2008).

Charm and tau decays at B factories

A. Zupanc

*Jozef Stefan Institute, Experimental Particle Physics Department,
Jamova 39, 1001 Ljubljana, Slovenia*

We discuss recent results on charm and tau physics obtained by the Belle and BaBar collaborations. In the charm section we present measurements of $D^0 - \bar{D}^0$ mixing parameters, measurements searches for CP violation in D^0 decays and a measurement of D_s meson decay constant. In the tau section the recent results on lepton flavor violation in tau decays to three leptons or a lepton and a vector meson are discussed.

1 Introduction

The cross-sections for $c\bar{c}$ and τ pair production are very similar to the $b\bar{b}$ production cross-section at the B factories. The Belle¹ and BaBar² detectors at the KEKB³ and PEP-II colliders have accumulated together over 1 ab^{-1} of data and therefore provide large samples and an excellent environment to study charm and τ decays.

2 $D^0 - \bar{D}^0$ mixing and search for CP violation in D^0 decays

Particle-antiparticle mixing has been observed in several systems of neutral mesons: neutral kaons, B_d and B_s mesons. Last year at this conference the first evidence for $D^0 - \bar{D}^0$ mixing^{4,5} was presented by both Belle and BaBar collaborations. As in the kaon and B-meson systems, the $D^0 - \bar{D}^0$ are produced in flavor eigenstates. The mixing occurs through weak interactions between the quarks and gives rise to two different mass eigenstates

$$|D_{1,2}\rangle = p|D^0\rangle \pm q|\bar{D}^0\rangle, \quad (1)$$

where $|p|^2 + |q|^2 = 1$. The time evolution of flavor eigenstate is then given by

$$|D^0(t)\rangle = \left[|D^0\rangle \cosh\left(\frac{ix+y}{2}t\right) + \frac{q}{p}|\bar{D}^0\rangle \sinh\left(\frac{ix+y}{2}t\right) \right] \times e^{-\frac{1}{2}(1+\frac{im}{\Gamma})t}, \quad (2)$$

Table 1: The mixing parameter y_{CP} and CP violating parameter ΔY measured by BaBar using the ratios of lifetimes for the decays of D^0 mesons to K^-K^+ , $\pi^-\pi^+$ and $K^-\pi^+$.

Sample	y_{CP}	ΔY
K^-K^+	$(+1.60 \pm 0.46 \pm 0.17)\%$	$(-0.40 \pm 0.44 \pm 0.12)\%$
$\pi^-\pi^+$	$(+0.46 \pm 0.65 \pm 0.25)\%$	$(+0.05 \pm 0.64 \pm 0.32)\%$
Combined	$(+1.24 \pm 0.39 \pm 0.13)\%$	$(-0.26 \pm 0.36 \pm 0.08)\%$

where the two parameters that describe the $D^0 - \bar{D}^0$ mixing x and y ,

$$x = \frac{m_1 - m_2}{\Gamma}, \quad (3)$$

$$y = \frac{\Gamma_1 - \Gamma_2}{2\Gamma}, \quad (4)$$

$$\Gamma = \frac{\Gamma_1 + \Gamma_2}{2} \quad (5)$$

are the mass and width difference of the two mass eigenstates. In the Standard Model (SM), $D^0 - \bar{D}^0$ mixing is strongly GIM and CKM suppressed, and is dominated by long distance effects⁶. As the mixing rate is expected to be small within the SM, it is sensitive to the contribution of new, as of now unobserved processes and particles. The largest SM predictions for the parameters x and y , which include the impact of long distance dynamics, are of order 1%⁶.

CP violating effects in decays of neutral D meson system would appear as a difference in the partial decay widths of D^0 and \bar{D}^0 mesons decaying to a CP eigenstate f

$$A_{CP} = \frac{\Gamma(D^0 \rightarrow f) - \Gamma(\bar{D}^0 \rightarrow \bar{f})}{\Gamma(D^0 \rightarrow f) + \Gamma(\bar{D}^0 \rightarrow \bar{f})}. \quad (6)$$

The contribution to the time-integrated asymmetry in neutral D meson decays can be separated into three parts: direct CP violation in decays to specific states, indirect CP violation in $D^0 - \bar{D}^0$ mixing, and indirect CP violation in interference between mixing and decay. Indirect CP violation is to a good approximation predicted to be universal for amplitudes with final CP eigenstates, but direct CP violation can be non-universal depending on the specifics of the new physics. Within the SM the expected level of CP violation is below the current experimental sensitivity⁷, therefore any positive signal would indicate physics beyond the SM.

BaBar measured $D^0 - \bar{D}^0$ mixing parameters using the ratios of lifetimes for the decays of neutral D mesons to CP even eigenstates K^-K^+ and $\pi^-\pi^+$ to the mixed-CP state $K^-\pi^+$ ⁸. The ratio of lifetimes

$$y_{CP} = \frac{\tau_{K\pi}}{\tau_{hh}} - 1, \quad h = K, \pi, \quad (7)$$

corresponds in the limit of conserved CP symmetry to the mixing parameter y defined above. By measuring the lifetime difference of D^0 and \bar{D}^0 mesons decaying to CP eigenstates the CP violating parameter

$$\Delta Y = \frac{\tau_{K\pi}}{\langle \tau_{hh} \rangle} A_{\Gamma}, \quad A_{\Gamma} = \frac{\tau_{hh}(D^0) - \tau_{hh}(\bar{D}^0)}{\tau_{hh}(D^0) + \tau_{hh}(\bar{D}^0)} \quad (8)$$

is measured. In the limit of CP conservation $\Delta Y = 0$.

The D^0 meson is required to be produced in a $D^{*+} \rightarrow D^0\pi^+$ decay^a. This requirement suppresses the background and tags the flavor of neutral D meson at the production with the charge of the pion. The D^0 lifetime is determined from an unbinned likelihood fit to the

^aCharge conjugation is implied throughout this paper.

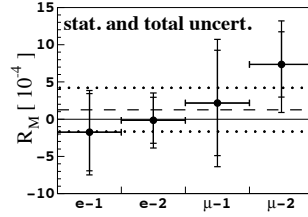


Figure 1: The R_M values of the four subsamples (e and μ , each for two different Belle detector configurations). Fit result to this four values is shown with dashed line, the dotted lines represent $\pm\sigma$ interval, and the solid line corresponds to no mixing.

reconstructed decay time and its estimated error, determined by a vertex-constrained combined fit to the D^0 decay and production vertices. The obtained value of y_{CP} given in Table 1, combined for both decay modes, represent evidence of $D^0 - \bar{D}^0$ mixing at the 3σ level. It confirms the lifetime ratio measurement made by Belle⁴. The comparison of measured lifetimes for D^0 and \bar{D}^0 decaying to CP eigenstates K^-K^+ , $\pi^-\pi^+$ shows now evidence for CP violation (Table 1).

Belle performed an improved search for $D^0 - \bar{D}^0$ mixing using semileptonic $D^0 \rightarrow K^{(*)-}\ell^+\nu_\ell$ decays⁹, where the lepton is either an electron or a muon. Neutral D mesons from $D^{*+} \rightarrow D^0\pi^+$ decays are used and tagged at production by the charge of the pion. The mixing parameter,

$$R_M \simeq \frac{x^2 + y^2}{2} = \frac{N_{WS}}{N_{RS}}, \quad (9)$$

is determined by measuring the numbers of reconstructed wrong (WS) and right sign (RS) events. The non-mixed decay results in a charge combination $\pi^+K^-\ell^+$ referred to as the RS charge combination while the mixing process results in a charge combination $\pi^+K^+\ell^-$ and is referred to as the WS charge combination. The reconstructed masses of D^0 and D^{*+} candidates are smeared since the neutrino is not directly reconstructed. The RS and WS yields are determined from the fits to the RS and WS distributions of mass difference $\Delta M = M(K\ell\nu\pi) - M(K\ell\nu)$, in which the uncertainty due to the neutrino four momentum cancels to a large extent. No significant WS signal is found in either the electron or muon samples and the most stringent experimental limit, obtained from semileptonic decays, on time integrated mixing rate is given, $R_M < 6.1 \times 10^{-4}$ at 90% C.L. The R_M values obtained for each subsample, e and μ , are shown on Fig. 1.

The Belle and BaBar collaborations performed measurements searching for CP violation in decays of neutral D mesons to K^-K^+ , $\pi^-\pi^+$ ¹⁰, $\pi^-\pi^+\pi^0$ ^{11,12} and $K^+K^-\pi^0$ ¹². The main experimental challenge in these analyses is precise tagging of a neutral D meson decaying to a CP eigenstate. The flavor of the D^0 meson at production is tagged, as in the mixing analyses described above, by reconstructing $D^{*+} \rightarrow D^0\pi^+$ decays. Beside the intrinsic asymmetry A_{CP} , defined by Eq. 6, there are two other contributions that create a difference in the numbers of reconstructed D^0 and \bar{D}^0 events. The first one is the forward-backward (FB) asymmetry in the production of D^{*+} in $e^+e^- \rightarrow c\bar{c}$ arising from $\gamma-Z$ interference and higher order QED effects and is an odd function of the cosine of the D^{*+} production polar angle in the center-of-mass system (CMS)¹³. The second one is the asymmetry in the reconstruction efficiencies of oppositely charged pions from D^{*+} decays. The effect of the latter is evaluated and corrected for by measuring the relative detection efficiency for tagging pions using the $D^0 \rightarrow K^-\pi^+$ decays with and without flavor tag. CP violation would appear as an asymmetry in the $D^0 - \bar{D}^0$ yields independent of any kinematic variable. However, the reconstruction efficiency of the tagging pion is polar angle dependent, therefore the CP asymmetry, $A_{CP} = \frac{N_{D^0} - N_{\bar{D}^0}}{N_{D^0} + N_{\bar{D}^0}}$, is measured

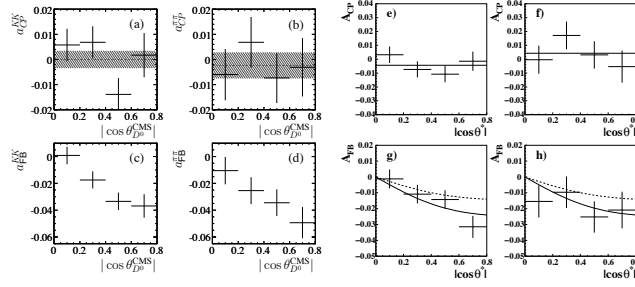


Figure 2: CP -violating asymmetries in KK (BaBar (a) and Belle (e)) and $\pi\pi$ (BaBar (b) and Belle (f)), and forward-backward asymmetries in KK (BaBar (c) and Belle (g)) and $\pi\pi$ (BaBar (d) and Belle (h)). In (a), (b), (e), and (f) the horizontal lines represent the central values.

Table 2: Measured CP asymmetry by the BaBar and Belle Collaborations in $D^0 \rightarrow K^-K^+$ and $D^0 \rightarrow \pi^-\pi^+$ decays.

A_{CP}^{hh}	BaBar	Belle
K^+K^-	$(0.00 \pm 0.34(\text{stat}) \pm 0.13(\text{syst}))\%$	$(-0.43 \pm 0.30(\text{stat}) \pm 0.11(\text{syst}))\%$
$\pi^+\pi^-$	$(-0.24 \pm 0.52(\text{stat}) \pm 0.22(\text{syst}))\%$	$(+0.43 \pm 0.52(\text{stat}) \pm 0.12(\text{syst}))\%$

in intervals of the cosine of the polar angle in the CMS. Any forward-backward asymmetry is canceled by averaging over symmetric intervals in the cosine of the polar angle in the CMS.

In Table 2 the measured CP asymmetry by the BaBar and Belle Collaborations in $D^0 \rightarrow K^-K^+$ and $D^0 \rightarrow \pi^-\pi^+$ decays is given. No CP violation is observed in either of the decay modes. The measurements are statistically limited. The main source of the systematic uncertainty is the statistics of the $D^0 \rightarrow K^-\pi^+$ samples, used to correct the charged pion reconstruction efficiency asymmetry and will thus also reduce with larger data samples.

The three-body decays $D^0 \rightarrow \pi^-\pi^+\pi^0$, $K^-K^+\pi^0$ proceed both via CP eigenstates and flavor states, making it possible to probe CP violation in both types of amplitudes and in the interference between them. Measuring interference effects in a Dalitz plot probes asymmetries in both the magnitudes and phases of the amplitudes, not simply in the overall decay rates. Belle measured time- and phase-space integrated CP asymmetry (Eq. 6) in $D^0 \rightarrow \pi^-\pi^+\pi^0$ decays and BaBar measured it in $D^0 \rightarrow \pi^-\pi^+\pi^0$ and $D^0 \rightarrow K^-K^+\pi^0$ decays. Measured asymmetries are given in Table 3. The asymmetry in reconstruction efficiency of tagging pions from D^{*+} decays was evaluated using independent $D^{*+} \rightarrow D^0(K_S\pi^0)\pi^+$ data and Monte Carlo simulated samples at Belle, while in BaBar's measurement it was evaluated using tagged and untagged data samples of $D^0 \rightarrow K^-\pi^+$ decays as described above. This difference explains the larger systematic uncertainty on measured CP asymmetry from Belle. The phase-space integrated CP asymmetry is insensitive to differences in the Dalitz plot shapes, so BaBar adopted three other approaches to search for CP violation in $D^0 \rightarrow \pi^-\pi^+\pi^0$, $K^-K^+\pi^0$ decays. First they quantified differences between the D^0 and \bar{D}^0 Dalitz plots in two dimensions by plotting normalized residuals (shown in Figure 3)

$$\Delta = (n_{\bar{D}^0} - Rn_{D^0}) / \sqrt{\sigma_{n_{\bar{D}^0}}^2 + R^2\sigma_{n_{D^0}}^2} \quad (10)$$

in the Dalitz plot area elements, and where n denotes the number of events, σ its uncertainty and R is the efficiency corrected ratio. From the calculated $\chi^2/\nu = (\sum_{DP} \Delta^2)/\nu$ value, where ν is the number of Dalitz plot elements, the one-sided Gaussian confidence levels for consistency with no CP violation are obtained: 32.8% for $\pi^-\pi^+\pi^0$ and 16.6% for $K^-K^+\pi^0$. In BaBar's second approach differences in the angular moments of the D^0 and \bar{D}^0 intensity distributions

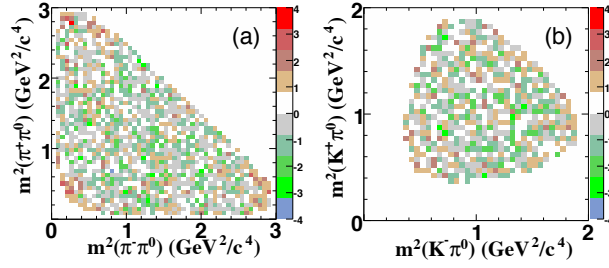


Figure 3: Normalized residuals Δ for $D^0 \rightarrow \pi^- \pi^+ \pi^0$ (left) and $D^0 \rightarrow K^- K^+ \pi^0$ (right) decays.

Table 3: Measured CP asymmetry by the Belle and BaBar Collaborations in $D^0 \rightarrow \pi^- \pi^+ \pi^0$ and $D^0 \rightarrow K^- K^+ \pi^0$ decays.

A_{CP}^f	Belle	BaBar
$\pi^+ \pi^- \pi^0$	$(0.43 \pm 0.41(\text{stat}) \pm 1.23(\text{syst}))\%$	$(-0.31 \pm 0.41(\text{stat}) \pm 0.17(\text{syst}))\%$
$K^+ K^- \pi^0$	-	$(+1.00 \pm 1.67(\text{stat}) \pm 0.25(\text{syst}))\%$

are looked for. The angular moments of the cosine of the helicity angle of the D^0 meson decay products reflect the spin and mass structure of intermediate resonant and nonresonant amplitudes. Similarly to the previous approach the one sided Gaussian confidence levels for consistency with no CP violation are obtained: 28.2% for the $\pi^+ \pi^-$, 28.4% for the $\pi^+ \pi^0$, 63.1% for the $K^+ K^-$, and 23.8% for the $K^+ \pi^0$ subsystems. In the third, model dependent approach, BaBar searched for CP violation in the amplitudes describing intermediate states in the D^0 and \bar{D}^0 decays. The Dalitz plot amplitude \mathcal{A} can be parametrized as a sum of amplitudes $A_r(s_+, s_-)$ for all relevant intermediate states r , each with a complex coefficient, i.e., $\mathcal{A} = \sum_r a_r e^{i\phi_r} A_r(s_+, s_-)$, where a_r and ϕ_r are real and s_+ and s_- are the squared invariant masses of the pair of final state particles with $+1$ and -1 net charge. In the absence of CP violation the values of a_r and ϕ_r are expected to be identical for D^0 and \bar{D}^0 decay. Comparison of amplitudes and relative phases, a_r and ϕ_r , obtained for D^0 and \bar{D}^0 decays showed, that the CP asymmetry in any amplitude, relative to that of the whole decay, is no larger than a few percent.

3 Measurement of $\mathcal{B}(D_s^+ \rightarrow \mu^+ \nu_\mu)$

One of the more important goals of particle physics is the precise measurement and understanding of the CKM matrix. To interpret results on B meson decays, theoretical calculations of form factors and decay constants are often needed (usually based on lattice gauge theory¹⁴). Decays of charmed hadrons in turn enable tests of the predictions for analogous quantities in the charm sector. It is necessary to have accurate measurements in the charm sector to check theoretical methods and predictions. In the SM the leptonic decays of mesons are mediated by a single virtual W^\pm boson. The decay rate for e.g. $D_s^+ \rightarrow \ell^+ \nu_\ell$ is given by

$$\Gamma(D_s^+ \rightarrow \ell^+ \nu_\ell) = \frac{G_F^2}{8\pi} f_{D_s}^2 m_\ell^2 m_{D_s} \left(1 - \frac{m_\ell^2}{m_{D_s}^2}\right)^2 |V_{cs}|^2, \quad (11)$$

where G_F is the Fermi coupling constant, V_{cs} is the corresponding CKM matrix element, m_ℓ and m_{D_s} are the masses of the lepton and D_s meson, respectively. The effects of the strong interaction are accounted for by the decay constant f_{D_s} . Since the decay rate is very small for

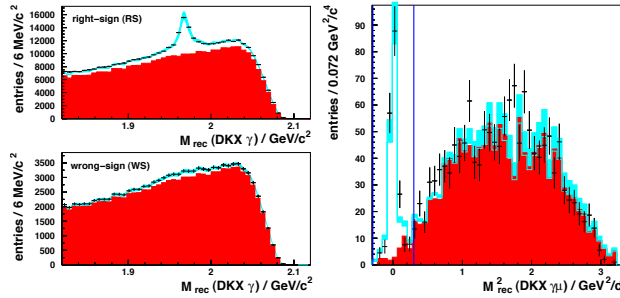


Figure 4: Recoil mass spectrum for D_s -tags for right-sign (left top) and wrong sign (left bottom) charge combinations of the D meson and kaon. (Right) Spectrum of missing mass squared for $D_s^+ \rightarrow \mu^+ \nu_\mu$ candidates. The signal peaks at zero, the background shape in red is obtained by reconstructing $D_s^+ \rightarrow e^+ \nu_e$ decays, where no signal is expected due to helicity suppression.

electrons due to helicity suppression and detection of τ 's involves additional neutrinos, the muon mode is experimentally the most accessible one.

The analysis performed at Belle uses events of the type $e^+e^- \rightarrow D_s^* D^{\pm,0} K^{\pm,0} X$, where X can be any number of pions and up to one photon¹⁵. The particles in the final state are divided into a tag and signal side. The tag side consists of a D meson and a kaon in any charge combination and tags the flavor of the D_s meson. The signal side is a D_s^* decaying to $D_s \gamma$. Reconstructing the tag side, and allowing for any possible set of particles in X , the signal side is identified by reconstruction of the recoil mass as shown in Figure 4. Within this sample of tagged inclusive D_s decays, decays of D_s meson to muon and neutrino are selected by requiring another charged track that is identified as a muon and has the same charge as the D_s candidate. The number of reconstructed $D_s^+ \rightarrow \mu^+ \nu_\mu$ decays is then determined from the fit to the recoil mass squared against all reconstructed particles, including the muon, as shown in Figure 4. Normalizing the number of reconstructed $D_s^+ \rightarrow \mu^+ \nu_\mu$ decays to the number of reconstructed tagged inclusive D_s decays an absolute branching ratio is measured

$$\mathcal{B}(D_s^+ \rightarrow \mu^+ \nu_\mu) = [6.44 \pm 0.76(\text{stat}) \pm 0.57(\text{syst})] \times 10^{-3}, \quad (12)$$

which is consistent with the world average¹⁶ and Babar's¹⁷ and Cleo-c's¹⁸ measurements. The obtained value of f_{D_s} using Eq. 11 is

$$f_{D_s} = (275 \pm 16(\text{stat}) \pm 12(\text{syst})) \text{ MeV}. \quad (13)$$

A simple average of the D_s meson decay constant obtained from the cited measurements has an uncertainty of 11 MeV. Recently a lattice QCD calculation of significantly improved precision was performed, with preliminary result $f_{D_s} = (241 \pm 3) \text{ MeV}$ ¹⁹. This value is somewhat lower than the experimental average and if it proves to be stable the comparison with the experimental results may point to some inconsistency between the two. More precise measurements are needed for a firm conclusion.

4 Search for lepton flavor violating τ decays

One of the currently most interesting questions in τ physics is whether there is a sizable lepton flavor violation (LFV) or not. LFV decays are expected even in the SM extended with the massive neutrinos²⁰, but the expected rate is very small and far beyond the reach of B factories. Many extensions of the SM however, predict LFV $\tau \rightarrow \ell \ell \ell$ decays at the level of $10^{-10} - 10^{-7}$ ²¹, which can be already probed at B factories with the current accumulated data. B factories provide very clean environment for measurements searching for LFV τ decays. Candidate signal events are required to have 1-3 topology, where the τ on the signal side yields three charged

Table 4: Improved 90% C.L. upper limits (UL) on $\mathcal{B}(\tau \rightarrow \ell\ell\ell)$.

Mode	Belle $\mathcal{B}_{\text{UL}}^{90}(\times 10^{-8})$	BaBar $\mathcal{B}_{\text{UL}}^{90}(\times 10^{-8})$
$\tau^- \rightarrow e^- e^+ e^-$	3.6	4.3
$\tau^- \rightarrow \mu^- \mu^+ \mu^-$	3.2	5.3
$\tau^- \rightarrow e^- \mu^+ \mu^-$	4.1	3.7
$\tau^- \rightarrow \mu^- e^+ e^-$	2.7	8.0
$\tau^- \rightarrow e^+ \mu^- \mu^-$	2.3	5.6
$\tau^- \rightarrow \mu^+ e^- e^-$	2.0	5.8
$\mathcal{L} \text{ (fb}^{-1}\text{)}$	535	376

Table 5: Improved 90% C.L. upper limits (UL) on $\mathcal{B}(\tau \rightarrow \ell V^0)$.

Mode	Belle $\mathcal{B}_{90}(\times 10^{-8})$	BaBar $\mathcal{B}_{90}(\times 10^{-8})$	Mode	Belle $\mathcal{B}_{\text{UL}}^{90}(\times 10^{-8})$	BaBar $\mathcal{B}_{\text{UL}}^{90}(\times 10^{-8})$
$\tau^- \rightarrow e^- \phi$	7.3	–	$\tau^- \rightarrow \mu^- \phi$	13	–
$\tau^- \rightarrow e^- \omega$	18	11	$\tau^- \rightarrow \mu^- \omega$	8.9	10
$\tau^- \rightarrow e^- K^{*0}$	7.8	–	$\tau^- \rightarrow \mu^- K^{*0}$	5.9	–
$\tau^- \rightarrow e^- \bar{K}^{*0}$	7.7	–	$\tau^- \rightarrow \mu^- \bar{K}^{*0}$	10	–
$\tau^- \rightarrow e^- \rho^0$	6.3	–	$\tau^- \rightarrow \mu^- \rho^0$	6.8	–
$\mathcal{L} \text{ (fb}^{-1}\text{)}$	543	384	$\mathcal{L} \text{ (fb}^{-1}\text{)}$	543	384

particles, while the second τ on the tag side yields one charged track. The event is easily divided into two hemispheres in the CMS. The signal side does not include any neutrinos in the final state, therefore signal events should peak at the nominal mass of the tau and at zero in the two dimensional distribution of the invariant mass versus energy difference.

Belle and BaBar reported improved upper limits on $\tau \rightarrow \ell\ell\ell$ branching ratios^{22,23}, where leptons in the final state are either electrons or muons, leading to six distinct decay modes: $e^- e^+ e^-$, $\mu^+ e^- e^-$, $\mu^- e^+ e^-$, $e^+ \mu^- \mu^-$, $e^- \mu^+ \mu^-$ and $\mu^- \mu^+ \mu^-$. In all cases the observed number of events in the signal region is consistent with the expected background. The improved upper limits on branching ratios, given in Table 4, are of order of 10^{-8} and they already restrict the parameter space of some beyond the SM models.

Belle reported improved upper limits on LFV τ decays to a lepton and vector meson, where the lepton is either an electron or a muon and vector meson is either ϕ , K^{*0} , \bar{K}^{*0} or ρ^0 ²⁴. For the first same a search for $\tau \rightarrow \ell\omega$ ($\ell = e, \mu$) decays was performed by Belle and BaBar^{24,25}. No significant signal was observed in any of the studied decay modes. The improved upper limits on $\mathcal{B}(\tau \rightarrow \ell V^0)$ range from $5.9\text{--}10 \times 10^{-8}$ and are given in Table 5.

5 Conclusions

Only one year after the first observation of $D^0 - \bar{D}^0$ mixing, the mixing parameter y_{CP} is known with relatively high precision. The current world averages of the mixing parameters x and y ²⁶ lie at the upper edge of still uncertain theoretical expectations, at the level of 1%, therefore making it impossible to conclude whether $D^0 - \bar{D}^0$ mixing is a purely SM effect or receives contributions from new physics. CP violation is expected to be small in the D meson system, below the sensitivity of current experimental data. If large CP violating phases are present in yet unknown processes the asymmetries could be increased to $\sim 1\%$. All measured CP asymmetries

in D^0 decays observe no CP violation.

Further measurements of the D_s meson decay constant are needed to resolve the discrepancy between the latest lattice QCD calculations and the experimental value.

The measurements searching for LFV tau decays are approaching the 10^{-8} level and already restrict the parameter space of many beyond the SM models.

References

1. A. Abashian *et al.*, Nucl. Instrum. Meth. A **479**, 117 (2002).
2. B. Aubert *et al.* [BABAR Collaboration], Nucl. Instrum. Meth. A **479**, 1 (2002).
3. S. Kurokawa, Nucl. Instrum. Meth. A **499**, 1 (2003).
4. M. Staric *et al.* [Belle Collaboration], Phys. Rev. Lett. **98**, 211803 (2007).
5. B. Aubert *et al.* [BABAR Collaboration], Phys. Rev. Lett. **98**, 211802 (2007).
6. I.I. Bigi, N. Uraltsev, Nucl. Phys. B **592**, 92 (2001); A.F. Falk, Y. Grossman, Z. Ligeti, A.A. Petrov, Phys. Rev. D **65**, 054034 (2002); A.F. Falk, Y. Grossman, Y. Nir, A.A. Petrov, Phys. Rev. D **69**, 114021 (2004).
7. I.I. Bigi, A.I. Sanda, *CP violation* (Cambridge University Press, Cambridge, 2000), p. 257; S. Bianco, F.L. Fabbri, D. Benson, I. Bigi, Riv. Nuovo Cim. **26N7**, 1 (2003); G. Burdman, I. Shipsey, Ann. Rev. Nucl. Part. Sci. **53**, 431 (2003).
8. B. Aubert *et al.* [BABAR Collaboration], arXiv:0712.2249 [hep-ex].
9. U. Bitenc *et al.* [BELLE Collaboration], arXiv:0802.2952 [hep-ex].
10. B. Aubert *et al.* [BaBar Collaboration], Phys. Rev. Lett. **100**, 061803 (2008).
11. K. Arinstein *et al.* [Belle Collaboration], Phys. Lett. B **662**, 102 (2008).
12. B. Aubert *et al.* [BABAR Collaboration], arXiv:0802.4035 [hep-ex].
13. F.A. Berends, K.J.F. Gaemers, R. Gastmans, Nucl. Phys B **63**, 381 (1973); R.W. Brown, K.O. Mikaelian, V.K. Cung, E.A. Paschos, Phys. Lett. B **43**, 403 (1973); R.J. Cashmore, C.M. Hawkes, B.W. Lynn, R.G. Stuart, Z. Phys. C **30**, 125 (1986).
14. A. S. Kronfeld [Fermilab Lattice Collaboration], J. Phys. Conf. Ser. **46**, 147 (2006).
15. L. Widhalm *et al.* [Belle Collaboration], arXiv:0709.1340 [hep-ex].
16. W.-M. Yao *et al.* [Particle Data Group], J. Phys. G **33**, 1 (2006).
17. B. Aubert *et al.* [BABAR Collaboration], Phys. Rev. Lett. **98**, 141801 (2007).
18. M. Artuso *et al.* [CLEO-c Collaboration], Phys. Rev. Lett. **99**, 071802 (2007).
19. E. Follana, C. T. H. Davies, G. P. Lepage and J. Shigemitsu [HPQCD Collaboration], Phys. Rev. Lett. **100**, 062002 (2008).
20. B. W. Lee and R. E. Shrock, Phys. Rev. D **16**, 1444 (1977); X. Y. Pham, Eur. Phys. J. C **8**, 513 (1999).
21. J. R. Ellis *et al.*, Phys. Rev. D **66**, 115013 (2002); J. P. Saha and A. Kundu, Phys. Rev. D **66**, 054021 (2002); A. Brignole *et al.*, Phys. Lett. B **566**, 217 (2003); A. Brignole and A. Rossi, Nucl. Phys. B **701**, 3 (2004); R. Barbier *et al.*, Phys. Rept. **420**, 1 (2005); P. Paradisi, JHEP **10**, 006 (2005); E. Arganda and M. J. Herrero, Phys. Rev. D **73**, 055003 (2006); M. Blanke *et al.*, JHEP **5**, 013 (2007); C.-X. Yue and Sh. Zhao, Eur. Phys. J. C **50**, 897 (2007); A. G. Akeroyd *et al.*, Phys. Rev. D **76**, 012004 (2007); A. Ilakovac, Phys. Rev. D **62**, 036010 (2000); A. Cordero-Cid *et al.*, Phys. Rev. D **72**, 117701 (2005); B. Bajc, M. Nemevsek and G. Senjanovic, Phys. Rev. D **76** (2007) 055011.
22. K. Abe *et al.* [Belle Collaboration], Phys. Lett. B **660**, 154 (2008).
23. B. Aubert *et al.* [BABAR Collaboration], Phys. Rev. Lett. **99**, 251803 (2007).
24. Y. Nishio *et al.* [Belle Collaboration], arXiv:0801.2475 [hep-ex].
25. B. Aubert *et al.* [BABAR Collaboration], Phys. Rev. Lett. **100**, 071802 (2008).
26. Heavy Flavor Averaging Group, <http://www.slac.stanford.edu/xorg/hfag/charm/index.html>

CONSTRAINING NEW PHYSICS FROM $D^0 - \bar{D}^0$ MIXING

ALEXEY A. PETROV

*Department of Physics and Astronomy, Wayne State University
Detroit, MI 48201, USA
Michigan Center for Theoretical Physics, University of Michigan
Ann Arbor, MI 48109, USA*



I review constraints on possible New Physics interactions from $D^0 - \bar{D}^0$ mixing measurements. I consider the most general low energy effective Hamiltonian and include leading order QCD running of effective operators. I discuss constraints from an extensive list of popular New Physics models, each of which could be discovered at the LHC, that can generate these operators. In most of the scenarios, strong constraints that surpass those from other search techniques could be placed on the allowed parameter space using the existent evidence for observation of D meson mixing.

1 Introduction

Meson-antimeson mixing has traditionally been of importance because it is sensitive to heavy degrees of freedom that propagate in the underlying mixing amplitudes. Estimates of the charm quark and top quark mass scales were inferred from the observation of mixing in the K^0 and B_d systems, respectively, before these particles were discovered directly.

This success has motivated attempts to indirectly detect New Physics (NP) signals by comparing the observed meson mixing with predictions of the Standard Model (SM). $K^0 - \bar{K}^0$ mixing has historically placed stringent constraints on the parameter space of theories beyond the SM and provides an essential hurdle that must be passed in the construction of models with NP. The large mixing signal in the B_d and B_s systems, observed at the B-factories and the Tevatron collider, can be precisely described in terms of the SM alone, which makes the parameter spaces of various NP models increasingly constrained. These facts influenced theoretical and experimental studies of D^0 flavor oscillations, where the SM mixing rate is sufficiently small that the NP component might be able to compete. There has been a flurry of recent experimental activity

regarding the detection of D^0 - \bar{D}^0 mixing, which marks the first time Flavor Changing Neutral Currents (FCNC) have been observed in the charged $+2/3$ quark sector. With the potential window to discern large NP effects in the charm sector and the anticipated improved accuracy for future mixing measurements, the motivation for a comprehensive up-to-date theoretical analysis of New Physics contributions to D meson mixing is compelling.

The phenomenon of meson-anti-meson mixing occurs in the presence of operators that change quark flavor by two units¹. Those operators can be generated in both the Standard Model and many possible extensions of it. They produce off-diagonal terms in the meson-anti-meson mass matrix, so that the basis of flavor eigenstates no longer coincide with the basis of mass eigenstates. Those two bases, however, are related by a linear transformation,

$$|D_{1,2}\rangle = p|D^0\rangle \pm q|\bar{D}^0\rangle, \quad (1)$$

where the complex parameters p and q are obtained from diagonalizing the D^0 - \bar{D}^0 mass matrix. Neglecting CP-violation leads to $p = q = 1/\sqrt{2}$. The mass and width splittings between those mass eigenstates are given by

$$x_D = \frac{m_1 - m_2}{\Gamma_D}, \quad y_D = \frac{\Gamma_1 - \Gamma_2}{2\Gamma_D}. \quad (2)$$

It is expected that x_D and y_D should be rather small in the Standard Model, which is usually attributed to the absence of superheavy quarks destroying Glashow-Iliopoulos-Maiani (GIM) cancellation. In Eq. (2), Γ_D is the average width of the two neutral D meson mass eigenstates. The quantities which are actually measured in most experimental determinations of the mass and width differences, $y_D^{(\text{CP})}$, x'_D , and y'_D , are defined as

$$\begin{aligned} y_D^{(\text{CP})} &= y_D \cos \phi - x_D \sin \phi \left(\frac{A_m}{2} - A_{\text{prod}} \right), \\ x'_D &= x_D \cos \delta_{K\pi} + y_D \sin \delta_{K\pi}, \\ y'_D &= y_D \cos \delta_{K\pi} - x_D \sin \delta_{K\pi}, \end{aligned} \quad (3)$$

where $A_{\text{prod}} = (N_{D^0} - N_{\bar{D}^0}) / (N_{D^0} + N_{\bar{D}^0})$ is the so-called production asymmetry of D^0 and \bar{D}^0 (giving the relative weight of D^0 and \bar{D}^0 in the sample) and $\delta_{K\pi}$ is the strong phase difference between the Cabibbo favored and double Cabibbo suppressed amplitudes², which is usually measured in $D \rightarrow K\pi$ transitions. In what follows we shall neglect CP-violating parameters ϕ and A_m . In this limit $y_D^{(\text{CP})} = y_D$. Please see recent reviews^{1,3,4} for more complete analysis.

2 Experimental Constraints on Charm Mixing

The recent interest in D^0 - \bar{D}^0 mixing started with the almost simultaneous observations by the BaBar⁶ and Belle⁷ collaborations of nonzero mixing signals at about the per cent level,

$$y'_D = (0.97 \pm 0.44 \pm 0.31) \cdot 10^{-2} \quad (\text{BaBar}), \quad (4)$$

$$y_D^{(\text{CP})} = (1.31 \pm 0.32 \pm 0.25) \cdot 10^{-2} \quad (\text{Belle}). \quad (5)$$

This was soon followed by the announcement by the Belle collaboration of mixing measurements from the Dalitz plot analyses of $D^0 \rightarrow K_S \pi^+ \pi^-$ ⁸,

$$x_D = (0.80 \pm 0.29 \pm 0.17) \cdot 10^{-2}, \quad y_D = (0.33 \pm 0.24 \pm 0.15) \cdot 10^{-2}. \quad (6)$$

A fit to the current database by the Heavy Flavor Averaging Group (HFAG) gives⁵

$$x_D = 9.8_{-2.7}^{+2.6} \cdot 10^{-3}, \quad y_D = (7.5 \pm 1.8) \cdot 10^{-3}, \quad (7)$$

which is obtained assuming no CP-violation affecting mixing. It is important to note that the combined analysis of x_D and y_D excludes the "no-mixing" point $x_D = y_D = 0$ by $6.7\sigma^5$. This fact adds confidence that charm mixing has indeed been observed. Then, a correct interpretation of the results is important. In addition, as with any rare low-energy transition, the question arises on how to use it to probe for physics beyond the Standard Model.

3 Standard Model "background" in $D^0 - \overline{D}^0$ mixing

Theoretical predictions for x_D and y_D obtained in the framework of the Standard Model historically span several orders of magnitude. I will not discuss predictions of the SM for the charm mixing rates here, instead referring the interested reader to recent reviews^{1,3,4}. It might be advantageous to note that there are two approaches to describe $D^0 - \overline{D}^0$ mixing, neither of which give very reliable results because m_c is in some sense intermediate between heavy and light.

The inclusive approach^{10,11} is based on the operator product expansion (OPE). In the formal limit $m_c \gg \Lambda$ limit, where Λ is a scale characteristic of the strong interactions, x_D and y_D can be expanded in terms of matrix elements of local operators. The use of the OPE relies on local quark-hadron duality, and on Λ/m_c being small enough to allow a truncation of the series after the first few terms. This, however, is not realized in charm mixing, as the leading term in $1/m_c$ is suppressed by four and six powers of the strange quark mass for x_D and y_D respectively. The parametrically-suppressed higher order terms in $1/m_c$ can have less powers of m_s , thus being more important numerically¹¹. This results in reshuffling of the OPE series, making it a triple expansion in $1/m_c$, m_s , and α_s . The (numerically) leading term contains over twenty matrix elements of dimension-12, eight-quark operators, which are difficult to compute reliably. A naive power counting then yields $x_D, y_D < 10^{-3}$. The exclusive approach¹² sums over intermediate hadronic states. Since there are cancellations between states within a given $SU(3)$ multiplet, one needs to know the contribution of each state with high precision. However, the D is not light enough that its decays are dominated by a few final states. In the absence of sufficiently precise data, one is forced to use some assumptions. Large effects in y_D appear for decays close to D threshold, where an analytic expansion in $SU(3)_F$ violation is no longer possible. Thus, even though theoretical calculations of x_D and y_D are quite uncertain, the values $x_D \sim y_D \sim 1\%$ are quite natural in the Standard Model¹³.

It then appears that experimental results of Eq. (7) are consistent with the SM predictions. Yet, those predictions are quite uncertain to be subtracted from the experimental data to precisely constrain possible NP contributions. In this situation the following approach can be taken. One can neglect the SM contribution altogether and assume that NP saturates the result reported by experimental collaborations. This way, however, only an upper bound on the NP parameters can be placed. A subtlety of this method of constraining the NP component of the mixing amplitude is related to the fact that the SM and NP contributions can have either the same or opposite signs. While the sign of the SM contribution cannot be calculated reliably due to hadronic uncertainties, x_D computed entirely within a given NP model can be determined rather precisely. This stems from the fact that NP contributions are generated by heavy degrees of freedom making short-distance OPE reliable. This means that only the part of parameter space of NP models that generate x_D of the same sign as observed experimentally can be reliably and unambiguously constrained.

4 New Physics contributions to $D^0 - \overline{D}^0$ mixing

Any NP degree of freedom will generally be associated with a generic heavy mass scale M , at which the NP interaction will be most naturally described. At the scale m_c of the charm

mass, this description will have been modified by the effects of QCD, which should be taken into account. In order to see how NP might affect the mixing amplitude, it is instructive to consider off-diagonal terms in the neutral D mass matrix,

$$\left(M - \frac{i}{2}\Gamma\right)_{12} = \frac{1}{2M_D} \langle \bar{D}^0 | \mathcal{H}_w^{\Delta C=-2} | D^0 \rangle + \frac{1}{2M_D} \sum_n \frac{\langle \bar{D}^0 | \mathcal{H}_w^{\Delta C=-1} | n \rangle \langle n | \mathcal{H}_w^{\Delta C=-1} | D^0 \rangle}{M_D - E_n + i\epsilon} \quad (8)$$

where the first term contains $\mathcal{H}_w^{\Delta C=-2}$, which is an effective $|\Delta C| = 2$ hamiltonian, represented by a set of operators that are local at the $\mu \simeq m_D$ scale. Note that a b -quark also gives a (negligible) contribution to this term. This term only affects x_D , but not y_D .

The second term in Eq. (8) is given by a double insertion of the effective $|\Delta C| = 1$ Hamiltonian $\mathcal{H}_w^{\Delta C=-1}$. This term is believed to give dominant contribution to $D^0 - \bar{D}^0$ mixing in the Standard Model, affecting both x and y . It is generally believed that NP cannot give any sizable contribution to this term, since $\mathcal{H}_w^{\Delta C=-1}$ Hamiltonian also mediates non-leptonic D -decays, which should then also be affected by this NP contribution. I will show that there is a well-defined theoretical limit where NP contribution *dominates* lifetime difference y_D and consider implications of this limit in "real world".

4.1 New Physics in $|\Delta C| = 1$ interactions.

Consider a non-leptonic D^0 decay amplitude, $A[D^0 \rightarrow n]$, which includes a small NP contribution, $A[D^0 \rightarrow n] = A_n^{(\text{SM})} + A_n^{(\text{NP})}$. Here, $A_n^{(\text{NP})}$ is assumed to be smaller than the current experimental uncertainties on those decay rates. This ensures that NP effects cannot be seen in the current experimental analyses of non-leptonic D-decays. One can then write y_D as

$$y_D \simeq \sum_n \frac{\rho_n}{\Gamma_D} A_n^{(\text{SM})} A_n^{(\text{SM})} + 2 \sum_n \frac{\rho_n}{\Gamma_D} A_n^{(\text{NP})} A_n^{(\text{SM})} \quad . \quad (9)$$

The first term of Eq. (schematic) represents the SM contribution to y_D . The SM contribution to y_D is known to vanish in the limit of exact flavor $SU(3)$. Moreover, the first order correction is also absent, so the SM contribution arises only as a *second* order effect¹³. This means that in the flavor $SU(3)$ limit the lifetime difference y_D is dominated by the second term in Eq. (9), i.e. New Physics contributions, even if their contributions are tiny in the individual decay amplitudes¹⁴! A calculation reveals that NP contribution to y_D can be as large as several percent in R-parity-violating SUSY models⁹ or as small as $\sim 10^{-10}$ in the models with interactions mediated by charged Higgs particles¹⁴.

This wide range of theoretical predictions can be explained by two observations. First, many NP affecting $|\Delta C| = 1$ transitions also affect $|\Delta B| = 1$ or $|\Delta S| = 1$ decays or kaon and B-meson mixings, which are tightly constrained. Second, a detailed look at a given NP model that can potentially affect y_D reveals that the NP contribution itself can vanish in the flavor $SU(3)$ limit. For instance, the structure of the NP interaction might simply mimic the one of the SM. Effects like that can occur in some models with extra space dimensions. Also, the chiral structure of a low-energy effective lagrangian in a particular NP model could be such that the leading, mass-independent contribution vanishes exactly, as in a left-right model (LRM). Finally, the NP coupling might explicitly depend on the quark mass, as in a model with multiple Higgs doublets. However, most of these models feature second order $SU(3)$ -breaking already at leading order in the $1/m_c$ expansion. This should be contrasted with the SM, where the leading order is suppressed by six powers of m_s and term of order m_s^2 only appear as a $1/m_c^6$ -order correction.

4.2 New Physics in $|\Delta C| = 2$ interactions.

Though the particles present in models with New Physics may not be produced in charm quark decays, their effects can nonetheless be seen in the form of effective operators generated by the

exchanges of these new particles. Even without specifying the form of these new interactions, we know that their effect is to introduce several $|\Delta C| = 2$ effective operators built out of the SM degrees of freedom.

By integrating out new degrees of freedom associated with new interactions at a scale M , we are left with an effective hamiltonian written in the form of a series of operators of increasing dimension. Operator power counting then tells us the most important contributions are given by the operators of the lowest possible dimension, $d = 6$ in this case. This means that they must contain only quark degrees of freedom and no derivatives. Realizing this, we can write the complete basis of these effective operators, which can be done most conveniently in terms of chiral quark fields,

$$\langle f | \mathcal{H}_{NP} | i \rangle = G \sum_{i=1} C_i(\mu) \langle f | Q_i | i \rangle(\mu) , \quad (10)$$

where the prefactor G has the dimension of inverse-squared mass, the C_i are dimensionless Wilson coefficients, and the Q_i are the effective operators:

$$\begin{aligned} Q_1 &= (\bar{u}_L \gamma_\mu c_L) (\bar{u}_L \gamma^\mu c_L) , & Q_5 &= (\bar{u}_R \sigma_{\mu\nu} c_L) (\bar{u}_R \sigma^{\mu\nu} c_L) , \\ Q_2 &= (\bar{u}_L \gamma_\mu c_L) (\bar{u}_R \gamma^\mu c_R) , & Q_6 &= (\bar{u}_R \gamma_\mu c_R) (\bar{u}_R \gamma^\mu c_R) , \\ Q_3 &= (\bar{u}_L c_R) (\bar{u}_R c_L) , & Q_7 &= (\bar{u}_L c_R) (\bar{u}_L c_R) , \\ Q_4 &= (\bar{u}_R c_L) (\bar{u}_R c_L) , & Q_8 &= (\bar{u}_L \sigma_{\mu\nu} c_R) (\bar{u}_L \sigma^{\mu\nu} c_R) . \end{aligned} \quad (11)$$

In total, there are eight possible operator structures that exhaust the list of possible independent contributions to $|\Delta C| = 2$ transitions. Since these operators are generated at the scale M where the New Physics is integrated out, a non-trivial operator mixing can occur when one takes into account renormalization group running of these operators between the scales M and μ , with μ being the scale where the hadronic matrix elements are computed. We shall work at the renormalization scale $\mu = m_c \simeq 1.3$ GeV. This evolution is determined by solving the RG equations obeyed by the Wilson coefficients,

$$\frac{d}{d \log \mu} \vec{C}(\mu) = \hat{\gamma}^T \vec{C}(\mu) , \quad (12)$$

where $\hat{\gamma}$ represents the matrix of anomalous dimensions of the operators in Eq. (11)¹⁵. Due to the relatively simple structure of $\hat{\gamma}$, one can easily write the evolution of each Wilson coefficient in Eq. (10) from the New Physics scale M down to the hadronic scale μ , taking into account quark thresholds. Corresponding to each of the eight operators $\{Q_i\}$ ($i = 1, \dots, 8$) is an RG factor $r_i(\mu, M)$. The first of these, $r_1(\mu, M)$, is given explicitly by

$$r_1(\mu, M) = \left(\frac{\alpha_s(M)}{\alpha_s(m_t)} \right)^{2/7} \left(\frac{\alpha_s(m_t)}{\alpha_s(m_b)} \right)^{6/23} \left(\frac{\alpha_s(m_b)}{\alpha_s(\mu)} \right)^{6/25} . \quad (13)$$

and the rest can be expressed in terms of $r_1(\mu, M)$ as

$$\begin{aligned} r_2(\mu, M) &= [r_1(\mu, M)]^{1/2} , & r_6(\mu, M) &= r_1(\mu, M) , \\ r_3(\mu, M) &= [r_1(\mu, M)]^{-4} , & r_7(\mu, M) &= r_4(\mu, M) , \\ r_4(\mu, M) &= [r_1(\mu, M)]^{(1+\sqrt{241})/6} , & r_8(\mu, M) &= r_5(\mu, M) . \\ r_5(\mu, M) &= [r_1(\mu, M)]^{(1-\sqrt{241})/6} , & & \end{aligned} \quad (14)$$

The RG factors are generally only weakly dependent on the NP scale M since it is taken to be larger than the top quark mass, m_t , and the evolution of α_s is slow at these high mass scales. In Table 1, we display numerical values for the $r_i(\mu, M)$ with $M = 1, 2$ TeV and $\mu = m_c \simeq 1.3$ GeV. Here, we compute α_s using the one-loop evolution and matching expressions for perturbative consistency with the RG evolution of the effective hamiltonian. A contribution to $D^0 - \bar{D}^0$

$M(\text{TeV})$	$r_1(m_c, M)$	$r_2(m_c, M)$	$r_3(m_c, M)$	$r_4(m_c, M)$	$r_5(m_c, M)$
1	0.72	0.85	3.7	0.41	2.2
2	0.71	0.84	4.0	0.39	2.3

Table 1: Dependence of the RG factors on the heavy mass scale M .

mixing from a particular NP model can be obtained by calculating matching conditions for the Wilson coefficients C_i at the scale M , running their values down to μ and computing the relevant matrix elements of four-quark operators. A generic model of New Physics would then give the following contribution x_D ,

$$x_D^{NP} = G \frac{f_D^2 B_D m_D}{\Gamma_D} \left[\frac{2}{3} [C_1(m_c) + C_6(m_c)] - \frac{5}{12} [C_4(m_c) + C_7(m_c)] + \frac{7}{12} C_3(m_c) - \frac{5C_2(m_c)}{6} + [C_5(m_c) + C_8(m_c)] \right]. \quad (15)$$

Here we simplified the result by assuming that all non-perturbative ('bag') parameters are equal to $B_D \simeq 0.82$. The Wilson coefficients at the scale μ are related to the Wilson coefficients at the scale M by renormalization group evolution,

$$\begin{aligned} C_1(m_c) &= r_1(m_c, M) C_1(M), \\ C_2(m_c) &= r_2(m_c, M) C_2(M), \\ C_3(m_c) &= \frac{2}{3} [r_2(m_c, M) - r_3(m_c, M)] C_2(M) + r_3(m_c, M) C_3(M), \\ C_4(m_c) &= \frac{8}{\sqrt{241}} [r_5(m_c, M) - r_4(m_c, M)] \left[C_4(M) + \frac{15}{4} C_5(M) \right] \\ &\quad + \frac{1}{2} [r_4(m_c, M) + r_5(m_c, M)] C_4(M), \\ C_5(m_c) &= \frac{1}{8\sqrt{241}} [r_4(m_c, M) - r_5(m_c, M)] [C_4(M) + 64C_5(M)] \\ &\quad + \frac{1}{2} [r_4(m_c, M) + r_5(m_c, M)] C_5(M), \\ C_6(m_c) &= r_6(m_c, M) C_6(M), \\ C_7(m_c) &= \frac{8}{\sqrt{241}} [r_8(m_c, M) - r_7(m_c, M)] \left[C_7(M) + \frac{15}{4} C_8(M) \right] \\ &\quad + \frac{1}{2} [r_7(m_c, M) + r_8(m_c, M)] C_7(M), \\ C_8(m_c) &= \frac{1}{8\sqrt{241}} [r_7(m_c, M) - r_8(m_c, M)] [C_7(M) + 64C_8(M)] \\ &\quad + \frac{1}{2} [r_7(m_c, M) + r_8(m_c, M)] C_8(M), \end{aligned} \quad (16)$$

A contribution of each particular NP model can then be studied using Eq. (15). Even before performing such an analysis, one can get some idea what energy scales can be probed by $D^0 - \bar{D}^0$ mixing. Setting $G = 1/M^2$ and $C_i(M) = 1$, we obtain $M \sim 10^3$ TeV. More realistic models can be probed in the region of several TeV, which is very relevant for LHC phenomenology applications.

A program described above has been recently executed¹⁵ for 21 well-motivated NP models, which will be actively studied at LHC. The results are presented in Table 2. As can be seen, out of 21 models considered, only four received no useful constraints from $D^0 - \bar{D}^0$ mixing. More informative exclusion plots can be found in that paper¹⁵ as well. It is interesting to note that

Model	Approximate Constraint
Fourth Generation	$ V_{ub'}V_{cb'} \cdot m_{b'} < 0.5$ (GeV)
$Q = -1/3$ Singlet Quark	$s_2 \cdot m_S < 0.27$ (GeV)
$Q = +2/3$ Singlet Quark	$ \lambda_{uc} < 2.4 \cdot 10^{-4}$
Little Higgs	Tree: See entry for $Q = -1/3$ Singlet Quark Box: Parameter space can reach observed x_D
Generic Z'	$M_{Z'}/C > 2.2 \cdot 10^3$ TeV
Family Symmetries	$m_1/f > 1.2 \cdot 10^3$ TeV (with $m_1/m_2 = 0.5$)
Left-Right Symmetric	No constraint
Alternate Left-Right Symmetric	$M_R > 1.2$ TeV ($m_{D_1} = 0.5$ TeV) $(\Delta m/m_{D_1})/M_R > 0.4$ TeV $^{-1}$
Vector Leptoquark Bosons	$M_{VLQ} > 55(\lambda_{PP}/0.1)$ TeV
Flavor Conserving Two-Higgs-Doublet	No constraint
Flavor Changing Neutral Higgs	$m_H/C > 2.4 \cdot 10^3$ TeV
FC Neutral Higgs (Cheng-Sher)	$m_H/ \Delta_{uc} > 600$ GeV
Scalar Leptoquark Bosons	See entry for RPV SUSY
Higgsless	$M > 100$ TeV
Universal Extra Dimensions	No constraint
Split Fermion	$M/ \Delta y > (6 \cdot 10^2)$ GeV
Warped Geometries	$M_1 > 3.5$ TeV
MSSM	$ (\delta_{12}^u)_{LR,RL} < 3.5 \cdot 10^{-2}$ for $\tilde{m} \sim 1$ TeV $ (\delta_{12}^u)_{LL,RR} < .25$ for $\tilde{m} \sim 1$ TeV
SUSY Alignment	$\tilde{m} > 2$ TeV
Supersymmetry with RPV	$\lambda'_{12k}\lambda'_{11k}/m_{\tilde{d}_{R,k}} < 1.8 \cdot 10^{-3}/100$ GeV
Split Supersymmetry	No constraint

Table 2: Approximate constraints on NP models from D^0 mixing.

some models *require* large signals in the charm system if mixing and FCNCs in the strange and beauty systems are to be small (as in, for example, the SUSY alignment model^{16,17}).

5 Conclusions

I reviewed implications of recent measurement of $D^0 - \bar{D}^0$ mixing rates for constraining models of New Physics. A majority of considered models received competitive constraints from $D^0 - \bar{D}^0$ mixing measurements despite hadronic uncertainties that plague SM contributions. It should be noted that vast majority of predictions of NP models do not suffer from this uncertainty, and can be computed reliably, if lattice QCD community provides calculations of matrix elements of four-fermion operators Eq. (11).

Another possible manifestation of new physics interactions in the charm system is associated with the observation of (large) CP-violation^{1,4,18}. This is due to the fact that all quarks that build up the hadronic states in weak decays of charm mesons belong to the first two generations. Since 2×2 Cabbibo quark mixing matrix is real, no CP-violation is possible in the dominant tree-level diagrams which describe the decay amplitudes. CP-violating amplitudes can be introduced in the Standard Model by including penguin or box operators induced by virtual b -quarks. However, their contributions are strongly suppressed by the small combination of CKM matrix elements $V_{cb}V_{ub}^*$. It is thus widely believed that the observation of (large) CP violation in charm decays or mixing would be an unambiguous sign for New Physics.

Acknowledgments

This work was supported in part by the U.S. National Science Foundation CAREER Award PHY-0547794, and by the U.S. Department of Energy under Contract DE-FG02-96ER41005.

References

1. M. Artuso, B. Meadows and A. A. Petrov, to appear in *Ann. Rev. Nucl. Part. Sci.*, arXiv:0802.2934 [hep-ph]; A. A. Petrov, *In the Proceedings of Flavor Physics and CP Violation (FPCP 2003), Paris, France, 3-6 Jun 2003, pp MEC05* [arXiv:hep-ph/0311371].
2. S. Bergmann, *et. al*, *Phys. Lett. B* **486**, 418 (2000); A. F. Falk, Y. Nir and A. A. Petrov, *JHEP* **9912**, 019 (1999).
3. E. Golowich, arXiv:0806.1868 [hep-ph].
4. S. Bianco, F. L. Fabbri, D. Benson and I. Bigi, *Riv. Nuovo Cim.* **26N7**, 1 (2003).
5. A. J. Schwartz, arXiv:0803.0082 [hep-ex].
6. B. Aubert *et al.* [BABAR Collaboration], *Phys. Rev. Lett.* **98**, 211802 (2007).
7. M. Staric *et al.* [Belle Collaboration], *Phys. Rev. Lett.* **98**, 211803 (2007).
8. K. Abe *et al.* [BELLE Collaboration], *Phys. Rev. Lett.* **99**, 131803 (2007).
9. A. A. Petrov and G. K. Yeghiyan, *Phys. Rev. D* **77**, 034018 (2008).
10. A. Datta, D. Kumbhakar, *Z. Phys. C* **27**, 515 (1985); A. A. Petrov, *Phys. Rev. D* **56**, 1685 (1997); E. Golowich and A. A. Petrov, *Phys. Lett. B* **625**, 53 (2005).
11. H. Georgi, *Phys. Lett. B* **297**, 353 (1992); T. Ohl, G. Ricciardi and E. Simmons, *Nucl. Phys. B* **403**, 605 (1993); I. Bigi and N. Uraltsev, *Nucl. Phys. B* **592**, 92 (2001).
12. J. Donoghue, E. Golowich, B. Holstein and J. Trampetic, *Phys. Rev. D* **33**, 179 (1986); L. Wolfenstein, *Phys. Lett. B* **164**, 170 (1985); P. Colangelo, G. Nardulli and N. Paver, *Phys. Lett. B* **242**, 71 (1990); T.A. Kaeding, *Phys. Lett. B* **357**, 151 (1995); E. Golowich and A. A. Petrov, *Phys. Lett. B* **427**, 172 (1998); A. A. Anselm and Y. I. Azimov, *Phys. Lett. B* **85**, 72 (1979).
13. A. F. Falk, Y. Grossman, Z. Ligeti and A. A. Petrov, *Phys. Rev. D* **65**, 054034 (2002); A. F. Falk, *et. al*, *Phys. Rev. D* **69**, 114021 (2004).
14. E. Golowich, S. Pakvasa and A. A. Petrov, *Phys. Rev. Lett.* **98**, 181801 (2007).
15. E. Golowich, J. Hewett, S. Pakvasa and A. A. Petrov, *Phys. Rev. D* **76**, 095009 (2007).
16. Y. Nir and N. Seiberg, *Phys. Lett. B* **309**, 337 (1993).
17. M. Ciuchini *et al.*, *Phys. Lett. B* **655**, 162 (2007).
18. A. A. Petrov, *In the Proceedings of International Workshop on Charm Physics (Charm 2007), Ithaca, New York, 5-8 Aug 2007, pp 11* [arXiv:0711.1564 [hep-ph]].

The CKM angle γ/ϕ_3 - B-factories results review

V. SORDINI

*Univertité Paris XI - LAL,
Btiment 200 91898 Orsay Cedex, France.
Università di Roma La Sapienza
P.le Aldo Moro 5, 00185 Roma, Italy.*



γ/ϕ_3 is the less precisely known of the Unitarity Triangle angles. The general problematics of measurements of this parameter are discussed and recent experimental results from *Babar* and *Belle* are presented.

1 Measurements of the CKM angle γ/ϕ_3

1.1 Introduction

In the Standard Model, *CP* violation is described by the presence of an irreducible phase in the CKM matrix, the unitary matrix that relates the weak interaction with the mass eigenstates. The CKM can be written as:

$$V_{CKM} = \begin{pmatrix} V_{ud} & V_{us} & V_{ub} \\ V_{cd} & V_{cs} & V_{cb} \\ V_{td} & V_{ts} & V_{tb} \end{pmatrix}$$

where $V_{q_1 q_2}$ is the coupling related to the transition $q_1 \rightarrow q_2$. Many parametrizations exist in literature, we use here a generalization of the *Wolfenstein parametrization*¹ as presented in², where the four independent parameters are λ , A , $\bar{\rho}$ and $i\bar{\eta}$ (where the latter is the *CP* violating phase). The matrix is written:

$$V_{CKM} = \begin{pmatrix} 1 - \frac{\lambda^2}{2} & \lambda & A\lambda^3(\bar{\rho} - i\bar{\eta}) \\ -\lambda & 1 - \frac{\lambda^2}{2} & A\lambda^2 \\ A\lambda^3(1 - \bar{\rho} - i\bar{\eta}) & -A\lambda^2 & 1 \end{pmatrix} + O(\lambda^4) \quad (1)$$

The unitarity of the V_{CKM} matrix implies several relations between its elements that can be represented as triangles in the $(\bar{\rho}, \bar{\eta})$ plane. We choose the relation $V_{ub}^*V_{ud} + V_{cb}^*V_{cd} + V_{tb}^*V_{td} = 0$, whose elements can be determined by B physics measurements. This triangle, represented in fig. 1, is particularly attracting from the experimental point of view, since it has all the sides of order λ^3 . The angles of the triangle are called either α , β and γ or ϕ_2 , ϕ_1 and ϕ_3 , we adopt

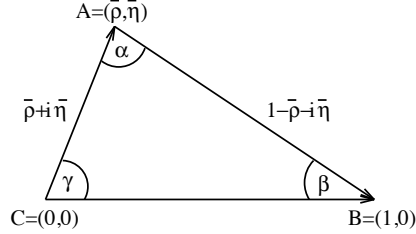


Figure 1: Unitarity Triangle, represented in the $(\bar{\rho}, \bar{\eta})$ plane.

here the first notation.

In the Wolfenstein parametrization the only complex elements, up to terms of order $O(\lambda^5)$, are V_{ub} and V_{td} and the phases γ and β can be directly related to them. In particular, for γ it can be written $V_{ub} = |V_{ub}|e^{-i\gamma}$. Several measurements, using different methods, constrain the weak phase γ from the analyses of $B^+ \rightarrow D^{(*)0}(D^{(*)0})K^{(*)+}$ and $B^0 \rightarrow D^{(*)0}(D^{(*)0})K^{(*)0}$ decays, exploiting the interference between $b \rightarrow u$ and $b \rightarrow c$ transitions whose decay amplitudes will be proportional to the V_{ub} and V_{cb} elements respectively.

1.2 Phenomenology of $B \rightarrow DK$ decays

The amplitudes for the $B \rightarrow DK$ decays of interest can be expressed:

$$\begin{aligned} A(B^+ \rightarrow \bar{D}^0 K^+) &= V_{us} V_{cb}^*(T + C), & A(B^0 \rightarrow \bar{D}^0 K^0) &= V_{us} V_{cb}^* C, \\ A(B^+ \rightarrow D^0 K^+) &= V_{cs} V_{ub}^*(\bar{C} + A), & A(B^0 \rightarrow D^0 K^0) &= V_{cs} V_{ub}^* \bar{C}. \end{aligned} \quad (2)$$

(3)

The T parameter will account for a *tree* diagram, C and \bar{C} for *color-suppressed* diagrams and A for an *annihilation* diagram. For the neutral $B \rightarrow DK$ decays, both the diagrams for the $b \rightarrow c$ and $b \rightarrow u$ transitions are *color-suppressed* and their amplitudes are described by the C and \bar{C} parameters respectively (see³ for a complete treatment).

1.3 Measuring a phase

The idea of measuring a relative phase ϕ through the interference between two amplitudes A_1 and $A_2 e^{i\phi}$ connecting the same initial and final states is based on the fact that the decay rate between these two states is proportional to: $|A_1 + A_2 e^{i\phi}|^2 = A_1^2 + A_2^2 + 2A_1 A_2 \cos \phi$ and hence the interference term gives sensitivity to the relative phase ϕ .

In fig. 2 we show an interference scheme for B^+ mesons decays giving sensitivity to γ . The B^+ can decay either to $\bar{D}^0 K^+$ through a $b \rightarrow c$ transition or to $D^0 K^+$ through a $b \rightarrow u$ transition. If both the D^0 and the \bar{D}^0 decay to the same final state f , the study of the decay $B^+ \rightarrow [f]K^+$ gives sensitivity to the relative phase between the two decay amplitudes. The amplitude for $b \rightarrow c$ and $b \rightarrow u$ transitions can be written as $A(b \rightarrow u) \equiv |V_{ub}|e^{i\gamma}A_u e^{i\delta_u}$ and $A(b \rightarrow c) \equiv |V_{cb}|A_c e^{i\delta_c}$, where $A_{u(c)}$ and $\delta_{u(c)}$ are the absolute value and the phase of the strong interaction contribution to the amplitude. If the neutral D decay is also considered, a term $A_D e^{i\delta_D}$ (or $A_{\bar{D}} e^{i\delta_{\bar{D}}}$) has to be included. In case of B^+ , the interference term in the decay rate will be proportional to $\cos(\delta + \gamma)$, where $\delta = \delta_D - \delta_{\bar{D}} + \delta_u - \delta_c$. A similar diagram can be

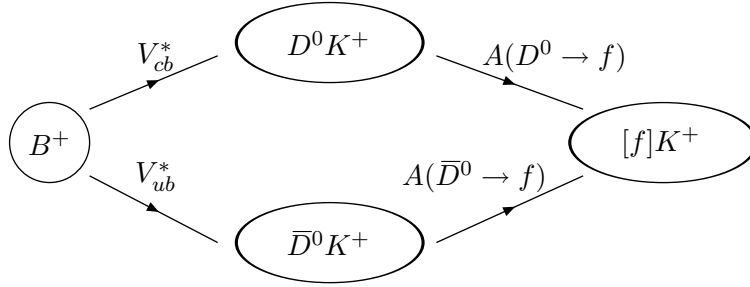


Figure 2: Interference between the $B^+ \rightarrow \bar{D}^0 K^+$ (a) and the $B^+ \rightarrow D^0 K^+$ decays.

drawn for the CP conjugate decay ($B^- \rightarrow [f]K^-$), in this case the interference term will be proportional to $\cos(\delta - \gamma)$, since the strong interactions conserve CP .

The example shown in fig. 2 refers to the $B^+ \rightarrow \bar{D}^0(D^0)K^+$, but equivalent arguments can be done for all the $B^+ \rightarrow \bar{D}^{(*)0}(D^{(*)0})K^+$ and $B^- \rightarrow D^{(*)0}(\bar{D}^{(*)0})K^-$ as well as for the $B^0 \rightarrow \bar{D}^{(*)0}(D^{(*)0})K^{(*)0}$ and $\bar{B}^0 \rightarrow D^{(*)0}(\bar{D}^{(*)0})\bar{K}^{(*)0}$ decays.

A fundamental quantity in all the measurements of γ is the parameter $r_B = \frac{|A(b \rightarrow u)|}{|A(b \rightarrow c)|}$. Being the absolute value of the ratio of the $b \rightarrow u$ to the $b \rightarrow c$ transition amplitudes, r_B leads the sensitivity to γ in each channel. Following the expressions for the decay amplitudes in 2, the r_B ratio for charged $B \rightarrow DK$ channels can be written as:

$$r_B(D^0 K^+) = \frac{|A(B^+ \rightarrow D^0 K^+)|}{|A(B^+ \rightarrow \bar{D}^0 K^+)|} = \frac{|V_{cs} V_{ub}^*| |\bar{C} + A|}{|V_{us} V_{cb}^*| |T + C|}, \quad (4)$$

and, for neutral decays, as:

$$r_B(D^0 K^0) = \frac{|A(B^0 \rightarrow D^0 K^0)|}{|A(B^0 \rightarrow \bar{D}^0 K^0)|} = \frac{|V_{cs} V_{ub}^*| |\bar{C}|}{|V_{us} V_{cb}^*| |C|}. \quad (5)$$

In the expressions 4 and 5, the term $\frac{|V_{cs} V_{ub}^*|}{|V_{us} V_{cb}^*|}$ only depends on absolute values of CKM parameters and is known to be $\sqrt{\bar{\rho}^2 + \bar{\eta}^2} = 0.372 \pm 0.012^4$, while the terms depending on the hadronic parameters are not easily predictable. For simple numerical evaluation, the following assumption can be used: $|C|/|T| \approx 0.3$ and $|A|/|T| \approx 0.5^5$, and one would expect $r_B^{CH} \approx 0.1$ for the charged $B \rightarrow DK$ channels and $r_B^{NEUT} \approx 0.4$ for the neutral $B \rightarrow DK$ ones.

The measurements of γ are difficult because $b \rightarrow u$ transitions are strongly suppressed with respect to $b \rightarrow c$ ones, as described by r_B ratios^a and, as shown from the sketch in fig. 2, the unknowns in any γ analysis are γ itself, the r_B ratio and a strong phase δ . These are usually called polar coordinates. Some analyses make use of the cartesian coordinates, defined in terms of the polar coordinates as $x_{\pm} = r_B \cos(\delta \pm \gamma)$ and $y_{\pm} = r_B \sin(\delta \pm \gamma)$.

In the following, we denote r_B^* and δ_B^* the amplitude ratio and strong phase relative to $B^+ \rightarrow \bar{D}^{*0}(D^{*0})K^+$ decays. In case of a presence of a K^* in the B decay final state, as in the $B^- \rightarrow D^0(\bar{D}^0)K^{*-}$ channel, the natural width of the K^* resonance has to be taken into account and effective variables are used, following the formalism shown in¹⁷. In case of the polar coordinates, these variables are γ (which stays unchanged), k , r_S and δ_S while, in case of the cartesian coordinates, they are called $x_{s\pm}$, $y_{s\pm}$.

1.4 Different experimental methods

There are several methods that aim to measure γ in $B \rightarrow DK$ decays (all based on the strategy sketched in fig. 2) that differ because of the neutral D final states f they reconstruct and

^aIt has to be stressed that the parameters r_B are ratios between amplitudes, the ratio between number of events from $b \rightarrow u$ and $b \rightarrow c$ transitions will be proportional to r_B^2 .

consequently because of different experimental analysis techniques they use.

The Gronau London Wyler method

In the GLW method^{6,7}, γ is measured from the study of B decays to $D_{\pm}^0 K$ final states, where D_{\pm}^0 is a CP eigenstate (i.e. it is reconstructed in a CP eigenstate final state) with eigenvalues ± 1 , defined starting from D^0 and \bar{D}^0 , as $|D_{\pm}^0\rangle = \frac{1}{2}(|D^0\rangle \pm |\bar{D}^0\rangle)$.

The following observables are measured:

$$R_{CP\pm} = \frac{\Gamma(B^+ \rightarrow D_{CP\pm}^0 K^+) + \Gamma(B^- \rightarrow D_{CP\pm}^0 K^-)}{\Gamma(B^+ \rightarrow D^0 K^+) + \Gamma(B^- \rightarrow \bar{D}^0 K^-)} = 1 + r_B^2 \pm 2r_B \cos \gamma \cos \delta_B$$

$$A_{CP\pm} = \frac{\Gamma(B^+ \rightarrow D_{CP\pm}^0 K^+) - \Gamma(B^- \rightarrow D_{CP\pm}^0 K^-)}{\Gamma(B^+ \rightarrow D_{CP\pm}^0 K^+) + \Gamma(B^- \rightarrow D_{CP\pm}^0 K^-)} = \frac{\pm 2r_B \sin \gamma \sin \delta_B}{R_{CP\pm}}$$

where δ_B is the relative strong phase between the two B decay amplitudes.

In the GLW method, four observables, $A_{CP\pm}$ and $R_{CP\pm}$, are measured to constraint three unknowns, γ , δ and r_B . This method suffers of an irreducible four-fold ambiguity on the determination of the phases and, with the actual available statistics, is very useful in measuring r_B , but has typically a low sensitivity to γ .

The Adwood Dunietz Soni method

In the ADS method^{8,9}, γ is measured from the study of $B \rightarrow DK$ decays, where D mesons decay into non CP eigenstate final states. In this method the B meson is reconstructed in final states which can be reached in two ways: either through a favored $b \rightarrow c$ B decay followed by a suppressed D decay ($D^0 \rightarrow f$, or $\bar{D}^0 \rightarrow \bar{f}$), or through a suppressed $b \rightarrow u$ B decay followed by a favored D decay ($D^0 \rightarrow \bar{f}$ or $\bar{D}^0 \rightarrow f$). In this way the two amplitudes are comparable and one can expect larger interference terms.

In the ADS method, one measures the observables:

$$R_{ADS} = \frac{\Gamma(B^+ \rightarrow \bar{f}K^+) + \Gamma(B^- \rightarrow fK^-)}{\Gamma(B^+ \rightarrow fK^+) + \Gamma(B^- \rightarrow \bar{f}K^-)} = r_D^2 + r_B^2 + 2r_B r_D \cos \gamma \cos(\delta_B + \delta_D) \quad (6)$$

$$A_{ADS} = \frac{\Gamma(B^- \rightarrow fK^-) - \Gamma(B^+ \rightarrow \bar{f}K^+)}{\Gamma(B^- \rightarrow fK^-) + \Gamma(B^+ \rightarrow \bar{f}K^+)} = r_B r_D [\cos(\delta + \gamma) + \cos(\delta - \gamma)] / R_{ADS}. \quad (7)$$

Here δ_D is the relative strong phase between the favored and suppressed D decay amplitudes, and r_D is the ratio between the absolute values of their amplitudes $r_D = |A(D^0 \rightarrow f)| / |A(D^0 \rightarrow \bar{f})|$. This method is very useful in measuring r_B , but normally it has very low sensitivity to γ .

The Giri Grossman Soffer Zupan method

In this method¹⁰, usually called Dalitz method, γ is measured from the $B \rightarrow DK$ decays with the D decaying to multi-body CP eigenstate final states. Multi-body decays are usually described by the isobar model, in which the decay amplitude is written as a sum of amplitudes with quasi two-body intermediate states and determined on independent neutral D samples. This information is used in input to the Dalitz analyses (that directly extracts from data γ , r_B and δ or the polar coordinates) where the complete and rich structure of the multi-body D decay is exploited and detectable interference terms are expected because of the presence of different strong phases. This method is indeed very powerful and it is the one that gives the best error on the weak phase γ .

2 Common experimental techniques

We present here the results obtained by the two B-factories experiments: *Babar* at the PEP-II asymmetric-energy e^+e^- collider, located at the Stanford Linear Accelerator Center (USA) and *Belle* at the KEK asymmetric-energy e^+e^- collider, located in Tsukuba (Japan). All the analyses presented reconstruct exclusively B decays and make use of some common techniques.

The B mesons are characterized by two almost independent kinematic variables: the beam-energy substituted mass $m_{ES}(M_{bc}) \equiv \sqrt{(E_0^{*2}/2 + \vec{p}_0 \cdot \vec{p}_B)^2/E_0^2 - p_B^2}$ and the energy difference $\Delta E \equiv E_B^* - E_0^*/2$, where E and p are the energy and the momentum respectively, the subscripts B and 0 refer to the candidate B and to the e^+e^- system respectively and the asterisk denotes the e^+e^- CM frame.

Since both PEP-II and KEK e^+e^- collide at $\sqrt{s} = M(\Upsilon(4S))$, the $\Upsilon(4S)$ resonance is produced almost at rest in the e^+e^- center of mass frame. Given the values of the masses of the $\Upsilon(4S)$ and of the B mesons, the latter have a very low residual momentum in the e^+e^- center of mass frame. On the other hand, in case of $e^+e^- \rightarrow q\bar{q}$ events, with $q = u, d, s, c$ (called continuum events), the two quarks are produced with large momentum and for this reason, these events have a jet-like spatial shape, different from the spherically distributed one for $B\bar{B}$ events.

Several variables account for these differences and are used in the analyses to fight continuum background, which is typically the main source of background to these analyses.

3 Experimental results on the charged B decays

We present here the recent results on γ from *Babar* and *Belle*, using the different methods.

3.1 Analyses using the GLW method

We report on the update of the GLW analysis¹² of $B^- \rightarrow D^0 K^-$, with $D^0 \rightarrow K^+ K^-$, $\pi^+ \pi^-$, $K_S \pi^0$ and $K_S \omega$ ^b using $383 \cdot 10^6$ $B\bar{B}$ pairs collected with the *Babar* detector. In this analysis, after a cut on m_{ES} and on a combination of event shape variables, the observables are extracted using a maximum likelihood fit to the variables ΔE and the Cerenkov angle of the charged K produced in the charged B decay.

The results obtained for the direct CP asymmetries and the ratios are the following:

$$\begin{aligned} R_{CP^+} &= 1.06 \pm 0.10 \pm 0.05, & A_{CP^+} &= 0.27 \pm 0.09 \pm 0.04, \\ R_{CP^-} &= 1.03 \pm 0.10 \pm 0.05, & A_{CP^-} &= -0.09 \pm 0.09 \pm 0.02, \end{aligned}$$

where the first error is statistical and the second one is systematic. For the first time for a GLW analysis, the results are extracted from data also in terms of the cartesian coordinates:

$$\begin{aligned} x_+ &= -0.09 \pm 0.05 \pm 0.02, \\ x_- &= +0.10 \pm 0.05 \pm 0.03, \\ r^2 &= +0.05 \pm 0.07 \pm 0.03, \end{aligned}$$

where the first error is statistical and the second one is systematic.

The uncertainties on A_{CP^\pm} (R_{CP^\pm}) are smaller by a factor of 0.7 (0.9) and 0.6 (0.6) than the previous *Babar*¹³ and *Belle*¹⁴ measurements, respectively.

^bthe $K^- \pi^+$ mode is also reconstructed for normalization

3.2 Analyses using the ADS method

We report on the update of the ADS analysis¹⁵ of $B^- \rightarrow D^0 K^-$, with $D^0 \rightarrow K^- \pi^+$ using 657 10^6 $B\bar{B}$ pairs collected with the *Belle* detector. In this analysis, after a cut on m_{ES} and on a combination of event shape variables, the observables are extracted using a maximum likelihood fit to the variable ΔE , giving the following results:

$$R_{ADS} = (8.0_{-5.7}^{+6.3+2.0})10^{-3}, \quad A_{ADS} = -0.13_{-0.88}^{+0.97} \pm 0.26,$$

where the first error is statistical and the second one is systematic.

The results obtained for R_{ADS} show that no evidence of $b \rightarrow u$ transition is found, even with the very high statistics used. This result implies an upper limit on the ratio r_B , $r_B < 0.19$ 90% C.L. . This result on r_B is consistent with the previous *Belle* and *Babar* analyses and confirms the expectation for a small value of r_B ($r_B \sim 0.1$) in charged $B \rightarrow DK$ decays.

3.3 Analyses using the GGSZ method

Both the *Babar* and *Belle* collaboration have presented at this conference new results using Dalitz technique, that strongly improve the precision on the determination of γ .

We first report on a new Dalitz analysis¹⁶ of $B^- \rightarrow D^0 K^-$ and $B^- \rightarrow D^{*0} K^-$, that for the first time uses neutral D reconstructed into the final state $D^0 \rightarrow K_s K^+ K^-$ and on the update of the Dalitz analysis of $B^- \rightarrow D^0 K^-$, $B^- \rightarrow D^{*0} K^-$ and $B^- \rightarrow D^0 K^{*-}$, with $D^0 \rightarrow K_S \pi^+ \pi^-$ using 383 10^6 $B\bar{B}$ pairs collected with the *Babar* detector. In this analysis, m_{ES} , ΔE and a combination of event shape variables are used in the maximum likelihood fit to extract the number of signal and background events and then a CP fit is performed to extract the cartesian coordinates for the three channels, $B^- \rightarrow D^0 K^-$, $B^- \rightarrow D^{*0} K^-$ and $B^- \rightarrow D^0 K^{*-}$. In the CP fit, the D Dalitz distribution, for $D^0 \rightarrow K_S \pi^+ \pi^-$ and $D^0 \rightarrow K_s K^+ K^-$, as they are determined on independent data samples, are used as an input. The results for the cartesian coordinates are shown in tab. 1, for the three analyzed channels (in the tables, the symbol \tilde{D}^0 indicates either a D^0 or a \bar{D}^0). The first error is statistical, the second is experimental systematic uncertainty and the third is the systematic uncertainty associated with the Dalitz models.

Parameters	$B^- \rightarrow \tilde{D}^0 K^-$	$B^- \rightarrow \tilde{D}^{*0} K^-$	$B^- \rightarrow \tilde{D}^0 K^{*-}$
x_- , x_-^* , x_{s-}	$0.090 \pm 0.043 \pm 0.015 \pm 0.011$	$-0.111 \pm 0.069 \pm 0.014 \pm 0.004$	$0.115 \pm 0.138 \pm 0.039 \pm 0.014$
y_- , y_-^* , y_{s-}	$0.053 \pm 0.056 \pm 0.007 \pm 0.015$	$-0.051 \pm 0.080 \pm 0.009 \pm 0.010$	$0.226 \pm 0.142 \pm 0.058 \pm 0.011$
x_+ , x_+^* , x_{s+}	$-0.067 \pm 0.043 \pm 0.014 \pm 0.011$	$0.137 \pm 0.068 \pm 0.014 \pm 0.005$	$-0.113 \pm 0.107 \pm 0.028 \pm 0.018$
y_+ , y_+^* , y_{s+}	$-0.015 \pm 0.055 \pm 0.006 \pm 0.008$	$0.080 \pm 0.102 \pm 0.010 \pm 0.012$	$0.125 \pm 0.139 \pm 0.051 \pm 0.010$

Table 1: CP -violating parameters $x_{\pm}^{(*)}$, $y_{\pm}^{(*)}$, $x_{s\pm}$, and $y_{s\pm}$, as obtained from the CP fit.

Using a frequentist analysis, the experimental results for $x_{\pm}^{(*)}$, $y_{\pm}^{(*)}$, $x_{s\pm}$, and $y_{s\pm}$ are interpreted in terms of the weak phase γ , the amplitude ratios r_B , r_B^* , and r_S , and the strong phases δ_B , δ_B^* , and δ_S , giving $\gamma = (76 \pm 22 \pm 5 \pm 5)^\circ \pmod{180^\circ}$, $r_B = 0.086 \pm 0.035 \pm 0.010 \pm 0.011$, $r_B^* = 0.135 \pm 0.051 \pm 0.011 \pm 0.005$, $kr_S = 0.163_{-0.105}^{+0.088} \pm 0.037 \pm 0.021$, $\delta_B = (109_{-31}^{+28} \pm 4 \pm 7)^\circ \pmod{180^\circ}$, $\delta_B^* = (-63_{-30}^{+28} \pm 5 \pm 4)^\circ \pmod{180^\circ}$, and $\delta_S = (104_{-41}^{+43} \pm 17 \pm 5)^\circ$. The first error is statistical, the second is the experimental systematic uncertainty and the third reflects the uncertainty on the D decay Dalitz models. The results for γ and the ratios r_B , r_B^* and r_S are shown in fig. 3.

We also report on the update of the Dalitz analysis¹⁹ of $B^- \rightarrow D^0 K^-$ and $B^- \rightarrow D^{*0} K^-$ ($D^{*0} \rightarrow D^0 \pi^0$), with $D^0 \rightarrow K_S \pi^+ \pi^-$ using 635 10^6 $B\bar{B}$ pairs collected with the *Belle* detector. In this analysis, M_{bc} , ΔE and a combination of event shape variables are used in the maximum

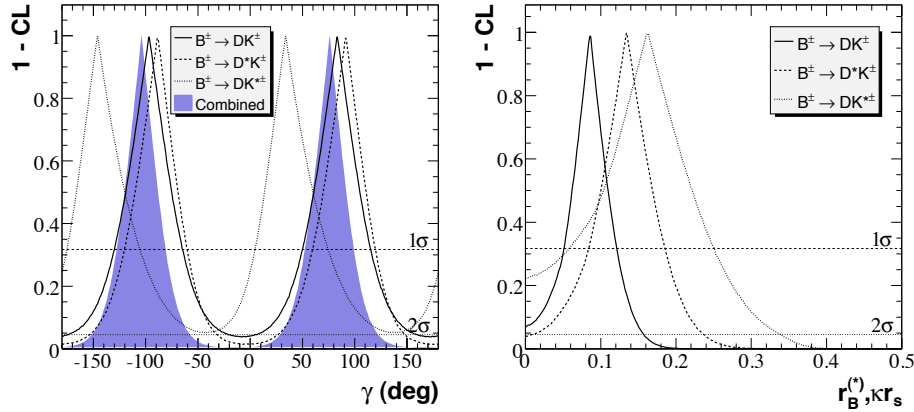


Figure 3: [*Babar* Dalitz analysis] $\alpha = 1 - \text{CL}$ as a function of γ (left plot) and of r_B , r_B^* and r_S (right plot) for $B^- \rightarrow \tilde{D}^0 K^-$, $B^- \rightarrow \tilde{D}^{*0} K^-$, and $B^- \rightarrow \tilde{D}^0 K^{*-}$ decays separately, and their combination, including statistical and systematic uncertainties and their correlations. The dashed (upper) and dotted (lower) horizontal lines correspond to the one- and two-standard deviation intervals, respectively.

likelihood fit to extract the number of signal and background events and then a CP fit is performed to extract the cartesian coordinates for the two channels, $B^- \rightarrow D^0 K^-$, $B^- \rightarrow D^{*0} K^-$ (with $D^{*0} \rightarrow D^0 \pi^0$). In the CP fit, the D Dalitz distribution for $D^0 \rightarrow K_S \pi^+ \pi^-$, as it is determined on independent data samples, is used as an input. The results are shown in tab. 2, where the first error is statistical and the second is experimental systematic uncertainty. The uncertainty associated with the Dalitz model is not shown and it is assumed to be equal to the one evaluated in the previous analysis by *Belle* collaboration¹⁸.

Parameter	$B^- \rightarrow \tilde{D}^0 K^-$	$B^- \rightarrow \tilde{D}^{*0} K^-$
x_-	$+0.105 \pm 0.047 \pm 0.011$	$+0.024 \pm 0.140 \pm 0.018$
y_-	$+0.177 \pm 0.060 \pm 0.018$	$-0.243 \pm 0.137 \pm 0.022$
x_+	$-0.107 \pm 0.043 \pm 0.011$	$+0.133 \pm 0.083 \pm 0.018$
y_+	$-0.067 \pm 0.059 \pm 0.018$	$+0.130 \pm 0.120 \pm 0.022$

Table 2: CP -violating parameters $x_{\pm}^{(*)}$ and $y_{\pm}^{(*)}$, as obtained from the CP fit.

Using a frequentist analysis, the experimental results for $x_{\pm}^{(*)}$ and $y_{\pm}^{(*)}$ are interpreted in terms of the weak phase γ , the amplitude ratios r_B , r_B^* and the strong phases δ_B , δ_B^* , giving $\gamma = \left(76_{-13}^{+12} \pm 4 \pm 9\right)^\circ \pmod{180^\circ}$, $\delta_B = \left(136_{-16}^{+14} \pm 4 \pm 23\right)^\circ \pmod{180^\circ}$, $\delta_B^* = \left(343_{-22}^{+20} \pm 4 \pm 23\right)^\circ \pmod{180^\circ}$, $r_B = 0.16 \pm 0.04 \pm 0.01 \pm 0.05$ and $r_B^* = 0.21 \pm 0.08 \pm 0.02 \pm 0.05$. The first error is statistical, the second is the experimental systematic uncertainty and the third reflects the uncertainty on the D decay Dalitz model. It can be noticed that this analysis finds slightly higher values for the r_B and r_B^* ratios with respect to the *Babar* analysis, which explains the smaller statistical errors on γ , also if the precision on the cartesian coordinates is similar. The results for γ and the ratios r_B and r_B^* are shown in fig. 4

4 Experimental results on the neutral B decays

Lately, within the *Babar* collaboration, there have been efforts to constrain γ and related quantities from the study of neutral $B \rightarrow DK$ decays. As already discussed, the r_B ratios in these channels are expected to be higher than in the charged ones, hence giving higher sensitivity to γ .

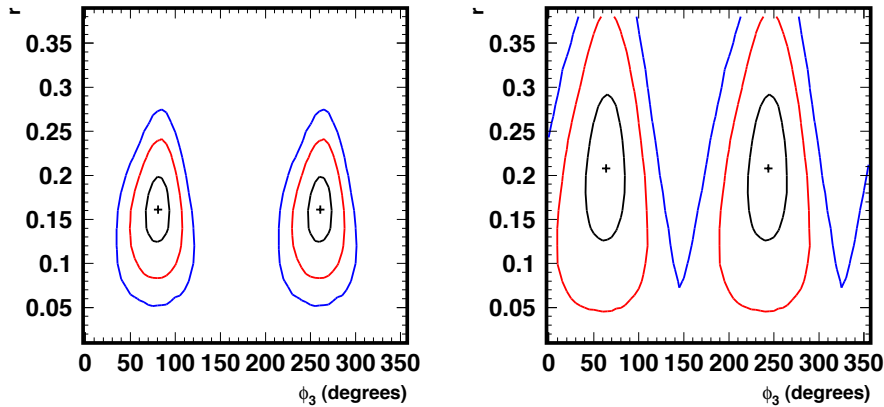


Figure 4: [*Belle* Dalitz analysis] Projections of confidence regions for the $B^- \rightarrow D^0 K^-$ (left plot) and $B^- \rightarrow D^{*0} K^-$ (right plot) mode onto the (r_B, γ) and (r_B^*, γ) planes respectively. Contours indicate projections of one, two and three standard deviation regions.

We first report on a new Dalitz analysis²¹ of $B^0 \rightarrow D^0 K^{*0}$, with $K^{*0} \rightarrow K^+ \pi^-$ and $D^0 \rightarrow K_S \pi^+ \pi^-$ using $371 \cdot 10^6$ $B\bar{B}$ pairs collected with the *Babar* detector. In this analysis, m_{ES} and a combination of event shape variables are used in the maximum likelihood fit to extract the number of signal and background events and then a CP fit is performed. A likelihood scan in polar coordinates $(\gamma, \delta_S^0, r_S^0)$ is extracted from data and combined with an external information on r_S^0 ²⁰. The results obtained are shown in tab. 3, where the first error is statistical, the second is the experimental systematic uncertainty and the third reflects the uncertainty on the D decay Dalitz model.

Parameters	
γ [$^\circ$]	$162 \pm 55 \pm 1.6 \pm 6.5 \pmod{180^\circ}$
δ_S^0 [$^\circ$]	$62 \pm 55 \pm 3.1 \pm 15.8 \pmod{180^\circ}$
r_S^0	< 0.55 95 % probability

Table 3: Results for γ , δ_S^0 and r_S^0 , as obtained from the CP fit.

We also report on a new time-dependent Dalitz plot analysis²² of $B^0 \rightarrow D^- K^0 \pi^+$ using $347 \cdot 10^6$ $B\bar{B}$ pairs collected with the *Babar* detector. This analysis studies the interference between $b \rightarrow u$ and $b \rightarrow c$ transitions through the B mesons mixing and hence gives sensitivity to the combination of CKM weak phases $2\beta + \gamma$. In this analysis, m_{ES} , ΔE and a combination of event shape variables are used in the maximum likelihood fit to extract the number of signal and background events and then a time-dependent fit to the neutral B Dalitz distribution is performed to extract $2\beta + \gamma$. In this fit, the ratio r_B^0 is assumed to be $r_B^0 = 0.3$ and the effect of this assumption is taken into account in the systematics evaluation by varying this ratio of ± 0.1 . The result obtained for $2\beta + \gamma$ is the following:

$$2\beta + \gamma = (83 \pm 53 \pm 20)^\circ \pmod{180^\circ},$$

where the first error is statistical and the second one is systematic.

5 Combined results and conclusions

From all the available measurements, including the new ones presented here, the knowledge of γ , according to the combination performed by the *UTfit* collaboration, is $\gamma = (80 \pm 13)^\circ$.

The combined results obtained for the other quantities are $r_B = 0.10 \pm 0.02$, $r_B^* = 0.09 \pm 0.04$, $r_S = 0.13 \pm 0.09$, $r_S^0 < 0.55$ 95 % probability and $2\beta + \gamma = (88 \pm 29)^\circ$.

In conclusion both the *Babar* and *Belle* collaboration have made enormous efforts to constrain the CKM angle γ and related quantities using many methods in different channels, leading to a precision in the determination that was not expected to be accessible at the B-factories experiments.

1. L. Wolfenstein, *Phys. Rev. Lett.* **51** (1983) 1945.
2. A. J. Buras, M. E. Lautenbacher and G. Ostermaier, *Phys. Rev. D* **50** (1994) 3433.
3. A. J. Buras e L. Silvestrini, “*Non-leptonic two-body B decays beyond factorization,*” *Nucl. Phys. B* **569** (2000) 3, [hep-ph/9812392](http://arxiv.org/abs/hep-ph/9812392).
4. Updated results on the web page <http://www.utfit.org>.
5. M. Gronau and J. L. Rosner, *Phys. Lett. B* **439**, 171 (1998) [[arXiv:hep-ph/9807447](http://arxiv.org/abs/hep-ph/9807447)].
B. Blok, M. Gronau and J. L. Rosner, *Phys. Rev. Lett.* **78**, 3999 (1997) [[arXiv:hep-ph/9701396](http://arxiv.org/abs/hep-ph/9701396)].
6. M. Gronau, D. Wyler, *Phys. Rev. Lett.* **B253** (1991) 483.
7. M. Gronau, D. London, *Phys. Rev. Lett.* **B265** (1991) 172.
8. I. Dunietz, *Phys. Rev. Lett.* **B270** (1991) 75; *Phys. Rev. Lett.* **D52** (1995) 3048.
9. D. Atwood, I. Dunietz and A. Soni, “*Enhanced CP violation with $B \rightarrow K D0$ (*anti-D0*) modes and extraction of the CKM angle gamma,*” *Phys. Rev. Lett.* **78**, 3257 (1997) [[arXiv:hep-ph/9612433](http://arxiv.org/abs/hep-ph/9612433)].
10. A. Giri, Y. Grossman, A. Soffer and J. Zupan, “*Determining gamma using $B^{+-} \rightarrow D K^{+-}$ with multibody D decays,*” *Phys. Rev. D* **68** (2003) 054018 [[arXiv:hep-ph/0303187](http://arxiv.org/abs/hep-ph/0303187)].
11. R. A. Fisher, *Annals Eugen.* **7**, 179 (1936).
12. B. Aubert *et al.* [BABAR Collaboration], [arXiv:0802.4052](http://arxiv.org/abs/0802.4052) [hep-ex].
13. *Babar* Collaboration, B. Aubert *et al.*, *Phys. Rev. D* **73**, 051105(R) (2006).
14. Belle Collaboration, K. Abe *et al.*, *Phys. Rev. D* **73**, 051106(R) (2006).
15. Y. Horii *et al.* [Belle Collaboration], [arXiv:0804.2063](http://arxiv.org/abs/0804.2063) [hep-ex].
16. B. Aubert *et al.* [BABAR Collaboration], [arXiv:0804.2089](http://arxiv.org/abs/0804.2089) [hep-ex].
17. M. Gronau, *Phys. Lett.* **B557** (2003) 198-206.
18. Belle Collaboration, A. Poluektov *et al.*, *Phys. Rev. D* **73**, 112009 (2006).
19. K. Abe *et al.* [Belle Collaboration], [arXiv:0803.3375](http://arxiv.org/abs/0803.3375) [hep-ex].
20. B. Aubert *et al.* (BABAR Collaboration), *Phys. Rev.* **D74**, 031101 (2006).
21. B. Aubert *et al.* [BABAR Collaboration], [[arXiv:0805.2001](http://arxiv.org/abs/0805.2001)] [hep-ex]].
22. B. Aubert *et al.* [BABAR Collaboration], *Phys. Rev. D* **77**, 071102 (2008) [[arXiv:0712.3469](http://arxiv.org/abs/0712.3469)] [hep-ex]].

***R* Value Measurements at 2.60, 3.07 and 3.65 GeV with BESII**

Haiming Hu^a
*Institute of High Energy Physics, 19(B) Yuquan Road,
 Beijing 100049, China
 for the BES Collaboration*



Using a data sample with a total integrated luminosity of 9998.3 nb^{-1} collected at 2.6, 3.07 and 3.65 GeV with BESII, the cross section for e^+e^- annihilating into hadronic final states (R values) are measured. The statistical errors are smaller than 1%, and the systematic errors are about 3.5%. The running coupling constant of the strong interaction $\alpha_s^{(3)}(s)$ and $\alpha_s^{(5)}(M_Z^2)$ are determined from the measured R values.

1 Instruction

The R ratio is defined as the lowest level hadronic cross section normalized by theoretical $\mu^+\mu^-$ production cross section in e^+e^- annihilation

$$R = \frac{\sigma_{had}^0(e^+e^- \rightarrow \gamma^* \rightarrow \text{hadrons})}{\sigma_{\mu\mu}^0(e^+e^- \rightarrow \gamma^* \rightarrow \mu^+\mu^-)}, \quad (1)$$

and is an important input parameter for precision tests of the Standard Model (SM). The errors on R values measurements below 5 GeV have significant influence on the uncertainties of calculations of the QED running electromagnetic coupling constant $\alpha(s)$, muon anomalous magnetic moment ($g-2$) and global fits for the Higgs mass^{1,2,3}. In addition, precision measurements of R values between 2.0 - 3.7 GeV provide a test of perturbative QCD and QCD sum rule calculations^{4,5,6}.

R value measurement is made at BESII⁷ based on the expression^{8,9}

$$R_{exp} = \frac{N_{had}^{obs} - N_{bg}}{\sigma_{\mu\mu}^0 L \epsilon_{trg} \epsilon_{had}^0 (1 + \delta_{obs})}, \quad (2)$$

^ae-mail: huhm@ihep.ac.cn

where N_{had}^{obs} is number of the observed hadronic events, N_{bg} is number of the remnant QED backgrounds (e^+e^- , $\mu^+\mu^-$, $\tau^+\tau^-$, $\gamma\gamma$, etc.), L is the integrated luminosity, ε_{trg} is the trigger efficiency for hadronic events, ε_{had}^0 is the hadronic efficiency without the simulation of the initial state radiation (ISR), and $(1 + \delta_{obs})$ is the effective factor of ISR in which the hadronic efficiencies for different bremsstrahlung energies are considered.

In 1998 and 1999, two series of R value measurements were made at 91 energy points between 2 - 5 GeV by the BESII⁷ experiments^{8,9}. The average statistical errors are 2 ~ 4%, and the systematical errors are 5 ~ 8% depending on the energy points. In 2004, large-statistics data samples were accumulated at the center-of-mass energies of 2.6, 3.07 and 3.65 GeV; the total integrated luminosity was 9998.3 nb⁻¹, and an additional 65.2 nb⁻¹ data sample was accumulated at 2.2 GeV for the purpose of tuning the parameters of the hadronic event generator. Some improvements in the event selection, tuning of generator parameters and luminosity measurement are made in order to decrease the systematic errors. The previously used EGS-based detector simulation has been replaced by a GEANT3-based one. The consistency between data and Monte Carlo (MC) has been validated using many high purity physics channels¹⁰. With these improvements, the errors on the new measured R values are reduced to about 3.5%.

2 Data analysis

The measurement scheme for this work is similar to that of used in previous one⁹. The strategy for selecting hadronic events is to subtract the QED backgrounds, cosmic ray and beam associated backgrounds, the remaining events are then selected with specialized hadronic criteria. Two large sources of error in the measurement arise from the event selection and hadronic efficiency, and these have strong correlations between them.

2.1 Selection of hadronic events

In the BEPC energy region, the processes that originate in the beam-beam interaction region are $e^+e^- \rightarrow e^+e^-$, $\mu^+\mu^-$, $\tau^+\tau^-$, $\gamma\gamma$, e^+e^-X (X means any possible final states), hadrons and beam associated backgrounds. The observed final state charged particles are e , μ , π , K and p . Different types of backgrounds are identified using specialized criteria, and most of them can be rejected with good efficiency^{8,9,11}.

Candidate hadronic events are classified by their number of charged tracks. The selection of hadronic events is done in two successive steps: one at the track level and the other at the event level^{8,9}. In the BEPC energy region, the number of events with one observed/reconstructed charged track in BESII accounts for about 8 - 13% of all hadronic events. In previous measurements, only hadronic events with two or more charged tracks ($n_{ch} \geq 2$) were selected^{8,9}. The omission of 0 and 1-track hadronic events introduces some uncertainty in the tuning of the hadronic event generator parameters; this in turn induces a sizable systematic error into the hadronic efficiency. However, for single-track events, contamination from beam-associated backgrounds is significant. Therefore, a more strict hadronic event selection is applied¹¹. The event must have one charged track with good helicity fitting (the event can have any number of charged tracks with bad helicity fitting) and at least one reconstructed π^0 are considered as single-track hadronic events.

Figure 1 shows the z -vertex distributions of the candidate hadronic events (including the residual beam-associated and QED backgrounds). The events produced by e^+e^- collisions originate near the collision point (in the neighborhood of $z = 0$), and the non-beam-beam backgrounds, such as those from beam-gas and beam-wall scattering, are distributed all along the beam-pipe. The number of observed hadronic events N_{had}^{obs} can be determined by fitting the distribution of event vertices along the beam direction with a Gaussian to describe the hadronic

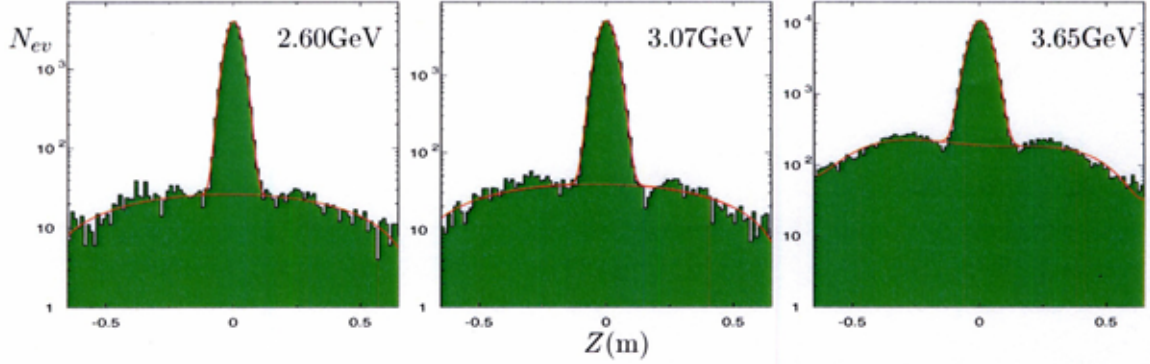


Figure 1: Distribution of vertices of data along the beam direction for candidate hadronic events. The vertices of the collision events and beam-associated backgrounds are fitted by the Gaussian form and polynomial, respectively. The width of bin is 0.0125 m.

events and a m -th degree polynomial for the residual beam associated backgrounds.

The numbers of residual QED backgrounds, N_{bg} in Eq.(2), are deduced statistically from MC. The QED event generators with 1% are used. The number of residual background events is determined as

$$N_{bg} = L[\epsilon_{ee}\sigma_{ee} - \epsilon_{\mu\mu}\sigma_{\mu\mu} - \epsilon_{\tau\tau}\sigma_{\tau\tau} - \epsilon_{\gamma\gamma}\sigma_{\gamma\gamma}], \quad (3)$$

where σ_{ee} is the production cross section for Bhabha events given by the corresponding generator, and ϵ_{ee} is the residual ratio of Bhabha events that pass the hadronic event selection criteria. Other symbols have the similar meanings. The fraction of the remaining background $e^+e^- \rightarrow e^+e^-X$ is much smaller than 1% and is neglected. The values of ϵ_{ee} and $\epsilon_{\mu\mu}$ are about 5×10^{-4} , and $\epsilon_{\tau\tau}$ is 36.45% at 3.65 GeV. The errors on N_{bg} are given in Table 2.

2.2 Tuning the LUARLW parameters

The hadronic efficiency is determined using the LUARLW hadronic event generator¹². The physical basis of LUARLW is the solution of the Lund area law¹³. The production of hadrons are described as the fragmentation of a semiclassical relativistic string¹⁴, the quark components of the string and decays of unstable particles are handed by subroutines in JETSET^{15,16,17}.

Both LUARLW and JETSET have some phenomenological parameters that have to be determined from the data. The basic method is to find a set of parameters that make various distributions (such as those sensitive to the efficiency) simulated by MC agree well with experimental data at all of the measured energies points. The distributions used in the data-MC comparison are: the multiplicities of charged and neutral tracks, the z vertices for charged tracks, the charged track momentum, the polar-angle between tracks and the beam direction, the deposited energy in the BSC, and fractions of π^\pm , K^\pm , and some other short-lived particles (π^0 , K_S , ϕ , Λ etc.). With these distributions, the systematic errors corresponding to each criteria used in the hadronic event selection can be determined. Figure 2 shows some comparisons between data and the LUARLW MC at 3.07 GeV, where reasonable agreement is evident. More distributions at other energy points can be found in Refs.^{11,19}.

2.3 Trigger

The trigger conditions are almost the same as those used for the R measurements reported in Refs.^{8,9}. Since single-track hadronic events are also included in this measurement, the TOF back-to-back hit trigger requirement is not used, thereby making the trigger conditions somewhat loser than before. The trigger table used in data taking is given in Ref.¹¹. The trigger efficiencies

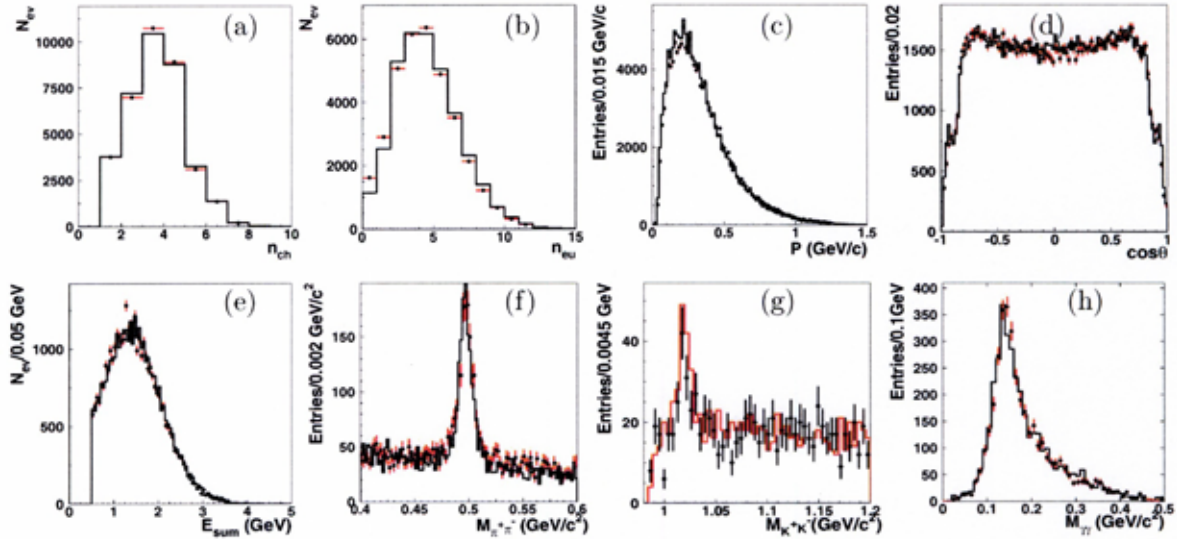


Figure 2: The normalized distributions for data (dots with error bars) and the LUARLW MC (histograms) at 3.07 GeV with full detector simulation: (a) charged track multiplicity; (b) neutral track multiplicity; (c) charged track momentum p ; (d) polar-angle between charged track and beam direction, $\cos\theta$; (e) deposited energy in the BSC; invariant masses of (f) $K_S \rightarrow \pi^+\pi^-$; (g) $\phi \rightarrow K^+K^-$ and (h) $\pi^0 \rightarrow \gamma\gamma$ decays.

ϵ_{trg} for hadronic events, listed in Table 1, are almost 99.8%, and their associated errors are conservatively estimated to be 0.5%.

2.4 Luminosity

The integrated luminosity is measured with wide angle Bhabha events. The measurement method is very similar to that described in Refs. ^{8,9}. In previous measurements, an EGS-based detector simulation was used. And for the measurement reported here, it has been replaced by a GEANT3-based package, which has better geometrical and material descriptions for the sub-detectors. In particular, the simulation of the BSC is significantly improved, and provides better consistency between MC and data. The Bhabha events are selected by using the BSC information. In order to decrease the uncertainty caused by events selection criteria, another Bhabha control sample only selected with MDC information is employed to correct the difference between data and MC. The efficiency correction factors of ranging from 0.994 to 1.026 are given in different energy points. In addition, the contribution from $e^+e^- \rightarrow \gamma\gamma$ process is taken into account. As a result, the measurement precision of luminosity is significantly improved and their systematic uncertainties are smaller than 2%.

2.5 Initial state radiative correction

An $\mathcal{O}(\alpha^3)$ Feynman-diagram-based calculation for the initial state radiative (ISR) correction is used in both calculation of the ISR factor $(1 + \delta_{obs})$ and the simulation of radiative events by LUARLW. The detailed description on the ISR treatment can be found in Refs. ^{20,21,22,23,24}. In the ISR simulations and calculations, the contributions from both continuum and resonances are considered (quantities related to the narrow J/ψ and ψ' are treat analytically). For comparison, another approach based on structure functions²⁵ is also used at all energy points. The differences between these two schemes for theoretical value of $(1 + \delta)$ are smaller than 1.1%. The uncertainty in the effective ISR factor $(1 + \delta_{obs})$ due to errors of the hadronic cross sections at the different effective energies for radiative events are also considered (the errors on the hadronic cross section

given in the PDG06 tables are used); these decrease with increasing of energy from 0.9% to 0.1%. The values of $(1 + \delta_{obs})$ and their errors are listed in Tables 1 and 2, respectively.

3 Error analysis

The Feynman-diagram-based ISR simulated angle and momentum distributions for the radiated photon is built into LUARLW, and the averaged hadronic efficiency $\bar{\epsilon}_{had}$ with radiative effects can be obtained. The number of hadronic events N_{had}^{obs} , the hadronic efficiency $\bar{\epsilon}_{had}$ and their errors are correlated. The equivalent number of hadronic events, which corresponds to the number of hadronic events produced at the collision point, is defined as

$$N_{had} = \frac{N_{had}^{obs}}{\bar{\epsilon}_{had}}. \quad (4)$$

The combined systematic error associated with the event selection and hadronic efficiency is denoted as ΔN_{had} . This error is caused by the discrepancy between data and MC samples for the selection hadronic criteria discussed in Section 2.1.

Except for the error mentioned above, an additional uncertainty of the parameters in the MC hadronization model is estimated to be about 1% by comparing different sets of tuned parameters, and is considered in error of hadronic event efficiency.

The error on N_{had}^{obs} due to the choice of degree for the polynomial used in the fitting is less than 0.7%. The fit errors for N_{had}^{obs} are 1.34% at 2.6 GeV, 1.11% at 3.07 GeV, and 0.73% at 3.65 GeV, which are calculated from the uncertainties in the fitted parameters of the Gaussian signal peaks. The total ΔN_{had} is the quadratic sum of all fractional errors.

A conclusion of the KLN theorem is that the radiative corrections due to final state radiation (FSR) are negligible for a measurement of the inclusive hadronic cross sections that sums over all hadronic final states²⁷. At the present level of precision, the FSR correction factor in Eq.(2) can be neglected. However, the absence of final state radiation in the event generator introduces some error into the determination of the hadronic event detection efficiency. The masses of the hadrons produced in the final states are much greater than that of the initial state e^\pm . As a result, the effect of FSR is much weaker than initial bremsstrahlung. Its influence is estimated to be 0.5% and is included in the error.

The 0-track events are not selected in this analysis, and the influence of 0-track events on the parameter tuning of LUARLW is not considered. This introduces some error into the hadronic event efficiency determination. Events with no charged tracks cannot be well separated from background. The fraction of 0-track events is estimated from the MC to be 3.4% at 2.6 GeV, 2.9% at 3.07 GeV, and 2.4% at 3.65 GeV. If the difference for 0-track events between MC and data is assumed to be 20%, the estimated errors for the lost/unobserved 0-track events are 0.7%, 0.6% and 0.5%, respectively. The error related to 0-track events is included into the error of N_{had} defined in Eq.(4).

In this analysis, hadronic events are classified according to their number of charged tracks. Therefore, errors in the tracking efficiency σ_{trk} , the differences in the track reconstruction between data and MC, introduce some error into the classification and counting of the number of events. For an event with n_{ch} charged tracks, the probability that n_{er} of n_{ch} tracks are wrongly constructed roughly obeys a binomial distribution $B(n_{er}; n_{ch}, \sigma_{trk})$, where the parameter $\sigma_{trk} \sim 2\%$ is the tracking error. Considering the distribution of charged multiplicity $P(n_{ch})$ for the inclusive hadronic sample (such as shown in Figure 2(a)), the effective error of tracking efficiency is

$$\Delta\epsilon_{trk} = \sum_{n_{ch} \geq 1} P(n_{ch})B(n_{er}; n_{ch}, \sigma_{trk}). \quad (5)$$

The R value measurement is, in fact, a counting of the number of hadronic events, so only those cases where all n_{ch} tracks in an event are wrongly reconstructed ($n_{er} = n_{ch}$) will cause an error in ΔN_{had} . The values of $\Delta\epsilon_{trk}$ estimated from Eq. (5) are listed in Table 2. Since the fraction of 1-track events decreases with increasing center-of-mass energy, the error $\Delta\epsilon_{trk}$ also decreases with energy.

The numbers of errors on the R value measurement are given in Table 2. As a cross check, the R values are measured using the relation

$$R_{exp} = \frac{N_{had}^{obs} - N_{bg}}{\sigma_{\mu\mu}^0 L \epsilon_{trg} \bar{\epsilon}_{had} (1 + \delta)}, \quad (6)$$

where $\bar{\epsilon}_{had}$ is the hadronic efficiency averaged over all of the ISR spectrum, and $(1 + \delta)$ is the corresponding theoretical ISR factor. The R values determined with Eq. (6) are $2.17 \pm 0.01 \pm 0.07$ at 2.6 GeV, $2.13 \pm 0.01 \pm 0.07$ at 3.07 GeV, and $2.16 \pm 0.01 \pm 0.08$ at 3.65 GeV. The R values measured with Eq. (2) and (6) are consistent to within 1%. Another cross check is also made by selecting hadronic events with $n_{ch} \geq 2$ as was done in Refs. ^{8,9}. In this case, the R values measured at the three energy points are $2.20 \pm 0.02 \pm 0.08$, $2.13 \pm 0.01 \pm 0.07$ and $2.15 \pm 0.01 \pm 0.08$, respectively. The differences in R values determined by selecting hadronic events with $n_{ch} \geq 1$ and $n_{ch} \geq 2$ are consistent within 1%.

Table 1: Items used in the determination of R at each energy point.

E_{cm}	L	N_{had}^{obs}	N_{bg}	$\epsilon_{trg}(\%)$	$\epsilon_{had}^0(\%)$	$(1 + \delta_{obs})$	R	σ_{sta}	σ_{sys}
2.60	1222.06	24026	193	99.85	63.81	1.08	2.18	0.02	0.08
3.07	2290.72	33933	208	99.79	67.63	1.11	2.13	0.02	0.07
3.65	6485.30	83767	4937	99.89	71.83	1.21	2.14	0.01	0.07

Table 2: Summary of the systematic errors in percent (%).

$E_{cm}(\text{GeV})$	$L(nb^{-1})$	N_{had}	N_{bg}	$\Delta\epsilon_{trk}$	ϵ_{trg}	$(1 + \delta_{obs})$	Total
2.60	2.00	2.79	0.05	0.32	0.50	1.18	3.68
3.07	1.96	2.53	0.05	0.29	0.50	1.15	3.45
3.65	1.38	2.74	0.35	0.26	0.50	1.10	3.33

4 Results and discussions

Tables 1 and 2 list the quantities used in the measurement of R with Eq. (2) and the contributions to the total error. The results are displayed in Fig. 3, together with previous measurements. The errors on the R values reported here are about 3.5%. The measured R values are consistent within errors with the prediction of perturbative QCD⁴.

Compared with our previous results^{8,9}, the measurement precision has been improved due to four main refinements to the analysis: (1) the simulation of BES with a GEANT3 based package that has a more detailed geometrical description and matter definition for the sub-detectors; (2) large data samples are taken at each energy point, with statistical errors that are smaller than 1%; (3) the selected hadronic event sample is expanded to include single-track events, which supplies more information to the tuning of LUARLW with resulting improved parameters; (4) the distributions used for parameter tuning are those related to the hadronic selection criteria; the better agreement between MC and data reduces the error on the hadronic event efficiency.

Based upon the measured R values and the perturbative QCD expansion that computes $R_{QCD}(\alpha_s)$ to an $\mathcal{O}(\alpha_s^3)$ approximation²⁶, the strong running coupling constant $\alpha_s^{(3)}(s)$ can be

determined at each energy point^{28,29} by solving the equation $R_{exp} \pm \sigma_{sts} \pm \sigma_{sys} = R_{QCD}(\alpha_s^{(3)})$. The obtained $\alpha_s^{(3)}(s)$ are evolved to 5 GeV, and the weighted average of $\bar{\alpha}_s^{(4)}(25\text{GeV}^2)$ is listed in Table 3. When evaluated at the M_Z scale, the resulting value is $\alpha_s^{(5)}(M_Z^2) = 0.117^{+0.012}_{-0.017}$, which agrees with the world average value within the quoted errors⁴.

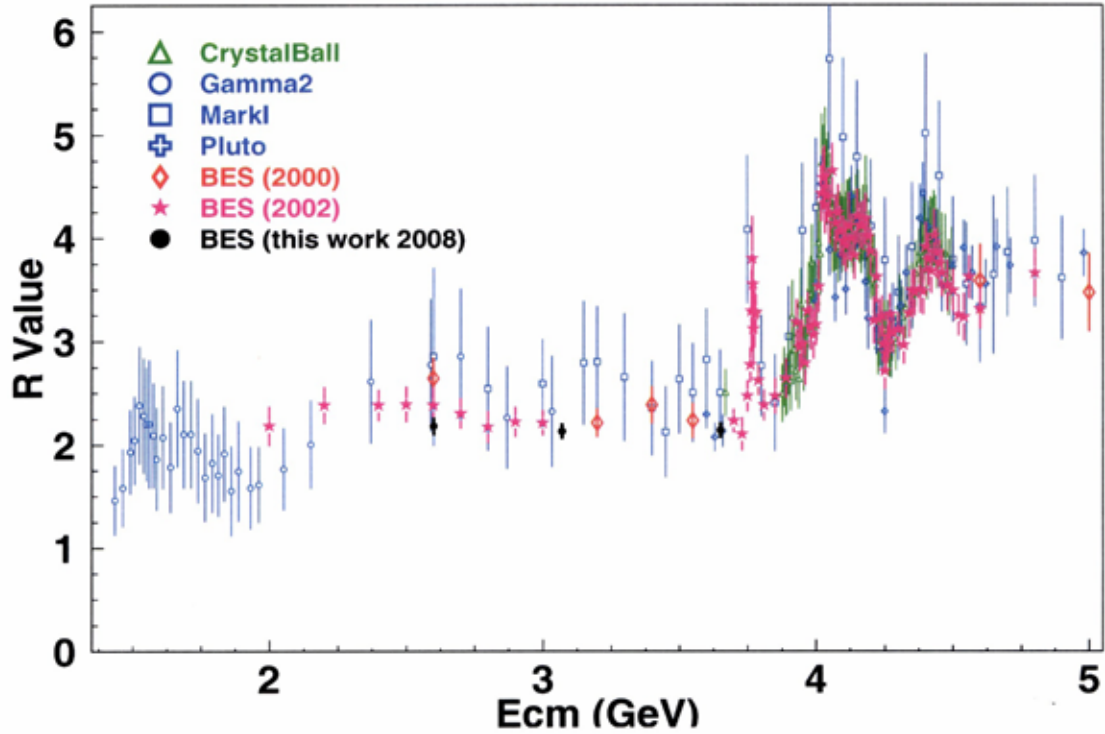


Figure 3: R values reported here together with other measurements below 5 GeV.

Table 3: $\alpha_s(s)$ determined from R values measured at 2.600, 3.070 and 3.650 GeV, and evolved to 5 GeV and M_Z . The first and second errors are statistical and systematic, respectively.

$\sqrt{s}(\text{GeV})$	$\alpha_s^{(3)}(s)$	$\alpha_s^{(4)}(25\text{GeV}^2)$	$\bar{\alpha}_s^{(4)}(25\text{GeV}^2)$	$\alpha_s^{(5)}(M_Z^2)$
2.60	$0.266^{+0.030+0.125}_{-0.030-0.116}$	$0.212^{+0.018+0.068}_{-0.019-0.086}$		
3.07	$0.192^{+0.029+0.103}_{-0.029-0.101}$	$0.169^{+0.022+0.074}_{-0.023-0.086}$	$0.209^{+0.044}_{-0.050}$	$0.117^{+0.012}_{-0.017}$
3.65	$0.207^{+0.015+0.104}_{-0.015-0.104}$	$0.189^{+0.012+0.082}_{-0.013-0.091}$		

References

1. B. Pietrzyk, Nucl. Phys. B(Proc. Suppl.) **162** 18 (2006)
2. F. Jegerlehner, Nucl. Phys. B(Proc. Suppl.) **162** 22 (2006)(hep-ph/0608329)
3. F. Ambrosino *et al.*, hep-ex/0603056, and reference therein.
4. Particle Data Group, Jour. Phys. **33**, (2006)116
5. M. Davier *et al.*, Phys. Lett. **B 419** (1998)419
6. M. Davier *et al.*, Eur. Phys. J. **C 27** (2003)497
7. BES Collaboration, J. Z. Bai *et al.*, Nucl. Instr. Meth. A **458**, 627 (2001).
8. BES Collaboration, Phys. Rev. Lett. **84**, (2000)594
9. BES Collaboration, Phys. Rev. Lett. **88**, (2002)101802
10. BES Collaboration, M. Ablikim *et al.*, Nucl. Instrum. Meth. A **552**, 344 (2005).

11. H. Hu et al. High Energy Physics and Nuclear Physics **31**, (2007)802
12. H.M. Hu et al., High Energy Phys. and Nucl. Phys. **25**, (2001)1035 (in Chinese)
13. B.Andersson and H.Hu, hep-ph/9810285
14. Bo Andersson, The Lund Model, Cambridge Unniversity press (1998)
15. Torbjorn Sjostrand, CERN-TH.7112/93
16. T.Sjöstrand, Computer Physics Commun. **39** (1986) 347
17. T.Sjöstrand, Computer Physics Commun. **43** (1987) 367
18. Armin Böhrer, Phys. Rep. **191**, (1997)107
19. Y. Weng et al. High Energy Physics and Nuclear Physics **31**, (2007)703
20. A. Osterheld et al. SLAC-PUB-4160, 1986
21. C. Edwards et al. SLAC-PUB-5160, 1990
22. H. Hu et al. High Energy Physics and Nuclear Physics **25**, (2001)701
23. G.Bonneau and F.Martin, Nucl. Phys. **B27**, (1971)381
24. F.A.Berends and R.Kleiss, Nucl. Phys. **B178**, (1981)141
25. E.A.Kureav and V.S.Fadin, Sov. Nucl. Phys. **41**, (1985)466
26. S.G.Gorishnii, *et al.*, Phys. Let. **B259**, (1991)144
27. Y.S. Tsai, SLAC-PUB-3129, May 1983 (T/E)
28. J.H.Kuhn and M.Steinhauser, arXiv:hep-ph/0109084 v3(2002).
29. J. Hu et al. High Energy Physics and Nuclear Physics **31**, (2007)1

Light Hadrons and New Enhancements in J/ψ Decays at BESII

Guofa XU
(for the BES Collaboration)
Institute of High Energy Physics, CAS, Beijing 100049, China

Based on 58 million J/ψ samples collected by the BESII detector at the BEPC, many mesons, baryons, and new resonances have been reported. Here, I will review some recent results of glueball candidates and new enhancement.

1 Introduction

In this paper, some recent BESII results are reported based on 58 million J/ψ events collected by the BESII detector at the BEPC. For much more detail, please see the references.

2 Scalars (0^{++})

As we know that so many scalars are listed in PDG06¹, but according to the quark model no enough room for all of these scalar particles. On the other hand, the Lattice QCD predicted that the ground state glueball is 0^{++} , and its mass is around 1.5~1.8 GeV. Theoretical physicists expect that glueballs will mix with nearby $q\bar{q}$ states of the same quantum numbers^{2,3}, it makes the situation more difficult for the glueball identification. Although the identification of a glueball is very complicated, there are several glueball candidates, such as $f_0(1500)$ and $f_0(1710)$, considering the possible mix with the ordinary $q\bar{q}$ meson, $f_0(1370)$, $f_0(1500)$, $f_0(1710)$, and $f_0(1790)$ have been analyzed for more detail by using the partial wave analyzes (PWA) method in $J/\psi \rightarrow \gamma\pi\pi$, $\gamma K\bar{K}$, $J/\psi \rightarrow \omega K\bar{K}$, and $J/\psi \rightarrow \phi\pi\pi$, $\phi K\bar{K}$ channels.

2.1 The Analysis of $J/\psi \rightarrow \gamma\pi\pi$ and $\gamma K\bar{K}$ Channels

The partial wave analyzes of $J/\psi \rightarrow \gamma\pi^+\pi^-$ and $J/\psi \rightarrow \gamma\pi^0\pi^0$ show the evidence for two 0^{++} states around the 1.45 and 1.75 GeV/ c^2 mass regions (Fig. 1, 2)⁴. The $f_0(1500)$ has

a mass of $1466 \pm 6 \pm 20 \text{ MeV}/c^2$, a width of $108_{-11}^{+14} \pm 25 \text{ MeV}/c^2$, and a branching fraction $\mathcal{B}(J/\psi \rightarrow \gamma f_0(1500) \rightarrow \gamma \pi^+ \pi^-) = (0.67 \pm 0.02 \pm 0.30) \times 10^{-4}$. The 0^{++} state in the $\sim 1.75 \text{ GeV}/c^2$ mass region has a mass of $1765_{-3}^{+4} \pm 13 \text{ MeV}/c^2$ and a width of $145 \pm 8 \pm 69 \text{ MeV}/c^2$.

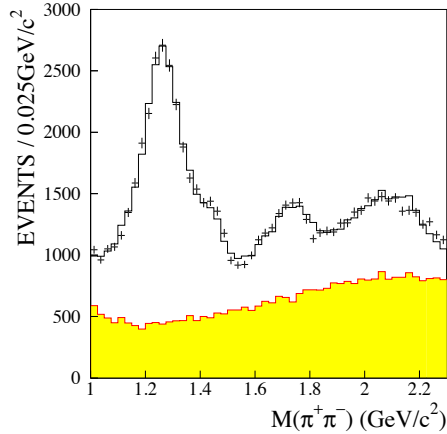


Figure 1: The $\pi^+ \pi^-$ invariant mass distribution from $J/\psi \rightarrow \gamma \pi^+ \pi^-$. The crosses are data, the full histogram shows the maximum likelihood fit, and the shaded histogram corresponds to the $\pi^+ \pi^- \pi^0$ background.

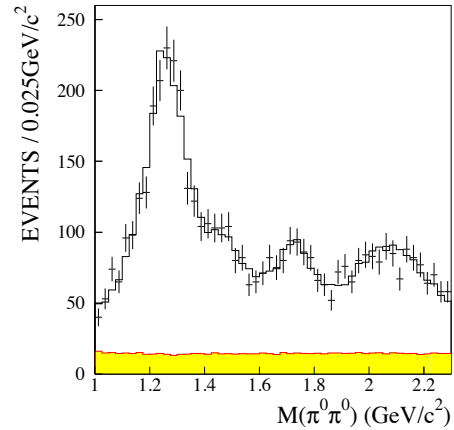


Figure 2: The $\pi^0 \pi^0$ invariant mass distribution from $J/\psi \rightarrow \gamma \pi^0 \pi^0$. The crosses are data, the full histogram shows the maximum likelihood fit, and the shaded histogram corresponds to the background.

The PWA of $J/\psi \rightarrow \gamma K^+ K^-$ and $J/\psi \rightarrow \gamma K_S^0 K_S^0$ show strong production of the $f_2'(1525)$ and the S-wave resonance $f_0(1710)$ (Fig. 3)⁵. The $f_0(1710)$ peaks at a mass of $1740 \pm 4_{-25}^{+10} \text{ MeV}$ with a width of $166_{-8-10}^{+5+15} \text{ MeV}$.

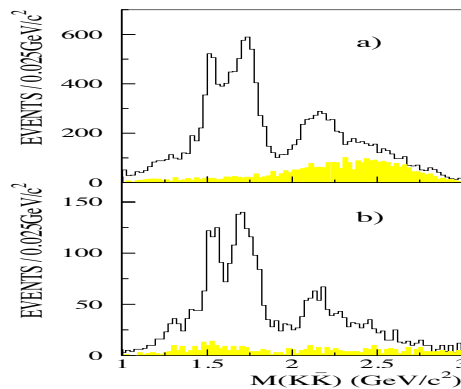


Figure 3: Invariant mass spectra of a) $K^+ K^-$, b) $K_S^0 K_S^0$ for $J/\psi \rightarrow \gamma K \bar{K}$ events, where the shaded histograms correspond to the estimated background contributions.

2.2 The Analysis of $J/\psi \rightarrow \omega K^+ K^-$ Channel

From Fig. 4, one can see that a dominant feature is $f_0(1710)$ ⁶. The fitted $f_0(1710)$ optimizes at $M = 1738 \pm 30 \text{ MeV}/c^2$, $\Gamma = 125 \pm 20 \text{ MeV}/c^2$.

2.3 The Analysis of $J/\psi \rightarrow \phi \pi^+ \pi^-$ and $\phi K^+ K^-$ Channels

After the partial wave analyzes for these $\phi \pi \pi$ and $\phi K K$ channels⁷, the data reported here have three important features. Firstly, the parameters of $f_0(980)$ are all well determined. Secondly,

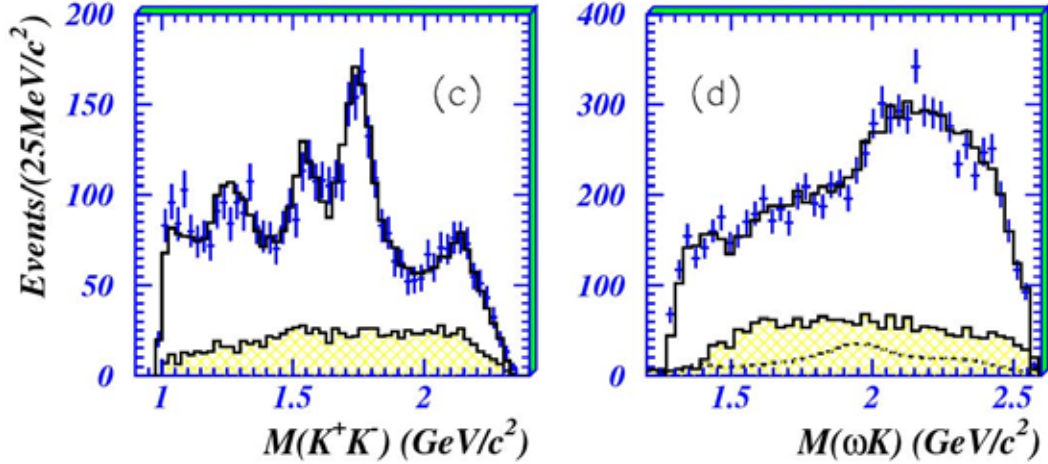


Figure 4: (c) and (d) are projections on to K^+K^- and ωK mass. Histograms show the maximum likelihood fit; the shaded region indicates the background estimated from sidebins; the dashed curve in (d) shows the magnitude of the $K_1(1400)$ contribution and a $K\omega$ contribution at $1945 \text{ MeV}/c^2$.

there is the clearest signal to date of $f_0(1370) \rightarrow \pi^+\pi^-$; a resonant phase variation is required, from interference with $f_2(1270)$. Thirdly, there is a clear peak in $\pi\pi$ at $1775 \text{ MeV}/c^2$, consistent with $f_0(1790)$; spin 2 is less likely than spin 0.

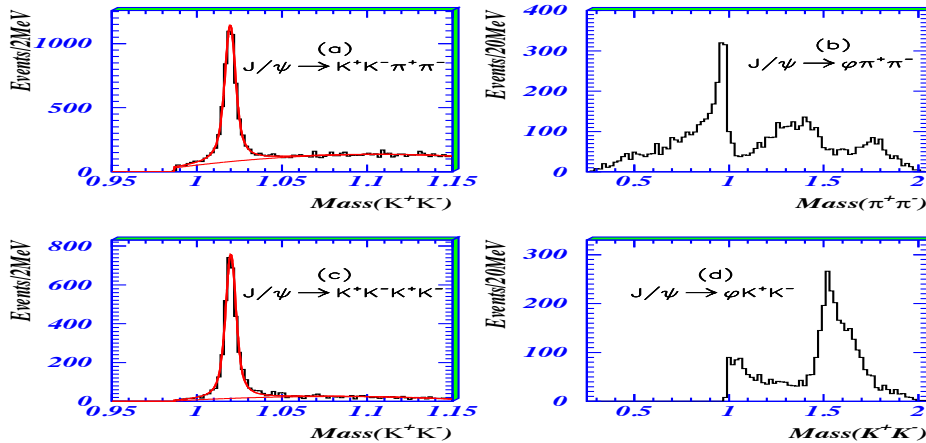


Figure 5: The K^+K^- invariant mass distributions for (a) $J/\psi \rightarrow K^+K^-\pi^+\pi^-$, (c) $J/\psi \rightarrow K^+K^-K^+K^-$; curves show the fitted background and a Gaussian fit to the ϕ ; (b) and (d) show mass projections for events selected within $\pm 15 \text{ MeV}/c^2$ of the ϕ .

In summary, (1) $f_0(1370)$ has been seen in $J/\psi \rightarrow \phi\pi\pi$, but not in $J/\psi \rightarrow \omega\pi\pi$. (2) No peak of the $f_0(1500)$ directly seen in $J/\psi \rightarrow \phi KK$, ωKK , $\phi\pi\pi$, and $\omega\pi\pi$, but in proton-proton scattering is quite clear. (3) $f_0(1710)$ is observed clearly in both $J/\psi \rightarrow \phi KK$ and $J/\psi \rightarrow \omega KK$, but with $Br(J/\psi \rightarrow \omega f_0(1710) \rightarrow \omega KK)/Br(J/\psi \rightarrow \phi f_0(1710) \rightarrow \phi KK) \sim 6$, which is against a simple $s\bar{s}$ configuration for this state. (4) $f_0(1790)$ which is seen in $\pi\pi$ rather than $K\bar{K}$.

Different models have different interpretations for these experimental results. One of the interpretations is from Cheng⁸, he explained that (1) $f_0(1710)$ is composed primarily of the scalar glueball. (2) $f_0(1500)$ is close to an $SU(3)$ octet. The glueball content of $f_0(1500)$ is very tiny because an $SU(3)$ octet does not mix with the scalar glueball. (3) $f_0(1370)$ consists of an approximate $SU(3)$ singlet with some glueball component ($\sim 10\%$).

3 Pseudo-scalars (0^{-+})

The first observation of $\eta(1440)$ was made in $p\bar{p}$ annihilation at rest into $\eta(1440)\pi^+\pi^-$, $\eta(1440) \rightarrow K\bar{K}\pi$ ⁹. Nowadays, The existence of two overlapping pseudo-scalar states has been suggested to instead of the $\eta(1440)$: one around 1405 MeV/ c^2 decays mainly through $a_0(980)\pi$ (or direct $K\bar{K}\pi$), and the other around 1475 MeV/ c^2 mainly to $K^*(892)\bar{K}$ ^{1,10}. It is therefore conceivable that the higher mass state is the $s\bar{s}$ member of the 2^1S_0 nonet^{11,12}, while the lower mass state may contain a large gluonic content^{13,14}.

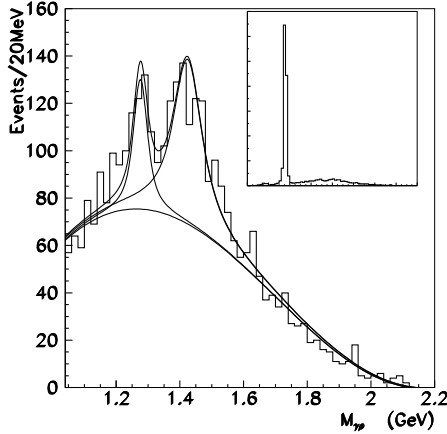


Figure 6: The $\gamma\rho$ invariant mass distribution. The insert shows the full mass scale where the $\eta(958)$ is clearly observed.

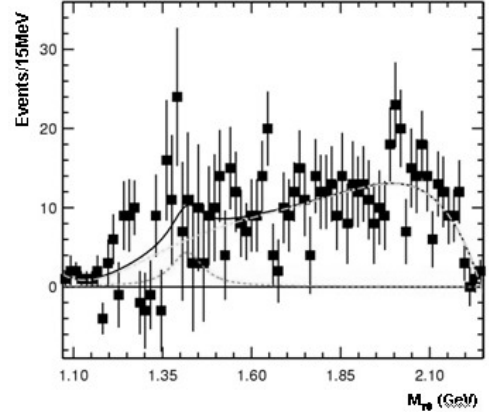


Figure 7: The invariant mass of $\gamma\phi$ after side-band background subtraction.

In our $J/\psi \rightarrow \gamma\gamma V$ analysis¹⁵, there is a resonance around 1424 MeV at the $J/\psi \rightarrow \gamma\gamma\rho$ channel. Comparing our result on the branching ratio $B(J/\psi \rightarrow \gamma X(1424) \rightarrow \gamma\gamma\rho) = (1.07 \pm 0.17 \pm 0.11) \times 10^{-4}$, and the upper limit of $B(J/\psi \rightarrow \gamma X(1424) \rightarrow \gamma\gamma\phi) < 0.82 \times 10^{-4}$ (95% C.L.), we cannot draw a definite conclusion on whether the $X(1424)$ is either a $q\bar{q}$ state or a glueball state.

We also analyzed the $\eta(1405)/\eta(1475)$ at $J/\psi \rightarrow \{\omega, \phi\}K\bar{K}\pi$ channels¹⁶. In the invariant mass spectra of $K_S^0 K^\pm \pi^\mp$ and $K^+ K^- \pi^0$ recoiling against the ω signal region, the resonance at 1.44 GeV/ c^2 is observed, while in the invariant mass spectra of $K_S^0 K^\pm \pi^\mp$ and $K^+ K^- \pi^0$ recoiling against the ϕ signal region, no significant structure near 1.44 GeV/ c^2 is seen and an upper limits on the J/ψ decay branching fractions at the 90% C.L. are given in Table 1.

Table 1: The mass, width, and branching fractions of J/ψ decays into $\{\omega, \phi\}X(1440)$.

$J/\psi \rightarrow \omega X(1440)$ ($X \rightarrow K_S^0 K^+ \pi^- + c.c.$)	$J/\psi \rightarrow \omega X(1440)$ ($X \rightarrow K^+ K^- \pi^0$)
$M = 1437.6 \pm 3.2 \text{ MeV}/c^2$	$M = 1445.9 \pm 5.7 \text{ MeV}/c^2$
$\Gamma = 48.9 \pm 9.0 \text{ MeV}/c^2$	$\Gamma = 34.2 \pm 18.5 \text{ MeV}/c^2$
$B(J/\psi \rightarrow \omega X(1440) \rightarrow \omega K_S^0 K^+ \pi^- + c.c.) = (4.86 \pm 0.69 \pm 0.81) \times 10^{-4}$	
$B(J/\psi \rightarrow \omega X(1440) \rightarrow \omega K^+ K^- \pi^0) = (1.92 \pm 0.57 \pm 0.38) \times 10^{-4}$	
$B(J/\psi \rightarrow \phi X(1440) \rightarrow \phi K_S^0 K^+ \pi^- + c.c.) < 1.93 \times 10^{-5}$	(90% C.L.)
$B(J/\psi \rightarrow \phi X(1440) \rightarrow \phi K^+ K^- \pi^0) < 1.71 \times 10^{-5}$	(90% C.L.)

4 New Enhancements

A narrow enhancement is observed in $J/\psi \rightarrow \gamma p\bar{p}$ ¹⁷. Assuming that the $p\bar{p}$ system is in an S-wave resulted in a resonance with mass $M = 1859^{+3+5}_{-10-25}$ MeV/c², width $\Gamma < 30$ MeV/c² (at the 90% C.L.) and product branching fraction $B(J/\psi \rightarrow \gamma X) \cdot B(X \rightarrow p\bar{p}) = (7.0 \pm 0.4(stat)_{-0.8}^{+1.9}(syst)) \times 10^{-5}$. The data not precise enough to determine the angular distribution. According to the theoretical calculation¹⁸, if the X is a bound state of $(p\bar{p})$, the decay channel ($X \rightarrow \eta 4\pi$) is favored over ($X \rightarrow \eta 2\pi, 3\eta$).

The decay channel $J/\psi \rightarrow \gamma \pi^+ \pi^- \eta'$ is analyzed using two η' decay modes, $\eta' \rightarrow \pi^+ \pi^- \eta$ and $\eta' \rightarrow \gamma \rho$ ¹⁹. A resonance, the $X(1835)$, is observed with a high statistical significance of 7.7σ in the $\pi^+ \pi^- \eta'$ invariant mass spectrum. From a fit with a Breit-Wigner function, the mass is determined to be $M = 1833.7 \pm 6.1(stat) \pm 2.7(syst)$ MeV/c², the width is $\Gamma = 67.7 \pm 20.3(stat) \pm 7.7(syst)$ MeV/c², and the product branching fraction is $B(J/\psi \rightarrow \gamma X) \cdot B(X \rightarrow \pi^+ \pi^- \eta') = (2.2 \pm 0.4(stat) \pm 0.4(syst)) \times 10^{-4}$. The mass and width of the $X(1835)$ are not compatible with any known meson resonance¹. If we redoing the S -wave BW fit to the $p\bar{p}$ invariant mass spectrum¹⁷ including the zero Isospin, S -wave final-state-interactions (FSI) factor²⁰, yields a mass $M = 1831 \pm 7$ MeV/c² and a width $\Gamma < 153$ MeV/c² (at the 90% C.L.), these values are in good agreement with the mass and width of $X(1835)$ reported here.

In the analysis of $J/\psi \rightarrow \omega p\bar{p}$ ²¹, no significant enhancement near the $p\bar{p}$ mass threshold is observed, and an upper limit of $B(J/\psi \rightarrow \omega X)B(X \rightarrow p\bar{p}) < 1.5 \times 10^{-5}$ is determined at the 95% confidence level.

5 Summary

Using the 58 M J/ψ events sample taken with the BESII detector at the BEPC storage ring, BES experiment provided many interesting results, especially for the study of the lowest glueball candidates, the structure of $\eta(1440)$, and the new enhancement of $X(1835)$, but since the limit of the statistics, the better results (with higher statistics and better accuracy) will be needed for well understanding. The upgraded BEPCII/BESIII will provide a huge J/ψ decay samples for the further analysis.

References

1. W.-M. Yao *et al.*, (Particle Physics Group), *J. Phys. G* **33**, 1 (2006).
2. C. Amsler and F.E. Close, *Phys. Rev. D* **53**, 295 (1996).
3. F.E. Close and A. Kirk, *Eur. Phys. J. C* **21**, 531 (2001).
4. M. Ablikim *et al.* [BES Collab.], *Phys. Lett. B* **642**, 441 (2006).
5. J.Z. Bai *et al.* [BES Collab.], *Phys. Rev. D* **68**, 052003 (2003).
6. M. Ablikim *et al.* [BES Collab.], *Phys. Lett. B* **603**, 138 (2004).
7. M. Ablikim *et al.* [BES Collab.], *Phys. Lett. B* **607**, 243 (2005).
8. H.Y. Cheng, *hep-ph/0609229*.
9. P.H. Baillon *et al.*, *Nuovo Cimento A* **50**, 393 (1967).
10. S. Godfrey and J. Napolitano, *Rev. Mod. Phys.* **71**, 1411 (1999).
11. M.G. Rath *et al.*, *Phys. Rev. D* **40**, 693 (1989).
12. A. Bertin *et al.*, *Phys. Lett. B* **361**, 187 (1995).
13. M. Acciarri *et al.*, *Phys. Lett. B* **501**, 1 (2001).
14. F. Close *et al.*, *Phys. Rev. D* **55**, 5749 (1997).
15. M. Ablikim *et al.* [BES Collab.], *Phys. Lett. B* **594**, 47 (2004).
16. M. Ablikim *et al.* [BES Collab.], *arXiv:0712.1411*.
17. J.Z. Bai *et al.* [BES Collab.], *Phys. Rev. Lett.* **91**, 022001 (2003).

18. G.J. Ding and M.L. Yan, *Phys. Rev. C* **72**, 015208 (2005).
19. M. Ablikim *et al.* [BES Collab.], *Phys. Rev. Lett.* **95**, 262001 (2005).
20. A. Sibirtsev *et al.*, *Phys. Rev. D* **71**, 054010 (2005).
21. M. Ablikim *et al.* [BES Collab.], *Eur. Phys. J. C* **53**, 15 (2008).

NA48 Results

G. Ruggiero

Scuola Normale Superiore, Pisa, Italy

Measured decay rates of $K^\pm \rightarrow e^\pm \pi^0 \nu_e$ and $K^\pm \rightarrow \mu^\pm \pi^0 \nu_\mu$ normalized to $K^\pm \rightarrow \pi^\pm \pi^0$ are presented. These measurements are based on K^\pm decays collected in a dedicated run in 2003 by the NA48/2 experiment at CERN. Using the PDG 2006 average for the $K^\pm \rightarrow \pi^\pm \pi^0$ normalization mode, the results are found to be larger than the current values given by the PDG 2006 and lead to a larger magnitude of the $|V_{us}|$ CKM element than previously accepted. When combined with the latest PDG 2006 value of $|V_{ud}|$, the result is in agreement with unitarity of the CKM matrix.

The ratio $R_K = \Gamma(K^\pm \rightarrow e^\pm \nu)/\Gamma(K^\pm \rightarrow \mu^\pm \nu)$ is calculated with very high precision within the Standard Model (SM), but corrections due to the presence of New Physics could be as high as 3%. The data obtained by the NA48/2 experiment in two years of data taking at the CERN SPS accelerator has been analyzed. The obtained result for R_K is two times more precise than the world average but is still insufficient to probe the existence of physics beyond the Standard Model. The status of the analysis of the data taken in 2007, aimed for a sub-percent precision of R_K , will be summarized.

1 Introduction

The NA48 experiment at CERN SPS is a fixed target experiment devoted to kaon physics operating since 1997. Until 2001 the experiment studied the neutral kaon decays and provided the final measurement of ϵ'/ϵ ¹. A charged kaon physics program (NA48/2) took place in 2003 and 2004: it was mainly devoted to the search for direct CP violation in the K^\pm decays into three pions². Beside this main topic, also semileptonic and rare charged kaon decays were studied. To this end dedicated runs with reduced intensity were taken in 2003 and 2004. The present work describes the final result of the measurement of the branching ratio of $K^\pm \rightarrow l^\pm \pi^0 \nu_l$ ($l = e, \mu$)³ using the 2003 data and the preliminary results of the measurement of the ratio $R_K = \Gamma(K^\pm \rightarrow e^\pm \nu_e)/\Gamma(K^\pm \rightarrow \mu^\pm \nu_\mu)$ based on the 2003 and 2004 data. The NA62 collaboration is currently carrying on the kaon physics program at CERN SPS. The first phase of this experiment aims

for a sub-percent precision measurement of R_K , for which data were taken in 2007 with the NA48/2 apparatus.

2 NA48/2 Experimental Setup

The experiment used simultaneous K^\pm beams produced by 400 GeV/c protons delivered by the SPS and impinging on a Be target with a duty cycle of 4.8 s spill over a 16.8 s accelerator period. The proton intensity on target was about 7×10^{11} proton per spill during the 2003 and 2004 normal runs. It was reduced during the special runs to allow data taking with a minimum bias trigger, while it was increased up to more than 10^{12} protons per spill during the 2007 run. A 100 m long beam line selected charged beams with 60 ± 3 GeV/c average momentum in 2003 and 2004 and 75 ± 2 GeV/c in 2007. The detector sits about 100 meter downstream to the end of the beam line and detected the products of the kaon decays happening in the evacuated region between the end of the beam line and the beginning of the detector. A detailed description of the NA48 apparatus can be found elsewhere⁴. The most relevant devices for the measurements described here were: the magnetic spectrometer, consisting of 4 drift chambers and one magnet and the high resolution liquid krypton electromagnetic calorimeter. The spectrometer worked with a reduced magnetic field in 2003 and 2004 and with full magnetic field in 2007 allowing a better momentum resolution. Other devices were the hodoscope for charged particle triggering and precise time measurement and a muon detector.

3 Measurement of the K_{l3} Branching Ratio

3.1 Theoretical aspects

The following master formula describes the branching ratio of the semileptonic charged kaon decays⁵:

$$BR(K_{l3}) = \tau_K \frac{G_F^2}{384\pi^3} m_K^5 S_{EW} |V_{us}|^2 |f_+(0)|^2 I_K^l (1 + \delta_{SU2}^K + \delta_{em}^{Kl})^2. \quad (1)$$

Here K_{l3} is a short-hand notation for $K^\pm \rightarrow l^\pm \pi^0 \nu_l$ with l equal to e or μ . τ_K is the average life time of K^\pm , G_F the Fermi constant and m_K the mass of the charged kaon. S_{EW} is the short distance radiative correction, δ_{SU2}^K and δ_{em}^{Kl} are the model dependent long distance corrections due to isospin breaking in strong and electromagnetic interactions. Two form factors, $f_+(t)$ and $f_0(t)$, describe the dynamic of the semileptonic decays. Their t dependence can be approximated as:

$$f_+(t) = f_+(0) \left(1 + \lambda'_+ \frac{t}{m_{\pi^+}^2} + \lambda''_+ \frac{t^2}{m_{\pi^+}^4} \right), \quad f_0(t) = f_+(0) \left(1 + \lambda_0 \frac{t}{m_{\pi^0}^2} \right). \quad (2)$$

$f_+(0)$ is the form factor at zero momentum transfer. The parameters λ'_+ , λ''_+ and λ_0 are measured⁶. I_K^l is the result over the phase space integration after factorizing out the $f_+(0)$ and depends on λ'_+ , λ''_+ and λ_0 , using the above approximation⁵. Finally V_{us} is the element of the CKM matrix which describes the u-s transitions.

It turns out that the measurement of the branching ratio of the charged K_{l3} decays allows a clean test of the u-s quark transitions. Moreover the ratio between the branching ratios of the K_{e3} and $K_{\mu3}$ provides also an experimental test of the μ - e universality.

3.2 Data taking and Analysis Strategy

Because of the impossibility to measure precisely the absolute kaon flux, NA48 measured the semileptonic branching ratios normalized to $K^\pm \rightarrow \pi^\pm \pi^0$, that is the ratios $\mathcal{R}_{K_{l3}/K_{2\pi}} \equiv$

$\Gamma(K_{l3})/\Gamma(K^\pm \rightarrow \pi^\pm \pi^0)$. It is relevant that the single track topology for both the signal and the normalization channel allows a first order cancellation of the systematics.

Hits in the hodoscope compatible with a one track decay were the only input of the trigger. The trigger efficiency was measured on data to be greater than 99.8%. An offline one track selection using the spectrometer informations and a π^0 identification based on the calorimeter data, defined a sample of K_{e3} , $K_{\mu3}$ and $K^\pm \rightarrow \pi^\pm \pi^0$ decays. Extra activity in the calorimeter was allowed to select inclusively also the corresponding radiative decays. Kinematical cuts exploiting the missing energy and the decay topology separated the semileptonic from the two pions decays. The particle identification was used to distinguish the electron from the muon channel. In particular the requirement $E_{LKr}/P > 0.95$ identified an electron, where E_{LKr} is the energy released by the particle in the calorimeter and P is the particle momentum measured by the spectrometer; the cut $E_{LKr}/P < 0.8$ defined a pion. Finally, the presence of a hit in the muon detector, matching in space and time with the track, tagged a muon. The total number of selected events per decay mode was: 87×10^3 K_{e3} , 77×10^3 $K_{\mu3}$ and 729×10^3 $K^\pm \rightarrow \pi^\pm \pi^0$.

The acceptance was computed using a GEANT⁷ based Monte Carlo simulation. The event generation made use of the previously described parametrization for the form factors, with λ'_+ , λ''_+ and λ_0 taken from reference⁶. The phase space was corrected according to the Ginsberg prescription⁸ to account for radiative corrections. The PHOTOS package⁹ provided the generation of real bremsstrahlung photons. The acceptance varied between 7% and 14% depending on the decay mode. Different expressions of the form factors were also considered¹⁰ and the corresponding variation of the final result quoted as systematic uncertainty. The particle identification was a source of inefficiency not canceled in the single ratio. It was measured on data and varied between 98.5% and 99.5%, depending on the particle type. The corresponding error was quoted as systematic uncertainty. The Monte Carlo simulation pointed out a background contamination below 0.1% for K_{e2} and at the level of 0.2% and 0.3% for $K_{\mu2}$ and $K^\pm \rightarrow \pi^\pm \pi^0$, respectively.

3.3 Results

The results are:

$$\begin{aligned} \mathcal{R}_{K_{e3}/K_{2\pi}} &= 0.2470 \pm 0.0009_{stat} \pm 0.0004_{syst} \\ \mathcal{R}_{K_{\mu3}/K_{2\pi}} &= 0.1636 \pm 0.0006_{stat} \pm 0.0003_{syst} \\ \mathcal{R}_{K_{\mu3}/K_{e3}} &= 0.663 \pm 0.003_{stat} \pm 0.001_{syst} \end{aligned} \quad (3)$$

Analysis of these results as a function of their basic distributions shown stability.

Taking the branching ratio of $K^\pm \rightarrow \pi^\pm \pi^0$ from⁶ the branching ratio for the semileptonic decays are:

$$\begin{aligned} BR(K_{e3}) &= 0.05168 \pm 0.00019_{stat} \pm 0.00008_{syst} \pm 0.00030_{norm} \\ BR(K_{\mu3}) &= 0.03425 \pm 0.00013_{stat} \pm 0.00006_{syst} \pm 0.00020_{norm} \end{aligned} \quad (4)$$

The uncertainty is dominated by the error on the measurement of the branching ratio of the $K^\pm \rightarrow \pi^\pm \pi^0$. Both the values are significantly above the PDG 2006 values. The $BR(K_{e3})$ agrees with the BNL E865¹¹ and the ISTRA+'07¹² measurements. Both the NA48 measurements, however, do not agree with the values measured by KLOE¹³ which are in agreement with⁶. The recent KLOE measurement of the $BR(K^\pm \rightarrow \pi^\pm \pi^0)$ ¹⁴, significantly lower than the PDG 2006 one, partially recover the difference between NA48 and KLOE.

The measurements 4 allow the extraction of V_{us} . To this end the following values were used: $S_{ew} = 1.023$ ¹⁵, $I_K^e = 0.1591$ and $I_K^\mu = 0.1066$ (λ'_+ , λ''_+ and λ_0 from⁶), $\delta_{SU2}^K = 2.31\%$, $\delta_{em}^{Ke} = 0.03\%$ and $\delta_{em}^{K\mu} = 0.2\%$ from^{16,8,17}, $G_F = 1.16637 \times 10^{-5} \text{ GeV}^{-2}$ ¹⁸ and m_K and τ_K from⁶. The result is

$$|V_{us}|f_+(0) = 0.2188 \pm 0.0012 \quad (5)$$

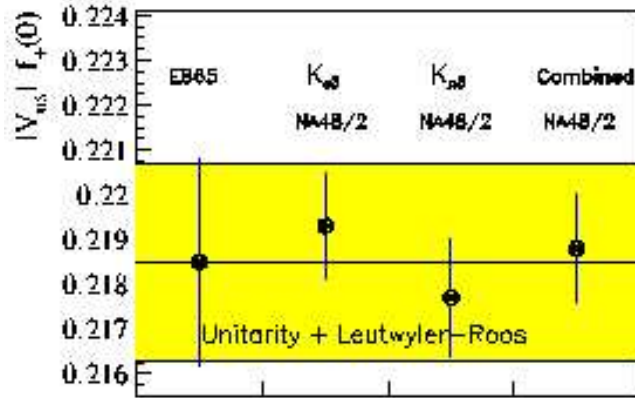


Figure 1: Comparison of the NA48 measurement of $|V_{us}|f_+(0)$ from K_{e3} , $K_{\mu3}$ and combined and the theoretical prediction computed as described in the text.

combined for K_{e3} and $K_{\mu3}$. The values obtained for the two decay modes separately are in agreement among themselves. The result is in agreement with the expected value computed using $V_{ud} = 0.9738 \pm 0.0003$ ¹⁹, $|V_{ub}| = (3.6 \pm 0.7) \times 10^{-36}$, $f_+(0) = 0.961 \pm 0.008$ ⁵ and assuming unitarity, as shown in figure 1. The results are compatible with the unitarity of the CKM matrix. Finally the measured value of $\mathcal{R}_{K_{\mu3}/K_{e3}}$ implies the μ -e universality violating quantity $g_{\mu}f_+^{\mu}(0)/g_e f_+^e(0) = 0.99 \pm 0.01$, consistent with one within the experimental errors.

4 Measurement of R_K

4.1 Theoretical aspects and experimental status

The measurement of $R_K \equiv R(K_{e2})/R(K_{\mu2})$ provides an accurate test of the lepton universality predicted in the SM. Here K_{l2} is a short-hand notation for $K^{\pm} \rightarrow l^{\pm}\nu_l$. Thanks to the cancellation in the ratio of the hadronic uncertainties, the SM predicts R_K with a sub-permille accuracy²⁰.

$$R_K = \frac{m_e^2}{m_{\mu}^2} \left(\frac{m_K^2 - m_e^2}{m_K^2 - m_{\mu}^2} \right)^2 (1 + \delta R_{QED}) = (2.477 \pm 0.001) \times 10^{-5}. \quad (6)$$

Here $m_{K,e,\mu}$ are the masses of the kaon, electron and muon and δR_{QED} is the correction for virtual photon processes and inner bremsstrahlung photon emission.

The helicity suppression makes R_K sensitive to new physics. A theoretical study²¹ suggests the possibility of up to some percent deviation from the SM value induced by lepton flavor violating effects, as those arising in supersymmetry extensions of SM. As a consequence a sub-percent precision measurement of R_K could probe physics beyond SM.

The PDG 2006 value, $R_K = (2.45 \pm 0.11) \times 10^{-5}$, is far from the accuracy needed. NA48 provided preliminary measurements at 2% precision using 2003 and 2004 data. More recently KLOE²² measured this quantity with 2% level accuracy. NA62 took data for 4 months in 2007 and collected more than 10^5 K_{e2} aiming for a 0.5% precision.

4.2 Analysis Strategy

The signal signature is one track in the final state compatible with a two body kinematics. Both kinematics and particle identification discriminate between the electron and the muon channel. The requirement $E_{LK\tau}/P > 0.95$ identifies an electron, like in the K_{l3} analysis previously described. Once data are collected using similar triggers for the two channels, systematics

cancels at zero order in the ratio. Background and particle identification efficiency, however, may affect numerator and denominator differently. Still a percent or even below measurement of R_K requires also a precise evaluation of the acceptance correction which can be as large as 10%. Since the main corrections depend on track momentum, the measurement takes advantage from an analysis in momentum bins. The background in the $K_{\mu 2}$ sample is below the percent level. On the contrary $K_{\mu 2}$ event can mimic $K_{e 2}$ in case of muons mis-identified as electrons and induce up to 10% background in the $K_{e 2}$ sample. This is a consequence of the about 10^{-6} probability of muon catastrophic energy loss in the liquid krypton calorimeter, which needs to be evaluated with percent accuracy. Muon contamination, however, depends on the kinematical discrimination power and affects $K_{e 2}$ with momentum higher than $35 \div 40$ GeV/c, where the kinematics of the two decay modes looks similar. A more than 1% level of background from $K_{e 2 \gamma}$ structure dependent decays is also expected and requires a knowledge of its branching ratio with 10% accuracy. Finally an electron identification efficiency at the level of $98 \div 99\%$, requires also to be evaluated with a 10% precision. Suitable control data can accomplish for that.

4.3 Preliminary results from 2003-2004 run

The number of $K_{e 2}$ collected by NA48 in 2003 and 2004 after background subtraction was $(4670 \pm 77_{stat}^{+29}_{-8}(syst))$ and $(3407 \pm 63_{stat} \pm 54_{syst})$, respectively. The systematic uncertainty refers to the background subtraction procedure. In particular the muon background in the $K_{e 2}$ sample was estimated at the level of 14%, using a pure $K_{e 2}$ sample at low momentum. The results are^{23,24}

$$\begin{aligned} R_K &= (2.416 \pm 0.043 \pm 0.024) \times 10^{-5} \quad (2003) \\ R_K &= (2.455 \pm 0.045 \pm 0.041) \times 10^{-5} \quad (2004) \end{aligned} \quad (7)$$

The 2003 data suffered from kinematical requests at trigger level which induced a large trigger efficiency correction. The choice of a minimum bias trigger for $K_{\mu 2}$ and and the minimum bias plus a further requirement on the total energy in the electromagnetic calorimeter for $K_{e 2}$, avoided that problem in 2004. The systematics of both the measurements are largely dominated by the uncertainty in the background subtraction. The other systematics are below 0.2%.

4.4 NA62 run: data collected and status of the analysis

NA62 took data in 2007. In comparison to the 2003-2004 run, the increase of the average beam momentum from 60 to 75 GeV/c and the shrink of the momentum bite from 3 to 2 GeV/c allowed a better background rejection. For the same purpose the spectrometer worked with a stronger magnetic field. The trigger was the same as in 2004. During the run an important accidental background appeared in the K^- data. For that reason only K^+ were taken for most of the period. The statistics collected matched the goal of the run: the total number of $K_{e 2}$ selected on-line was, in fact, $1,1 \times 10^5$. Figure 2 a) shows the squared invariant missing mass distribution, m_{miss}^2 , for selected $K_{e 2}$ -like events, where m_{miss}^2 is defined as the square of the difference between the kaon and the measured track four momenta. The number of good $K_{e 2}$ refers to the events under the peak.

Part of the data were taken with a lead bar 18.0 cm wide and $9 X_0$ thick in front of the liquid krypton calorimeter to measure the probability of muon catastrophic energy loss. The presence of the bar induced about 18% loss in $K_{e 2}$ acceptance. The lead acted as a muon filter selecting a pure sample of muons without electron contamination. More precisely this bar was placed just in front of six scintillator counters of the hodoscope used to disentangle muons not interacting in lead. The normal data taking provided more than 2000 μ with momentum greater than 35 GeV/c faking an electron. Other 2000 μ of that type came from special muon runs. The preliminary result of the muon catastrophic energy loss probability as a function of momentum measured using un-calibrated data from the special runs only is shown figure 2

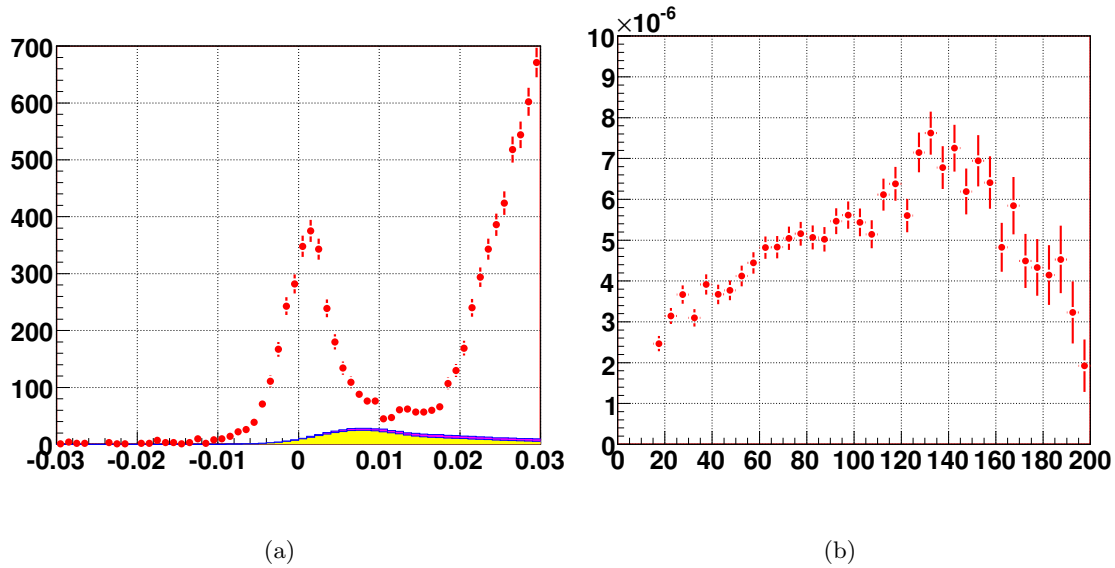


Figure 2: (a) m_{miss}^2 in GeV^4/c^2 for K_{e2} events collected during the 2007 run. The prediction for the $K_{\mu 2}$ and the $K_{e2\gamma}$ structure dependent contamination are also shown. (b) Probability that a muon releases in the liquid krypton calorimeter more than 95% of its energy as a function of muon momentum in GeV/c .

(b). It corresponds to a $K_{\mu 2}$ contamination in the K_{e2} sample of $7.5 \pm 0.1\%$. The background level, therefore, can be controlled with the requested accuracy. Special runs with the kaon beam dumped and with K^- only were also taken to study the residual accidental background in K^+ data. Finally a measurement of the electron identification efficiency on the overall K_{e2} momentum spectrum required also special runs with K_L beam, which allow the selection of a pure sample of electron through $K_L \rightarrow e^+\pi^-\nu$ decays.

The analysis of the 2007 data is already started and preliminary results are expected soon.

References

1. A. Lai *et al*, *Eur Phys. J. C* **22**, 231 (2001),
J.R. Batley *et al*, *Phys. Lett. B* **544**, 97 (2002).
2. J.R. Batley *et al*, *Eur. Phys. J. C* **52**, 875 (2007).
3. J.R. Batley *et al*, *Eur. Phys. J. C* **50**, 329 (2007) [Erratum-ibid. C **52**, 1021 (2007)].
4. V. Fanti *et al*, *Nucl. Instrum. Methods A* **574**, 433 (2007).
5. H. Leutwyler and M. Roos, *Z. Phys. C* **25**, 91 (1984).
6. W-M. Yao *et al* [Particle Data Group], *J. Phys. G* **33** 2006.
7. GEANT Detector Description and Simulation Tool, CERN Program Library Long Write-up W5013 1994.
8. E.S. Ginsberg, *Phys. Rev. D* **1**, 229 (1970).
9. E. Barberio and Z. Was, *Comput. Phys. Com.* **79** 1994,
P. Golonka and Z. Was, *Eur. Phys. J. C* **45**, 97 (2006)
10. C. Gatti, *Eur. Phys. J. C* **45**, 417 (2006)
11. A. Sher *et al*, *Phys. Rev. Lett.* **91**, 261802 (2)003.
12. V.I. Romanovsky *et al*, arXiv:0704.2052.
13. F. Ambrosino *et al*, arXiv:0707.2532.
14. F. Ambrosino *et al*, arXiv:0804.4577.
15. A. Sirlin, *Nucl. Phys. B* **196**, 83 (1982)

16. V. Cirigliano *et al*, *Eur. Phys. J. C* **35**, 53 (2004),
V. Cirigliano *et al*, *Eur. Phys. J. C* **23**, 121 (2002).
17. E. Blucher *et al*, Proceedings of the CKM 2005 Workshop (WG1), UC San Diego, 15-18 March 2005.
18. A. Czarnecki, W.J. Marciano and A. Sirlin, *Phys. Rev. D* **70**, 093006 (2004).
19. W.J. Marciano, and A. Sirlin, *Phys. Rev. Lett.* **96**, 032002 (2006).
20. V. Cirigliano and I. Rosell, *J. High Energy Phys.* **10**, 005 (2007).
21. A. Masiero, P. Paradisi and R. Petronzio, *Phys. Rev. D* **74**, 011701 (2006).
22. F. Ambrosino *et al.*, arXiv:0707.4623.
23. L. Fiorini, PoS (HEP2005) 288 2005.
24. V. Kozhuharov, PoS (KAON) 049 2007.

$\Sigma^+ \rightarrow p\mu^+\mu^-$: Standard Model or New Particle?

G. Valencia

Department of Physics, Iowa State University, Ames, IA 50011

The HyperCP collaboration observed three events for the decay $\Sigma^+ \rightarrow p\mu^+\mu^-$. They suggested that new physics may be required to understand the implied decay rate and the observed $m_{\mu\mu}$ distribution. Motivated by this result, we re-examine this mode. First within the standard model, and then assuming there is a new particle. Within the SM we find that $\Sigma^+ \rightarrow p\mu^+\mu^-$ is long-distance dominated and its rate falls within the range suggested by the HyperCP measurement. We then examine the conditions under which the observation is consistent with a light Higgs boson and find an explicit example that satisfies all the constraints: the light pseudoscalar Higgs boson in the next-to-minimal supersymmetric standard model (NMSSM).

1 Introduction

The HyperCP collaboration has observed three events for the mode $\Sigma^+ \rightarrow p\mu^+\mu^-$ ¹. A striking feature of the result is that the three events have the same muon pair invariant mass, 214.3 MeV. HyperCP estimates the probability for this clustering at 0.8% using a “form factor” distribution for the standard model expectations².

This observation invites two calculations and we report on the results in this talk. First we present the best possible prediction for the Standard Model expectation. Since there are no known particles of mass 214 MeV, we do not expect a peak at that muon pair invariant mass. However, we need to know whether the SM distribution is narrower or wider than the form used by HyperCP to assess the significance of the clustering. Even if the three events represent new physics, it is necessary to know the SM level in order to determine if HyperCP should have seen events at other values of $m_{\mu\mu}$.

The second calculation involves assuming that the observed events are indeed evidence for a new particle and confronting this observation with existing constraints from kaon and B physics. In particular we study the conditions under which the observation is consistent with a light Higgs boson and find an explicit candidate for the new particle: the lightest CP-odd Higgs boson in the NMSSM, the A_1^0 .

2 Standard Model Calculation

We first present the ingredients that enter the calculation within the SM³. The short distance contribution is too small to explain these events by four orders of magnitude, this decay is long distance dominated as is the case in similar kaon modes.

The long distance contributions to $\Sigma^+ \rightarrow p\mu^+\mu^-$ can be pictured schematically as arising from the $\Sigma^+ \rightarrow p\gamma^*$ process. There are four independent form factors allowed by electromagnetic

gauge invariance,

$$\mathcal{M}(B_i \rightarrow B_f \gamma^*) = -eG_F \bar{B}_f \left[i\sigma^{\mu\nu} q_\mu (a + b\gamma_5) + (q^2 \gamma^\nu - q^\nu \not{q})(c + d\gamma_5) \right] B_i \varepsilon_\nu. \quad (1)$$

Two of the form factors, $a(q^2)$ and $c(q^2)$, are parity conserving whereas $b(q^2)$ and $d(q^2)$ are parity violating. In addition, two of the form factors are non-zero at $q^2 = 0$ and contribute to the radiative decay $\Sigma^+ \rightarrow p\gamma$: $a(0)$ and $b(0)$. All four form factors are complex and receive imaginary parts from $N\pi$ intermediate states.

We estimate these imaginary parts by taking the weak vertex $\Sigma^+ \rightarrow N\pi$ from experiment and using the $N\pi \rightarrow p\gamma^*$ scattering at lowest order in χ PT (both conventional and heavy baryon). We check that our calculations agree with the existing ones at $q^2 = 0$.

To estimate the real part of the form factors we use $a(0)$ and $b(0)$, as determined from the width and decay distribution of the radiative decay $\Sigma \rightarrow p\gamma$ up to a discrete ambiguity. We then assume that value for the range of q^2 needed. This is consistent with our finding that the imaginary parts of the form factors are smooth and slowly varying over the q^2 range of interest. Finally, the real parts of $c(q^2)$ and $d(q^2)$ are obtained using a vector meson dominance model.

There is some uncertainty in the calculation, but the resulting range, $1.6 \times 10^{-8} \leq \mathcal{B}(\Sigma^+ \rightarrow p\mu^+\mu^-)_{SM} \leq 9.0 \times 10^{-8}$, is in good agreement with the measured rate, $\mathcal{B}(\Sigma^+ \rightarrow p\mu^+\mu^-) = (8.6_{-5.4}^{+6.6} \pm 5.5) \times 10^{-8}$ ¹. The predicted $m_{\mu\mu}$ distribution shows no peaks near 214 MeV (or elsewhere) and is slightly flatter than the form factor used by HyperCP. This leads us to conclude that the probability of having the three events at the same invariant mass is about 0.5%. Furthermore, the lower end of the range predicted for the rate is consistent with no events for HyperCP, allowing for the possibility of all three events being consistent with new physics.

3 A new Particle with mass 214 MeV?

We now turn to the interpretation of the 3 HyperCP events as a new particle¹ with $M_{P^0} = 214.3$ MeV and $\mathcal{B}(\Sigma^+ \rightarrow p\mu^+\mu^-)_{P^0} = (3.1_{-1.9}^{+2.4} \pm 1.5) \times 10^{-8}$. The observation implies that this hypothetical new light state, P^0 , is short lived, does not interact strongly, is narrow and decays only into $\mu^+\mu^-$, e^+e^- or $\gamma\gamma$, and has a $\Delta S = 1$, $\Delta I = 1/2$ coupling to $\bar{s}d$ quarks. There are three questions to be answered and we address them in order. Why hasn't it been seen before? Is there a candidate for such a state? Where else could it be observed?

3.1 Why hasn't it been seen before?

The most stringent constraint on a possible new particle P^0 is its non-observation in kaon decay. After all, the modes $K \rightarrow \pi\mu^+\mu^-$ proceed via the same quark level transition as $\Sigma^+ \rightarrow p\mu^+\mu^-$: $s \rightarrow d\mu^+\mu^-$. Of the three experiments that have studied these modes: BNL865⁴, HyperCP⁵ and NA48⁶ the one with most statistics was BNL865⁴ with 430 events, 30 of which were in their lowest bin $2m_\mu \lesssim m_{\mu\mu} \lesssim 225$ MeV where the signal would have been observed. Their observation shows no peaks in the $m_{\mu\mu}$ distribution, which is consistent with long distance SM physics. On that basis, the most optimistic scenario for the new physics hypothesis is to assume that all the 30 events in the first bin were due to P^0 which leads to a 95% confidence limit bound $\mathcal{B}(K^+ \rightarrow \pi^+ P^0) \leq 8.7 \times 10^{-9}$ ⁷ (assuming that statistical errors dominate). This translates into a rate for $\Sigma^+ \rightarrow pP^0$ some 25 times too small to explain the HyperCP events. Similar results are obtained from the other kaon experiments, none of which saw a peak in their $m_{\mu\mu}$ distribution.

Another constraint arises from the non-observation of the hypothetical new particle in $b \rightarrow s\mu^+\mu^-$. In this case both Belle and BaBar⁸ have results that can be interpreted as a 95% confidence level bound⁷ $\mathcal{B}(B \rightarrow X_s P^0) \leq 8 \times 10^{-8}$.

In Figure 1, we can see schematically how it is possible for the new state to be observed in Σ decay while not in K^+ decay: the kaon decay modes with only one pion in the final state only

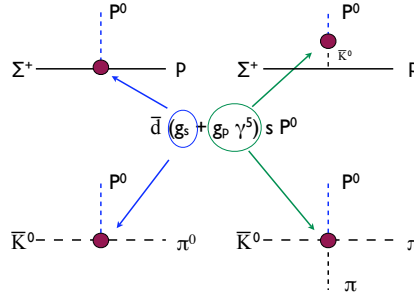


Figure 1: sd FCNC at the quark level: a scalar coupling only affects $K \rightarrow \pi P^0$ and a pseudoscalar coupling only affects $K \rightarrow \pi\pi P^0$. However, both affect $\Sigma \rightarrow pP^0$.

constrain the effective $|\Delta S| = 1$ scalar coupling of the new state whereas the Σ decay is sensitive also to the effective $|\Delta S| = 1$ pseudoscalar coupling. Any viable model for P^0 will then have an effective scalar coupling about 25 times smaller than the corresponding pseudoscalar coupling⁹.

In a similar manner, the constraints from B decay require that the effective bs coupling of P^0 be about an order of magnitude smaller than the corresponding sd coupling scaled by m_b/m_s and $(V_{ts}V_{tb}^*)/(V_{ts}V_{td}^*)$. The latter scaling is the appropriate one for one-loop Higgs penguins dominated by a top-quark and a W boson in the intermediate state. A successful model for P^0 can not have these penguin diagrams dominating the effective FCNC of P^0 to down-type quarks.

We have also considered additional processes that can, in principle, constrain the interactions of the hypothetical P^0 . $K - \bar{K}$ mixing allows an effective pseudoscalar coupling up to 50 times as large as required to explain the 3 HyperCP events. $K_L \rightarrow \mu^+\mu^-$ combined with the muon $g - 2$ allow an effective pseudoscalar coupling as large as required. The muon $g - 2$ allows a P^0 coupling to muons $g_{P\mu} \lesssim 5 \times 10^{-4}$ which interestingly is about m_μ/v ^{9,10}.

3.2 Is there a candidate for P^0 ?

The possibility that P^0 is a light sgoldstino has been explored to some extent in the literature¹¹. Here, we pursue the possibility that P^0 is a light Higgs boson. For detailed phenomenology of kaon and hyperon decays involving a light Higgs particle it is necessary to recall that there are two types of contributions that are generally of similar size⁷. There are two-quark ‘‘Higgs penguin’’ contributions that arise at one loop order and depend on the details of the flavor changing sector of the model. There are also ‘‘four-quark’’ contributions arising from a tree-level, SM W mediated $|\Delta S| = 1$ decay, in which the light Higgs is radiated from any of the u, d, s quarks or the W boson via the tree-level flavor diagonal couplings of the Higgs. Both of these contributions can be calculated in chiral perturbation theory¹², and we do so at leading order. Given our discussion in the previous section we concentrate on CP-odd or pseudoscalar Higgs bosons.

One possible candidate for P^0 is the A_1^0 of the NMSSM. The Higgs sector of the NMSSM contains the usual two Higgs doublets H_D and H_U that appear in the MSSM plus the Higgs singlet N . In the physical spectrum there are two CP-odd scalars, of which the A_1^0 is the lightest. It has been proposed in the literature that this A_1^0 can be naturally light due to a global $U(1)$ symmetry¹³.

The main features of the couplings of the A_1^0 to SM fields are as follows. Its coupling to Zh (h being the lightest CP even Higgs) is suppressed by $\tan\beta$ with respect to the MSSM ZhA coupling allowing an evasion of LEP bounds in the large $\tan\beta$ regime. Its couplings to quarks are also suppressed by $\tan\beta$ with respect to those of the A in the MSSM. This results, for large $\tan\beta$, in negligible couplings to up-type quarks. The couplings to down-type quarks are

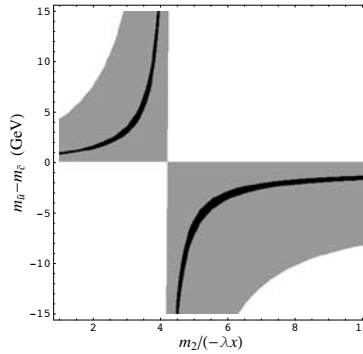


Figure 2: Parameter space for $m_{\tilde{u}} - m_{\tilde{c}}$ and $m_2/(-\lambda x)$ where A_1^0 can explain the HyperCP events (gray regions) and simultaneously satisfy the kaon bounds (black regions). The horizontal axis corresponds to parameters in the chargino mass matrix.

independent of $\tan\beta$ and can be written in terms of one parameter, l_d , which can be of order one¹⁴: $\mathcal{L} = -l_d m_d \bar{d} \gamma_5 d (iA_1^0)/v - l_d m_\ell \bar{\ell} \gamma_5 \ell (iA_1^0)/v + \dots$

The four-quark contributions to A_1^0 production in light meson and hyperon decay are thus proportional to l_d and independent of other parameters in the model. It is then straightforward to compute these contributions to the HyperCP case. We find¹⁵, $\mathcal{B}_{4q}(\Sigma^+ \rightarrow p A_1^0) = 1.7 \times 10^{-7} |l_d|^2$, which matches the central value of the HyperCP result for $l_d \sim 0.4$. The bad news is that this then leads to $\mathcal{B}_{4q}(K^+ \rightarrow \pi^+ A_1^0) \sim 10^{-6}$, two orders of magnitude larger than the limit from BNL E865. The conclusion illustrated by this calculation is that it is relatively easy to have a light Higgs that matches the HyperCP observation but it is very hard to avoid seeing it in kaon decay as well.

However, there are also the two-quark contributions to the amplitudes and it is possible to arrange a cancellation between amplitudes that satisfies the kaon bounds. The two-quark contributions are much more model dependent than the four-quark contributions, but also suffer from additional constraints due to non-observation of P^0 in B decay. We have not performed a full parameter scan, but rather illustrated that it is possible to satisfy all constraints. To this effect we start with the specific model considered by Hiller¹⁴ and modify it accordingly. To suppress the FCNC in B decay we consider $m_{\tilde{t}} = m_{\tilde{c}}$ and negligible squark mixing. The strength of the two-quark contribution to kaon decay is then tuned with $m_{\tilde{u}} - m_{\tilde{c}}$. We further consider (large) $\tan\beta = 30$, $m_{\tilde{t}} \sim 2.5$ TeV and $-\lambda x = 150$ GeV to obtain neutralino masses in the 100-1500 GeV range¹⁵. In Figure 2 we show our results¹⁵: the light shaded region corresponds to parameters that reproduce the HyperCP observation. The dark shaded region corresponds to those points that also satisfy the kaon bounds. As mentioned before the overlapping region is significantly smaller due to the cancellation required to satisfy the kaon bounds.

3.3 Where else can P^0 be observed?

Finally, we explore other processes that can test the new particle hypothesis for the HyperCP result. We begin by considering only the effect of two-quark operators, assuming that the existing kaon bounds are bypassed because the effective sd coupling is pseudoscalar. In this case the new state would show up in kaon decay modes with two pions in the final state and we can easily derive from the HyperCP measurement that (the errors reflect the experimental error only)⁹

$$\begin{aligned} \mathcal{B}(K_L \rightarrow \pi^+ \pi^- P^0) &\approx (1.8_{-1.4}^{+1.6}) \times 10^{-9} \\ \mathcal{B}(K_L \rightarrow \pi^0 \pi^0 P^0) &\approx (8.3_{-6.6}^{+7.5}) \times 10^{-9}. \end{aligned} \quad (2)$$

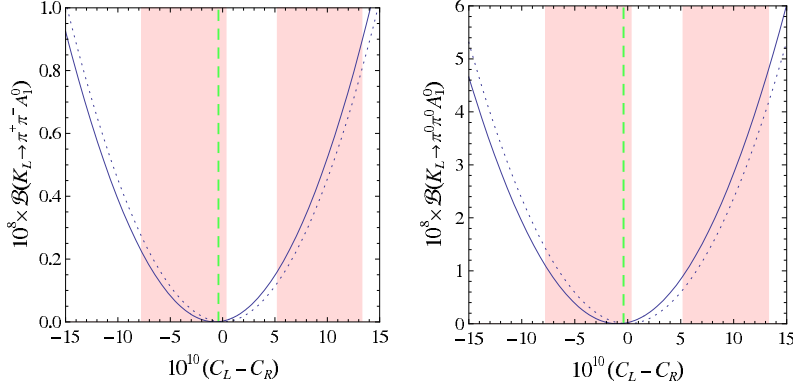


Figure 3: Predicted branching ratios (solid curves) for $K_L \rightarrow \pi^+ \pi^- A_1^0$ and $K_L \rightarrow \pi^0 \pi^0 A_1^0$ with $l_d = 0.35$. The horizontal axis corresponds to the size of g_P .

Both of these represent very significant enhancements over the corresponding SM rates and may be accessible to KTeV or NA48. In a similar manner this scenario results in^{9,7}

$$\mathcal{B}(\Omega^- \rightarrow \Xi^- P^0) \approx (2.0_{-1.2}^{+1.6}) \times 10^{-6}. \quad (3)$$

The best upper bound for this mode, also from HyperCP¹⁶, is 6.1×10^{-6} .

If the new state P^0 is a light Higgs, then there are other processes that are sensitive only to its flavor diagonal couplings¹⁹ (or four-quark operators). For example the modes $V \rightarrow \gamma A_1^0$ have been proposed in the literature¹⁷. The results are that $\mathcal{B}(\Upsilon_{1S} \rightarrow \gamma A_1^0)$ can reach about $1 \times 10^{-4} l_d^2$ and may be accessible to the B factories. Similarly $\mathcal{B}(\phi \rightarrow \gamma A_1^0)$ can reach $1.4 \times 10^{-8} l_d^2$ and may be accessible to DAΦNE¹⁷. In a similar spirit we have proposed the modes $\eta \rightarrow \pi \pi A_1^0$ where we can predict¹⁸ $\mathcal{B}(\eta \rightarrow \pi^+ \pi^- A_1^0) = 5.4 \times 10^{-7} l_d^2$, again possibly accessible to DAΦNE.

When the four-quark contributions are added to the two-quark contributions in the NMSSM (using parameters as in Hiller¹⁴ and Xiandong²⁰) the results of Eq. 2 are modified. An example of the resulting predictions for the rate of the kaon modes is shown in Fig. 3. Full details can be found in the paper¹⁸, but the x -axis is related to the strength of the two-quark contribution though an effective g_P and the strength of the four-quark contribution is kept fixed. The dotted curves result from the two-quark contributions alone. The shaded (pink) bands indicate the allowed ranges of $C_L - C_R$ when the two and four-quark contributions have the same sign¹⁸. Each vertical (green) dashed line corresponds to the special case¹⁵ of chargino dominated penguins.

4 Conclusions

The decay $\Sigma^+ \rightarrow p \mu^+ \mu^-$ within the SM is long distance dominated and the predicted rate is in the right range to explain the HyperCP observation. However, the predicted $m_{\mu\mu}$ distribution makes it unlikely to find the three events at the same mass ($P \lesssim 0.8\%$). Existing constraints from kaon and B physics allow a new particle interpretation of the HyperCP result provided that the FCNC couplings of the new particle are mostly pseudoscalar and smaller for $b \rightarrow s$ transitions than naive scaling with CKM angles would predict.

The NMSSM has a CP-odd Higgs boson, the A_1^0 that could be as light as the required 214 MeV. Its diagonal couplings to quarks and muons in the large $\tan\beta$ limit can have the right size as well. There are several modes that can test this hypothesis independently from the details of the flavor changing sector of the model: $\Upsilon_{1S} \rightarrow \gamma A_1^0$, $\phi \rightarrow \gamma A_1^0$ and $\eta \rightarrow \pi \pi A_1^0$.

It is harder to suppress the effective scalar sd coupling that appears in this model to the level required to satisfy the existing kaon bounds, but it is possible for certain values of the relevant

parameters. The measurement of one of the modes $K_L \rightarrow \pi\pi\mu^+\mu^-$ can confirm or refute this scenario.

Acknowledgments

This work was done in collaboration with Jusak Tandean and Xiao-Gang He. It was supported in part by DOE under contract number DE-FG02-01ER41155.

References

1. H. Park *et al.* [HyperCP Collaboration], Phys. Rev. Lett. **94**, 021801 (2005) [arXiv:hep-ex/0501014].
2. L. Bergstrom, R. Safadi, and P. Singer, Z. Phys. C **37**, 281 (1988).
3. X.G. He, J. Tandean, and G. Valencia, Phys. Rev. D **72**, 074003 (2005) [arXiv:hep-ph/0506067].
4. H. Ma *et al.* [E865 Collaboration], Phys. Rev. Lett. **84**, 2580 (2000) [arXiv:hep-ex/9910047].
5. H.K. Park *et al.* [HyperCP Collaboration], *ibid.* **88**, 111801 (2002) [arXiv:hep-ex/0110033].
6. J.R. Batley *et al.* [NA48/1 Collaboration], Phys. Lett. B **599**, 197 (2004) [arXiv:hep-ex/0409011].
7. X.G. He, J. Tandean, and G. Valencia, Phys. Rev. D **74**, 115015 (2006) [arXiv:hep-ph/0610274], and references therein.
8. B. Aubert *et al.* [BABAR Collaboration], Phys. Rev. Lett. **93**, 081802 (2004) [arXiv:hep-ex/0404006]; M. Iwasaki *et al.* [Belle Collaboration], Phys. Rev. D **72**, 092005 (2005) [arXiv:hep-ex/0503044].
9. X.G. He, J. Tandean, and G. Valencia, Phys. Lett. B **631**, 100 (2005) [arXiv:hep-ph/0509041].
10. Other studies leading to some of the conclusions in this section are: N.G. Deshpande, G. Eilam, and J. Jiang, Phys. Lett. B **632**, 212 (2006) [arXiv:hep-ph/0509081]. C.Q. Geng and Y.K. Hsiao, Phys. Lett. B **632**, 215 (2006) [arXiv:hep-ph/0509175], C.H. Chen and C.Q. Geng, Phys. Lett. B **645**, 189 (2007) [arXiv:hep-ph/0612142];
11. D.S. Gorbunov and V.A. Rubakov, Phys. Rev. D **73**, 035002 (2006) [arXiv:hep-ph/0509147]; S.V. Demidov and D.S. Gorbunov, JETP Lett. **84**, 479 (2007) [arXiv:hep-ph/0610066].
12. See for example, J.F. Gunion, H.E. Haber, G.L. Kane, and S. Dawson, SCIPP-89/13, and references therein. In particular, also B. Grzadkowski and J. Pawelczyk, Phys. Lett. B **300**, 387 (1993).
13. B.A. Dobrescu and K.T. Matchev, JHEP **0009**, 031 (2000) [arXiv:hep-ph/0008192].
14. G. Hiller, Phys. Rev. D **70**, 034018 (2004) [arXiv:hep-ph/0404220].
15. X.G. He, J. Tandean, and G. Valencia, Phys. Rev. Lett. **98**, 081802 (2007) [arXiv:hep-ph/0610362].
16. N. Solomey, DPF 5-8 April 2003, Philadelphia, Pennsylvania, USA.
17. M.L. Mangano and P. Nason, Mod. Phys. Lett. A **22**, 1373 (2007) [arXiv:0704.1719 [hep-ph]].
18. X. G. He, J. Tandean and G. Valencia, arXiv:0803.4330 [hep-ph].
19. J. Prades and A. Pich, Phys. Lett. B **245**, 117 (1990).
20. G. Xiangdong, C.S. Li, Z. Li, and H. Zhang, arXiv:0712.0257 [hep-ph].

MEASUREMENTS FROM KTeV OF RARE DECAYS OF THE K_L^0 AND π^0

E. D. ZIMMERMAN
University of Colorado
Boulder, Colorado 80302 USA

The KTeV collaboration at Fermi National Accelerator Laboratory has recently completed searches for and measurements of several decay modes of the neutral kaon and pion. These include new searches for lepton flavor violating decays (which have not been seen), and a new study of the parity properties of the decay $\pi^0 \rightarrow e^+e^-e^+e^-$.

1 The KTeV Detector

Fermilab's KTeV detector (Fig. 1) was constructed for Experiments 799 and 832. The two experiments were designed to concentrate on different aspects of neutral kaon physics: E799 on rare decays of the K_L and E832 on measurement of $\text{Re}(\epsilon'/\epsilon)$. A primary proton beam with energy 800 GeV struck a BeO target at a targeting angle of 4.8 mrad, and collimation and sweeping magnets produced two parallel neutral hadron beams. The beams entered a 60 m long vacuum decay region, which ended at a Mylar-Kevlar vacuum window. Decay products were tracked with a series of drift chambers surrounding a dipole analysis magnet. Downstream of the drift chambers were a series of transition radiation detectors (TRD) (in E799 only) and a pure CsI electromagnetic calorimeter, an active hadron beam absorber, and a set of muon detectors behind steel shielding. Photon veto detectors surrounded the fiducial volume in the transverse directions. The detector is described in more detail in Ref. ¹.

2 The decay $\pi^0 \rightarrow e^+e^-e^+e^-$ and the parity of the π^0

The neutral pion's parity has historically been studied in two ways: indirectly via the cross-section of π^- capture on deuterons^{2,3}, or directly via the double Dalitz decay $\pi^0 \rightarrow e^+e^-e^+e^-$ ⁴. While both sets of results are consistent with the negative parity, the direct measurement has only 3.6 σ significance. KTeV has now reported results⁵ that conclusively confirm the negative π^0

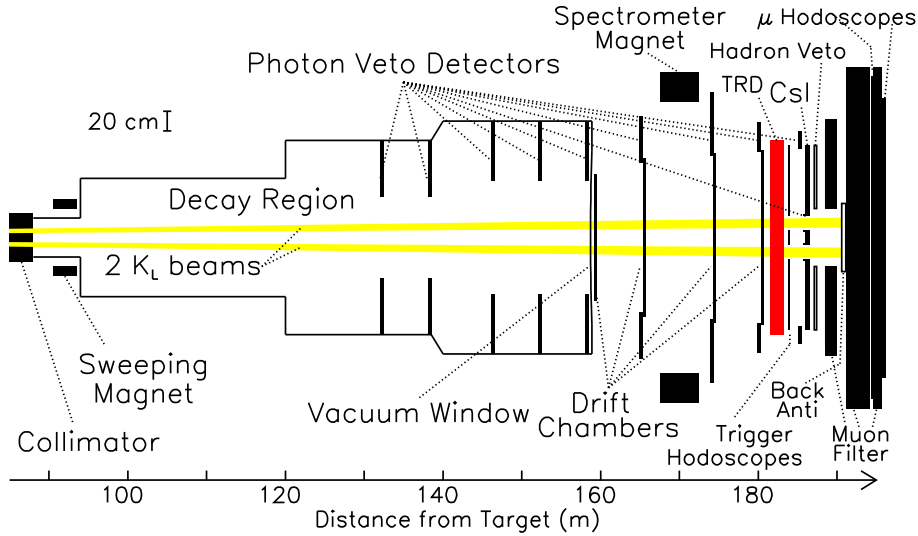
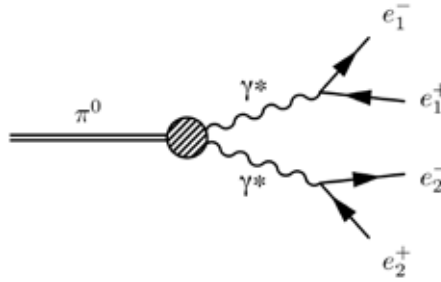


Figure 1: The KTeV spectrometer as configured for E799.


 Figure 2: Lowest order Feynman diagram for $\pi^0 \rightarrow e^+e^-e^+e^-$. The direct contribution is shown; a second diagram exists with e_1^+ and e_2^+ exchanged.

parity as well as the first-ever searches for parity and CPT violation, and the first measurements of the electromagnetic form factor, in this mode.

The $\pi^0 \rightarrow e^+e^-e^+e^-$ decay proceeds through a two-photon intermediate state (Fig. 2). The most general interaction Lagrangian for the $\pi^0 \rightarrow \gamma^*\gamma^*$ transition can be written⁶:

$$\mathcal{L} \propto C_{\mu\nu\rho\sigma} F^{\mu\nu} F^{\rho\sigma} \Phi \quad (1)$$

where $F^{\mu\nu}$ and $F^{\rho\sigma}$ are the photon fields, Φ is the pion field, and the coupling has the form

$$C_{\mu\nu\rho\sigma} \propto f(x_1, x_2) [\cos \zeta \epsilon_{\mu\nu\rho\sigma} + \sin \zeta e^{i\delta} (g_{\mu\rho} g_{\nu\sigma} - g_{\mu\sigma} g_{\nu\rho})]. \quad (2)$$

The first term in $C_{\mu\nu\rho\sigma}$ is the expected pseudoscalar coupling and the second term introduces a scalar coupling with a mixing angle ζ and a phase difference δ . Nuclear parity violation would introduce a nonzero ζ , while CPT violation would cause the phase δ to be nonzero. We assume the standard parity-conserving form for the $\gamma^* \rightarrow e^+e^-$ conversion.

The form factor $f(x_1, x_2)$ is expressed in terms of the momentum transfer of each of the virtual photons, or equivalently the invariant masses of the two Dalitz pairs: $x_1 \equiv (m_{e_1^+e_1^-}/M_{\pi^0})^2$; $x_2 \equiv (m_{e_2^+e_2^-}/M_{\pi^0})^2$. In calculating the phase space variables for an individual event, there is an intrinsic ambiguity in assigning each electron to a positron to form a Dalitz pair. KTeV's analysis uses a matrix element model that includes the exchange diagrams and therefore avoids

the need to enforce a pairing choice. The form factor is parametrized using a model based on that of D'Ambrosio, Isidori, and Portolés (DIP)⁷, but with an additional constraint that ensures the coupling vanishes at large momenta⁸. In terms of the remaining free parameters, the form factor is:

$$f_{\text{DIP}}(x_1, x_2; \alpha) = \frac{1 - \mu(1 + \alpha)(x_1 + x_2)}{(1 - \mu x_1)(1 - \mu x_2)}, \quad (3)$$

where $\mu = M_{\pi^0}^2/M_\rho^2 \approx 0.032$.

The parity properties of the decay can be extracted from the angle ϕ between the planes of the two Dalitz pairs in Fig. 2, where pair 1 is defined as having the smaller invariant mass. The distribution of this angle from the dominant direct contribution has the form $d\Gamma/d\phi \sim 1 - A \cos(2\phi) + B \sin(2\phi)$, where $A \approx 0.2 \cos(2\zeta)$ and $B \approx 0.2 \sin(2\zeta) \cos \delta$. A pure pseudoscalar coupling, therefore, would produce a negative $\cos(2\phi)$ dependence.

The branching ratio measurement, which we describe here first, makes use of a normalization mode in which two pions decay via $\pi^0 \rightarrow e^+e^-\gamma$ and the third $\pi^0 \rightarrow \gamma\gamma$. This ‘‘double single-Dalitz’’ mode, denoted $K_L \rightarrow \pi^0 \pi_D^0 \pi_D^0$ where π_D^0 refers to $\pi^0 \rightarrow e^+e^-\gamma$, has the same final state particles as the signal mode. Both modes are fully reconstructed in the detector and the total invariant mass is required to match the kaon's. The two modes are distinguished by a χ^2 formed of the three reconstructed π^0 masses. This serves to identify the best pairing of particles for a given decay hypothesis, as well as to select the more likely hypothesis of the two. The similarity of these modes allows cancellation of most detector-related systematic effects in the branching ratio measurement, but also allows each mode to be a background to the other.

Radiative corrections complicate the definition of the Dalitz decays in general. We define the signal mode $\pi^0 \rightarrow e^+e^-e^+e^-$ to be inclusive of radiative final states where the squared ratio of the invariant mass of the four electrons to the neutral pion mass $x_{4e} \equiv (M_{4e}/M_{\pi^0})^2$ is greater than 0.9, while events with $x_{4e} < 0.9$ (approximately 6% of the total rate) are treated as $\pi^0 \rightarrow e^+e^-e^+e^-\gamma$. For normalization, the decay $\pi^0 \rightarrow e^+e^-\gamma$ is understood to include all radiative final states, for consistency with previous measurements of this decay⁹. Radiative corrections in this analysis are taken from an analytic calculation to order $\mathcal{O}(\alpha^2)$ ⁶.

Radiative corrections complicate the definition of the Dalitz decays in general. The signal mode $\pi^0 \rightarrow e^+e^-e^+e^-$ is defined to be inclusive of radiative final states where the squared ratio of the invariant mass of the four electrons to the neutral pion mass $x_{4e} \equiv (M_{4e}/M_{\pi^0})^2$ is greater than 0.9, while events with $x_{4e} < 0.9$ (approximately 6% of the total rate) are treated as $\pi^0 \rightarrow e^+e^-e^+e^-\gamma$. Radiative corrections in this analysis are taken from an analytic calculation to order $\mathcal{O}(\alpha^2)$ ⁶.

The final event sample contains 30 511 signal candidates with 0.6% residual background and 141 251 normalization mode candidates with 0.5% background (determined from the Monte Carlo simulation). The background in the signal sample is dominated by mistagged events from the normalization mode. v KTeV finds the following the ratio of decay rates:

$$\frac{B_{eeee}^{x>0.9} \cdot B_{\gamma\gamma}}{B_{ee\gamma}^2} = 0.2245 \pm 0.0014(\text{stat}) \pm 0.0009(\text{syst}). \quad (4)$$

The $\pi^0 \rightarrow e^+e^-e^+e^-$ branching ratio can be calculated from the double ratio using the known values $B_{\gamma\gamma} = 0.9980 \pm 0.0003$ and $B_{ee\gamma} = (1.198 \pm 0.032) \times 10^{-2}$ ¹⁰. This yields $B_{eeee}^{x>0.9} = (3.26 \pm 0.18) \times 10^{-5}$, where the error is dominated by the uncertainty in the $\pi^0 \rightarrow e^+e^-\gamma$ branching ratio. KTeV uses the radiative corrections model⁶ to extrapolate to all radiative final states, finding:

$$\frac{B_{eeee(\gamma)} \cdot B_{\gamma\gamma}}{B_{ee\gamma}^2} = 0.2383 \pm 0.0015(\text{stat}) \pm 0.0010(\text{syst}), \quad (5)$$

and $B_{eeee(\gamma)} = (3.46 \pm 0.19) \times 10^{-5}$. This branching ratio result is in good agreement with previous measurements⁴.

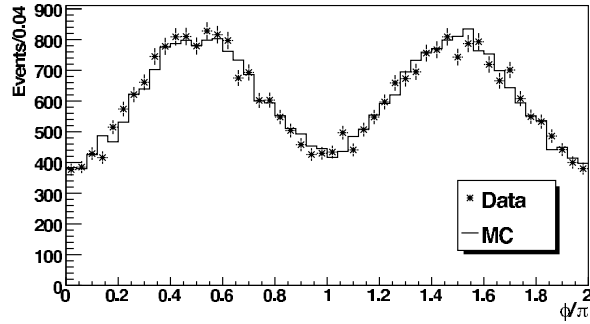


Figure 3: Distribution of the angle ϕ , in units of π , between the planes of the two e^+e^- pairs for $\pi^0 \rightarrow e^+e^-e^+e^-$ candidate decays. The solid histogram shows the Monte Carlo expectation for negative parity.

The parameters of the $\pi^0\gamma^*\gamma^*$ coupling are found by maximizing an unbinned likelihood function composed of the differential decay rate in terms of ten phase-space variables. The first five are $(x_1, x_2, y_1, y_2, \phi)$, where x_1, x_2 , and ϕ are described above and the remaining variables y_1 and y_2 describe the energy asymmetry between the electrons in each Dalitz pair in the π^0 center of mass⁶. The remaining five are the same variables, but calculated with the opposite choice of e^+e^- pairings. The likelihood is calculated from the full matrix element including the exchange diagrams and $\mathcal{O}(\alpha^2)$ radiative corrections.

The fit yields the DIP α parameter and the (complex) ratio of the scalar to the pseudoscalar coupling. For reasons of fit performance, the parity properties are fit to the equivalent parameters κ and η , where $\kappa + i\eta \equiv \tan \zeta e^{i\delta}$. The shape of the minimum of the likelihood function indicates that the three parameters α, κ , and η are uncorrelated. Acceptance-dependent effects are included as a normalization factor calculated from Monte Carlo simulations.

Systematic error sources on α and κ are similar to those for the branching ratio measurement. The dominant systematic error is due to variation of cuts, resulting in a total systematic error of 0.9 and 0.011 on α and κ respectively. For the η parameter, the primary uncertainty results from the resolution on the angle ϕ between the two lepton pairs. This behavior was studied with Monte Carlo simulation and a correction was calculated. The uncertainty on this correction results in a systematic error of 0.031.

The ϕ distribution is shown in Fig. 3. For plotting the data a unique pairing of the four electrons is chosen such that $x_1 < x_2$ and the product x_1x_2 is minimized: this choice represents the dominant contribution to the matrix element. It is clear that the pseudoscalar coupling dominates, as expected, with no evidence for a scalar component. The distributions of all five phase space variables agree well with the Monte Carlo simulation.

The parameters κ and η are transformed into limits on the pseudoscalar-scalar mixing angle ζ under two hypotheses. If CPT violation is allowed, then the limit is set by the uncertainties in η , resulting in $\zeta < 6.9^\circ$ at the 90% confidence level. If instead, CPT conservation is enforced, η must be zero, and the limit derives from the uncertainties on κ , resulting in $\zeta < 1.9^\circ$, at the same confidence level. These limits on ζ limit the magnitude of the scalar component of the decay amplitude, relative to the pseudoscalar component, to less than 12.1% in the presence of CPT violation, and less than 3.3% if CPT is assumed conserved. The limits on scalar contributions apply to all π^0 decays with two-photon intermediate or final states.

This analysis confirms the negative parity of the neutral pion with much higher statistical significance than the previous result, and places tight limits on nonstandard scalar and CPT -violating contributions to the $\pi^0 \rightarrow e^+e^-e^+e^-$ decay.

3 Lepton Flavor Violation

Lepton Flavor Violation (LFV) in weak decays is a key signature of several beyond-Standard Model physics scenarios. Supersymmetry¹¹, new massive gauge bosons^{12,13}, and technicolor¹⁴ all can lead to LFV decays which might be within reach of current experiments. Searches in K_L decays are complementary to searches in the charged lepton sector, since K_L decays probe the $s \rightarrow d\mu e$ transition¹². KTeV-E799 has searched for the decays $K_L \rightarrow \pi^0 \mu^\pm e^\mp$ and $\pi^0 \rightarrow \mu^\pm e^\mp$, and has made the first reported search for $K_L \rightarrow \pi^0 \pi^0 \mu^\pm e^\mp$ ¹⁵.

In each case, the analysis required two charged tracks, one of which was identified as a muon and the other an electron. The key detector elements for particle identification were E/p in the CsI calorimeter, response of the TRD, and muon hodoscopes downstream of the muon filter steel. Clusters in the CsI with no tracks pointing to them were considered photons.

3.1 $K_L \rightarrow \pi^0 \mu^\pm e^\mp$

The dominant background for $K_L \rightarrow \pi^0 \mu^\pm e^\mp$ was the decay $K_L \rightarrow \pi^\pm e^\mp \nu_e$ (K_{e3}), with a π^\pm decay or punch through to the muon hodoscopes, accompanied by two accidental photons faking a π^0 . Since accidental photons were often accompanied by other accidental activity, we removed events with evidence of additional in-time activity in the detector. Additionally, the two photons were required to form a good π^0 mass, and the square of the π^0 momentum in the K_L rest frame was required to be positive and therefore physical.

The signal and control regions were defined using a likelihood variable \mathbf{L} derived from p_t^2 , the sum of the momentum components of all final-state particles perpendicular to the kaon flight line, and $M_{\pi^0 \mu e}$, the invariant mass of the $\pi^0 \mu e$ system. The signal (control) region was defined by a cut on \mathbf{L} chosen to retain 95% (99%) of signal Monte Carlo events after all other cuts. Expected background levels were 0.66 ± 0.23 events in the signal region and 4.21 ± 0.53 events in the control region. Both the signal and control regions were blind during the analysis. Figure 4 shows the $p_t^2 - M_{\pi^0 \mu e}$ plane after all cuts: five events were found in the control region and zero in the signal. The resulting limit is $B(K_L \rightarrow \pi^0 \mu^\pm e^\mp) < 7.56 \times 10^{-11}$ at 90% CL, a factor of 82 improvement over the previous best limit for this mode.¹⁶

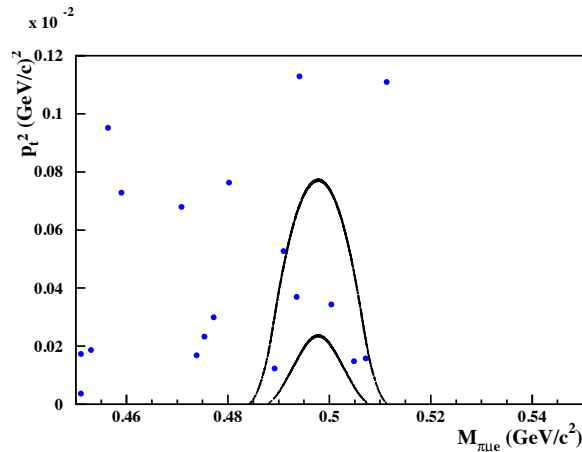


Figure 4: Surviving events in the $p_t^2 - M_{\pi^0 \mu e}$ plane for the $K_L \rightarrow \pi^0 \mu^\pm e^\mp$ search data. The signal and control regions are shown as the inner and outer solid contours.

3.2 Other lepton flavor violating modes

KTeV has also searched for the decay $K_L \rightarrow \pi^0 \pi^0 \mu^\pm e^\mp$. Reconstructing a second π^0 greatly reduces the backgrounds, so some particle identification and anti-accidental cuts were relaxed to improve the signal acceptance. A similar analysis, including a cut on a kinematic likelihood variable, yielded no events in either the control region or the signal region. This resulted in a limit $B(K_L \rightarrow \pi^0 \pi^0 \mu^\pm e^\mp) < 1.64 \times 10^{-10}$. This is the first limit reported for this decay.

The decay chain $K_L \rightarrow \pi^0 \pi^0 \pi^0$, $\pi^0 \rightarrow \mu^\pm e^\mp$ gives the same final state particles as $K_L \rightarrow \pi^0 \pi^0 \mu^\pm e^\mp$, and therefore the same analysis procedure applies with the additional requirement that the invariant mass $M_{\mu e} \approx M_{\pi^0}$. Since no events were found, the limit is $B(\pi^0 \rightarrow \mu^\pm e^\mp) < 3.59 \times 10^{-10}$. This limit on $\pi^0 \rightarrow \mu^\pm e^\mp$ is equally sensitive to both charge modes, while the previous best limits were not¹⁷. Assuming equal contributions from both charge combinations, KTeV's result is about a factor of two better than the previous best limit on $\pi^0 \rightarrow \mu^+ e^-$ and about a factor of 10 greater than the previous best limit on $\pi^0 \rightarrow \mu^- e^+$.

4 Conclusion

KTeV has completed several measurements recently on the decays of neutral K and π mesons. The measurement of $\pi^0 \rightarrow e^+ e^- e^+ e^-$ represents the best direct determination of the parity of the π^0 and the first searches for nonstandard parity and CPT violation in this mode. It also yields the best branching ratio and the first measurement of the form factor in this mode. The limits on lepton flavor violation are now the most stringent in the world for these decay modes.

Acknowledgments

KTeV acknowledges the support and effort of the Fermilab staff and the technical staffs of the institutions. This work was supported in part by the U.S. DOE, NSF, Ministry of Education and Science of Japan, Fundao de Amparo a Pesquisa do Estado de S Paulo-FAPESP, Conselho Nacional de Desenvolvimento Cientifico e Tecnologico-CNPq and CAPES-Ministerio Educao.

References

1. E. Abouzaid *et al.*, *Phys. Rev. D* **75**, 012004 (2007).
2. W. K. H. Panofsky, R. L. Aamodt, and J. Hadley, *Phys. Rev.* **81**, 565 (1951).
3. W. Chinowsky and J. Steinberger, *Phys. Rev.* **95**, 1561 (1954).
4. N. Samios *et al.*, *Phys. Rev.* **126**, 1844 (1962).
5. E. Abouzaid *et al.*, *Phys. Rev. Lett.* **100**, 182001 (2008).
6. A. R. Barker, H. Huang, P. A. Toale, and J. Engle, *Phys. Rev. D* **67**, 033008 (2003).
7. G. D'Ambrosio, G. Isidori, and J. Portolés, *PLB* **423**, 385 (1998).
8. P. A. Toale, PhD Thesis, The University of Colorado at Boulder (2004).
9. M. A. Schardt *et al.*, *PRD* **23**, 639 (1981).
10. W.-M. Yao *et al.*, *J. Phys. G* **33** 1 (2006).
11. A. Belyaev *et al.*, *Eur. Phys. J.* **C22**, 715 (2002).
12. L. G. Landsberg, *Phys. Atom. Nuc.* **68**, 1190 (2005).
13. R. N. Cahn and H. Harari, *Nuc. Phys.* **B176**, 135 (1980).
14. S. Dimopoulos and J. Ellis, *Nucl. Phys.* **B182**, 505 (1981); T. Appelquist, N. Christensen, M. Piai, and R. Shrock, *Phys. Rev* **D70**, 093010 (2004).
15. E. Abouzaid *et al.*, *PRL* **100**, 131803 (2008)
16. K. Arisaka *et al.*, *Phys. Lett* **B432**, 230 (1998).
17. R. Appel *et al.*, *Phys. Rev. Lett.* **85**, 2450 (2000); *Phys. Rev. Lett.* **85**, 2877 (2000).

Recent results from KLOE

Marianna Testa for the KLOE Collaboration^a
INFN-LNF, Via E. Fermi 40,
I-00044 Frascati, Italy

In this report I will present the recent results on K mesons from the KLOE experiment at the DAFNE e^+e^- collider working at the center of mass energy $\sim 1\text{GeV} \sim m_\phi$. They include V_{us} determinations, the test on the unitarity of the first row of the CKM matrix and the related experimental measurements. Tests of lepton universality from leptonic and semileptonic decays will be also discussed. Then I will present tests of quantum coherence, CPT and Lorentz symmetry performed by studying the time evolution of the neutral kaon system.

1 The KLOE experiment

The KLOE detector operates at DAΦNE, an e^+e^- collider working at the center of mass energy $W \sim m_\phi \sim 1.02\text{ GeV}$. The ϕ mesons are produced essentially at rest and decay to $K_S K_L$ ($K^+ K^-$) $\sim 34\%$ ($\sim 49\%$) of the times. The K mesons are produced in a pure $J^{PC} = 1^{--}$ coherent quantum state, so that observation of a K_S (K^+) in an event signals (tags) the presence of a K_L (K^-) and vice-versa: highly pure, almost monochromatic, back-to-back K_S (K^+) and K_L (K^-) beams can be obtained. Moreover K_S and K_L are distinguishable on the basis of their decay length: $\lambda_S \sim 0.6\text{ cm}$ and $\lambda_L \sim 340\text{ cm}$.

^aF. Ambrosino, A. Antonelli, M. Antonelli, F. Archilli, C. Bacci, P. Beltrame, G. Bencivenni, S. Bertolucci, C. Bini, C. Bloise, S. Bocchetta, F. Bossi, P. Branchini, R. Caloi, P. Campana G. Capon, T. Capussela, F. Ceradini, F. Cesario, S. Chi, G. Chiefari, P. Ciambrone, F. Crucianelli, E. De Lucia, A. De Santis, P. De Simone, G. De Zorzi, A. Denig, A. Di Domenico, C. Di Donato, B. Di Micco, A. Doria, M. Dreucci, G. Felici, A. Ferrari, M. L. Ferrer, S. Fiore, C. Forti, P. Franzini, C. Gatti, P. Gauzzi, S. Giovannella, E. Gorini, E. Graziani, W. Kluge, V. Kulikov, F. Lacava, G. Lanfranchi, J. Lee-Franzini, D. Leone, M. Martemianov, M. Martini, P. Massarotti, W. Mei, S. Meola, S. Miscetti, M. Moulson, S. Müller, F. Murtas, M. Napolitano, F. Nguyen, M. Palutan, E. Pasqualucci, A. Passeri, V. Patera, F. Perfetto, M. Primavera, P. Santangelo, G. Saracino, B. Sciascia, A. Sciubba, A. Sibidanov, T. Spadaro, M. Testa, L. Tortora, P. Valente, G. Venanzoni, R. Versaci, G. Xu.

The KLOE detector consists essentially of a drift chamber (DC), surrounded by an electromagnetic calorimeter (EMC). The DC¹ is a cylinder of 4 m diameter and 3.3 m in length which constitutes a large fiducial volume for K_L decays ($\sim 1/2$ of λ_L). The momentum resolution for tracks at large polar angle is $\sigma_p/p \leq 0.4\%$. The EMC² is a lead-scintillating fiber calorimeter consisting of a barrel and two endcaps, which cover 98% of the solid angle. The energy resolution is $\sigma_E/E \sim 5.7\%/\sqrt{E(\text{GeV})}$. The intrinsic time resolution is $\sigma_T = 54\text{ps}/\sqrt{E(\text{GeV})} \oplus 50\text{ps}$. A superconducting coil surrounding the barrel provides a 0.52 T magnetic field. The present report is based on a first data sample of $\sim 500 \text{ pb}^{-1}$, except for quantum coherence, CPT and Lorentz symmetry tests; at present KLOE has about 2.2 fb^{-1} on disk.

2 V_{us} determination

In the Standard Model, the coupling of the W boson to the weak charged current is written as

$$\frac{g}{\sqrt{2}} W_\alpha^+ (\bar{\mathbf{U}}_L \mathbf{V}_{\text{CKM}} \gamma^\alpha \mathbf{D}_L + \bar{e}_L \gamma^\alpha \nu_{eL} + \bar{\mu}_L \gamma^\alpha \nu_{\mu L} + \bar{\tau}_L \gamma^\alpha \nu_{\tau L}) + \text{h.c.}, \quad (1)$$

where $\mathbf{U}^T = (u, c, t)$, $\mathbf{D}^T = (d, s, b)$ and L is for lefthanded. In the coupling above there is only one coupling constant for leptons and quarks. Quarks are mixed by the Cabibbo-Kobayashi-Maskawa matrix, \mathbf{V}_{CKM} , which must be unitary.

The most precise check on the unitarity of the \mathbf{V}_{CKM} matrix is provided by measurements of $|V_{us}|$ and $|V_{ud}|$, the contribution of V_{ub} being at the level of 10^{-5} . $|V_{us}|$ may be extracted by the measurements of the semileptonic decay rates, fully inclusive of radiation, which are given by:

$$\Gamma(K_{\ell 3}(\gamma)) = \frac{C_K^2 G_F^2 M_K^5}{192\pi^3} S_{\text{EW}} |V_{us}|^2 |f_+(0)|^2 I_{K\ell} \left(1 + \delta_K^{\text{SU}(2)} + \delta_{K\ell}^{\text{EM}}\right)^2. \quad (2)$$

In the above expression, the index K denotes $K^0 \rightarrow \pi^\pm$ and $K^\pm \rightarrow \pi^0$ transitions, for which $C_K^2 = 1$ and $1/2$, respectively. M_K is the appropriate kaon mass, S_{EW} is the universal short-distance electroweak correction³ and $\ell = e, \mu$. Following a common convention, $f_+(0) \equiv f_+^{K^0\pi^-}(0)$. The mode dependence is contained in the δ terms: the long-distance electromagnetic (EM) corrections, which depend on the meson charges and lepton masses and the SU(2)-breaking corrections, which depend on the kaon species⁴. $I_{K\ell}$ is the integral of the dimensionless Dalitz-plot density over the physical region for non radiative decays and includes $|\tilde{f}_{+,0}(t)|^2$, the reduced form factor, defined below.

$|V_{us}|$ can be also extracted from $K \rightarrow \mu\nu$ decays using the relation

$$\frac{\Gamma(K_{\mu 2}(\gamma))}{\Gamma(\pi_{\mu 2}(\gamma))} = \frac{|V_{us}|^2}{|V_{ud}|^2} \frac{f_K^2}{f_\pi^2} \frac{m_K \left(1 - m_\mu^2/m_K^2\right)^2}{m_\pi \left(1 - m_\mu^2/m_\pi^2\right)^2} \times (0.9930 \pm 0.0035), \quad (3)$$

where f_π and f_K are the pion- and kaon-decay constants and the uncertainty in the numerical factor is dominantly from structure-dependent radiative corrections. This ratio can be combined with direct measurements of $|V_{ud}|$ to obtain $|V_{us}|$.

The measurement of V_{us} from leptonic and semileptonic kaon decays allows both the test the unitarity of the CKM matrix and the leptonic quark universality. Moreover the universality of electron and muon interactions can be tested by measuring the ratio $\Gamma(K \rightarrow \pi\mu\nu)/\Gamma(K \rightarrow \pi e\nu)$ and the comparison between the measurement of V_{us} from leptonic decays and that from semileptonic decays allows to put bounds on new physics.

The experimental inputs to eq. 2 and 3 are the semileptonic and leptonic decay rates, fully inclusive of radiation, *i.e.* branching ratios (BR) and lifetimes, and the reduced form factors $\tilde{f}_+(t)$ and $\tilde{f}_0(t)$, whose behaviour as a function of t , the 4-momentum transfer squared $(P_K - p_\pi)^2$,

is obtained from the decay pion spectra. Details on the measurements and the treatment of correlations can be found in ref. ⁵. In this report I will present the recent measurement of the $K_{\mu 3}$ form factors, the charged kaon life time, the $\text{BR}(K_{13}^{\pm})$ and the $\text{BR}(K^+ \rightarrow \pi^+ \pi^0)$

3 $K_{\mu 3}$ from factors

The largest uncertainty in calculating $|V_{us}|$ from the decays rates is due to the difficulties in computing the matrix element $\langle \pi | J_{\alpha}^{had} | K \rangle$ which has the form:

$$\langle \pi | J_{\alpha}^{had} | K \rangle = f_+(0) \times ((P+p)_{\alpha} f_+(t) + (P-p)_{\alpha} (f_0(t) - f_+(t) \Delta_{K\pi}/t)) \quad (4)$$

where $P(p)$ is the $K(\pi)$ momentum, $t = (P-p)^2$ and $\Delta_{K\pi} = M_K^2 - m_{\pi}^2$. The above equation defines the vector and scalar form factors (FF) $f_+(t) = f_+(0) \tilde{f}_+(t)$ and $f_0(t) = f_+(0) \tilde{f}_0(t)$, which take into account the non point-like structure of the pions and kaons. The term $f_+(0)$ has been factored out, since the FFs must have the same value at $t = 0$. If the FFs are expanded in powers of t up to t^2 as $\tilde{f}_{+,0}(t) = 1 + \lambda'_{+,0} \frac{t}{m^2} + \frac{1}{2} \lambda''_{+,0} \left(\frac{t}{m^2} \right)^2$, four parameters (λ'_{+} , λ''_{+} , λ'_0 and λ''_0) need to be determined from the decay pion spectrum in order to be able to compute the phase-space integral. However, this parametrization of the form factors is problematic, because the values for the λ s obtained from fits to the experimental decay spectrum are strongly correlated ⁶. It is therefore necessary to obtain a form for $\tilde{f}_0(t)$ and $\tilde{f}_+(t)$ with at least t and t^2 terms but with only one parameter. The Callan-Treiman relation ⁷ fixes the value of scalar FF at $t = \Delta_{K\pi}$ (the so-called Callan-Treiman point) to the ratio of the pseudoscalar decay constants f_K/f_{π} . $\tilde{f}_0(\Delta_{K\pi}) = \frac{f_K}{f_{\pi}} \frac{1}{f_+(0)} + \Delta_{CT}$, where Δ_{CT} , SU(2)-breaking correction ⁸, is of $\mathcal{O}(10^{-3})$. A recent dispersive parametrization for the scalar form factor ⁹, $\tilde{f}_0(t) = \exp \left[\frac{t}{\Delta_{K\pi}} (\ln C - G(t)) \right]$, allows the constraint given by the Callan-Treiman relation to be exploited, such that $C = \tilde{f}_0(\Delta_{K\pi})$ and $\tilde{f}_0(0) = 1$. $G(t)$ is derived from $K\pi$ scattering data. As suggested in ref. ⁹, a good approximation to the dispersive parametrization is $\tilde{f}_0(t) = 1 + \lambda_0 \frac{t}{m^2} + \frac{\lambda_0^2 + p_2}{2} \left(\frac{t}{m^2} \right)^2 + \frac{\lambda_0^3 + 3p_2\lambda_0 + p_3}{6} \left(\frac{t}{m^2} \right)^3$ with p_2 and p_3 given in ref. ⁹. Also for the vector FF we make use of a dispersive parameterization ¹⁰, twice subtracted at $t = 0$, $\tilde{f}_+(t) = \exp \left[\frac{t}{m_{\pi}^2} (\Lambda_+ + H(t)) \right]$, where $H(t)$ is obtained from $K\pi$ scattering data and Λ_+ has to be determined from the fit to experimental data. At KLOE energies clean and efficient

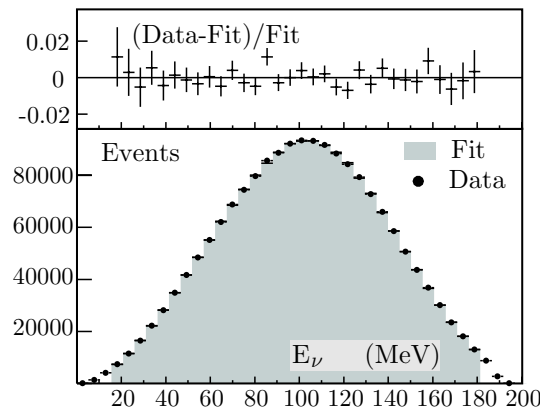


Figure 1: Residuals of the fit (top plots) and E_{ν} distribution for data events superimposed on the fit result (bottom plot)

π/μ separation, required to measure the t spectrum, is difficult. The FF parameters have

been therefore obtained from fits to the distribution of the neutrino energy E_ν after integration over the pion energy. About 1.8 Million of $K_{\mu 3}$ are selected by means of kinematic cuts, time of flight (TOF) measurements and calorimetric information. Details on the analysis can be found in ref. ¹¹. Using the dispersive parameterizations for the vector and scalar FF's and combining the $K_{\mu 3}$ and $K_{e 3}$ data, we find $\lambda_+ = (25.7 \pm 0.4 \pm 0.4 \pm 0.2_{\text{param}}) \times 10^{-3}$ and $\lambda_0 = (14.0 \pm 1.6 \pm 1.3 \pm 0.2_{\text{param}}) \times 10^{-3}$ with $\chi^2/\text{dof} = 2.6/3$ and a correlation coefficient of -0.26 . The result of the fit on $K_{\mu 3}$ data is shown in figure 1. Preliminary results based on $1fb^{-1}$ have been also obtained and averaged with that presented above: $\lambda_+ = (26.0 \pm 0.5_{\text{stat+syst}}) \times 10^{-3}$ and $\lambda_0 = (15.1 \pm 1.4_{\text{stat+syst}}) \times 10^{-3}$

4 $\tau(K^\pm)$, $\text{BR}(K_{l3}^\pm)$ and $\text{BR}(K^+ \rightarrow \pi^+\pi^0)$

We have combined the recent published measurements of the semileptonic BRs and the charged kaon lifetime to use them in the evaluation of $|V_{us}|$.

At KLOE, two methods are used to reconstruct the proper decay time distribution for charged kaons. The first is to obtain the decay time from the kaon path length in the DC, accounting for the continuous change in the kaon velocity due to ionization energy losses. A fit to the proper-time distribution in the interval from 15–35 ns ($1.6\tau_\pm$) gives the result $\tau_\pm = 12.364 \pm 0.031_{\text{stat}} \pm 0.031_{\text{syst}}$ ns. Alternately, the decay time can be obtained from the precise measurement of the arrival times of the photons from $K^+ \rightarrow \pi^+\pi^0$ decays. In this case, a fit to the proper-time distribution in the interval from 13–42 ns ($2.3\tau_\pm$) gives the result $\tau_\pm = 12.337 \pm 0.030_{\text{stat}} \pm 0.020_{\text{syst}}$ ns. Taking into account the statistical correlation between these two measurements ($\rho = 0.307$), we obtain the average value $\tau_\pm = 12.347 \pm 0.030$ ns, see ¹².

To measure $\text{BR}(K_{e3}^\pm)$ and $\text{BR}(K_{\mu 3}^\pm)$, we use both $K \rightarrow \mu\nu$ and $K \rightarrow \pi\pi^0$ decays as tags. We measure the semileptonic BRs separately for K^+ and K^- . Therefore, $\text{BR}(K_{e3})$ and $\text{BR}(K_{\mu 3})$ are each determined from four independent measurements (K^+ and K^- decays; $\mu\nu$ and $\pi\pi^0$ tags). Two-body decays are removed by kinematics and the photons from the π^0 are reconstructed to reconstruct the K^\pm decay point. From the TOF and momentum measurement for the lepton tracks, we obtain the m_l^2 distribution shown in figure 2. Further details are given in ¹³. Using the

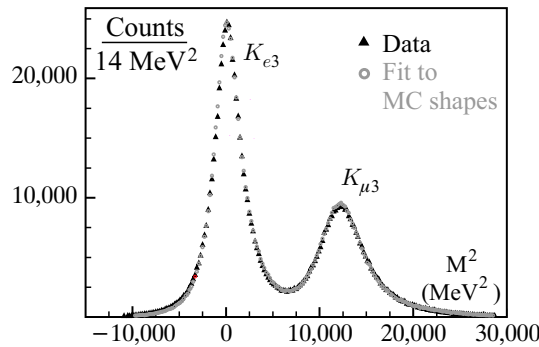


Figure 2: Distribution of m_l^2 , from TOF information, for K_{l3}^\pm events.

above result for τ_\pm to estimate the fiducial volume acceptance, we obtain $\text{BR}(K_{e3}) = 0.04972 \pm 0.00053$ and $\text{BR}(K_{\mu 3}) = 0.03273 \pm 0.00039$, which we use in our evaluation of $|V_{us}|$.

We have also obtained a preliminary result on the $\text{BR}(K^+ \rightarrow \pi^+\pi^0)$, which is crucial to perform the fit of all K^\pm BRs and for the $|V_{us}|$ determination of several experiments (NA48, ISTRA+, E865) in the normalization of the BRs (K_{l3}^\pm). About 800000 $K^+ \rightarrow \pi^+\pi^0$ have been select with kinematic cuts. Our preliminary result, $\text{BR}(K^+ \rightarrow \pi^+\pi^0) = (20.658 \pm 0.065 \pm 0.090)\%$, is lower than the PDG value ¹⁴ of about 1.3%. Further details can be found in ref. ¹⁵.

5 $|f_+(0)V_{us}|$ and lepton universality

Using the $\text{BR}(K_{l3}^{0,\pm})$, $\tau(K_L)$, $\tau(K^\pm)$ and the FFs from the KLOE results and $\tau(K_S)$ from the PDG¹⁴, the values of $|f_+(0)V_{us}|$ has been evaluated for K_{Le3} , $K_{L\mu3}$, K_{Se3} , K_{e3}^\pm and $K_{\mu3}^\pm$ decay modes. The inputs from theory, according to eq. 2, are the SU(2)-breaking correction evaluated with ChPT to $\mathcal{O}(p^4)$, as described in¹⁶, the long distance EM corrections to the full inclusive decay rate evaluated with ChPT to $\mathcal{O}(e^2p^2)$ ¹⁶ using low-energy constants from ref.¹⁷.

The average on the five different determination obtained taking into account all correlations is: $|f_+(0)V_{us}| = 0.2157 \pm 0.0006$ with $\chi^2/\text{dof} = 7.0/4$.

Comparison of the values of $|f_+(0)V_{us}|$ for K_{e3} and $K_{\mu3}$ modes provides a test of lepton universality. We calculate the following quantity

$$r_{\mu e} \equiv \frac{|f_+(0)V_{us}|_{\mu3, \text{exp}}^2}{|f_+(0)V_{us}|_{e3, \text{exp}}^2} = \frac{\Gamma_{\mu3}}{\Gamma_{e3}} \frac{I_{e3}(1 + \delta_{Ke})^2}{I_{\mu3}(1 + \delta_{K\mu})^2}, \quad (5)$$

where $\delta_{K\ell}$ stands for $\delta_K^{\text{SU}(2)} + \delta_{K\ell}^{\text{EM}}$. In the SM $r_{\mu e} = 1$. Averaging between charged and neutral modes, we find $r_{\mu e} = 1.000 \pm 0.008$. The sensitivity of this result is competitive with that obtained for $\pi \rightarrow l\nu$ and $\tau \rightarrow l\nu$ decays^{18,19} whose accuracy is $\sim 0.4\%$.

6 Test of CKM unitarity

To get the value of $|V_{us}|$ we have used the recent determination of $f_+(0) = 0.9644 \pm 0.0049$ from RBC and UKQCD Collaborations obtained from a lattice calculation with $2+1$ flavors of dynamical domain-wall fermions²². Using their value for $f_+(0)$, our K_{l3} results give $|V_{us}| = 0.2237 \pm 0.0013$. Additional information is provided by the determination of the ratio $|V_{us}/V_{ud}|$, using eq. 3. From our measurements of $\text{BR}(K_{\mu2})$ and τ_\pm , $\Gamma(\pi_{\mu2})$ from ref.¹⁴ and the recent lattice determination of f_K/f_π from the HPQCD/UKQCD collaboration, $f_K/f_\pi = 1.189 \pm 0.007$ ²¹, we obtain $|V_{us}/V_{ud}|^2 = 0.0541 \pm 0.0007$. We perform a fit to the above ratio and our result $|V_{us}|^2 = 0.05002 \pm 0.00057$ together with the result $|V_{ud}|^2 = 0.9490 \pm 0.0005$ from superallowed β -decays²⁰. We find $1 - |V_{us}|^2 - |V_{ud}|^2 = 0.0004 \pm 0.0007$ ($\sim 0.6\sigma$) and confirm the unitarity of the CKM quark mixing matrix as applied to the first row. The result of the fit is shown in figure 3.

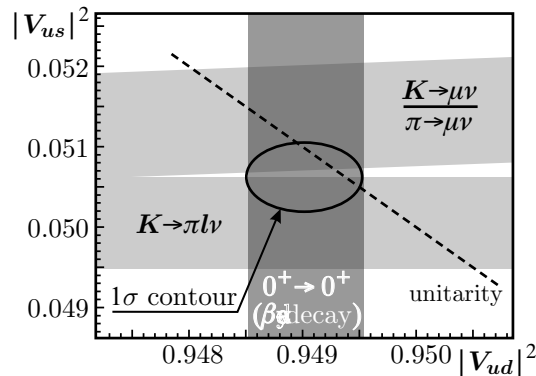


Figure 3: KLOE results for $|V_{us}|^2$, $|V_{us}/V_{ud}|^2$ and $|V_{ud}|^2$ from β -decay measurements, shown as 2σ wide grey bands. The ellipse is the 1σ contour from the fit. The unitarity constraint is illustrated by the dashed line.

7 Bounds on new physics from K_{l2} decays

The comparison between the values for $|V_{us}|$ obtained from helicity-suppressed K_{l2} decays and helicity-allowed K_{l3} decays allows to put bounds on new physics. We study the quantity $R_{l23} =$

$\left| \frac{V_{us}(K_{\mu 2})}{V_{us}(K_{\ell 3})} \times \frac{V_{ud}(0^+ \rightarrow 0^+)}{V_{ud}(\pi_{\mu 2})} \right|$, which is unity in the SM, but would be affected only in $V_{us}(K_{\mu 2})$ by the presence of non-vanishing scalar or right-handed currents. A scalar current due to a charged Higgs exchange is expected to lower the value of $R_{\ell 23}$, which becomes (see²³): $R_{\ell 23} = \left| 1 - \frac{m_{K^+}^2}{m_{H^+}^2} \left(1 - \frac{m_{\pi^+}^2}{m_{K^+}^2} \right) \frac{\tan^2 \beta}{1 + \epsilon_0 \tan \beta} \right|$ with $\tan \beta$ the ratio of the two Higgs vacuum expectation values in the MSSM and $\epsilon_0 \approx 0.01$ ²⁴. Using our result on $K_{\mu 2}$ and $K_{\ell 3}$ decays, the lattice determinations of $f_+(0)$ and f_K/f_π and the value of $|V_{ud}|$ discussed above, we obtain $R_{\ell 23} = 1.008 \pm 0.008$. Fig. 4 shows the region in the $\{m_{H^+}, \tan \beta\}$ plane excluded at 95% CL by our result for $R_{\ell 23}$.

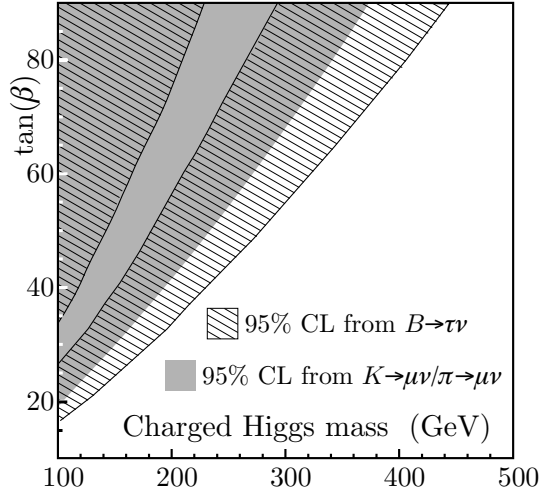


Figure 4: Region in the m_{H^+} - $\tan \beta$ plane excluded by our result for $R_{\ell 23}$; the region excluded by measurements of $\text{BR}(B \rightarrow \tau \nu)$ is also shown.

The ratio $R_K = \frac{\text{BR}(K_{e 2})}{\text{BR}(K_{\mu 2})}$ is extremely well known in the SM, being almost free on hadronic uncertainties. Since the electron channel is helicity suppressed R_K is sensitive to contributions from physics beyond the SM. Deviations up to few percent on R_K are expected in minimal supersymmetric extensions of the SM and should be dominated by lepton-flavour violating contributions with tauonic neutrinos emitted²⁵. KLOE has selected about 8000 $K_{e 2}$ events on 1.7 pb^{-1} by performing a direct search without the tag of the other kaon. Background from $K_{\mu 2}$ has been reduced by means of kinematic cuts and calorimeter particle identification. Our preliminary result, $R_K = (2.55 \pm 0.05 \pm 0.5) \times 10^{-5}$, allows to put bounds on the charged Higgs mass and $\tan \beta$ for different slepton mass matrix off-diagonal elements $\Delta_{1,3}$. An accuracy of $\sim 1\%$ is expected increasing the data sample analyzed, the control sample and Monte Carlo statistics.

8 Test of quantum coherence, CPT and Lorentz symmetry with the neutral kaons

Test of quantum mechanics (QM) can be performed by studying the time evolution of the quantum correlated $K_S K_L$ system, in particular studying the interference pattern of the decay $K_L K_S \rightarrow \pi^+ \pi^- \pi^+ \pi^-$. The distribution of the difference decay times is given by:

$$I(|\Delta t|) \propto e^{-|\Delta t| \Gamma_L} + e^{-|\Delta t| \Gamma_S} - 2 \cos(\Delta m |\Delta t|) e^{-\frac{\Gamma_S + \Gamma_L}{2} |\Delta t|} \quad (6)$$

One of the most direct ways to search for deviations from QM is to introduce a decoherence parameter ζ ²⁶, *i.e.* multiplying by a factor $(1 - \zeta)$ the interference term in the last equation. The definition of ζ depends on the basis chosen for the initial state²⁷ $|i\rangle \propto |K_S(+\vec{p})\rangle |K_L(-\vec{p})\rangle - |K_L(+\vec{p})\rangle |K_S(-\vec{p})\rangle$ or $|i\rangle \propto |K^0(+\vec{p})\rangle |\bar{K}^0(-\vec{p})\rangle - |\bar{K}^0(+\vec{p})\rangle |K^0(-\vec{p})\rangle$.

The case $\zeta = 1$ (*i.e.* total decoherence) corresponds to the spontaneous factorization of states (known as Furry's hypothesis²⁸). Selecting a pure sample of $K_L K_S \rightarrow \pi^+ \pi^- \pi^+ \pi^-$ and fitting eq. 6 to data, KLOE has obtained the following preliminary result based on $1fb^{-1}$: $\zeta_{SL} = 0.009 \pm 0.022_{\text{stat}}$ and $\zeta_{00} = (0.03 \pm 0.12_{\text{stat}}) \times 10^{-5}$ consistent with QM predictions.

In a quantum gravity framework, space-time fluctuations at the Planck scale ($\sim 10^{-33}$ cm), might induce a pure state to evolve into a mixed one²⁹. This decoherence, in turn, necessarily implies *CPT* violation³⁰. In this context the *CPT* operator may be "ill-defined" and *CPT* violation effects might also induce a breakdown of the correlation in the initial state^{31,32} which can be parametrized in general as: $|i\rangle \propto |K_S(+\vec{p})\rangle|K_L(-\vec{p})\rangle - |K_L(+\vec{p})\rangle|K_S(-\vec{p})\rangle + \omega (|K_S(+\vec{p})\rangle|K_S(-\vec{p})\rangle - |K_L(+\vec{p})\rangle|K_L(-\vec{p})\rangle)$ where ω is a complex parameter describing *CPT* violation. Its order of magnitude might be at most $|\omega| \sim \sqrt{(M_K^2/M_{\text{Planck}})/\Delta\Gamma} \sim 10^{-3}$, with $\Delta\Gamma = \Gamma_S - \Gamma_L$. KLOE has improved its limit on the ω parameter using about $1fb^{-1}$. The preliminary results, obtained by fitting the $I(\Delta t; \pi^+ \pi^- \pi^+ \pi^-)$ distribution, are $\text{Re}\omega = (-2.5_{-2.3}^{+3.1}) \times 10^{-4}$ and $\text{Im}\omega = (-2.2_{-3.1}^{+3.4}) \times 10^{-4}$, consistent with quantum coherence and *CPT* symmetry. The accuracy reaches the interesting region of the Planck's scale.

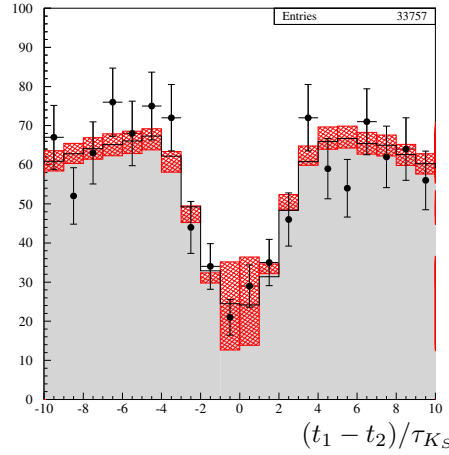


Figure 5: Fit of the difference $t_1 - t_2$ of the decay times of $K_S \rightarrow \pi^+ \pi^-$ and $K_L \rightarrow \pi^+ \pi^-$, where t_1 is the time of the kaon having $\cos\theta > 0$, in the range $0 < t_{\text{sid}} < 4h$. The black points are the experimental data, the histogram is the fit results and the hatched area is the uncertainty arising from the efficiency, the resolution and the background evaluation

Another possibility for *CPT* violation is based on spontaneous breaking of Lorentz symmetry in the context of the Standard Model Extension (SME)^{33,34}. In the SME *CPT* violation manifests to lowest order only in the δ parameter, describing *CPT* violation in the time evolution, which exhibits a dependence on the kaon 4-momentum:

$$\delta(p, \theta, t_{\text{sid}}) = \frac{1}{2\pi} \int_0^{2\pi} \delta(\vec{p}, t_{\text{sid}}) d\phi = \frac{isin\phi_{SW} e^{i\phi_{SW}} \gamma}{\Delta m} \quad (7)$$

$$(\Delta a_0 + \beta \Delta a_Z \cos \chi \cos \theta + \beta \Delta a_Y \sin \chi \cos \theta \sin \Omega t_{\text{sid}} + \beta \Delta a_X \sin \chi \cos \theta \cos \Omega t_{\text{sid}})$$

after integration on ϕ , where θ and ϕ are the conventional polar and azimuthal angles defined in the laboratory frame around the z axis. Δa_μ are four *CPT* and Lorentz symmetry violating coefficients for the two valence quarks, β is the kaon velocity, $\gamma = 1/\sqrt{1-\beta^2}$, ϕ_{SW} is the superweak angle, χ is the angle between the z laboratory axis and the Earth's rotation axis and Ω is Earth's sidereal frequency. The sidereal time (t_{sid}) dependence arises from the rotation

of the Earth. KLOE has measured the $\Delta a_{X,Y,Z}$ parameters by using the channel $K_S K_L \rightarrow \pi^+ \pi^- \pi^+ \pi^-$ and performing an analysis on the polar angle θ and the sidereal time t_{sid} . Fitting the distribution of the decay times difference $I(t_1 - t_2; \pi^+ \pi^- (\cos \theta_1 > 0) \pi^+ \pi^- (\cos \theta_2 < 0); t_{sid})$ we obtain the preliminary results based on $1fb^{-1}$: $\Delta a_X = (-6.3 \pm 6.0) \times 10^{-18}$ GeV, $\Delta a_Y = (-2.8 \pm 5.9) \times 10^{-18}$ GeV and $\Delta a_Z = (-2.4 \pm 9.7) \times 10^{-18}$ GeV. The result of the fit is shown in fig. 5. A limit on the Δa_0 parameter has been obtained through the difference on the K_S and K_L semileptonic charge asymmetry integrated on t_{sid} and on a symmetrical polar angle region. Our preliminary result is $\Delta a_0 = (0.4 \pm 1.8) \times 10^{-17}$ GeV

References

1. M. Adinolfi *et al.* (KLOE Collaboration), *Nucl. Instrum. Methods* **A488** (2002) 51
2. M. Adinolfi *et al.* (KLOE Collaboration), *Nucl. Instrum. Methods* **A482** (2002) 364
3. A. Sirlin *Nucl. Phys.* **B196** (1982) 83.
4. V. Cirigliano *et al.*, *Eur Phys. J* **23** (2002) 121.
5. F. Ambrosino *et al.* (KLOE Collaboration), *J. High Energy Phys.* **04** (2008) 059
6. P. Franzini, Opening remarks, PoS(KAON)002 (2007).
7. C.G. Callan, S.B. Treiman, *Phys. Rev. Lett.* **16** (1966) 153.
8. J. Gasser, H. Leutwyler, *Nucl. Phys.* **B250** (1985) 465.
9. V. Bernard, M. Oertel, E. Passemar and J. Stern, *Phys. Lett.* **B638** (2006) 480.
10. V. Bernard, M. Oertel, E. Passmar and J. Stern, private communication. They compute a dispersion relation for $\ln f_+$ twice subtracted at $t = 0$, using $K\pi$ p -wave scattering data, as done in Ref.9.
11. F. Ambrosino, *et al.* (KLOE Collaboration), *J. High Energy Phys.* **12** (2007) 105
12. F. Ambrosino, *et al.* (KLOE Collaboration), *J. High Energy Phys.* **01** (2008) 073.
13. F. Ambrosino *et al.* (KLOE Collaboration), *J. High Energy Phys.* **02** (2008) 098
14. W.-M. Yao. *et al.* (Particle Data Group), *J. Phys.* **G33** (2006) 1 and 2007 web updates.
15. F. Ambrosino, *et al.* (KLOE Collaboration), [arXiv:0804.4577](https://arxiv.org/abs/0804.4577)
16. V. Cirigliano *et al.* *Eur Phys. J* **23** (2002) 121
17. S. Descotes-Genon and B. Moussallam, *Eur Phys. J* **C42** (2005) 403
18. M.J. Ramsey-Musolf, S. Su and S. Turlin, *Phys. Rev.* **C76** (2007) 095017.
19. M. Davier, A. Höcker and Z. Zhang, *Rev. Mod. Phys* **78** (2006) 1043.
20. I.S. Towner and J.C. Hardy, [arXiv:0710.3181](https://arxiv.org/abs/0710.3181).
21. E. Follana *et al.*, (HPQCD/UKQCD Collaboration), [arXiv:0706.1726](https://arxiv.org/abs/0706.1726)
22. P.A. Boyle *et al.*, (RBC/UKQCD Collaboration), [arXiv:0710.5136](https://arxiv.org/abs/0710.5136)
23. G. Isidori and P. Paradisi, *Phys. Lett.* **B639** (2006) 499
24. G. Isidori and A. Retico, *J. High Energy Phys.* **11** (2001) 001
25. A. Masiero, P. Paradisi, R. Petronzio, *Phys. Rev.* **D74** (2006) 011701
26. P. H. Eberhard, "Tests of Quantum Mechanics at a ϕ factory" in *The second DaΦne handbook*, ed. L. Maiani, G. Pancheri, N. Paver, Vol.I
27. R. A. Bertlmann *et al.*, *Phys. Rev.* **D60** (1999) 114032
28. W. H. Furry, *Phys. Rev.* **D49** (1936) 393
29. S. Hawking, *Commun. Math. Phys.* **87** (1982) 395
30. R. Wald, *Phys. Rev.* **D21** (1980) 2742
31. J. Bernabeu, N. Mavromatos, J. Papavassiliou, *Phys. Rev. Lett.* **92** (2004) 131601
32. J. Bernabeu, N. Mavromatos, J. Papavassiliou, A. Waldron-Lauda, *Nucl. Phys.* **B744** (2006) 180
33. V. A. Kostelecky, *Phys. Rev.* **61** (1999) 016002
34. V. A. Kostelecky, *Phys. Rev.* **64** (2001) 076001

MEASUREMENT OF DIRECT CP VIOLATION PARAMETER $Re(\epsilon'/\epsilon)$ IN THE NEUTRAL KAON SYSTEM

A GLAZOV

On behalf of the KTeV Collaboration

DESY, Notkestrasse 85, Hamburg, 22607, Germany



The final measurement of the direct CP violation parameter $Re(\epsilon'/\epsilon)$ performed by the KTeV collaboration is presented. The new result, $Re(\epsilon'/\epsilon) = [19.2 \pm 1.1_{\text{stat}} \pm 1.8_{\text{syst}}]$, improves precision of the previous measurement¹ and is consistent with it. Along with the measurement of $Re(\epsilon'/\epsilon)$, new measurements of the $K_L - K_S$ mass difference, Δm , the K_S lifetime, τ_S , the phase $\phi_\epsilon = \arg(\epsilon)$ and the phase difference $\Delta\phi$ are performed. The data are consistent with CPT symmetry, the value of $Re(\epsilon'/\epsilon)$ is consistent with the NA48 result².

1 Introduction

Violation of CP symmetry in weak interactions was first discovered in 1964 when the decay $K_L \rightarrow \pi^+\pi^-$ was observed. It was realized in the following experiments that the main reason for the effect is a small difference between $K^0 \rightarrow \bar{K}^0$ and $\bar{K}^0 \rightarrow K^0$ transition rates, which is termed as indirect CP violation. CP can be also violated directly in a decay amplitude, a search for this process has been performed by experiments at CERN^{3,2} and Fermilab^{4,1}. In this letter, the final measurement of direct CP violation by the KTeV experiment at Fermilab is reported.

Direct CP violation manifests itself as a difference in the level of CP violation for different decay modes. For neutral kaons, $K \rightarrow \pi^+\pi^-$ and $K \rightarrow \pi^0\pi^0$ decay amplitudes can be compared:

$$\begin{aligned}\eta_{+-} &= \frac{A(K_L \rightarrow \pi^+\pi^-)}{A(K_S \rightarrow \pi^+\pi^-)} = \epsilon + \epsilon' \\ \eta_{00} &= \frac{A(K_L \rightarrow \pi^0\pi^0)}{A(K_S \rightarrow \pi^0\pi^0)} = \epsilon - 2\epsilon'.\end{aligned}\tag{1}$$

Here ϵ quantifies common indirect CP violation while ϵ' parameterizes a difference between the two modes and thus is a direct CP violation parameter.

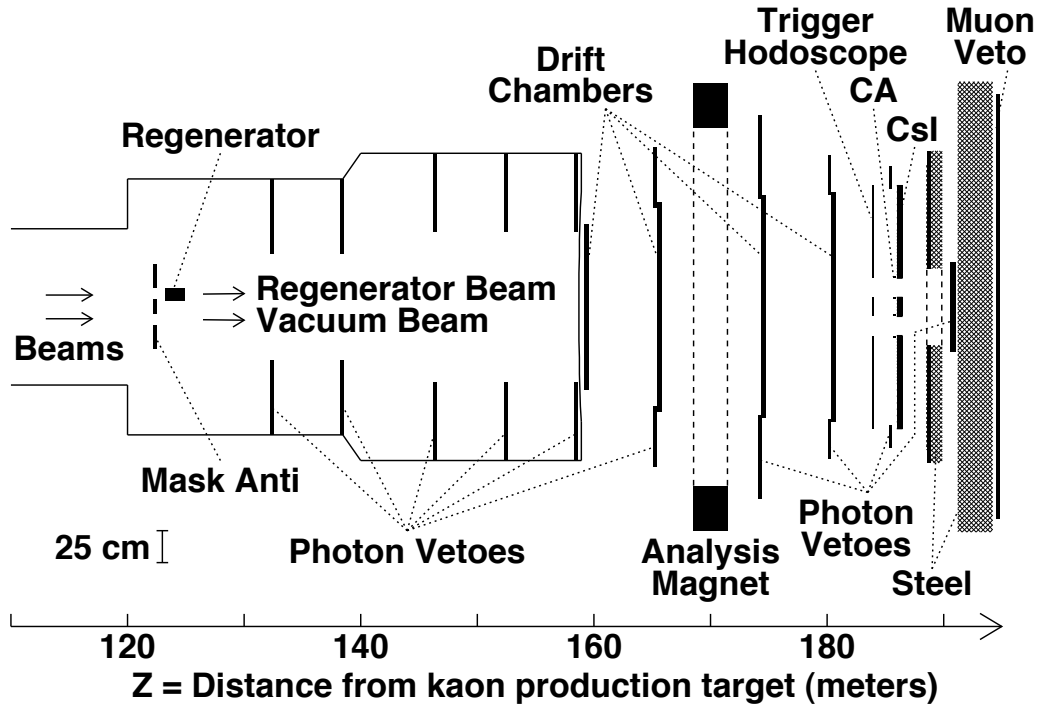


Figure 1: Schematic view of the KTeV detector

CPT invariance imposes additional constraints on the complex parameters ϵ and ϵ' . In particular phase of ϵ must be equal to the “superweak” phase, $\phi_\epsilon = \phi_{SW} \equiv \arctan(2\Delta m/\Delta\Gamma)$, where $\Delta m \equiv m_L - m_S$ is the $K_L - K_S$ mass difference and $\Delta\Gamma \equiv \Gamma_S - \Gamma_L$ is the difference in the decay widths. CPT invariance together with measurements of the strong phase shifts⁵ also requires that $\phi_\epsilon \approx \phi_{\epsilon'}$. Therefore, $Re(\epsilon'/\epsilon)$ is a measure of direct CP violation while $Im(\epsilon'/\epsilon)$ is a measure of CPT violation. Experimentally, $Re(\epsilon'/\epsilon)$ is determined using double ratio of the decay rates:

$$\frac{\Gamma(K_L \rightarrow \pi^+\pi^-)/\Gamma(K_S \rightarrow \pi^+\pi^-)}{\Gamma(K_L \rightarrow \pi^0\pi^0)/\Gamma(K_S \rightarrow \pi^0\pi^0)} = \left| \frac{\eta_{+-}}{\eta_{00}} \right|^2 \approx 1 + 6Re(\epsilon'/\epsilon), \quad (2)$$

while $Im(\epsilon'/\epsilon)$ can be determined from the phase difference of the decay amplitudes:

$$\Delta\phi \equiv \phi_{00} - \phi_{+-} \approx -3Im(\epsilon'/\epsilon). \quad (3)$$

Previous measurements of $Re(\epsilon'/\epsilon)$ have established that it has small non-zero value. This letter presents the final KTeV measurement of $Re(\epsilon'/\epsilon)$ which is based on complete data sample, including new 1999 data period that about doubles the statistics of the previous KTeV publication¹, and significantly improved experimental procedure.

2 KTeV Detector and Data Analysis

The KTeV apparatus (see Fig. 1) uses double beam technique to simultaneously collect the four decay modes $K_{L,S} \rightarrow \pi^+\pi^- (\pi^0\pi^0)$. The two neutral beams are formed from secondary particles produced by 800 GeV/c protons colliding on a beryllium oxide target using a system of collimators, absorbers and sweeping magnets. The neutral kaon decays are detected in 110 – 158 m range from the production target (for the KTeV coordinate system this corresponds to a positive Z direction). The kaon energies used in this analysis are in 40 – 160 GeV range. At

125 m from the production target one of the beams passes through a plastic regenerator which produces coherent mixture of K_L and K_S states, for $K \rightarrow \pi\pi$ decays the K_S state dominates. The regenerator alternates between the two neutral beams during the periods with no proton collisions on target, at about once per minute rate, in order to reduce systematic differences between K_L and K_S decays. The kaon beam with the regenerator is termed in the following as the regenerator beam while the other beam is termed as the vacuum beam.

The charged decay products are detected in a drift chamber spectrometer. The spectrometer is equipped with two chambers before and two after an analyzing magnet. Each chamber measures charged particle tracks in horizontal and vertical views. The neutral decay products are measured in a CsI crystal calorimeter, located after the spectrometer at 186 m from the production target. The crystals of the calorimeter have transverse dimensions of 2.5×2.5 cm² for the central region surrounded by 5×5 cm crystals in the outer range, there are 3100 crystals in total.

An extensive veto system rejects background events coming from interactions in the regenerator, semileptonic and $K_L \rightarrow \pi^0\pi^0\pi^0$ decays. The background levels, which include non- $K \rightarrow \pi\pi$ decays as well as $K \rightarrow \pi\pi$ decays in which the kaon scatters in the regenerator, after all selection cuts do not exceed 0.1% for the $\pi^+\pi^-$ (“charged”) and 1.2% for the $\pi^0\pi^0$ (“neutral”) mode.

The reconstruction of $K \rightarrow \pi^+\pi^-$ mode starts from selecting events with two track measured in the spectrometer. Each track is matched to a cluster in CsI calorimeter and $E/p < 0.85$ is required to reject $K \rightarrow \pi^\pm e^\mp \nu$ events. No signal is allowed in the muon veto system, located behind the CsI calorimeter, to reject $K \rightarrow \pi^\pm \mu^\mp \nu$ events. A high efficiency of the muon system is ensured by imposing $p > 8$ GeV/c condition for momentum of each track. The invariant mass of the two tracks, assuming the tracks are charged pions, is selected in $488 \text{ MeV}/c^2 < m_{\pi^+\pi^-} < 508 \text{ MeV}/c^2$ range. The transverse momentum squared of the kaon is required to be $p_T^2 < 250 \text{ MeV}^2/c^2$ in order to reject events in which the kaon undergoes scattering in the regenerator or in an upstream collimator.

To measure $K \rightarrow \pi^0\pi^0$ decays four photon clusters of energy are detected in the CsI calorimeter. The clusters are paired together to reconstruct $\pi^0 \rightarrow \gamma\gamma$ decays. For each pairing the Z coordinate of the decay point with respect to the calorimeter surface is calculated as $Z_{12} = r_{12}\sqrt{E_1 E_2}/m_{\pi^0}$, where $E_{1,2}$ are the photon energies, r_{12} is the distance between the photons and m_{π^0} is the nominal π^0 mass. All six pairings are considered and the one which leads to the most consistent Z_{12} determination is used. The decay Z vertex position is estimated using an error weighted average of Z_{12} . The kaon transverse vertex position is reconstructed by using a center of energy of the clusters, it is required to be situated inside the beam profile in order to reduce scattering background. The kaon energy is measured as a sum of the cluster energies. A cut on total invariant mass is imposed $488 \text{ MeV}/c^2 < m_{\pi^0\pi^0} < 508 \text{ MeV}/c^2$ which rejects $K \rightarrow \pi^0\pi^0\pi^0$ events.

Distributions of the Z coordinate of $K_S \rightarrow \pi\pi$ and $K_L \rightarrow \pi\pi$ decay vertices have very different shape because of the difference in the lifetimes. To take this into account, KTeV uses a detailed Monte Carlo simulation (MC). Quality of this simulation can be tested by comparing the Z vertex distribution in the vacuum beam, see Fig 2. A linear slope in the ratio of the data to MC distributions can be directly translated into uncertainty of $Re(\epsilon'/\epsilon)$ using a difference of an average Z position of the decay vertex for K_S and K_L decays. The systematic uncertainty is derived based on $K_L \rightarrow \pi^+\pi^-$ decays for the charged and $K_L \rightarrow \pi^0\pi^0\pi^0$ decays for the neutral mode.

Compared to the previous KTeV publication¹, several significant improvements of the measurement procedure were introduced. These include improvements for the 1999 data taking (i.e. better duty cycle for the proton extraction and repaired electronics of CsI calorimeter), for the data analysis (i.e. better model for drift chamber resolution which lead to $\sim 15\%$ increase of $m_{\pi^+\pi^-}$ resolution), while the main improvements were made for the detector simulation. The

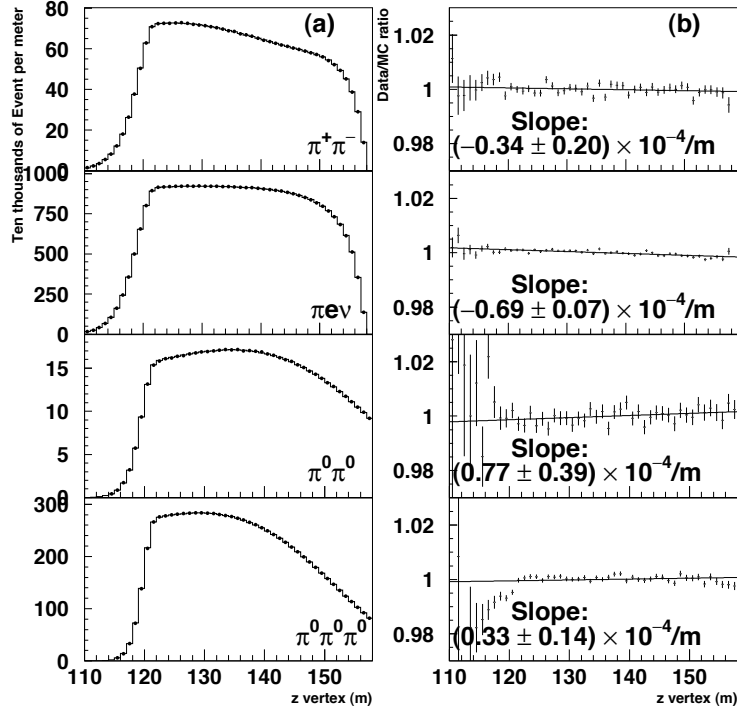


Figure 2: Z coordinate of the kaon decay point in the vacuum beam for data (dots) and MC (histogram), (a), and the ratio of data to MC distributions, (b), for (from top to bottom) $K_L \rightarrow \pi^+ \pi^-$, $K_L \rightarrow \pi^\pm e^\mp \nu$, $K_L \rightarrow \pi^0 \pi^0$ and $K_L \rightarrow \pi^0 \pi^0 \pi^0$ decays.

updates in MC include new charged particle tracing in the detector, which were also used for the KTeV measurement of the parameter V_{us} ⁶ and better description of the photon showers, using a new GEANT-based⁷ shower library. The new simulation of the photon showers leads to significant reduction of the energy scale uncertainty, which is the main source of the error for $Re(\epsilon'/\epsilon)$, this error is reduced from 1.3×10^{-4} to 0.65×10^{-4} .

3 Results

For the full combined dataset, the result of the analysis is

$$Re(\epsilon'/\epsilon) = [19.2 \pm 1.1_{\text{stat}} \pm 1.8_{\text{syst}}] \times 10^{-4} = [19.2 \pm 2.1] \times 10^{-4}. \quad (4)$$

The result is in a good agreement with the previous KTeV publication¹: $Re(\epsilon'/\epsilon) = [20.7 \pm 1.5_{\text{stat}} \pm 2.4_{\text{syst}}] \times 10^{-4}$. A comparison of the KTeV measurement with other experiments is presented in Fig. 3. A good agreement between different results is observed; the world average, $Re(\epsilon'/\epsilon) = [16.8 \pm 1.4] \times 10^{-4}$, corresponds to a measurement of the direct CP violation parameter with 8% precision.

Decays in the regenerator beam are sensitive to $K_L - K_S$ interference and thus allow to measure Δm , ϕ_ϵ and $Im(\epsilon'/\epsilon)$. Measurements of Δm and ϕ_ϵ depend strongly on the properties of the kaon regeneration and transmission in the regenerator beam. The transmission in the regenerator beam has been re-measured using a high statistics sample of $K \rightarrow \pi^+ \pi^- \pi^0$ events collected in 1999. A dedicated study of the screening corrections allowed to significantly reduce uncertainty arising from the kaon regeneration. As a result, the measurement of ϕ_ϵ is significantly improved compared to previous KTeV publication¹ providing a better CPT symmetry test. For

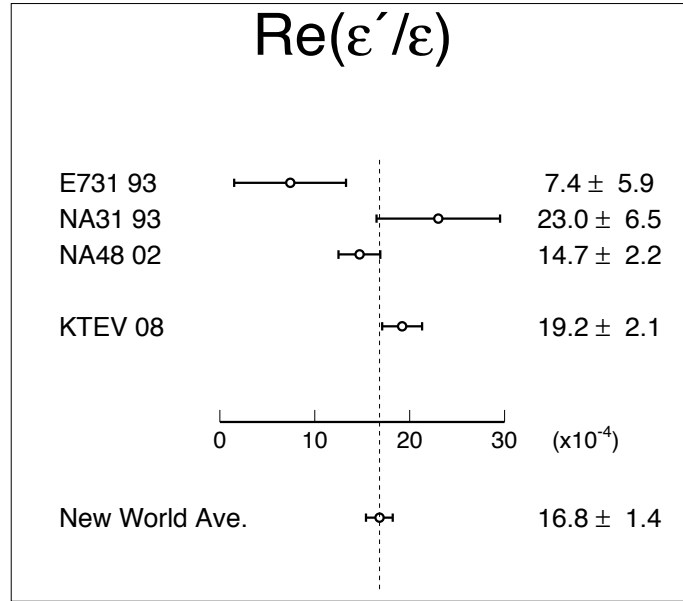


Figure 3: $Re(\epsilon'/\epsilon)$ measured by E731⁴, NA31³, NA48² and KTeV¹ collaborations together with an average of these four measurements labeled as “New World Ave.”.

an analysis without CPT constraints, KTeV obtains:

$$\begin{aligned}
 \tau_S &= [89.589 \pm 0.070] \times 10^{-12} \text{ s}, \\
 \Delta m &= [5279.7 \pm 19.5] \times 10^6 \text{ h/s}, \\
 \phi_\epsilon &= [43.86 \pm 0.63]^\circ, \\
 Im(\epsilon'/\epsilon) &= [-17.20 \pm 20.20] \times 10^{-4}.
 \end{aligned} \tag{5}$$

The measured $Im(\epsilon'/\epsilon)$ corresponds to $\Delta\phi = [0.30 \pm 0.35]^\circ$. The data are consistent with CPT symmetry: $Im(\epsilon'/\epsilon)$ and $\delta\phi = \phi_\epsilon - \phi_{SW} = [0.40 \pm 0.56]^\circ$ are consistent with zero. Imposing the CPT conservation as an additional constraint allows to reduce uncertainties on τ_S and Δm . This is illustrated in Fig. 4 which shows correlations of τ_S , Δm and ϕ_ϵ together with a band derived from $\delta\phi = 0$ condition. The resulting τ_S and Δm are:

$$\begin{aligned}
 \tau_S &= [89.623 \pm 0.047] \times 10^{-12} \text{ s}, \\
 \Delta m &= [5269.9 \pm 12.3] \times 10^6 \text{ h/s}.
 \end{aligned} \tag{6}$$

Using these values KTeV determines $\phi_{SW}|_{cpt} = [43.419 \pm 0.058]^\circ$.

4 Conclusions

The final measurement of $Re(\epsilon'/\epsilon)$ and other kaon system parameters by the KTeV collaboration based on complete dataset is presented. Increase of the data sample and improvements of the analysis techniques allow to reduce the total uncertainties compared to the previous publication¹. The world measurements of $Re(\epsilon'/\epsilon)$ are consistent with each other and establish firmly the presence of direct CP violation in the kaon decays. With improved precision, the data do not show any indication of CPT symmetry violation.

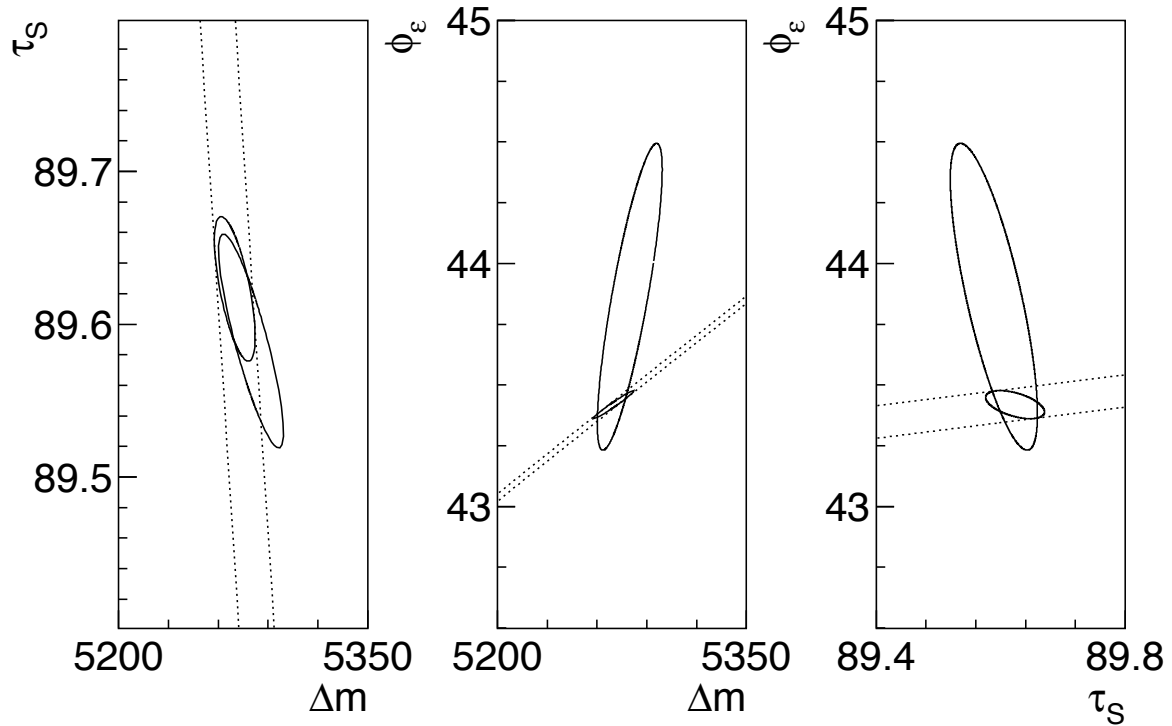


Figure 4: $\delta\chi^2 = 1$ contours of total uncertainty for (a) Δm and τ_S , (b) ϕ_ϵ and Δm , (c) τ_S and ϕ_ϵ . Dashed lines show $\phi_\epsilon = \phi_{SW}$ CPT constraint. Larger (smaller) ellipses correspond to results without (with) assumption of CPT symmetry conservation.

References

1. A. Alavi-Harati *et al* (KTeV), *Phys. Rev. D* **67**, 012005 (2003).
2. A. Lai *et al.* (NA48) *Eur. Phys. J. C* **62**, 231 (2001).
3. G. D. Barr *et al.* (NA31) *Phys. Lett. B* **317**, 233 (1993).
4. L. K. Gibbons *et al.* (E731) *Phys. Rev. Lett.* **70**, 1203 (1993).
5. W. Ochs, *πN Newsletter* **3**, 25 (1994).
6. A. Alavi-Harati *et al* (KTeV), *Phys. Rev. D* **70**, 092006 (2004).
7. R. Brun *et al*, GEANT 3.21, CERN, Geneva.

Status of the CKM matrix

S. Descotes-Genon, on behalf of the CKMfitter group

Laboratoire de Physique Théorique (UMR 8627), CNRS/Univ. Paris-Sud 11, 91405 Orsay, France

I review the status of Cabibbo-Kobayashi-Maskawa matrix within the Standard Model, with a focus on exclusive $b \rightarrow (d, s)\gamma$ transitions and on charm and strange physics.

In the Standard Model (SM), the weak charged-current transitions mix quarks of different generations, which is encoded in the unitary Cabibbo-Kobayashi-Maskawa (CKM) matrix. In the case of three generations of quarks, the physical content of this matrix reduces to four real parameters, among which one phase, the only source of CP violation in the Standard Model (the lepton sector can also exhibit similar sources of CP violation once masses, provided by New Physics (NP), are considered). One can define these four real parameters as:

$$\lambda^2 = \frac{|V_{us}|^2}{|V_{ud}|^2 + |V_{us}|^2} \quad A^2\lambda^4 = \frac{|V_{cb}|^2}{|V_{ud}|^2 + |V_{us}|^2} \quad \bar{\rho} + i\bar{\eta} = -\frac{V_{ud}V_{ub}^*}{V_{cd}V_{cb}^*}. \quad (1)$$

This parametrisation is exact, unitary to all orders in λ and independent of phase conventions. A Wolfenstein-like parametrisation of the CKM matrix can be derived up to an arbitrary power in the Cabibbo angle $\lambda = \sin(\theta_C)$, using the unitarity of the matrix to determine all its elements. A challenge for both experimentalists and theorists consist in extracting information on the underlying mechanism of CP violation from the wealth of data currently available, in the presence of the strong interaction that binds quarks into hadrons. Does the above CKM mechanism describe accurately the data? If yes, what are the values of λ , A , $\bar{\rho}$ and $\bar{\eta}$? If no, what is (are) the source(s) of CP violation beyond the Standard Model?

The CKMfitter group follows this program within the Rfit frequentist approach¹. The likelihood function \mathcal{L} is defined as the product $\mathcal{L}(y_{mod}) = \mathcal{L}_{exp}(x_{exp} - x_{the}(y_{mod})) \cdot \mathcal{L}_{the}(y_{QCD})$ where x_{exp} denote experimental measurements and x_{the} the corresponding theoretical predictions. x_{the} depends on y_{mod} which are either free parameters of the theory (e.g., the CKM matrix parameters) or hadronic quantities (e.g., form factors, decay constants... denoted y_{QCD}). Each

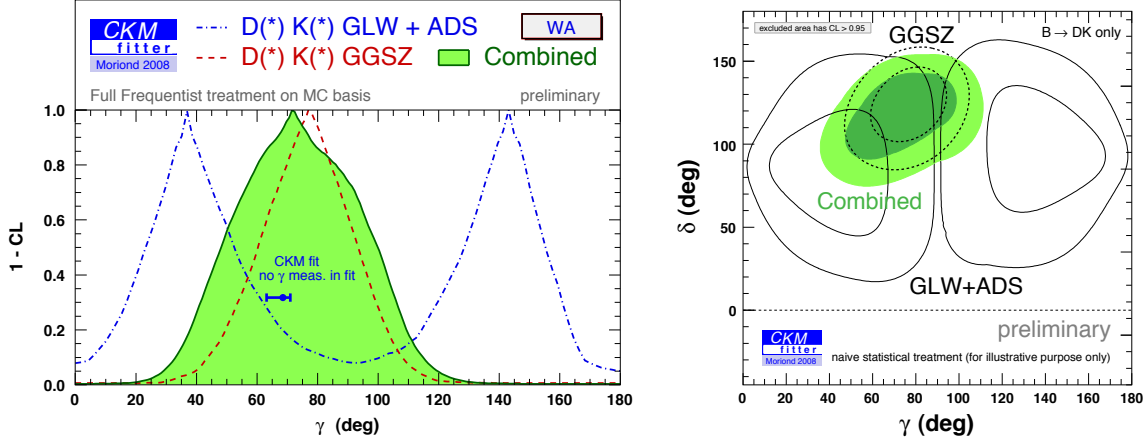


Figure 2: CL profile for γ (left) and correlation between γ and the strong phase δ for the different methods based on $B \rightarrow DK$ (right).

eral slightly incompatible solutions, the frequentist statistical treatment treats all the solutions on the same footing, leading to a broadening of the confidence intervals for γ (a Bayesian analysis would integrate over hadronic parameters, so that different incompatible solutions sharing the same value of γ yield an increase degree of belief in this value, reducing the uncertainty in the posterior p.d.f of γ)².

The outcome of the global fit is shown in Fig. 1 in the usual $(\bar{\rho}, \bar{\eta})$ plane

$$A = 0.795^{+0.025}_{-0.015}, \quad \lambda = 0.2252^{+0.0008}_{-0.0008}, \quad \bar{\rho} = 0.135^{+0.033}_{-0.016}, \quad \bar{\eta} = 0.345^{+0.015}_{-0.018} \quad (2)$$

but also in the $(\bar{\rho}_s, \bar{\eta}_s)$ plane defined as $\bar{\rho}_s + i\bar{\eta}_s = -(V_{us}V_{ub}^*)/(V_{cs}V_{cb}^*)$ and more suitable to discuss the CKM mechanism for the B_s sector. The corresponding triangle $(V_{us}V_{ub}^*)/(V_{cs}V_{cb}^*) + 1 + (V_{ts}V_{tb}^*)/(V_{cs}V_{cb}^*) = 0$ is squashed, with 2 sides of $O(\lambda^0)$ and 1 side of $O(\lambda^2)$. $\beta_s = \arg[-V_{cs}V_{cb}^*/(V_{ts}V_{tb}^*)]$, the angle opposite to the small side, is related to B_s mixing in the SM. The global fit yields a small and well-predicted value $\beta_s = -0.0183^{+0.0009}_{-0.0008}$ rad, with which recent flavour-tagged $B_s^0 \rightarrow J/\psi\phi$ analysis from CDF and D0 present some tension³. The two experiments used different assumptions for their analyses (strong phases, width of the B_s meson) and obtained nontrivial likelihoods. It seems sensible to wait for a combined analysis within a common framework and for a larger data sample before claiming a hint of NP in the B_s sector.

2 $B \rightarrow V\gamma$

It has been known for a long time that the loop processes $b \rightarrow (d, s)\gamma$ can give an access to $|V_{t(d,s)}|$ which complement $\Delta m_{d,s}$ in an interesting fashion: we can test penguin versus box diagrams, so that an inconsistency between the two determinations, and with the global fit, would teach us in which direction to look for NP. Inclusive $B \rightarrow X_s$ decays have been computed with a high accuracy⁴, but one can also consider exclusive $B \rightarrow V\gamma$ decays. The first attempts to compute the corresponding amplitudes used a factorisation approach^{5,6,7}. It was in particular used to determine

$$R_{\rho/\omega} = \frac{\bar{\mathcal{B}}(\rho^\pm\gamma) + \frac{\tau_{B^\pm}}{\tau_{B^0}} [\bar{\mathcal{B}}(\rho^0\gamma) + \bar{\mathcal{B}}(\omega\gamma)]}{\bar{\mathcal{B}}(K^{*\pm}\gamma) + \frac{\tau_{B^\pm}}{\tau_{B^0}} [\bar{\mathcal{B}}(K^{*0}\gamma)]} = \left| \frac{V_{td}}{V_{ts}} \right|^2 \left(\frac{1 - m_\rho^2/m_B^2}{1 - m_{K^*}^2/m_B^2} \right)^3 \frac{1}{\xi^2} [1 + \Delta R] \quad (3)$$

where ξ is a ratio of form factors and ΔR is a correction from hadronic physics estimated as $\Delta R = 0.1 \pm 0.1$. This important step left many questions open. What is the dependence of ΔR

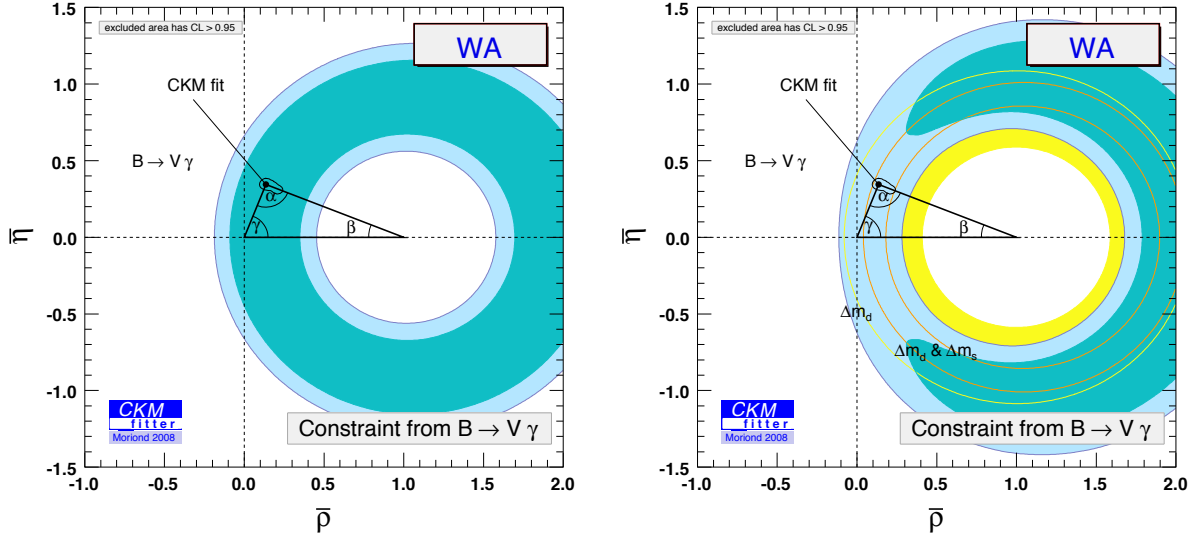


Figure 3: Constraints on the unitarity triangle from $B \rightarrow V\gamma$ using the simplified expression of $R_{\rho/\omega}$ (left) and considering the available branching ratios and their theoretical expressions with $1/m_b$ corrections (right).

on the CKM matrix elements? Can one estimate and exploit isospin breaking? How to estimate weak annihilation processes, which for $(\rho, \omega)\gamma$ occurs at tree level and can be large, despite a formal $1/m_b$ suppression. A further step was proposed by estimating $1/m_b$ -suppressed terms, missed in QCD factorisation or in SCET, through light-cone sum rules⁸. For each final state, all contributions can be expressed as a factor to the leading amplitude, i.e., the magnetic operator $Q_7 = (e/8\pi^2)m_b \bar{D}\sigma^{\mu\nu}(1 + \gamma_5)F_{\mu\nu}b$:

$$\bar{A} \equiv \frac{G_F}{\sqrt{2}} \left(\lambda_u^D a_7^u(V) + \lambda_c^D a_7^c(V) \right) \langle V\gamma | Q_7 | \bar{B} \rangle \quad \lambda_U^D = V_{UD}^* V_{Ub}, \quad (4)$$

where $D = d, s$ and the coefficient $a_7^U(V) = a_7^{U, \text{QCDF}}(V) + a_7^{U, \text{ann}}(V) + a_7^{U, \text{soft}}(V)$ is the sum of three terms. QCDF denotes the result from QCD factorisation at leading-order in $1/m_b$ and up to $O(\alpha_s)$ corrections, whereas ann and soft correspond to weak-annihilation and soft-gluon contributions. The latter are $1/m_b$ -suppressed contributions which can be computed within QCD factorisation, but can be estimated through light-cone sum rules.

In this approach, each decay is described individually and the short- and long-distance contributions of u and c internal loops can be identified (they are not combined in a single correction ΔR). For the evaluation, we followed refs.^{6,8} and for the expressions of a_7 's and hadronic inputs (form factors, distribution amplitudes), using leading-order Wilson coefficients and the HFAG averages for the branching ratios (in units of 10^{-6})⁹:

$$K^{*-}\gamma : 40.3 \pm 2.6, \quad K^{*0}\gamma : 40.1 \pm 2.0, \quad \rho^+\gamma : 0.88_{-0.26}^{+0.28}, \quad \rho^0\gamma : 0.93_{-0.18}^{+0.19}, \quad \omega\gamma : 0.46_{-0.17}^{+0.20},$$

together with the Belle value $B(B_s \rightarrow \phi\gamma) = (57_{-15}^{+18+12}) \cdot 10^{-6}$. Fig. 3 shows the improvement from the previous treatment. The constraint is not a perfectly circular ring, due to the (previously neglected) sensitivity to other CKM matrix elements in the decay amplitude. The constraints from $B \rightarrow V\gamma$ and from neutral B meson mixing have been superimposed to illustrate the compatibility of the two determinations, and their complementarity (we compare box and penguin processes with different theory sources). The study of CP asymmetries should provide further information on the apex of the B -meson unitarity triangle.

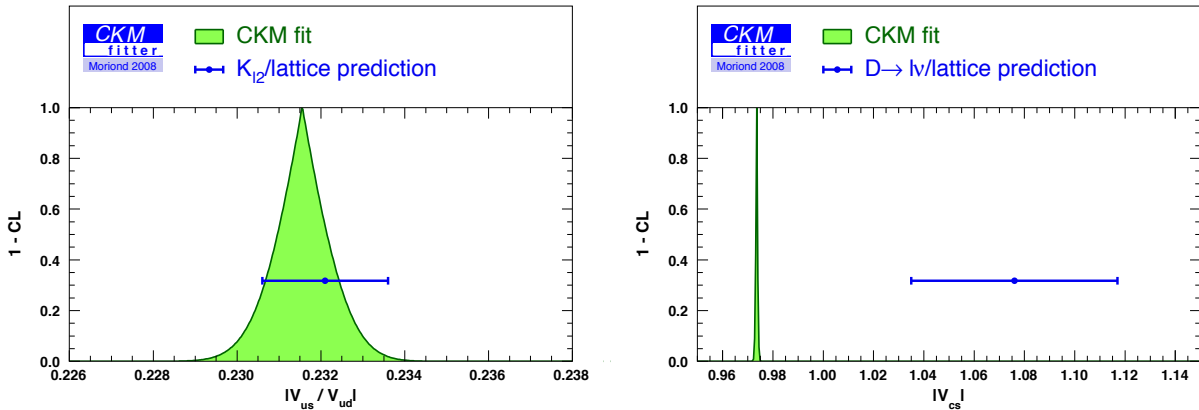


Figure 4: Constraints on $|V_{us}/V_{ud}|$ (left) and $|V_{cs}|$ (right). On each plot, the direct determination is compared to the prediction based on the global fit.

3 Lighter quarks and the lattice

The above constraints derived from b transitions can be translated into values of CKM matrix elements involving lighter quark and they can be compared to direct measurements which have recently improved. Indeed, some lattice simulations with three dynamical light quarks (unquenched) are available with astoundingly small systematics, thus reducing QCD uncertainties.

As a first example, $|V_{ud}|$ has benefited from an improved analysis of super-allowed β decays of nuclei, whereas $|V_{us}|$ has a shrinking uncertainty due to recent experimental results on $K_{\ell 3}$ and an improved lattice estimate of the relevant form factor $f_+(0) = 0.964(5)$ (domain-wall fermions, UKQCD+RBC)^{10,11}. Both values are used in the global fit, but an interesting cross-check consists in comparing the value of $|V_{us}/V_{ud}|$ from the fit with the value obtained by combining the measured ratio of leptonic decays $K \rightarrow \ell\nu/\pi \rightarrow \ell\nu$ with the lattice ratio of decay constant $f_K/f_\pi = 1.189(7)$ (staggered fermions, HPQCD+UKQCD)¹². The agreement shown on the left of Fig. 4 is remarkable, f_K/f_π being notoriously very difficult to compute on the lattice (it involves only light quarks and the chiral extrapolation can yield large uncertainties).

A second example is the charm sector, which has always been thought of as a favourite place to test lattice QCD, since m_c is close to the typical hadronic scale of 1 GeV. Lattice computations of form factors and decay constants should pin down $|V_{cd}|$ and $|V_{cs}|$ to a high accuracy. We illustrate the current improvement in the field in Fig. 5. The constraints on the nucleon and the kaon provide only a mild constraint, since $|V_{ud}| \simeq |V_{cs}|$ and $|V_{cd}| \simeq |V_{us}|$ only at first non trivial order in λ (one needs an input from another sector to fix higher orders). The B sector alone constrains $|V_{cd}|$ and $|V_{cs}|$ tightly and the combination of all indirect constraints turns out to be very powerful. We have also represented the direct constraints for $|V_{cd}|$, from νN scattering, and for $|V_{cs}|$ from charmed-tagged W decays (left) and from CLEO-c results on $D \rightarrow K\ell\nu$ (right)¹³. The distorted shape of these regions comes from $|V_{cd}|^2 + |V_{cs}|^2 \leq 1$.

These results for lighter quarks seem to confirm both the consistency of the CKM picture and the high accuracy advocated by lattice results. However, a recent result has shattered this beautiful convergence. Indeed, CLEO-c and Belle have both measured the leptonic decay $D_s \rightarrow \ell\nu$, whereas a related unquenched lattice result $f_{D_s} = 241 \pm 3$ MeV (staggered, HPQCD+UKQCD)¹². This yields to $|V_{cs}| = 1.076 \pm 0.041$ in flat disagreement with unitarity and with the fit value $|V_{cs}| = 0.97351^{+0.00020}_{-0.00022}$, as shown on Fig. 4 (right)¹⁴. This result is quite unsettling since the D_s involves only strange and charm valence quarks and should be an ideal place for lattice simulations, whereas NP is not supposed to play a major role for such mesons. Paradoxically, the much more complicated f_K/f_π led to an impressive agreement of experiment

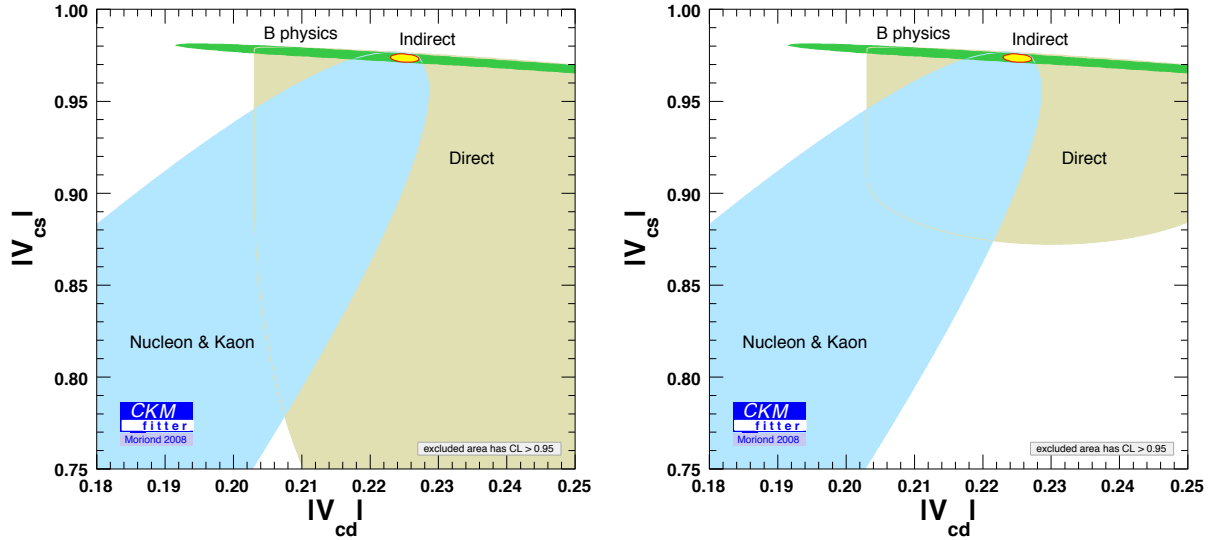


Figure 5: Constraints on $|V_{cd}|$ and $|V_{cs}|$ using PDG 07 (left) and with the new CLEO-c data on $D \rightarrow K l \nu$ (right).

and theory, while f_{D_s} points towards either uncontrolled systematics in unquenched lattice simulations (due to dynamical quarks?), overlooked systematics in the experimental measurements (radiative corrections?), or NP¹⁵. In any case, interesting news should come from this sector.

Acknowledgments

I would like to thank all the members of the CKMfitter group for the very enjoyable collaboration on the various topics covered in this presentation. This work was supported by the ANR contract ANR-06-JCJC-0056 and the EU Contract No. MRTN-CT-2006-035482, “FLAVIANet”.

References

1. CKMfitter Group (J. Charles et al.), Eur. Phys. J. C **41**, 1-131 (2005), updated results and plots available at: <http://ckmfitter.in2p3.fr>
2. V. Sordini, this conference.
3. G. P. Di Giovanni, this conference.
4. U. Haisch, this conference.
5. A. Ali, E. Lunghi and A. Y. Parkhomenko, Phys. Lett. B **595**, 323 (2004).
6. S. W. Bosch and G. Buchalla, Nucl. Phys. B **621** (2002) 459.
7. M. Beneke, T. Feldmann and D. Seidel, Eur. Phys. J. C **41** (2005) 173.
8. P. Ball, G. W. Jones and R. Zwicky, Phys. Rev. D **75**, 054004 (2007).
9. Heavy Flavour Averaging group, <http://www.slac.stanford.edu/xorg/hfag/>
10. M. Antonelli *et al.* [FlaviaNet Working Group on Kaon Decays], arXiv:0801.1817 [hep-ph].
11. P. Boyle [RBC Collaboration], PoS **LAT**, 005 (2007) [arXiv:0710.5880 [hep-lat]].
12. E. Follana, C. T. H. Davies, G. P. Lepage and J. Shigemitsu [HPQCD Collaboration], Phys. Rev. Lett. **100** (2008) 062002 [arXiv:0706.1726 [hep-lat]].
13. I. Shipsey, CLEO-c Aspen workshop, Jan 2008.
14. J. L. Rosner and S. Stone, arXiv:0802.1043 [hep-ex].
15. B. A. Dobrescu and A. S. Kronfeld, arXiv:0803.0512 [hep-ph].

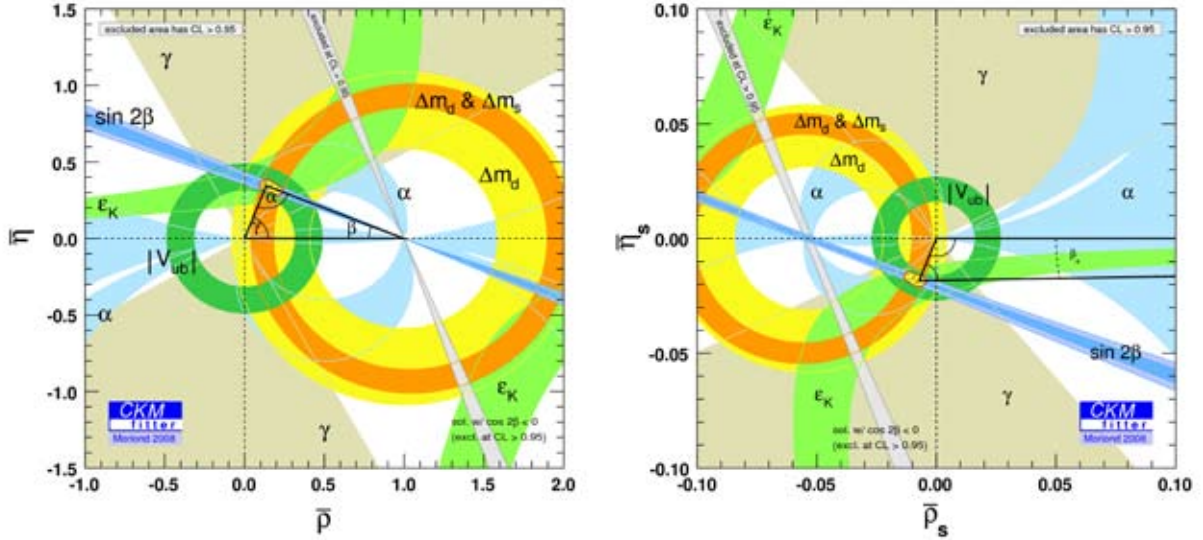


Figure 1: Constraints on the unitarity triangles corresponding to the B_d (left) and B_s (right) mesons.

individual measurement entering \mathcal{L}_{exp} is considered as Gaussian by default (in the case of a non-Gaussian experimental measurement, the exact description of the associated likelihood is directly used in the fit) and correlations, if known, are taken into account. The uncertainties on the theoretical parameters y_{QCD} define the allowed range of values for each parameter: $\mathcal{L}_{the}(y_{QCD}(i))$ is one within the allowed range and zero outside. The fit is performed on all the parameters y_{mod} by minimizing $\chi^2(y_{mod}) \equiv -2 \ln(\mathcal{L}(y_{mod}))$. For metrology (assuming a good agreement between data and theory), one splits $y_{mod} = (a, \mu)$, where a are the parameters of interest (e.g., $\bar{\rho}, \bar{\eta}$) and μ are the remaining parameters. The minimum value $\chi^2_{min;\mu}(a)$ is computed for a set of fixed values a while μ is allowed to vary. The Confidence Level represented on the plots is obtained from the χ^2 difference $\Delta\chi^2(a) = \chi^2_{min;\mu}(a) - \chi^2_{min}$.

1 The global fit

The global fit involves a large set of constraints. At the time of the conference, recent and significant changes occurred for $|V_{ud}|$ and $|V_{us}|$, which will be discussed below. In addition, BABAR and Belle have presented new determinations of γ , based on the interference between the colour-allowed $B^- \rightarrow D^0 K^-$ and colour-suppressed $B^- \rightarrow \bar{D}^0 K^-$ decays. The accuracy of the method is driven by the size of $r_B = |A_{suppr}|/|A_{favour}| \simeq |V_{ub}V_{cs}^*|/|V_{cb}V_{us}^*| \times O(1/N_c)$ typically of order 0.1-0.2, and the different methods try to improve on this ratio by different choices of D decay channels (GLW: D into CP eigenstates, ADS: $D^{(*)}$ into doubly Cabibbo-suppressed states, GGSZ: $D^{(*)}$ into 3-body state and Dalitz analysis). For the GGSZ analysis, BABAR and Belle have increased their statistics and BABAR includes neutral D into $K_S^0 K^+ K^-$. There has also been a DK update from BABAR for GLW, and a similar update from Belle for ADS².

Combining these results yields $\gamma = (72^{+34}_{-30})^\circ$ (68% CL) which shows a rather mild improvement at 2 and 3 σ with respect to combinations showed at previous conferences. The various methods provide values for γ , but also for the hadronic quantities such as r_B or the relative strong phase δ between the two amplitudes. The current values for these quantities are not completely consistent among the methods, as illustrated in Fig. 2: the methods yield similar ranges for γ but rather different values of the hadronic parameters. In such a situation with sev-